



Immobilization of Alcohol Dehydrogenase - Development of Support Materials and Immobilization Methods

Sigurdardóttir, Sigyn Björk

Publication date:
2020

Document Version
Publisher's PDF, also known as Version of record

[Link back to DTU Orbit](#)

Citation (APA):
Sigurdardóttir, S. B. (2020). *Immobilization of Alcohol Dehydrogenase - Development of Support Materials and Immobilization Methods*. Technical University of Denmark.

General rights

Copyright and moral rights for the publications made accessible in the public portal are retained by the authors and/or other copyright owners and it is a condition of accessing publications that users recognise and abide by the legal requirements associated with these rights.

- Users may download and print one copy of any publication from the public portal for the purpose of private study or research.
- You may not further distribute the material or use it for any profit-making activity or commercial gain
- You may freely distribute the URL identifying the publication in the public portal

If you believe that this document breaches copyright please contact us providing details, and we will remove access to the work immediately and investigate your claim.

Immobilization of Alcohol Dehydrogenase - Development of Support Materials and Immobilization Methods

PhD Thesis by
Sigyn Björk Sigurðardóttir

Supervisor:

Associate Professor Manuel Pinelo

Co-Supervisors:

Associate Professor Andreas Kaiser

Associate Professor Wenjing (Angela) Zhang

May, 2020

Immobilization of Alcohol Dehydrogenase - Development of Support Materials and Immobilization Methods

PhD Thesis
May, 2020

By
Sigyn Björk Sigurðardóttir

Copyright: Reproduction of this publication in whole or in part must include the customary bibliographic citation, including author attribution, report title, etc.

Published by: DTU, Department of Chemical and Biochemical Engineering, Søltøfts Plads, 228A, 2800 Kgs. Lyngby, Denmark
www.kt.dtu.dk

ISSN: [0000-0000] (electronic version)

ISBN: [000-00-0000-000-0] (electronic version)

ISSN: [0000-0000] (printed version)

ISBN: [000-00-0000-000-0] (printed version)

Preface

This thesis summarizes the topics and results of my PhD project entitled *New concepts for efficient immobilization of enzymes in inorganic membrane reactors*.

The project was a collaboration between DTU Chemical Engineering and DTU Energy, which consisted of two PhD students, three supervisors, and two researchers. My project was supervised by Associate Professor Manuel Pinelo from DTU Chemical Engineering and co-supervised by Associate Professor Andreas Kaiser from DTU Energy and Associate Professor Wenjing (Angela) Zhang from DTU Environment.

The work was supported by The Danish Council for Independent Research, Grant no.: 6111-00232B

The work corresponds to 180 ECTS points and includes course work, conference participations, supervision of students, external research stay, and own research. The work was carried out from June 2017 to May 2020, initially at the Center for Bioprocess Engineering (BioEng) and later at the Process and Systems Engineering Centre (PROSYS), Department of Chemical and Biochemical Engineering, DTU. A part of the work was conducted at Yale University, in the research group of Professor Menachem Elimelech at the Department of Chemical and Environmental Engineering (January 2019 – April 2019).

The PhD thesis is based on three scientific papers that were published in connection with the project. Furthermore, results from ongoing work are reported and discussed. The thesis is organized as follows:

Chapter 1 is an introduction to the topic and the scope of the project. The background and motivation for applying enzyme immobilization are discussed, the project is defined, and the different project phases are described.

Chapter 2 describes the state-of-the-art in enzyme immobilization techniques and is based on Paper 1, which is a review about enzyme immobilization on inorganic surfaces for membrane reactor applications. A special introduction to aluminosilicate nanofiber membranes as support for enzyme immobilization is given, as well as to enzyme immobilization by polyelectrolyte layer-by-layer assembly and interfacial polymerization, as these materials and methods are involved in the experimental part.

Chapter 3 describes the experimental results involving the immobilization of alcohol dehydrogenase (ADH). The discussion is divided into three parts involving the immobilization of ADH on i) inorganic raw powders and ii) aluminosilicate nanofiber membranes by covalent bonding and physical adsorption, and iii) on polymeric membranes by the polyelectrolyte layer-by-layer assembly method and interfacial polymerization. The chapter is partly based on Paper 2, which is a research paper about the immobilization of ADH on inorganic raw powders. The interactions between ADH and different inorganic raw materials was investigated, as well as the effects of different immobilization methods on the catalytic properties of the immobilized enzyme.

Chapter 4 is based on Paper 3, which reports the results of the project I worked on during my external research stay at Yale University. The project involved the use of polyelectrolyte LbL assembly for the fabrication of nanofiltration membranes with controllable properties and the investigation of solute transport and energy barriers to anion transport through the membranes.

Chapter 5 includes concluding remarks and future perspectives.

Working on this project has been an enriching experience for me on a professional and a personal level. I want to thank my supervisors, collaborators, and colleagues at DTU and Yale University for their part in this PhD project. First and foremost, I want to thank my supervisor, Manuel Pinelo, for giving me the opportunity to work on the project and for his limitless encouragement and excellent guidance and supervision throughout the process. Similarly, I appreciate the guidance and supervision of my co-supervisors Andreas Kaiser and Wenjing (Angela) Zhang, as well as the collaboration with Jonas Lehman, Jean-Claude Grivel, Simona Ovtar, Michela Della Negra, and Iram Aziz, which included fruitful scientific discussions, constructive feedback, and knowledge sharing. I am grateful for the opportunity to join the Elimelech research group at Yale University and for the valuable learnings and inspiration I received from students and scientists in the group. I want to thank Professor Menachem Elimelech for welcoming me in his group and for the productive and educative collaboration we had, along with Razi Epsztein and Ryan DuChanois, whom I want to thank as well. Finally, a big thanks goes to all my colleagues from the BioEng and PROSYS centers at DTU and from Yale University. I am lucky to have met so many great people and friends in these groups who made me look forward to going to work every day. A special thanks goes to Gúndi for his love and care and for being my main supporter during the writing of the thesis, and to my family and friends who are always there for me.

Copenhagen, May 2020

Sigyn Björk Sigurðardóttir
PhD Student

Abstract

On the path towards a sustainable society, enzyme catalysis becomes ever more important as an environmentally friendly alternative for the industrial production of chemicals. Enzyme immobilization is a principal technique to facilitate the widespread implementation of enzymes in the industry. Enzyme immobilization enables enzyme reuse and enzyme stabilization for increased viability in continuous operations.

Enzyme immobilization involves the attachment of enzymes to a solid support by physical or chemical interactions. The immobilization method and support are decisive factors in the success of enzyme immobilization systems (i.e., the activity retention, stability, and reusability of the immobilized enzyme). The objective of this project was to investigate enzyme immobilization for applications in inorganic membrane reactors using a holistic approach, where we studied enzyme immobilization techniques and membrane fabrication together to guide the design of immobilization methods and inorganic membranes with properties tailored for enzyme immobilization. Inorganic membranes were supplied by project collaborators, who applied the principles of material science and ceramic engineering for the development and fabrication of the inorganic membranes in a parallel project.

The main motivation for utilizing inorganic support materials for enzyme immobilization is the high stability of the materials, including chemical, thermal, and mechanical stability, which allows a stable operation and enables support regeneration when the process efficiency decreases due to fouling of the support or enzyme deactivation. Besides high stability, inorganic membranes offer several other advantages, such as high permeability and long service life. Furthermore, inorganic membranes have high microbial stability and are well-suited for enzyme immobilization. We started our investigations by studying the interactions between enzymes and different inorganic raw materials that are commonly used for membrane fabrication to identify suitable materials and important design parameters for membrane fabrication. Alcohol dehydrogenase (ADH) was used as a model enzyme and was immobilized on raw powders of aluminum oxide, silicon carbide, titanium oxide, and yttria stabilized zirconia by physical adsorption and covalent bonding. The stability and activity of the immobilized ADH were evaluated based on the properties of the inorganic powders (i.e., surface area, particle size distribution, and surface charge). Enzyme loading on the particles and enzyme activity were greatly affected by the surface area and surface charge of the powders. Aluminum oxide and silicon carbide powders provided suitable conditions for the immobilization of ADH.

Subsequently, aluminosilicate nanofiber membranes were fabricated by project collaborators using electrospinning. The nanofiber membranes offered a large surface area ($11.7 \text{ m}^2 \text{ g}^{-1}$), a high porosity, and pore sizes fit for the immobilization of ADH. These properties combined ensured high permeability and high enzyme loading in the membranes—the enzymes could penetrate the membranes but were retained within the nanofiber structure. Similarly, the membranes offered favorable conditions for enzyme immobilization. Up to 96% immobilization efficiency was observed when the enzyme immobilization was conducted in filtration mode, which resulted in enzyme entrapment in the nanofiber membranes. The immobilized enzymes showed high activity, with near-complete substrate conversion in a single pass through the biocatalytic membranes, however, the enzyme stability was limited by leakage from the membranes. Moreover, the nanofiber membranes were extremely fragile, which limited their applications in general. It was proposed to seal the membranes by depositing a layer of polyelectrolytes on the membranes, for example by the layer-by-layer (LbL) assembly method, to prevent enzyme leakage from

the membranes and thus maintain high enzyme activity.

We demonstrated how polyelectrolyte LbL assembly could be used to tailor the properties of nanofiltration membranes, including the pore size, membrane thickness, and surface charge, and could thus be used to promote favorable conditions for enzyme immobilization. We studied solute transport in polyelectrolyte multilayer membranes of different thicknesses and pore sizes to evaluate the effects of membrane thickness on solute transport in the membranes, which could have possible implications for enzyme immobilization. We investigated alternative methods for enzyme immobilization on membranes that could simultaneously be used to control the transport properties of the membranes, including immobilization by polyelectrolyte LbL assembly and interfacial polymerization. We described how the polyelectrolyte LbL assembly method could be used as a versatile and reversible method for enzyme immobilization. Similarly, we described how immobilization by interfacial polymerization provided a facile method for the fabrication of stable biocatalytic membranes with controllable properties. In experiments involving the immobilization of ADH on polymeric ultrafiltration membranes by interfacial polymerization, we observed a decrease in water permeability by increasing the polymerization time and thus the degree of cross-linking of the biocatalytic membrane. Furthermore, we observed 100% immobilization efficiency and up to 70% substrate conversion in a single pass through the biocatalytic membranes.

In summary, we investigated the possibility of fabricating inorganic membranes with properties tailored for enzyme immobilization. We applied inorganic nanofiber membranes for the immobilization of ADH and found that the membranes offered excellent conditions for the immobilization of the enzyme, with high enzyme loading and activity. However, the fragility of the membranes limited their applications at this stage. Nevertheless, the promising results should be an encouragement to continue the development of inorganic nanofiber membranes with higher stability and mechanical flexibility. We further demonstrated how membranes surface modification could be used to promote favorable conditions for enzyme immobilization.

Dansk sammenfatning

Med øget fokus på grøn omstilling bliver enzymkatalyse et vigtigere alternativ i industriel produktion af kemikalier. Enzymimmobilisering faciliterer implementering af enzymer i industrielle processer ved at stabilisere enzymerne og muliggøre deres genanvendelse i kemiske processer.

Ved enzymimmobilisering bliver enzymet forbundet til en understøtning via fysiske eller kemiske interaktioner. Immobiliseringsmetoden og understøtningen er afgørende faktorer for succes af enzymimmobiliseringssystemet (dvs. enzymaktivitet, stabilitet og genanvendelighed efter immobilisering).

Formålet med dette projekt var, at undersøge enzymimmobilisering for anvendelse i uorganiske membranreaktorer ved en holistisk tilgang. Enzymimmobiliseringsmetoder og membranfremstilling blev studeret side om side for at udvikle uorganiske membraner med egenskaber skræddersyet til enzymimmobilisering. Uorganiske membraner blev leveret af samarbejdspartnere, der anvendte principper for materialevidenskab og keramikteknik til udvikling og fremstilling af de uorganiske membraner i et samarbejdsprojekt.

Motivationen for, at anvende uorganiske materialer til enzymimmobilisering er den høje kemiske, termiske, og mekaniske stabilitet af disse materialer, hvilket tillader stabil drift og muliggør regenerering af understøtningen, når proceseffektiviteten falder på grund af begroning af understøtningen eller enzym deaktivering. Udover høj stabilitet tilbyder uorganiske membraner flere andre fordele, såsom høj permeabilitet og lang levetid. Desuden har uorganiske membraner høj mikrobiel stabilitet og er velegnede til enzymimmobilisering. Vi startede vores undersøgelser med at studere interaktioner mellem enzymer og forskellige uorganiske råmaterialer, der ofte bruges til membranfremstilling, for at identificere egnede materialer og vigtige designparametre til membranfremstilling. Alkoholdehydrogenase (ADH) blev anvendt som et modelenzym og blev immobiliseret på partikler af aluminiumoxid, siliciumcarbide, titaniumoxid og yttria-stabiliserede zirkonier ved fysisk adsorbering og kovalent binding. Stabiliteten og aktiviteten af det immobiliserede ADH blev evalueret baseret på egenskaberne af de uorganiske partikler (dvs. overfladeareal, partikelstørrelsesfordeling, og overfladeladning). Immobiliseringseffektiviteten og enzymaktiviteten blev stærkt påvirket af partiklernes overfladeareal og overfladeladning. Aluminiumoxid- og siliciumcarbide viste passende betingelser for immobilisering af ADH.

Efterfølgende blev aluminiumsilicat-nanofibermembraner fremstillet af projektsamarbejdspartnere ved anvendelse af elektrospinning. Nanofibermembranerne havde et stort overfladeareal ($11.7 \text{ m}^2 \text{ g}^{-1}$), en høj porøsitet og porestørrelser, der var egnet til immobilisering af ADH. Disse egenskaber sikrede høj membranpermeabilitet og høj immobiliseringseffektivitet —enzymerne kunne trænge ind i membranen, men sad fast i nonfiberstrukturen. Tilsvarende tilbød membranerne gunstige betingelser for enzymimmobilisering. Op til 96% immobiliseringseffektivitet blev observeret, når enzymimmobiliseringen blev udført i filtreringsmodus, hvilket resulterede i, at enzymerne sad fast i nanofibermembranerne. De immobiliserede enzymer udviste høj aktivitet, men enzymstabiliteten var begrænset af enzymlækage fra membranerne. Derudover var nanofibermembranerne ekstremt skrøbelige, hvilket begrænsede deres anvendelser. Det blev således foreslået at forsegle membranerne ved at afsætte et lag af polyelektrolytter på membranerne, for eksempel ved layer-by-layer (LbL) samlingsmetode, for at forhindre enzymlækage fra membranerne og derved opretholde høj enzymaktivitet.

Vi demonstrerede hvordan polyelektrolyt LbL-samling kunne bruges til fremstilling af nanofiltreringsmembraner med skræddersyede egenskaber, herunder porestørrelse, membran-

tykkelse og overfladeladning, og kunne således bruges til at fremme gunstige betingelser for enzymimmobilisering. Vi studerede transport i polyelektrolyt flerlagsmembraner med forskellige tykkelser og porestørrelser for at evaluere indflydelsen af membrantykkelse på transport i membranerne, hvilket kunne muligvis have implikationer for enzymimmobilisering. Vi undersøgte alternative metoder til enzymimmobilisering på membraner, der samtidig kunne bruges til at kontrollere membranernes transportegenskaber, herunder immobilisering ved hjælp af polyelektrolyt LbL-samling og grænsefladepolymerisation. Vi beskrev, hvordan polyelektrolyt LbL-metoden kunne bruges som en alsidig og reversibel metode for enzymimmobilisering. Ligeledes beskrev vi, hvordan immobilisering ved grænsefladepolymerisation kunne anvendes som en simpel metode til fremstilling af stabile biokatalytiske membraner med kontrollerbare egenskaber. I foreløbige eksperimenter med immobilisering af ADH på polymeriske ultrafiltreringsmembraner ved grænsefladepolymerisation observerede vi et fald i vandpermeabilitet ved at øge polymerisationstiden og dermed graden af tværbinding af den biokatalytiske membran. Derudover observerede vi 100% immobiliseringseffektivitet og op til 70% substratkonvertering i en enkelt gennemgang gennem de biokatalytiske membraner.

Sammenfattende undersøgte vi muligheden for at fremstille uorganiske membraner med egenskaber, der er skræddersyet til enzymimmobilisering. Vi anvendte uorganiske nanofibermembraner til immobilisering af ADH og fandt, at membranerne sikrede passende betingelser for immobiliseringen af enzymet med høj immobiliseringseffektivitet og enzyrneaktivitet. Dog begrænsede membranernes skrøbelighed deres anvendelser. Ikke desto mindre bør de lovende resultater være en opmuntring til at fortsætte udviklingen af uorganiske nanofibermembraner med højere stabilitet og mekanisk fleksibilitet. Vi demonstrerede yderligere, hvordan membranoverfladeforandring kunne bruges til at fremme gunstige betingelser for enzymimmobilisering.

List of publications

The PhD project is based on the work reported in the following publications:

- i Enzyme Immobilization on Inorganic Surfaces for Membrane Reactor Applications: Mass Transfer Challenges, Enzyme Leakage and Reuse of Materials
Sigyn Björk Sigurðardóttir, Jonas Lehmann, Simona Ovtar, Jean-Claude Grivel, Michela Della Negra, Andreas Kaiser, Manuel Pinelo
Advanced Synthesis and Catalysis. 2018; 360 (14): 2578–2607. <https://doi.org/10.1002/adsc.201800307> (Published)
- ii Alcohol dehydrogenase on inorganic powders: Zeta potential and particle agglomeration as main factors determining activity during immobilization
Sigyn Björk Sigurðardóttir, Jonas Lehmann, Jean-Claude Grivel, Wenjing Zhang, Andreas Kaiser, Manuel Pinelo
Colloids and Surfaces B: Biointerfaces. 2018; 175: 136–42. <https://doi.org/10.1016/j.colsurfb.2018.11.080> (Published)
- iii Energy Barriers to Anion Transport in Nanofiltration Membranes: Role of Intra-Pore Diffusion
Sigyn B. Sigurðardóttir, Ryan M. DuChanois, Razi Epsztein, Manuel Pinelo, Menachem Elimelech
Journal of Membrane Science. 2020; 117921. <https://doi.org/10.1016/j.memsci.2020.117921> (Published)
- iv Influence of fabrication parameters on electrospun Al₂O₃/SiO₂ nanofibers and their impact on the immobilization of Alcohol dehydrogenase
Iram Aziz, Sigyn Björk Sigurðardóttir, Jonas Lehmann, Wenjing Zhang, Manuel Pinelo, Andreas Kaiser
(In preparation)

Other publication that I participated in during my PhD:

- v Efficient ionic liquid-based platform for multi-enzymatic conversion of carbon dioxide to methanol
Zhibo Zhang, Jan Muschiol, Yuhong Huang, Sigyn Björk Sigurðardóttir, Nicolas von Solms, Anders E Daugaard, Jiang Wei, Jianquan Luo, Bao-Hua Xu, Suojiang Zhang, Manuel Pinelo
Green Chemistry. 2018; 20 (18): 4339-48 <https://doi.org/10.1039/C8GC02230E> (Published)
- vi Membrane compaction, internal fouling, and membrane preconditioning as major factors affecting performance of solvent resistant nanofiltration membranes in methanol solutions
Sigyn Björk Sigurðardóttir, Mohd Shafiq Mohd Sueb, Manuel Pinelo
Separation and Purification Technology. 2019; 227: 11568 <https://doi.org/10.1016/j.seppur.2019.115686> (Published)
- vii Charge exclusion as a strategy to control retention of small proteins in polyelectrolyte-modified ultrafiltration membranes
Mingbo Ji, Xianhui Li, Maryam Omidvarkordshouli, Sigyn Björk Sigurðardóttir, John Woodley, Anders Egede Daugaard, Jianquan Luo, Manuel Pinelo
Separation and Purification Technology. 2020; 247: 116963 [doi:10.1016/j.seppur.2020.116936](https://doi.org/10.1016/j.seppur.2020.116936) (Published)

Contents

Preface	iii
Abstract	v
Dansk sammenfatning	vii
List of publications	ix
1 Introduction	1
1.1 Enzyme immobilization for applications in membrane reactors	1
1.2 Defining the research project	5
2 Enzyme immobilization on inorganic surfaces	9
2.1 Immobilization supports	9
2.2 Immobilization methods	11
2.3 Reusability of immobilized enzymes	16
3 Immobilization of alcohol dehydrogenase for applications in membrane reactors	17
3.1 Materials and methods	18
3.2 Results and discussion	21
4 Investigating solute transport in polyelectrolyte multilayer membranes with controllable properties	31
4.1 Materials and methods	32
4.2 Results and discussion	33
5 Conclusion and future perspectives	35
5.1 Conclusion	35
5.2 Future perspectives	38
Bibliography	39
Appendix	47
A1 Paper 1: Enzyme Immobilization on Inorganic Surfaces for Membrane Reactor Applications: Mass Transfer Challenges, Enzyme Leakage and Reuse of Materials	47
A2 Paper 2: Alcohol dehydrogenase on inorganic powders: Zeta potential and particle agglomeration as main factors determining activity during immobilization	78
A3 Paper 3: Energy barriers to anion transport in polyelectrolyte multilayer nanofiltration membranes: Role of intra-pore diffusion	86
A4 Experimental results of immobilization of alcohol dehydrogenase by polyelectrolyte layer-by-layer assembly and interfacial polymerization	96
A5 Supplementary material	99

1 Introduction

1.1 Enzyme immobilization for applications in membrane reactors

1.1.1 Enzyme catalysis

Enzymes are bioactive molecules that were developed by nature to catalyze reactions vital to sustaining life. With millions of years of evolution behind them, enzymes have remarkable catalytic efficiency. Enzymes can speed up reactions many million-fold, with record rate-enhancements reported as 10^{21} -fold [1]. Furthermore, they present exceptional specificity and selectivity due to the precise enzyme architecture, which is a result of the sequence and folding of the amino acid chain making up the enzyme [2], [3].

Scientists have long been intrigued by the catalytic power of enzymes and have implemented them in various processes and applications. The main applications of enzymes are in food and beverage processing, technical applications (e.g., detergents, textile, pulp and paper, production of biofuels), and in animal feed [4], [5]. The use of enzymes in organic synthesis is likewise an important and growing application, following continuous advances in biotechnology [6], [7]. The increasing importance of enzymes is reflected in the global market for industrial enzymes, which has grown from US\$ 0.6 billion in 1989 to an estimated US\$ 7 billion in 2021 [8]. The demand for industrial enzymes is expected to increase even further in the coming years, in line with the shift of focus towards a sustainable society.

Enzyme catalysis is highly relevant for the development of sustainable processes. It complies with the twelve principles of green chemistry [9], and it can contribute to the realization of many of the United Nations Sustainable Developments Goals (e.g., goals number 6, 7, and 12-15, regarding clean water and energy, responsible production, and more) [10]. As the native role of enzymes is in reaction mechanisms in natural systems, the optimal reaction conditions are usually in aqueous environments, at ambient temperature and pressure [11], [12]. These factors render enzyme catalysis less hazardous and more energy-efficient than conventional thermochemical processes [11], [13]. Moreover, enzymes are biodegradable and safe catalysts and the high catalytic efficiency allows the synthesis of complex products by short and simple biocatalytic routes, often replacing multi-step chemical routes that require harsh process conditions, specialized equipment, use of organic solvents, and substantial waste disposal [3], [6], [8], [14].

The use of enzymes is an environmentally friendly and economical alternative for the industrial production of chemicals [13], [15]. Nevertheless, the record of enzyme catalysis in organic synthesis and industrial production of chemicals is relatively short [6]. Historically, the application of natural enzymes in industrial catalysis was limited by low stability, lack of availability, and high cost of such enzymes [15]. Starting in the 1970s, the advent of and subsequent progress in enzyme engineering and recombinant DNA techniques have been key factors in making enzymes a relevant option in industrial catalysis [6], [8], [15]. Today, engineered enzymes with improved catalytic properties and stability can be produced cost-effectively on an industrial scale by recombinant DNA technology [2], [8], [15]. The target properties of enzymes that are commonly manipulated by enzyme engineering include thermostability, pH tolerance, and substrate specificity [16]. Microbial biotechnology is an active research field, and modern biotechnology tools are widely applied for the discovery and development of new and better enzymes for biocatalytic processes [12].

1.1.2 Enzyme immobilization

As enzymes have become widely available at a competitive price, a following decisive factor in their successful implementation in industrial processes is process design. Here, a critical objective is to design for enzyme stabilization and reusability to ensure efficient and long-term use of the enzymes. Enzyme immobilization is a predominant technique to stabilize enzymes and facilitate their reuse in industrial processes [17], [18]. The increased stability and reusability of immobilized enzymes have a positive effect on product quality, as well as on the process economy and environmental footprint [6].

Enzyme immobilization has a long history both in academia and industry. The modern history of enzyme immobilization goes hand-in-hand with the rise in biotechnology and increasing interest in using enzymes in industrial applications [19], [20]. Immobilized enzymes are applied in several well-established industrial processes, ranging from the production of bulk chemicals to complex pharmaceutical compounds, of which the production of high fructose corn syrup by immobilized glucose isomerase is the most important, with an annual production of 10^7 tons [3], [21]. Commercial processes applying immobilized enzymes represent only a small fraction of enzyme-catalyzed processes in general, but the number is increasing steadily, motivated by the potential of economic and environmental sustainability [21].

By immobilization, enzymes are attached to a support (e.g., organic or inorganic nanoparticles, beads, resins, or membranes) or to other enzymes to form cross-linked enzyme crystals or aggregates [22]. The enzymes are made insoluble upon immobilization, and the increased size of the enzyme-support complex enables a simple recovery from the process medium. Furthermore, immobilization generally results in enhanced enzyme stability by preventing enzyme unfolding and denaturation due to heat, pH, organic solvent, and other process parameters [6], [15], [22]. On the other hand, enzyme immobilization can result in loss of enzyme activity and increased mass transfer limitations due to conformational changes in the enzyme structure and restricted substrate accessibility upon confining the enzyme to a carrier [19], [22]. The balance between enzyme stability and activity upon immobilization depends on several parameters of the respective immobilization system, including the immobilization method, support, and reactor configuration [22], [23]. Consequently, a vast number of immobilization strategies have been proposed in academic and industrial research, with the aim of optimizing the performance of immobilization systems. The most common enzyme immobilization methods and their effects on the catalytic properties of enzymes upon immobilization on inorganic carriers were reviewed and reported in Paper 1 (Appendix A1).

1.1.3 Immobilization supports

Decades of research have led to the development of a variety of immobilization supports that come in different materials, morphologies, and structures. The support becomes an integral part of the catalyst upon immobilization, so it must be stable in a process medium and fulfill specific criteria to provide high enzyme loading and a suitable microenvironment for the enzymes. The surface properties are particularly important for a successful immobilization, as the immobilization occurs through physical and chemical interactions between the enzyme and support material. The ideal surface properties depend on the enzyme and immobilization method in question, and the support material and morphology must be selected accordingly [22]. Support materials are broadly categorized as organic (e.g., synthetic polymers, biopolymers, resins) and inorganic (e.g., ceramics, metals, graphene oxide), whereas hybrid materials are becoming more widely available [24]. Ceramic support materials offer the advantage of high chemical, thermal, and mechanical stability over organic materials, and thereby prolonged service life and the ability of

support regeneration by harsh chemical and thermal cleaning methods [25]. Ceramics can be produced in various structures, and their material and surface properties can be tuned by an appropriate selection of raw materials and processing conditions [26]. The surface properties of the ready-made ceramic materials may be further modified by different surface treatments to promote favorable conditions for enzyme immobilization [27], [28].

The selection of a suitable support structure depends mainly on the given application and reactor configuration. Support structures range from nanomaterials to membranes. Nanomaterials have a high surface-to-volume ratio and introduce little mass transfer limitations to the process, whereas larger support structures allow easy recovery and different configurations, such as fluidized bed reactors [15], [29]. Reactor configuration is a fundamental part of process design and has a large effect on the process efficiency. Processes involving immobilized enzymes have been operated in various reactor types, including stirred tank reactors, packed bed reactors, and membrane reactors [15], [21].

Enzyme immobilization on membranes is a practical solution for biocatalytic reactions. Membranes offer a large surface area for immobilization, both on the membrane surface as well as inside the membrane pores, which can afford high enzyme loading [30]. Furthermore, the contact between the substrate and enzyme is aided by the controlled, pressure-driven convection of the substrate through the biocatalytic membrane, where the reaction occurs without diffusion limitations [31]. Membranes with immobilized enzymes are operated in enzymatic membrane reactors (EMRs).

1.1.4 Enzymatic membrane reactors

The EMR is a particularly advantageous unit for biocatalytic reactions employing immobilized enzymes. The EMR is the combination of a bioreaction and a membrane operation [32], where the primary role of the membrane is to retain the enzyme within the process [33]. The unit offers a high degree of operational flexibility and can accommodate both free and immobilized enzymes. The enzymes can be suspended in the reactor (in free or immobilized form) and retained by the membrane, or they can be immobilized directly on the membrane, where the membrane functions as a selective barrier and a scaffold for the enzymes [33], [34]. The EMR leads to process intensification by combining reaction and separation in one unit and it aids the reaction efficiency by continuously removing products upon conversion, thereby shifting the reaction equilibrium and reducing product inhibition. Furthermore, the EMR gives a product stream free of enzymes, which eliminates the steps of deactivating and removing the enzymes from the products, which is costly and can have a negative impact on product quality [35], [36]. The EMR offers many important solutions in the development of sustainable processes. Research in the field is focused on optimizing conditions, including immobilization methods and supports, for the myriad of potential applications.

Various types of membrane modules have been operated as EMRs, including hollow fiber, spiral wound, tubular, and plate-and-frame, using polymeric and ceramic membranes [34], [37]. Hollow fiber membranes generally offer the highest surface area and packing density, and have been found favorable for enzyme immobilization for that reason [38], [39]. However, hollow fibers are especially susceptible to membrane fouling, which complicates their applications [40]. Membrane fouling and enzyme activity decay are the main challenges involved in EMR operations [33], [41], [42]. As biomolecules, enzymes inevitably lose their activity with time, even though enzyme immobilization may serve to stabilize the enzymes. These challenges call for the development of stable and robust membrane materials that can withstand strategies for fouling mitigation (e.g., membrane vibration and

backshocking) and chemical, thermal, and mechanical cleaning methods for the removal of fouling and deactivated enzymes [22]. Similarly, reversible immobilization methods are advantageous regarding the removal of deactivated enzymes from the immobilization support to reuse the support with fresh enzymes.

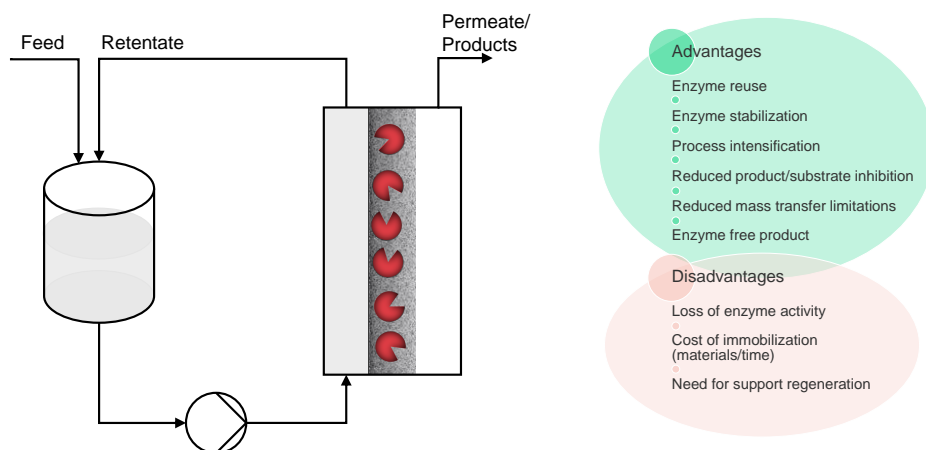


Figure 1.1: Schematic illustration of an enzymatic membrane reactor employing immobilized enzymes

Enzyme immobilization can be extended to multiple enzymes for cascade enzyme reactions. Cascade reactions are inspired by nature's intra-cellular processes and have received considerable attention recently as potential sustainable processes [15], [43], [44]. In cascade catalysis, multiple process steps are conducted together in one unit without the need to recover and purify intermediate products. The design saves both energy, auxiliaries, space, and time, and simultaneously, it enhances product yield by shifting the reaction equilibrium towards the product side, as well as by reducing product inhibition and loss of intermediates [45], [46]. Intra-cellular cascade reactions are often aided by inherent enzyme immobilization schemes, including compartmentalization to prevent product inhibition and separate competing reactions, and formation of multi-enzyme complexes to promote substrate channeling between subsequent enzymes in a pathway [47], [48]. Scientists have mimicked nature's immobilization schemes to facilitate both single and multi-enzyme catalysis, for instance, by the formation of fusion enzymes and polymericomes, and by polyelectrolyte layer-by-layer (LbL) assembly [49], [50].

1.1.5 Enzyme immobilization by polyelectrolyte layer-by-layer assembly

Enzyme immobilization by polyelectrolyte LbL assembly is based on enzyme entrapment inside polyelectrolyte multilayer (PEM) films or electrostatic attachment to a PEM surface [51]–[53]. Alternatively, enzymes can be encapsulated inside polyelectrolyte capsules fabricated by LbL assembly on a sacrificial template [54]. The properties of PEM films can be controlled to a considerable extent by controlling the deposition conditions (e.g., types and concentrations of polyelectrolytes, background ionic strength, deposition times, and the number of layers) [55], [56]. The deposition conditions can thus be selected to promote favorable conditions for enzyme immobilization. Polyelectrolyte LbL assembly is particularly advantageous for multi-enzyme immobilization, as the sequence and spatial confinement of the enzymes can be controlled by immobilizing different enzymes in con-

secutive layers [57]. Furthermore, the immobilization may be reversed by applying a high salt concentration or an acidic solution to the biocatalytic PEM membrane to regenerate the immobilization carrier [52], [58].

1.1.6 Scope of the research project

In this work, enzyme immobilization and membrane fabrication were investigated together for the development of membranes, notably ceramic membranes, with properties tailored for enzyme immobilization. Materials and methods were selected and developed to ensure both high enzyme loading and activity retention, as well as long-term stability of the immobilized enzyme and the ability of support regeneration. Alcohol dehydrogenase (ADH) was selected as a model enzyme. This enzyme is a part of a three enzyme cascade process for the conversion of CO₂ to methanol [59]. The industrial applications of ADH are generally hampered by instability of the free enzyme, and they are likewise complicated by the need for a cofactor [3], [60]. Immobilization is a promising method to stabilize ADH.

The state-of-the-art in enzyme immobilization techniques, with a special emphasis on inorganic support materials and membranes, was explored through recently published literature and reviewed in Paper 1 (Appendix A1). The literature research gave an overview of conventional materials and methods used for enzyme immobilization, as well as recent advances in the field, and guided further research in this project. In the experimental part, the interactions between ADH and different inorganic raw materials were investigated by immobilizing ADH on the materials by two common immobilization methods, namely, physical adsorption and covalent bonding. The results were used to identify suitable materials and other design parameters for membrane fabrication. The results were reported in Paper 2 (Appendix A2). Subsequently, ceramic membranes were fabricated by project collaborators and used for the immobilization of ADH by the common immobilization methods (i.e., physical adsorption and covalent bonding). Additionally, alternative immobilization methods, including enzyme immobilization by polyelectrolyte LbL assembly and interfacial polymerization, were investigated and applied for the immobilization of ADH on polymeric membrane substrates. The ability to tailor the properties of PEM membranes by controlling the polyelectrolyte deposition conditions was studied and then PEM membranes with controlled thickness and pore sizes were fabricated and applied in transport studies to evaluate the effect of membrane thickness on solute transport through the membranes (e.g., solute rejection and energy barriers to anion transport through the membranes). The results of transport studies in PEM membranes were reported in Paper 3 (Appendix A3).

1.2 Defining the research project

1.2.1 Problem statement

Despite the many benefits of enzyme immobilization and extensive research efforts within the field, the method is comparatively rarely applied in industrial biocatalysis. The main obstacles to implementing immobilized enzymes in industry include the cost and complexity of the catalyst preparation, which is sometimes followed by a decrease in enzyme activity. For enzyme immobilization to be feasible, it must have a positive outcome for the process economy. The economic benefits of stabilization and reusability of the enzymes and the accompanying process intensification, must thus surpass the cost of immobilization (i.e., cost of the support, chemicals, and utilities used for immobilization, labor hours, and potential loss of specific enzyme activity). Consequently, the design of an immobilization system comprises two main considerations:

- Catalytic properties of the enzymes: Design for high enzyme stability, reusability, and activity retention
- Immobilization method and support: Design for simplicity and low cost

The two considerations listed above are interdependent, as the catalytic properties and the balance between them depend on the immobilization method and support used. While a more simple immobilization method might be favorable for high activity retention, it typically results in less stabilization, and vice versa for a more complex immobilization method [22]. Similarly, simplicity implies lower cost of immobilization, as a simpler procedure of catalyst preparation requires less use of chemicals, fewer steps, and less active time of preparation. The cost of the immobilization system may further be reduced by reusing the support. Reversible immobilization methods, such as polyelectrolyte LbL assembly, and stable support materials, such as ceramics, are advantageous in that regard [52], [58].

1.2.2 Research question

The design criteria listed previously led to the research question driving this project: Is it feasible to promote conditions for enzyme immobilization on membranes by fabricating membranes with properties tailored to the enzyme in question?

1.2.3 Hypotheses

Based on the aforementioned, the following hypotheses were formulated:

- H1. The properties of the support material and the immobilization method affect the catalytic properties of enzymes upon immobilization
- H2. Ceramic membranes can be fabricated as stable and robust immobilization supports with properties specifically designed for enzyme immobilization
- H3. Membrane surface properties may be modified to provide conditions fit for enzyme immobilization
- H4. Membrane thickness may be increased without affecting solute rejection by the membrane

1.2.4 Objectives

The hypotheses were tested by means of several main objectives. ADH was used a model enzyme in the investigations, where relevant. However, the results could potentially be extrapolated to other enzymes. The objectives included:

- O1. To study the effects of support material properties and immobilization methods on the catalytic properties of ADH by immobilization on inorganic raw powders using two different immobilization methods
- O2. To identify materials and design parameters for the fabrication of ceramic membranes for the immobilization of ADH
- O3. To study the effects of ceramic processing conditions during membrane fabrication on the success of immobilization of ADH on the ceramic membranes
- O4. To investigate alternative immobilization methods and membrane modification techniques for single- and multi enzyme immobilization
- O5. To fabricate membranes with controllable properties by altering polyelectrolyte LbL deposition condition

- O6. To calculate energy barriers to anion transport through membranes of different thicknesses to evaluate the effect of membrane thickness on the membrane transport properties

1.2.5 Project phases

To realize the project objectives, the work was divided into phases dealing with specific parts of the project. Phases A1, A2, and A3 were conducted in series and were built on one another, while phase B was a parallel project that was connected to the research question. The methods developed in phase B could further be applied to phase A, particularly phase A3. A project diagram describing the different project phases and research outputs in connection to the phases is presented in Figure 1.2 and a further description of the phases is given below.

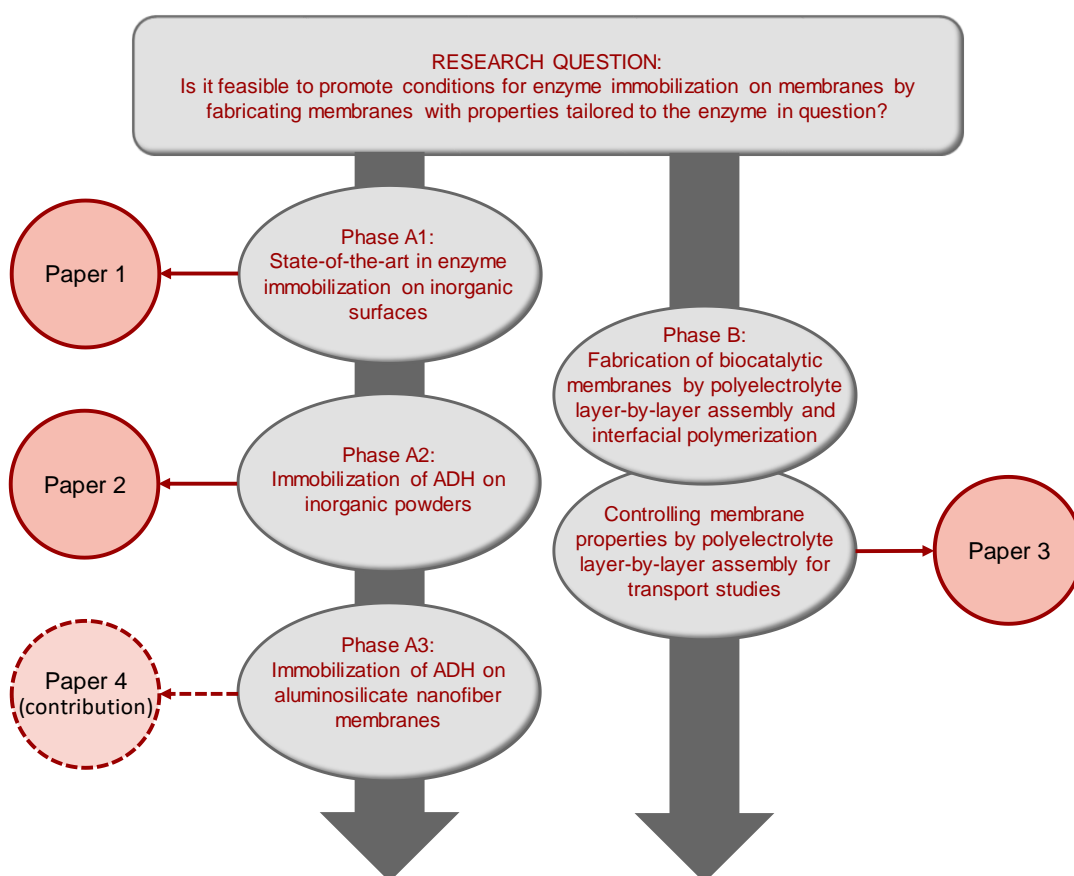


Figure 1.2: Project diagram describing the different project phases and research outputs in connection to the phases

Phase A1: Literature research on enzyme immobilization on inorganic support materials. The knowledge gathered was used for familiarizing with the state-of-the-art within the field of enzyme immobilization. A special emphasis was put on inorganic support materials, notably ceramic membranes. The effects of different immobilization methods and support materials on the catalytic properties of the enzyme were evaluated, as well as enzyme leakage, and the ability to regenerate and reuse the immobilization support.

Phase A2: Immobilization of ADH on inorganic raw powders by covalent bonding and physical adsorption. The objective was to study the effects of the material properties and

immobilization methods on the activity and stability of the immobilized enzyme. Materials and design parameters for membrane fabrication were identified.

Phase A3: Immobilization of ADH on electrospun ceramic nanofiber membranes. The membranes were fabricated by project collaborators at DTU Energy. The results of the experiments with the immobilization of ADH on inorganic raw powders were taken into account for material selection. ADH was immobilized on the membranes by similar protocols as on the inorganic raw powders to evaluate the effects of different support structures and ceramic processing conditions on the success of immobilization.

Phase B: Investigating alternative methods for enzyme immobilization on membranes that can simultaneously be used to control the transport properties of the membranes. Immobilization by polyelectrolyte LbL assembly and interfacial polymerization were investigated through literature research and experimentally. Furthermore, the ability to control the properties of PEM membranes by altering conditions during polyelectrolyte LbL assembly was investigated. Membranes of different thicknesses and pore sizes were fabricated and used in transport studies to evaluate the effect of membrane thickness on the separation properties of the membranes.

2 Enzyme immobilization on inorganic surfaces

The first example of enzyme immobilization was reported in 1916 when invertase was adsorbed onto charcoal and aluminium hydroxide [61]. Much progress has been made within the field of enzyme immobilization ever since, and countless immobilization strategies have been proposed for a myriad of different applications [20]. Early on, research in the field could be divided into distinct phases, starting with the development of different immobilization methods, then focusing investigations on new immobilization supports, and finally, designing immobilization systems for improved catalyst properties [19], [62]. Today, all these factors are under continuous development in parallel with advances in related fields of technology, such as biotechnology, membrane technology, material science, and nanotechnology [63]. Furthermore, research is influenced by potential applications of immobilized enzymes, including biofuel cells for clean energy production, industrial biocatalysis for sustainable production of chemicals, biosensors, and waste-water treatment. At the same time, even the immobilization of glucose isomerase, which is the most successful and widely applied immobilized enzyme, is under continuous development to bring the technology up to date with the latest scientific advancements [21]. The system configurations vary depending on the intended application, but equally important for any application is the immobilization method and support.

Different immobilization systems (immobilization methods and supports) were reviewed in Paper 1, *Enzyme Immobilization on Inorganic Surfaces for Membrane Reactor Applications: Mass Transfer Challenges, Enzyme Leakage and Reuse of Materials* (Appendix A1). The systems were described and evaluated in terms of their performance, including enzyme activity, stability, reusability, and leakage. A comprehensive discussion on inorganic supports was given, including a description of the properties of inorganic support materials and their influences on enzyme immobilization. The main topics of Paper 1 are briefly presented below, along with an introduction of aluminosilicate nanofiber membranes, as well as enzyme immobilization by polyelectrolyte LbL assembly and interfacial polymerization, which are materials and methods that are involved in the experimental part of the project.

2.1 Immobilization supports

The immobilization support plays a critical role in a successful enzyme immobilization system. Both the material, morphology, and structure of the support are important factors regarding the stability and catalytic properties of the immobilized enzyme and must be selected carefully for a given application. Common types of enzyme immobilization supports and their properties and considerations that influence enzyme immobilization are listed in Table 2.1.

A support must meet several requirements to be eligible for enzyme immobilization. First of all, the support must be compatible with the given enzyme to allow the immobilization to occur through physical or chemical interactions, while it must be stable and inert towards the reaction medium. A high surface area permits high enzyme loading, while a proper pore size of porous materials is important for protection and mass transfer. Enzymes can be protected from the external process conditions inside porous supports, whereas access to the enzyme's active site can be limited, especially when bulky substrates are

Table 2.1: Common types of enzyme immobilization supports and their properties and considerations that influence enzyme immobilization (non-exhaustive list)

Support	Type	Properties/Considerations
Material	Organic	Surface charge Functional groups Hydrophobicity Stability (thermal, pH, microbial, etc.) Regenerability
	Inorganic	
Morphology	Pore size	Surface area
	Porosity	Protection (within pores)
	Roughness	Mass transfer limitations
		Fouling Enzyme leakage
Structure	Particles (nano/micro)	Surface area
	Magnetic nanoparticles	Surface-to-volume ratio
	Beads	Mass transfer limitations
	Nanofibers	Ease of recovery
	Nanotubes	Reactor configuration
	Membranes	

involved. The stability of the support material is important for a stable operation as well as for regeneration and reuse of the material in multiple operation cycles [22]. Finally, the support should preferably be available at a low cost and impart a low environmental footprint to the process.

Ceramic materials present exceptional thermal, chemical, mechanical, and microbial stability. Moreover, the structure and properties of ceramics may be controlled by the selected raw materials and processing methods. Besides being robust and versatile enzyme carriers, ceramic materials are particularly advantageous regarding carrier reusability. The high stability of ceramic materials allows regeneration of their native properties by harsh chemical and thermal cleaning methods when the process becomes hampered by fouling or enzyme deactivation [22]. Carrier reusability is an important aspect of enzyme immobilization, considering both the economic viability and environmental impact of the process since carriers can be costly, and the production thereof can have a large environmental footprint, as revealed by life cycle assessment (LCA) studies [21]. Better utilization of the carriers (i.e., carrier reuse) would improve these factors and simultaneously reduce waste generation.

Alumina and silica-based materials are some of the most commonly used inorganic membrane materials, yielding ceramic membranes with excellent chemical, thermal, and mechanical properties, as well as high mass transfer rates [25], [64], [65]. Alumina and silica-based membranes include α -alumina, γ -alumina, silicon carbide, silicon nitride, porous glass, and zeolite membranes [64]. Additionally, aluminosilicate materials offer outstanding properties for membranes, such as high thermostability, mechanical and chemical stability, high surface area, and tuneable pore structure [66]–[68], they can be fabricated from low-cost raw materials [69], [70], and they have been used as support materials for enzyme immobilization with good success [68], [71]–[73]. Aluminosilicate membranes

may be fabricated by conventional ceramic processing methods, such as tape casting and extrusion [69], or by more novel methods such as electrospinning.

Electrospinning is a simple and cost-effective technique for the fabrication of nanofibers. The procedure involves loading an electrospinning solution of the desired fiber material in a syringe equipped with a feed pump, ejecting the solution under high voltage, and collecting the fibers on a grounded fiber collector at a fixed distance from the needle tip [74]. The fiber diameters vary from a few nanometers to several micrometers, resulting in nanofiber membranes with large surface areas and high porosity [74], [75]. Electrospinning is mainly used for the fabrication of polymeric nanofibers, whereas ceramic nanofibers are attracting increasing attention [76]. Numerous examples of enzyme immobilization on nanofiber membranes have been reported [65], [75], [77]. Besides immobilizing enzymes on nanofiber membranes by standard immobilization methods such as physical adsorption and covalent bonding, enzymes have been mixed with the electrospinning solution so they become a consolidated part of the nanofiber membrane material [78], [79]. The latter method is mostly restricted to polymeric nanofiber membranes as the required high-temperature calcination of ceramic nanofibers would inactivate the enzymes.

2.2 Immobilization methods

The first reported method of enzyme immobilization was physical adsorption, where it was found that the adsorption of invertase onto charcoal did not affect the activity of the enzyme [61]. Indeed, physical adsorption is the simplest immobilization method, it is reversible and it is found to have little effects on enzyme activity in general. On the other hand, physical adsorption has limited stabilizing effects on the enzymes, and processes involving physically adsorbed enzymes are often hampered by enzyme leakage. Physical adsorption occurs through physical or electrostatic interactions between the enzymes and the support, such as Van der Waals forces, hydrogen bonds, ionic bonds, and hydrophobic interactions [80], [81].

In an attempt to improve the performance of immobilized enzyme systems, alternative immobilization methods were proposed. One of those methods is covalent bonding, where the enzymes are attached to the support via covalent bonds, which provide a stable attachment to the support and thereby reduced enzyme leakage. Covalent bonding thus favors a stable operation, however, it typically results in loss of enzyme activity due to conformational changes in the enzyme structure induced by the chemical modification of the enzyme. Covalent bonding often requires modification of the support to promote functional groups on the support surface, through which the enzymes are attached. Such modification techniques include functionalization by amine or epoxy groups and activation with aldehydes that can react with specific amino acid residues on the surface of the enzyme [22], [80], [81].

The trade-off between enzyme activity and stability is a common consequence of any immobilization method. In addition to physical adsorption and covalent bonding, other well-known immobilization methods include entrapment (e.g., fouling induced entrapment in membranes [82] and entrapment in polyelectrolyte multilayers (PEMs) [51]), encapsulation (e.g., in polyelectrolyte capsules [83] and micelles [84]), affinity attachment (e.g. via biotin-avidin affinity binding [85]), and enzyme cross-linking (e.g., cross-linked enzyme crystals [86] or aggregates [87]). The methods differ in their complexity as well as in their effects on the activity and stability of the immobilized enzymes.

Enzyme immobilization on membranes is commonly achieved with physical adsorption,

covalent bonding, or entrapment (Figure 2.1). Alternatively, enzymes can be incorporated in the membrane fabrication process so they become an integrated part of the separation layer of the membrane. These methods include immobilization by polyelectrolyte LbL assembly [52], [53] and the recently proposed enzyme immobilization by interfacial polymerization [88], [89]. In the latter method, the enzyme polymerizes with an organic monomer on a membrane surface to form a biocatalytic membrane skin layer. The polyelectrolyte LbL assembly method has been widely used for single and multi-enzyme immobilization [90]–[96], whereas interfacial polymerization is a novel method for enzyme immobilization with only two published studies (to the best of the author’s knowledge), both of which report single-enzyme immobilization [88], [89]. Both of these methods show the potential to tune the properties of the membrane separation layer to a certain extent, and thus present interesting opportunities for the fabrication of membranes with properties tailored for enzyme immobilization, as described in the following two subsections.

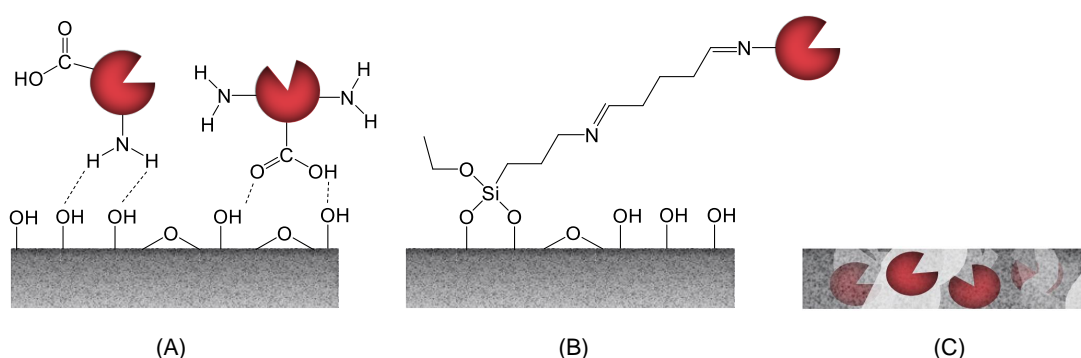


Figure 2.1: Schematic illustration of common methods for enzyme immobilization on/in membranes: (A) Physical adsorption, (B) covalent bonding, and (C) entrapment.

2.2.1 Enzyme immobilization by polyelectrolyte layer-by-layer assembly

Polyelectrolyte LbL assembly is based on the alternating deposition of anionic and cationic polyelectrolytes onto a substrate to form a PEM film [97]. The polyelectrolytes assemble by means of electrostatic interactions and entropy gain that results from releasing salt counterions associated with fixed charges of the polyelectrolytes [55], [98], [99]. Enzyme immobilization by polyelectrolyte LbL assembly is based on the entrapment of enzymes between layers of polyelectrolytes or electrostatic attachment to the PEM surface (Figure 2.2) [51]–[53]. Enzyme immobilization by entrapment and physical interactions generally means that the enzymes have high activity retention, whereas the long-term stability may be hampered by enzyme leakage from the support [22], [80]. Enzyme immobilization by polyelectrolyte LbL assembly has been combined with cross-linking in attempts to prevent enzyme leakage from the PEM [57], [99], [100].

The activity and stability of enzymes immobilized in PEM films are largely decided by the position of the enzyme layers in the PEM films, as suggested by Guedidi et al. [53]. They found that when enzymes were immobilized as the top-layer of PEM films prepared by the deposition of polyethylenimine (PEI) and alginate onto polyacrylonitrile membrane substrates, the enzymes exhibited higher activity than enzymes that were covered by additional layers of polyelectrolytes. On the contrary, the stability of enzymes immobilized inside the PEM was higher than the stability of enzymes attached as the top-layer of the PEM. When the enzymes were immobilized inside the PEM, the additional lay-

ers of polyelectrolytes covering the enzyme layer prevented enzyme leakage but induced mass transfer limitation, thereby resulting in higher stability and lower activity. The activity of the immobilized enzymes in the study was only 1-10% of the activity of the free enzyme since the reactions were conducted in soaking mode (without substrate convection through the membrane). Hence, the contact between the enzymes and substrates was restricted by diffusion limitations. Efficient mass transfer plays a critical role in reactions with immobilized enzymes. Datta et al. [52] described how the activity of glucose oxidase immobilized inside the pores of polyelectrolyte LbL modified microfiltration (MF) membranes increased from 0.1-21 $\text{mM min}^{-1} \text{mg enzyme}^{-1}$ when the reaction configuration was changed from soaking mode to convective mode. The membranes were modified by the deposition of one layer of poly-L-lysine (PLL), followed by three bilayers of poly(sodium 4-styrenesulfonate) (PSS) and poly(allylamine hydrochloride) (PAH) (i.e., PLL-(PSS-PAH)₃) inside the pores of an MF membrane. They further found that the enzyme activity was lower when the enzymes were immobilized on a three-layer PEM (PLL-PSS-PAH) than on a seven-layer PEM (PLL-(PSS-PAH)₃) since the three-layer PEM left a larger core-region in the membrane pores (the region in the pore center that is void of polyelectrolytes and enzymes) and thus a considerable amount of substrate was convected through the core region without coming into contact with the enzyme. The mass transfer was also influenced by the permeate flow. An optimal permeate flow-substrate conversion relationship existed—a too high flow resulted in decreased conversion due to insufficient residence time, while a too low permeate flow would decrease the conversion due to reduced mass transfer [52].

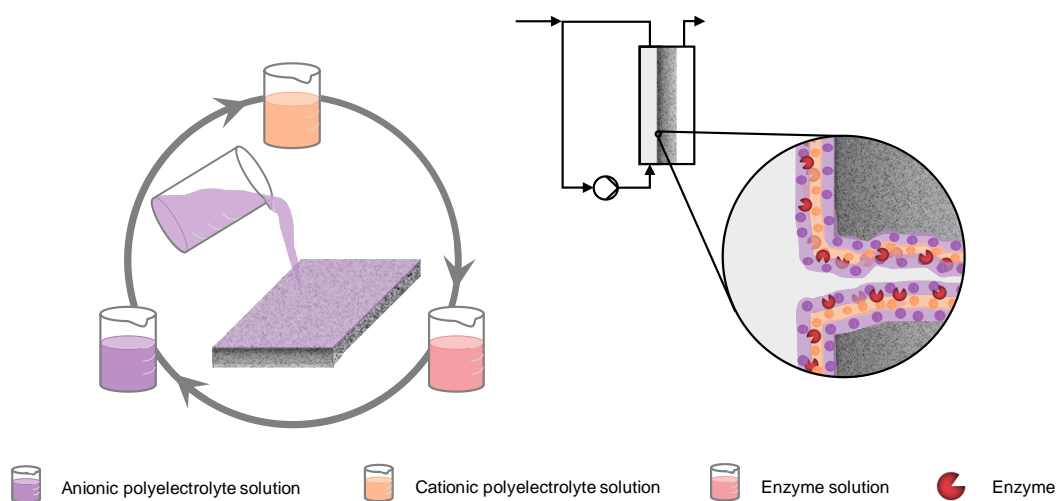


Figure 2.2: Illustration of enzyme immobilization by polyelectrolyte layer-by-layer assembly on a porous membrane substrate

Permeate flow is readily controllable in PEM membranes, both by deposition conditions and by operating conditions. The water permeability decreases by the addition of polyelectrolyte layers and by changing the polyelectrolyte concentrations of the deposition solutions [56]. To match the permeability and enzyme activity, enzyme loading can be controlled by immobilizing the enzymes in multiple layers [51], [57], [101]. The water permeability in stimuli-responsive PEM membranes can be controlled by changing the pH or temperature during operation, thus inducing swelling, or shrinking of the PEM films [95], [96]. Furthermore, the water permeability can be tuned to some extent by altering the concentrations of polyelectrolytes and background ionic strength of the depositions solu-

tions, since these parameters are found to influence the pore size and thickness of PEM films [55].

The polyelectrolyte-salt balance is an important consideration in polyelectrolyte LbL assembly. Besides influencing the structure of the PEM film (pore size and thickness), the surface charge is likewise affected. Against intuition, PEM membranes terminated with an anionic polyelectrolyte, such as PSS, are not necessarily negatively charged, notably when the PEM is built up of the common polyelectrolyte pair PDADMAC/PSS [56], [102]. This effect is caused by an overcompensation of PDADMAC in the PEM film, which yields a positively charged membrane. Salt annealing (exposing the PEM film to high salt concentration) has been proposed and applied as a method to revert the surface charge of PEM films [56], [102], [103]. Salt annealing can thus become an important tool for controlling the surface charge of PEM membranes to mediate an efficient electrostatic attachment of enzymes to the PEMs.

Not only can salt concentration and electrostatic conditions influence the surface charge and immobilization efficiency of biocatalytic PEM membranes, these factors can also be used to reverse the immobilization and thereby remove deactivated enzymes from the PEM membranes to load the membranes with fresh enzymes or remove the PEM film entirely [52], [58]. Datta et al. [52] removed glucose oxidase from a seven-layer polyelectrolyte LbL modified nylon membrane (PLL-(PSS/PAH)₃) by filtering water at pH 3 through the membrane. The electrostatic interactions between the enzyme (isoelectric point of 4.2) and the outer PAH layer (isoelectric point of 9.5) were reduced at pH 3 so the enzymes were released from the PEM membrane. The enzymes were reloaded onto the same membrane without significant loss of activity. Ceramic alumina membranes modified by the LbL deposition of three bilayers of PDADMAC/PSS were regenerated using high salt concentrations (5 M NaCl) in combination with cationic and anionic surfactants to dissolve the PEM film [58]. The high salt concentration screened the charges of the polyelectrolytes while the surfactants formed complexes with the polyelectrolytes of opposite charge so the interactions between the polyelectrolytes were weakened. The PEM film was thus gradually dissolved with a near-complete recovery of the water permeability of the pristine membrane (1100 and 1040 L m⁻² h⁻¹ bar⁻¹, for the pristine ceramic membrane and the ceramic membrane after PEM dissolution, respectively).

The preceding examples described some of the many features of the polyelectrolyte LbL assembly method. The examples demonstrated the versatility of the method and the opportunities to selectively tune the properties of PEM films, which can be extended to enzyme immobilization to provide favorable conditions for a wide variety of enzymes. The ability to remove and reload the enzymes and regenerate the pristine membranes are particularly important given the complications with fouling and enzyme deactivation involved in biocatalytic membrane operations. An additional benefit of polyelectrolyte LbL assembly is the use of safe chemicals and procedures during PEM fabrication. However, the procedure is relatively slow, it requires many steps of preparation, and often large volumes of chemicals are wasted. Optimization can likewise prove difficult due to the large number of interacting parameters involved in the procedure.

2.2.2 Enzyme immobilization by interfacial polymerization

A novel and facile approach to enzyme immobilization on membranes was proposed by Raaijmakers et al. [88] in a recent study. By this approach, an ultra-thin pepsin membrane was fabricated by polycondensation of pepsin (an enzyme) and trimesoylchloride (TMC, an organic monomer) on the surface of a porous polyacrylonitrile membrane substrate. The procedure was inspired by interfacial polymerization, a well-known method for

the fabrication of thin film composite membranes by the polymerization of aqueous and organic monomers at the interface of two immiscible solvents on the surface of a porous support membrane [104]. The resulting pepsin membrane was obtained by a simple and fast procedure, and the enzyme retained high enzyme activity and showed little enzyme deactivation in two reaction cycles of 30h.

Interfacial polymerization is the principal method for the fabrication of the separation layer of NF and reverse osmosis membranes. Briefly, a porous membrane substrate is wetted with an aqueous monomer (diamine), which is dissolved in an aqueous solvent, and then an organic monomer (polyacyl chloride) dissolved in an organic solvent is applied to the membrane substrate and the polymerization occurs at the interface between the two immiscible solvents [104]–[106]. The enzyme can be used as the aqueous monomer, whereby it becomes integrated into the skin layer of the membrane (Figure 2.3).

Raaijmakers et al. [88], investigated the effect of TMC concentration on the preparation and performance of polymerized pepsin-TMC membranes and found that when the TMC concentration was increased from 0.2-0.5 wt%, the degree of cross-linking decreased from 40-5 TMC molecules per enzyme. The decrease in cross-linking at higher TMC concentration was explained by acidification of the aqueous solution due to the release of hydrogen chloride upon polymerization, which hampered the reactivity of amine groups of the pepsin. The more cross-linked membrane (0.2 wt% TMC) presented higher enzyme activity, indicating that the high degree of covalent bonding did not compromise enzyme activity. The lower activity of the less cross-linked membrane (0.5 wt% TMC) was explained by the acidification of the aqueous solution upon polymerization. A higher degree of cross-linking resulted in higher retention of large molecules, the molecular weight cut off of the membrane prepared with 0.2 wt% TMC was measured as 9.5 kDa [88].

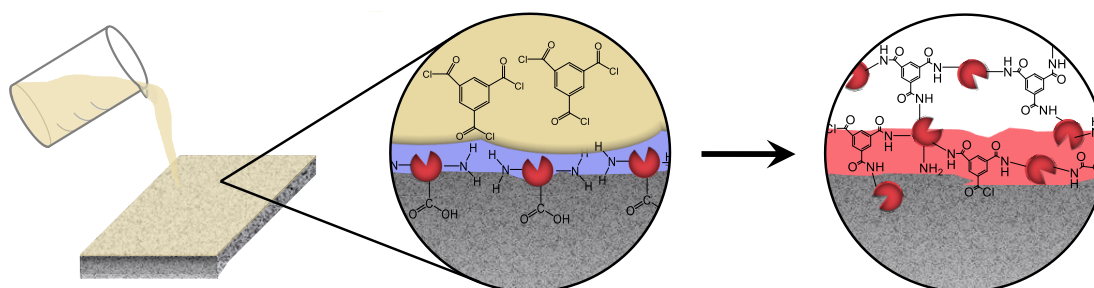


Figure 2.3: Illustration of enzyme immobilization by interfacial polymerization on a porous support membrane

Wang et al. [89] fabricated lysozyme membranes by the interfacial polymerization of lysozyme and TMC on a polyethersulfone membrane substrate with 10 kDa molecular weight cut off. The authors observed a higher degree of cross-linking with higher TMC concentration, which contradicted the study of Raaijmakers et al [88], but was explained by the different enzymes involved and their different resistance to changes in acidity. The lysozyme membranes maintained the activity of the native enzyme and showed good antimicrobial and separation properties. The solute rejection values and water flux varied based on the lysozyme and TMC concentrations used for the fabrication, which suggested that the membrane properties could be tailored by controlling these parameters.

Enzyme immobilization by interfacial polymerization can potentially provide a more stable

and simple alternative to immobilization in PEMs. The downside to immobilization by interfacial polymerization compared with immobilization in PEMs includes the use of organic solvents and the non-reversibility of the method. However, it could be feasible to regenerate ceramic membrane substrates by thermal treatments to remove the biocatalytic skin layer upon membrane fouling and enzyme deactivation.

2.3 Reusability of immobilized enzymes

The principal motivation for enzyme immobilization is to enable enzyme reuse in multiple reaction cycles or in continuous operations. These goals can be reached via three main solutions offered by enzyme immobilization. First, the stabilization of enzymes resulting from enzyme immobilization allows an efficient and long-term use of the enzymes, second, the increased size brought about by attaching the enzyme to a carrier facilitates the recovery and reuse of the enzyme-carrier complex, and finally, the immobilization of enzymes on stationary supports allows their use in continuous operations (e.g., in packed bed or membrane reactors).

For continuous operations, relevant reactor configurations depend on the support structure. Thus, magnetic nanoparticles and particles of sufficient density are suited for (magnetically stabilized) fluidized bed reactors, while various supports structures, ranging from nano- to macro-sized, are applicable in packed bed and membrane reactors [15], [107]–[109]. Membrane reactors can be operated with suspended enzymes (free or immobilized) circulating on the feed side of the membrane or with enzymes immobilized directly on/inside the membrane, where the reaction occurs as the substrate passes through the membrane [31]. The membrane unit can be either submerged in the bioreactor or external to the reactor [39] (Figure 2.4). In batch mode, immobilized enzymes are easily recovered by filtration or centrifugation, or by applying a magnetic field, in the case of magnetic supports [110].

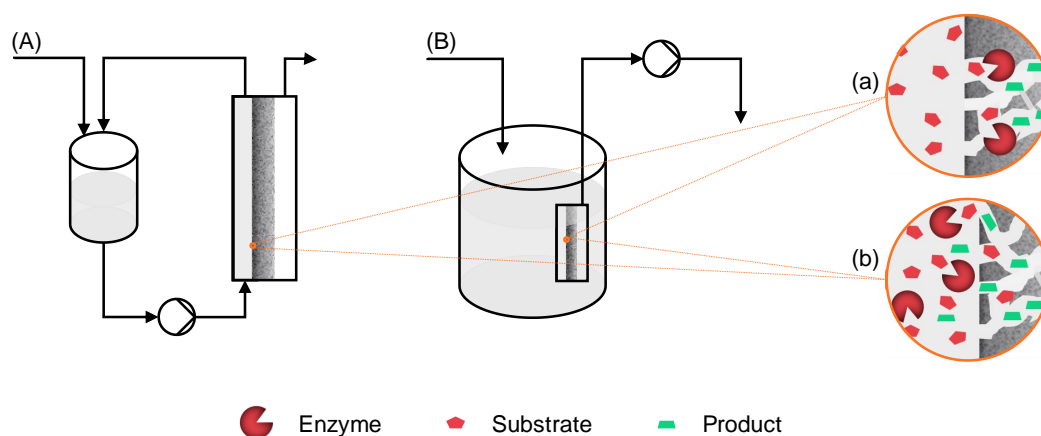


Figure 2.4: Configurations of enzymatic membrane reactors (EMRs) with free or immobilized enzymes. (A) EMR with an external membrane module, (B) EMR with a submerged membrane module, (a) EMR with enzymes immobilized on the membrane, and (b) EMR with free or immobilized enzymes suspended in the reactor and recirculated at the feed side of the membrane.

The reusability of immobilized enzymes depends on the reactor configuration, support structure, and the immobilization method. Hence, all three factors must be evaluated together to ensure an effective and stable enzyme immobilization system.

3 Immobilization of alcohol dehydrogenase for applications in membrane reactors

The immobilization of ADH for applications in EMRs was investigated. Two main aspects of the immobilization were considered, i) the interactions between ADH and different inorganic support materials were studied for the development of inorganic membranes with properties tailored to the immobilization of ADH, and ii) the investigation of methods for the immobilization of ADH on membranes with tunable surface and transport properties. For these purposes, ADH was immobilized on i) inorganic raw powders and inorganic (aluminosilicate) nanofiber membranes by physical adsorption and covalent bonding, and ii) by polyelectrolyte LbL assembly and interfacial polymerization on polymeric membrane substrates. The discussion herein is divided into three parts involving the immobilization of ADH on inorganic powders, inorganic membranes, and on polymeric membranes.

First, ADH was immobilized on inorganic powders of different materials to identify suitable materials for the fabrication of ceramic membranes with properties tailored for enzyme immobilization. The selected supports were raw powders of common membrane materials, namely aluminum oxide, silicon carbide, titanium oxide, and yttria stabilized zirconia. The inorganic materials were characterized to understand which properties influenced the immobilization of ADH and how the respective properties influenced the immobilization. Thus, the activity of ADH immobilized on the different inorganic powders was explained considering the surface area, particle size, and surface charge of the inorganic materials. ADH was immobilized on the inorganic powders by two different methods, physical adsorption and covalent bonding, to investigate the effects of the two immobilization methods on enzyme activity, recyclability, and storage stability. For covalent bonding, the inorganic powders were modified using (3-aminopropyl)triethoxysilane (APTES) and glutaraldehyde prior to immobilization. The commonly used functionalizing and activating agents were selected based on reports from the literature that describe successful covalent enzyme immobilization using the agents. The results of this study were presented in Paper 2, *Alcohol dehydrogenase on inorganic powders: Zeta potential and particle agglomeration as main factors determining activity during immobilization*, which is attached in Appendix A2.

In the study with the immobilization of ADH on inorganic powders, Al_2O_3 and SiC powders were found to provide favorable conditions for the immobilization of ADH. Subsequently, aluminosilicate nanofiber membranes were fabricated and supplied by project collaborators and were then applied for the immobilization of ADH by physical adsorption and covalent bonding. Electrospinning was used for the fabrication of the membranes and the effects of processing conditions during membrane fabrication on the membrane properties and their implications for enzyme immobilization were studied. The results of this part of the study were produced as a contribution to the manuscript *Influences of fabrication parameters on electrospun $\text{Al}_2\text{O}_3/\text{SiO}_2$ nanofibers and their impact on the immobilization of alcohol dehydrogenase*, which is in preparation. The focus of the paper is on membrane fabrication, specifically, the development of procedures for the fabrication of ceramic membranes with high surface area and properties tailored for enzyme immobilization. The development of the membrane fabrication procedures was not a part

of this PhD project, but a separate, collaborative PhD project. Hence, the details about the material science and processing conditions are left out of the discussion given here, and the discussion is restricted to the immobilization of alcohol dehydrogenase (ADH) on the nanofiber membranes. The investigation conducted in this part was limited by low availability and extremely high fragility of the aluminosilicate nanofiber membranes. The membranes would easily fracture and break when pressure was applied to them during filtration experiments. Nevertheless, the membranes were used as scaffolds for enzyme immobilization to test different parameters of the immobilization. The immobilization of ADH on the nanofibers membranes was compared to the immobilization of ADH on inorganic raw powders to investigate the effects of the support structure and processing conditions on the immobilization. ADH was immobilized on the aluminosilicate nanofibers with and without filtration to test the immobilization efficiency by different modes of immobilization. The storage stability of physically adsorbed and covalently bonded ADH was investigated.

The immobilization of ADH on inorganic raw powders and aluminosilicate nanofiber membranes revealed that the immobilization of ADH was hampered by the fragility of the aluminosilicate nanofiber membranes and by low storage stability. The storage stability of ADH immobilized on inorganic particles was hampered by particle agglomeration, whereas the storage stability of ADH immobilized on inorganic nanofiber membranes was hampered by enzyme leakage from the membranes. It was proposed that the enzyme leakage could be reduced by sealing the membranes with a layer of polyelectrolytes applied to the membrane surface via polyelectrolyte LbL assembly. Polyelectrolyte LbL assembly and interfacial polymerization were introduced as immobilization methods with controllable surface and transport properties. The use of polyelectrolyte LbL assembly and interfacial polymerization for the immobilization of ADH was investigated.

The different studies involved some of the main objectives of the project, including objectives O1-O4, regarding the effect of the support material and immobilization method on the catalytic properties of the immobilized ADH, the fabrication of ceramic membranes and membranes surface modification for the immobilization of ADH, and thus simultaneously address hypotheses H1-H3.

3.1 Materials and methods

3.1.1 Immobilization of alcohol dehydrogenase on inorganic powders

ADH was immobilized on four different inorganic raw powders of common membrane materials, namely aluminum oxide, silicon carbide, titanium oxide, and yttria stabilized zirconia, by physical adsorption and covalent bonding. APTES and glutaraldehyde were used as functionalizing and activating agents for the covalent bonding of ADH to the powders. The reader is referred to the Materials and methods section of Paper 2, in Appendix A2, for further information.

3.1.2 Immobilization of alcohol dehydrogenase on aluminosilicate nanofiber membranes

Membranes and materials

Aluminosilicate nanofiber membranes were provided by project collaborators from DTU Energy. The membranes were fabricated by electrospinning using a mixture of polymer solution and inorganic precursor sol. The electrospinning solution contained 5.5 wt% Polyvinylpyrrolidone 1.3M (PVP), 14 mmol $\text{AlCl}_3 \cdot 6\text{H}_2\text{O}$, and 7 mmol tetraethyl orthosilicate (TEOS). The electrospinning was done at 35 kV applied voltage and calcining of the nanofibers was conducted at 1100°C. GRM0.1PP microfiltration (MF) membrane (polysulfone, 0.1 μm pore diameter) was from Danish Separation Systems AS.

Alcohol dehydrogenase from *Saccharomyces cerevisiae* (yeast ADH, EC 1.1.1.1), β -nicotinamide adenine dinucleotide reduced disodium salt hydrate (NADH, $\geq 97\%$), formaldehyde (37% in H₂O), (3-aminopropyl)triethoxysilane (APTES, 99%), glutaraldehyde (25% in H₂O), 2-(N-Morpholino)ethanesulfonic (MES) acid, MES potassium salt, sodium hydroxide, Bradford reagent and albumin standard (BSA, 2 mg/mL) were purchased from Sigma-Aldrich (Steinheim, Germany). Ethanol (99%) was purchased from WVR (Søborg, Denmark). All chemicals were used as received. Ultrapure water was used for solution preparation and cleaning of membranes and equipment.

Immobilization procedures

The following solutions were used for immobilization on each membrane: 10 mL of 4% APTES in 90% ethanol and 10 mL of 2.5% glutaraldehyde in MilliQ water was used for functionalization and activation, respectively, for covalent bonding. 10 mL of 20 mg L⁻¹ ADH in MES buffer (40 mM, pH 6.5) was used for immobilization. The membranes were soaked in ultrapure water before first use. Membranes with immobilized ADH were stored in MES buffer at 4°C.

For covalent bonding, the membranes were first exposed to the APTES solution for 90 min at 70°C, and then washed three times with 90% ethanol and subsequently dried in an oven (BINDER, Germany) at 60°C for 60 min. Next, the membranes were exposed to the glutaraldehyde solution for 30 min at room temperature. The membranes were washed three times with water afterwards and then dried at 60°C for 90 min. For immobilization, the pristine (physical adsorption) or surface modified (covalent bonding) membranes were exposed to the enzyme solution for 90 min, at room temperature, and 100 rpm agitation. After the immobilization, the enzyme solutions were removed and the membranes were washed three times with buffer. The enzyme and wash solutions were stored for protein concentration measurements.

Two different procedures were used for the immobilization - immobilization by soaking and by filtration. By soaking, the membranes were immersed in the immobilization solutions in 50 mL falcon tubes, which were placed in a water bath shaker (JULABO GmbH, Germany). After the immobilization, the solutions were removed by pouring them from the tubes, and then the membranes were washed in a similar manner. By filtration, the immobilization was conducted in a 10 mL ultrafiltration cell (Amicon 8010, Millipore Corp., USA), the solutions were removed from the cell by filtration at 1 bar applied pressure, and the membranes were washed by filtering the washing solutions through the membranes at 1 bar pressure. When the nanofiber membranes were used in the filtration cell, a polysulfone MF membrane (GRM0.1PP) was placed underneath the ceramic membrane as a support to prevent fracturing of the ceramic membranes. The polysulfone membrane was pretreated by soaking in 0.1% NaOH for 30 min at 30 rpm rotation on a rotary shaker, followed by three similar 30-min washing cycles in water. The GRM0.1PP membranes were previously found not to retain ADH and were thus assumed not to interfere with the immobilization. The polysulfone membranes showed no enzyme activity when the ceramic membranes were removed from the filtration cell and normal reaction procedures were tested with the polysulfone support membranes.

Additionally, ADH was immobilized on aluminosilicate nanofiber membrane fractions by physical adsorption. The immobilization was conducted in 2 mL Eppendorf tubes, with 4.0 mg of membrane fractions mixed with 2 mL of enzyme solution (100 mg L⁻¹ ADH in MES buffer) for 1.5, 4, and 24h at 4°C. The enzyme solutions were removed with a pipette, and the membranes were washed three times with 2 mL MES buffer.

Immobilization efficiency

Immobilization efficiency was calculated from protein concentrations of the ADH feed solutions before and after enzyme immobilization and of the washing solutions. Protein concentrations were measured using a Bradford microassay. The protein samples were mixed with Bradford reagent in a 1:1 ratio, vortexed, and incubated for five min before measuring the absorbance at 595 nm on a SHIMADZU UV-1280 spectrophotometer (SHIMADZU Corp., Japan). The protein concentration of the samples was read from a standard curve, which was made with BSA.

Reactions

Reactions with the biocatalytic membranes were conducted in a 10 mL ultrafiltration cell. The reaction involved the ADH catalyzed conversion of formaldehyde to methanol with simultaneous oxidation of NADH to NAD⁺. The reactions were initiated by adding 4 mL of substrate solution (30 mM formaldehyde and 100 μ M NADH in MES buffer) to the reactor, the substrate solution was stirred at 150 rpm and the filtration cell was pressurized to 1 bar by nitrogen gas to filter the substrate solution through the biocatalytic membrane. The filtration was stopped when 2 mL permeate was collected. The NADH concentrations of the feed, retentate, and permeate were calculated from absorbance measurements at 340 nm and were used to calculate the conversion of NADH during a single pass through the membrane and potential retention of NADH in the reactor. The membranes were rinsed after the reactions by filtering MilliQ water through them to remove any substrate remaining inside the membrane pores. The membranes were stored in MES buffer at 4°C until the next use.

3.1.3 Immobilization of alcohol dehydrogenase by polyelectrolyte layer-by-layer assembly and interfacial polymerization

Membranes and materials

GRM0.1PP MF membrane (polysulfone, 0.1 μ m) and GR61PP, GR51PP, and GR40PP ultrafiltration (UF) membranes (polysulfone, 20, 50, and 100 kDa, respectively) were from Danish Separation Systems AS.

Alcohol dehydrogenase from *Saccharomyces cerevisiae* (yeast ADH, EC 1.1.1.1), β -nicotinamide adenine dinucleotide reduced disodium salt hydrate (NADH, \geq 97%), formaldehyde (37% in H₂O), sodium hydroxide, sodium chloride, 2-(N-Morpholino)ethanesulfonic (MES) acid, MES potassium salt, Trizma base, hydrochloric acid (37%), dopamine hydrochloride, poly(diallyldimethylammonium chloride) (PDADMAC, 20 wt% in H₂O), poly(sodium 4-styrenesulfonate) (PSS, \sim 70.000 Da), polyethylenimine (PEI, 50wt% in H₂O, 270.000 Da), trimesoylchloride (TMC), hexane, Bradford reagent, and albumin standard (BSA, 2 mg/mL) were purchased from Sigma-Aldrich (Steinheim, Germany). All chemicals were used as received. Ultrapure water was used for solution preparation and cleaning of membranes and equipment.

Immobilization procedures

The parameters that were tested for the immobilization of ADH by polyelectrolyte LbL assembly included polyelectrolyte concentrations (0.01-1 wt%), the mode of immobilization (static or filtration mode), number of polyelectrolyte layers (0-7 layers), different polysulfone UF and MF support membranes (20, 50, and 100 kDa, 0.1 μ m), membrane surface modification prior to LbL assembly (i.e., deposition of a polydopamine (PDA)/PEI layer on the support membrane), and the pH of the enzyme feed solution during immobilization (pH 6.5-8.5). For the immobilization by interfacial polymerization, tested parameters included aqueous solvents for the enzyme feed solution (water, MES buffer, Tris buffer), polymerization time (2-30 min), different polysulfone UF membrane substrates (20 and 50 kDa), reactant concentrations (100-571 mg L⁻¹ ADH, 0.05-0.5 wt% TMC in hexane), and different modes of immobilization (with and without filtration of the enzyme feed solution).

Selected experimental results with the immobilization of ADH by polyelectrolyte LbL assembly and interfacial polymerization are presented here. The water permeability of the membranes was measured gravimetrically, and the immobilization efficiency and the catalytic activity of the immobilized enzymes were measured by Bradford assay and in reactions with formaldehyde and NADH, similarly to the methods explained in Section 3.1.2, with the immobilization of ADH on aluminosilicate membranes. Due to the variation in immobilization procedures between different experiments, the experimental procedures are described in the respective figure and table captions.

3.2 Results and discussion

3.2.1 Immobilization of alcohol dehydrogenase on inorganic powders

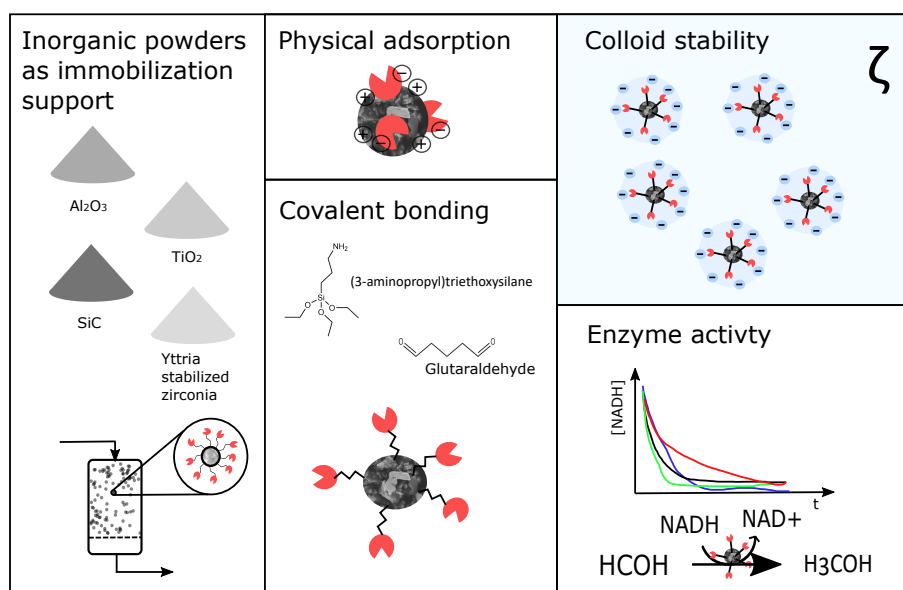


Figure 3.1: Graphical abstract of Paper 2. ADH was immobilized on inorganic raw powders of common membrane materials (aluminum oxide, silicon carbide, titanium oxide, and yttria stabilized zirconia) by physical adsorption and covalent bonding. The activity, stability, and recyclability of the immobilized enzymes were evaluated based on the properties of the support materials and the immobilization method [111].

The results obtained from the immobilization of ADH on inorganic powders highlighted not only the important effects of the immobilization method and support material on the activity and stability of the immobilized enzyme but also the importance of the conditions during reaction and storage. The buffer selection proved critical in the present case. Preliminary experiments revealed that the use of Tris-HCl buffer (pH 7, 100 mM) was problematic due to interactions with the substrate, formaldehyde, which led to a decrease in the pH of the reaction mixture from pH 7 to around pH 5. The low pH was detrimental to the enzyme activity and likewise increased the spontaneous degradation of the cofactor, NADH. Different biological buffers were tested for the ADH catalyzed reaction of formaldehyde to methanol, of which MES buffer (pH 6.5, 40 mM) was found to provide stable reaction conditions with high enzyme activity.

Besides affecting reaction conditions, the buffer affected the storage stability of silicon carbide powder with immobilized ADH, presumably due to particle agglomeration. The surface zeta potential of the silicon carbide was low in the MES buffer (around 3 mV), which is considerably lower than that required to ensure a stable particle suspension,

which is found to be around ± 30 mV [22]. Although the chemical modification and adsorption of enzymes onto a support introduce new charges to the support, which leads to changes in the surface zeta potential, it was assumed that the surface zeta potential of the silicon carbide powder with immobilized ADH was well within ± 30 mV. In the current system, the immobilization of ADH (isoelectric point (IEP) of 5.4-5.8) introduced negative charges to the silicon carbide powder in the MES buffer at pH 6.5, however, a relatively little amount of enzyme was immobilized and the IEP of the enzyme was relatively close to the pH of the storage buffer. Consequently, the particles agglomerated in the MES buffer during storage, which hindered mass transfer and impeded enzyme activity in following reaction cycles.

The surface zeta potential measurements helped to elucidate the influences of electrostatic forces on the immobilization, notably when physical adsorption was applied as the immobilization method. The TiO_2 powder was the only powder with a negative surface zeta potential in the MES buffer, while the Al_2O_3 , SiC, and YSZ-8 (yttria stabilized zirconia) powders were positively charged in the MES buffer. The activity of physically adsorbed ADH was considerably lower on TiO_2 than on the other three powders (Figure 3.2). ADH had an overall negative surface charge in the MES buffer at pH 6.5, and thus the immobilization of ADH on TiO_2 was likely hampered by electrostatic repulsion. However, electrostatic attraction is one of many mechanisms involved in physical adsorption, and the adsorption of charged enzymes onto similarly charged supports is not uncommon [112]. The highly negative surface of the TiO_2 powder may also have provided an unfavorable microenvironment for the enzymes by attracting hydrogen ions from the solution into the electrical double layer surrounding the particles, and thereby increasing local acidity at the surface of the particles [53]. It was previously observed that increasing the acidity of the reaction mixture had detrimental effects on the activity of ADH. The effects of the zeta potential of the raw powders on the activity of covalently immobilized enzymes were less clear. In this case, the introduction of functionalizing and activating agents to the support surface likely altered the surface charge, so the surface zeta potential became more similar between the different powders.

The enzyme activity was generally lower when covalent bonding was applied as the immobilization method, than when physical adsorption was used. The activity of physically adsorbed ADH was similar between ADH immobilized on Al_2O_3 , SiC, and YSZ-8 powders. The enzyme loading was lower on Al_2O_3 than on SiC and YSZ-8, possibly due to lower surface area, which suggested that the specific activity was higher on the Al_2O_3 powder. It was noteworthy that the immobilization efficiency was always lower by covalent bonding than by physical adsorption. This effect was likely caused by cross-linking of the inorganic particles during activation with glutaraldehyde, thus increasing the size of the cross-linked particles and lowering the surface area available for immobilization. Particle size distribution measurements of silicon carbide powder with immobilized ADH revealed that the particles with covalently bonded ADH were larger than the particles with physically adsorbed ADH. Guedidi et al. [53] discussed the importance of the available surface area for high enzyme loading. The authors observed a much higher maximum immobilization concentration of trypsin (23.8 kDa) than urease (545 kDa) on polyacrylonitrile membranes, which they explained by a larger surface area being available to trypsin than urease since trypsin could penetrate the membrane pores and thus adsorb to the external membrane surface and inside the membrane pores, while the larger urease could only adsorb to the external membrane surface. Similarly, de Cazes et al. [113] observed a higher laccase loading in α -alumina membranes with pore sizes of 1.4 μm than 0.2 μm since the enzyme, which was covalently bonded to a gelatin layer deposited on the mem-

brane surface, could penetrate the pores of the membranes with the larger pores but not the membranes with the smaller pores, and thus a larger surface area was available for the enzymes in the 1.4 μm membranes.

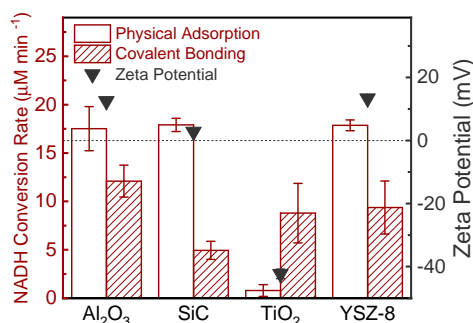


Figure 3.2: Immobilization of ADH on inorganic raw powders of aluminum oxide, silicon carbide, titanium oxide, and yttria stabilized zirconia by covalent bonding and physical adsorption. NADH conversion rate (activity of immobilized enzyme) compared to the surface zeta potential of the inorganic raw powders.

3.2.2 Immobilization of alcohol dehydrogenase on aluminosilicate nanofiber membranes

Properties of aluminosilicate nanofiber membranes

The calcination of the electrospun nanofiber membranes at 1100°C yielded a mullite crystal structure with the chemical formula $3\text{Al}_2\text{O}_3 \cdot 2\text{SiO}_2$. The membranes were 25 mm in diameter with an average weight of $0.0175 \text{ g} \pm 0.0031$ (Figure 3.3). The average fiber diameter was 129 nm and the specific BET surface area was $11.7 \text{ m}^2 \text{ g}^{-1}$. The surface area was higher or comparable to the surface area of the raw inorganic powders used previously (e.g., the BET surface area of Al_2O_3 powder was $5.4 \text{ m}^2 \text{ g}^{-1}$), even though the nanofiber membranes were shaped into ordered structures, as opposed to discrete particles. The high surface area of the nanofiber membranes was resulted from the nanometer-sized fiber diameters and mesopores (2-50 nm pore diameters) inside the fibers and confirmed that electrospinning can be used to fabricate membranes with an ultra-high surface area.

Immobilization efficiency on aluminosilicate nanofibers

ADH was immobilized on the aluminosilicate nanofiber membranes by physical adsorption and covalent bonding. The immobilization was conducted in filtration mode (with filtration of the enzyme feed solution through the membrane after a predefined immobilization time) and soaking mode (without filtration of the enzyme feed solution through the membrane). The immobilization efficiency was much higher in filtration mode than in soaking mode. When the enzyme feed solution was filtered through the membranes after 90 min immobilization time, the immobilization efficiency reached 80-96% (membrane with filtration, Figure 3.4A), whereas the immobilization efficiency was 11-17% when the enzyme feed solution was removed by pouring it off of the membranes after 90 min of immobilization (membrane without filtration, Figure 3.4A). The results suggested that the enzymes were entrapped in the membranes upon filtration, and thus the immobilization with filtration was a combination of physical adsorption/covalent bonding and entrapment. Considering the large difference in immobilization efficiency with and without filtration, a large proportion of the enzymes was likely entrapped inside the nanofiber membranes upon filtration.

During filtration, the rate of mass transfer through the membranes was limited by the polymeric support membrane, rather than the ceramic nanofiber membrane. Nevertheless,

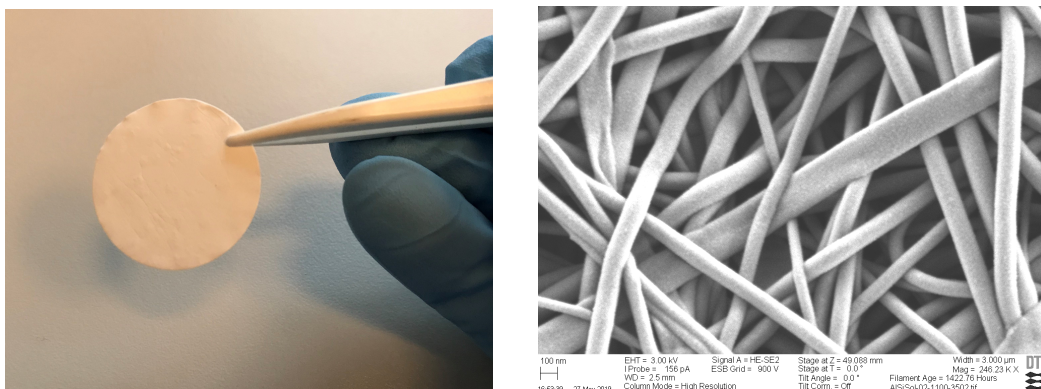


Figure 3.3: Left: A photograph of an aluminosilicate nanofiber membrane with a diameter of 25 mm. Right: An SEM image of an aluminosilicate membrane. The nanofibers on the SEM image were produced using 6 wt% PVP, instead of 5.5 wt% PVP as in the membranes used for immobilization, resulting in average fiber diameter and surface area of 185 nm and $13.7 \text{ m}^2 \text{ g}^{-1}$, respectively. Processing conditions were otherwise similar.

the ADH was immobilized in the nanofiber membrane, as could be confirmed by measuring the catalytic activity of the polymeric support membrane, which showed no catalytic activity in the absence of the ceramic nanofiber membranes. ADH was thus retained inside the porous and entangled nanofiber structure.

The low immobilization efficiency on the nanofiber membranes without filtration was likely due to insufficient mass transfer. This observation can be supported by comparing the difference in immobilization efficiencies on the nanofiber membranes without filtration on one hand and on raw Al_2O_3 and SiC powders on the other, which were measured as 34-75% in a previous study. The immobilization conditions were similar for the nanofiber membranes and the powders (10 mL of 20 mg L^{-1} ADH in 40 mM MES buffer at pH 6.5, 90 min, room temperature, 100 rpm agitation) and the surface area of the powders was lower than that of the nanofiber membranes (the BET surface area of the powders was 5.4 and $13.0 \text{ m}^2 \text{ g}^{-1}$ for Al_2O_3 and SiC, respectively, while it was $11.7 \text{ m}^2 \text{ g}^{-1}$ for the nanofibers membranes, and the amount of powder used in each experiment was 10 mg while the nanofiber membranes weighed on average 17.5 mg). However, the powders were well dispersed in the enzyme feed solutions during immobilization, whereas the bulkier nanofiber membranes were confined to the bottom of the falcon tubes. The good mixing of the particle dispersion aided the mass transfer and may have resulted in higher immobilization efficiency. The activity of membrane immobilized enzymes has been found to be severely impeded by mass transfer limitation when the reactions are operated in soaking mode (membrane soaked in the substrate solution) as compared with convective mode (substrate solution filtered through the membrane) [52]. Here, the immobilization of ADH in soaking mode was likely hampered by poor contact between the enzymes and the nanofiber membrane, resulting in low immobilization efficiency.

The immobilization efficiency of physically adsorbed ADH immobilized on aluminosilicate nanofibers in soaking mode increased from 22-54% by increasing the adsorption time from 1.5-24h (Figure 3.4B), which further suggested that the adsorption of ADH on the nanofibers was hampered by diffusion limitations. The lower immobilization efficiency on the nanofiber membranes compared with the powders may also have been caused by the elimination of hydroxyl and other functional groups from the surface of the nanofibers upon calcination at 1100°C [114], [115]. However, the immobilization efficiency on the

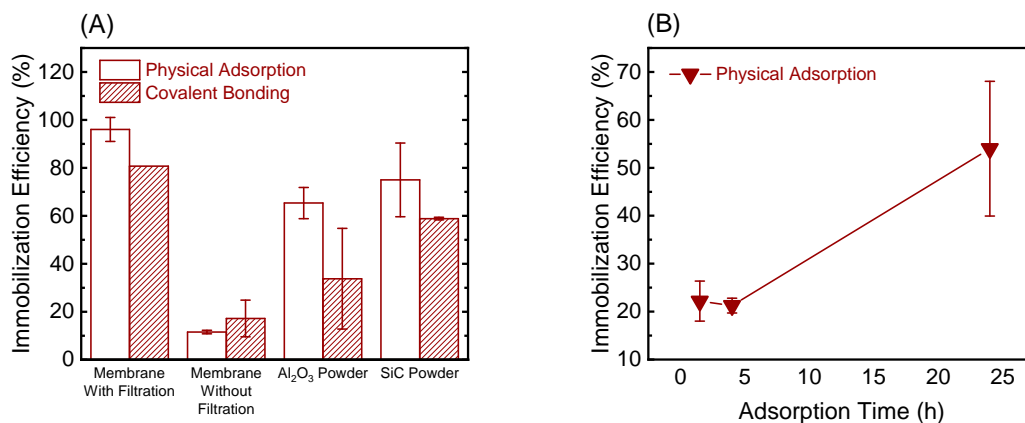


Figure 3.4: Immobilization efficiency on aluminosilicate nanofiber membranes and inorganic raw powders. (A) Immobilization efficiency on nanofiber membranes, with and without filtration of the enzyme feed solution through the membrane and on raw powders of Al₂O₃ and SiC. The membranes and powders were soaked in 10 mL 20 mg L⁻¹ ADH solution in MES buffer for 90 min at room temperature and 100 rpm agitation. (B) The effects of adsorption time on immobilization efficiency. ADH was physically adsorbed on aluminosilicate nanofiber membranes. The immobilization was conducted in 2 mL Eppendorf tubes with 4 mg of membrane fractions and 2 mL of 100 mg L⁻¹ ADH solution in MES buffer, at 4°C for 1.5, 4, and 24h, without agitation. Note that only one replicate of immobilization efficiency for covalent bonding with filtration was available since two out of three membranes broke during the experiments. The error bars in the other cases report the standard deviations of two independent experiments.

nanofiber membranes without filtration was higher with covalently bonded enzymes than with physically adsorbed enzymes, which indicated the presence of surface groups on the nanofiber surface through which the functionalizing and activating agents were successfully attached and thus provided linkers for the covalent attachment of the ADH to the surface of the nanofiber membranes. The presence of molecular linkers on the support surface does not restrain the enzymes from physically adsorbing to the surface, too, so the immobilization with covalent bonding can be a combination of covalent bonding and physical adsorption. Better mixing and longer reaction times between the nanofiber membranes and the functionalizing and activating agents might be required to increase the number of molecular linkers on the nanofiber surface and thus provide higher immobilization efficiency.

Performance of alcohol dehydrogenase immobilized on aluminosilicate nanofiber membranes

The activity and storage stability of ADH immobilized on aluminosilicate nanofiber membranes was investigated by measuring the activity of the biocatalytic membranes immediately upon immobilization and after storage in MES buffer at 4°C for up to 12 days with repeated reaction cycles (Figure 3.5). The membranes prepared by immobilization with filtration were used in this study. Note that only one replicate of the membrane with covalently bonded ADH is provided, as two out of three membranes with covalently bonded ADH broke during the experiments.

The initial activity of the biocatalytic membranes (Day 0) was high for both physically adsorbed and covalently bonded ADH, with almost 100% conversion of NADH in a single pass through the membranes. The substrate solutions were filtered through the bio-

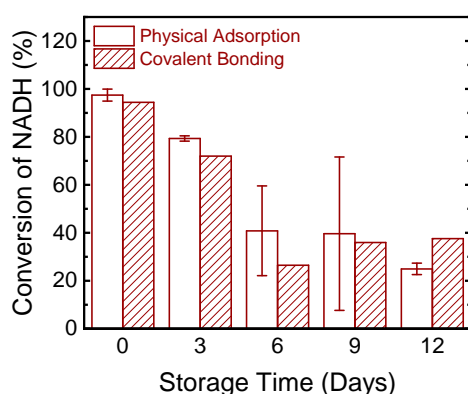


Figure 3.5: Activity and storage stability of ADH immobilized on aluminosilicate nanofiber membranes by physical adsorption and covalent bonding. The enzyme feed solutions were filtered through the membranes after 90 min of immobilization. The membranes were stored in MES buffer at 4°C between use. Reactions were initiated by adding 4 mL of substrate solution (30 mM formaldehyde, 100 μM NADH in MES buffer) to the reactor, the solution was agitated at 150 rpm and the filtration cell was pressurized to 1 bar by nitrogen gas, the filtration was stopped when 2 mL permeate was collected. Note that only one replicate for covalent bonding was available since two out of three membranes were broken during the process. The error bars for physical adsorption report the standard deviation of two independent experiments.

catalytic membranes at 1 bar applied pressure and 2 mL of permeate was collected in approximately 1.5 minutes. The NADH concentration of the retentate was similar to the initial NADH concentration of the substrate solution, which showed that NADH was not retained in the reactor and the conversion of NADH primarily occurred as the NADH passed through the membrane. This observation indicated that the ADH was mostly immobilized inside the nanofiber membranes, rather than on the surface [52], which agrees with the immobilization being a combination of physical adsorption/covalent bonding and entrapment, with a large contribution from enzyme entrapment. The high immobilization efficiency ensured high conversion in the reactions.

The activity of the biocatalytic membranes was measured every three days after the initial reaction to investigate the storage stability of the biocatalytic membranes. The membranes were removed from the filtration cells and stored in MES buffer at 4°C between reactions. The activity decreased gradually with storage time, which was presumably mostly due to leakage of the entrapped and physically adsorbed enzymes from the membranes during storage [116]. The decrease in enzyme activity was similar between the physically adsorbed and covalently bonded enzymes, which suggested that enzyme entrapment was the main immobilization mechanism in both membranes. The covalently bonded enzymes seemingly retained a higher activity than the physically adsorbed enzyme on day 12. Covalent bonding is known to provide higher stability than physical adsorption and entrapment [80], [117], so the activity remaining after 12 days of storage was likely higher with the covalently bonded enzymes since at this point the entrapped enzymes and much of the physically adsorbed enzymes had leaked from the membranes and thus a higher enzyme loading remained in the membrane with covalently bonded enzymes than the membranes with physically adsorbed enzymes. Although immobilization by physical adsorption is known to retain a higher enzyme activity than covalent bonding

[22], it should be kept in mind that the membranes with covalently bonded enzymes can have physically adsorbed enzymes on them too, and the catalytic activity of the membranes provided by physically adsorbed enzymes and covalently bonded enzymes are additive. However, the discussion provided here must be taken with a grain of salt, given the lack of replicates.

To increase the storage stability of the biocatalytic membranes, the membranes could potentially be coated with a layer of polyelectrolytes by the layer-by-layer assembly method [118], or the enzymes could be cross-linked post immobilization to prevent enzyme leakage [119]. The effects of polyelectrolyte coating on enzyme stability were observed in a study involving the immobilization of trypsin and urease by polyelectrolyte layer-by-layer assembly on polyacrylonitrile membranes. The residual activity of trypsin after 100 days of storage and repeated reaction cycles increased from approximately 60% when trypsin was immobilized as the top layer of the membrane, to 95% when the trypsin layer was coated with an additional layer of alginate. Similarly, the stability of urease was improved by coating the enzyme with a layer of polyethylenimine. The residual urease activity increased from approximately 25% after 25 days of storage and repeated reaction cycles, to approximately 50% after 28 days of storage and reactions by coating the urease with a layer of polyethylenimine [53].

The aluminosilicate nanofiber membranes provided suitable conditions for the immobilization of ADH with high enzyme loading and high activity retention. However, the fragility of the aluminosilicate nanofiber membranes was a major issue in handling the membranes and applying them in filtration experiments. Patel et al. [120] reported the immobilization of horseradish peroxidase in mesoporous silica-based nanofibers with excellent catalytic properties, high thermal stability, and good mechanical flexibility. The silica sol-gel precursor was made of tetramethyl orthosilicate and polyvinyl alcohol and contained glucose as pore former and to increase the viscosity of the electrospinning solution. The enzyme was mixed in the electrospinning solution and was thereby immobilized inside the nanofibers. However, instead of calcining the fibers upon electrospinning, the polymer and glucose template was removed by extraction using phosphate buffer. In a different study, TiO₂ nanofiber membranes were prepared by coating a glass filter substrate with electrospun TiO₂ nanofibers by vacuum filtration. The membrane was subsequently compressed by hot pressing at 5 bar and 120°C. The resulting membrane performed well in pressure-driven filtration [121]. The two examples describe two very different approaches to the fabrication of ceramic nanofiber membranes with favorable properties. It would be worth exploring more options for the fabrication of ceramic nanofiber membranes with higher stability and flexibility for enzyme immobilization.

3.2.3 Immobilization of alcohol dehydrogenase by polyelectrolyte layer-by-layer assembly and interfacial polymerization

ADH was immobilized on PEM membranes prepared by the deposition of seven layers of polyelectrolytes (one layer of PDA/PEI followed by three bilayers of PDADMAC and PSS) on a polysulfone MF substrate. The water permeability decreased by 86-92% upon the deposition of seven layers of polyelectrolytes and one layer of ADH due to increased mass transfer resistance exerted by the polyelectrolytes and enzymes (Figure 3.6). The immobilization of ADH on the PEM membranes resulted in a 20±9% decrease in water permeability. Similar values were reported by Datta et al. [52], who observed a 96% decrease in water permeability after the deposition of seven layers of polyelectrolytes and one layer of glucose oxidase. The decrease in water permeability was more pronounced with the additions of the first layers of polyelectrolytes, likely since the first few layers were deposited inside the membrane pores and thus caused pore narrowing. As the pores were

filled up, the layers started building up on the membrane surface with less distinct effects on the water permeability.

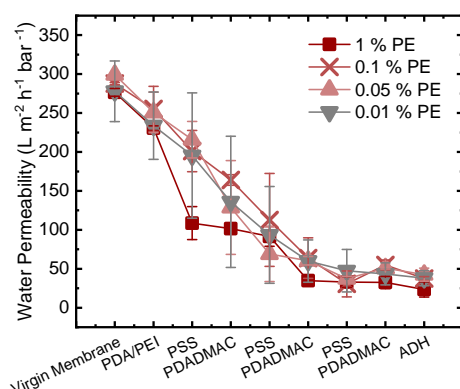


Figure 3.6: Water permeability of PEM membranes prepared by the deposition of layers of PDADMAC and PSS onto a GRM0.1PP MF membrane substrate (polysulfone, 0.1 μm). The water permeability of the virgin membrane was measured before modifying the membrane, then a layer of PDA/PEI was applied to the membrane as the first layer (10 mL of 2 mg/mL dopamine-HCl and 0.1 mg/mL PEI, 100 rpm, room temperature, 1h) followed by thorough rinsing with water and water permeability measurements. Layers of PSS and PDADMAC were then added to the membrane in an alternating fashion. 5 mL of 0.01-0.1wt% polyelectrolyte (PE) solutions in 20 mM NaCl were applied to the substrate for 20 min, at room temperature, without stirring. The polyelectrolyte solutions were discarded and the membranes were washed thoroughly with water between layers, followed by water permeability measurements. The water permeability was measured gravimetrically. The enzyme layer was immobilized by applying 5 mL of 10 mg L⁻¹ ADH in Tris buffer, pH 8.5, to the PEM membrane for 30 min, at 4°C. The enzyme solution was filtered through membrane at 1 bar after the immobilization.

The effects of polyelectrolyte deposition on the water permeability and transport properties of the PEM membrane must be taken into consideration for the selection of a suitable membrane substrate to ensure efficient process conditions during operations with the PEM membranes. We observed that polyelectrolyte LbL assembly on a polysulfone UF membrane substrate with 20 kDa pore size would result in low water permeability and retention of NADH by the biocatalytic PEM membrane (Table 3.1). The cofactor was thus partially hindered from entering the membrane, which hampered the reaction efficiency. Increasing the pore size of the UF membrane substrate from 20 to 100 kDa resulted in a biocatalytic PEM membrane with much higher water permeability and no observed retention of NADH by the membrane. The enzyme loading on the 100 kDa membranes was increased considerably by changing the enzyme feed solution buffer from MES buffer at pH 6.5 to Tris buffer at pH 8.5. The increased enzyme loading was not reflected in higher NADH conversion upon passing through the membranes, possibly due to an unfavorable orientation of the adsorbed enzymes at a higher pH. Given the electrostatic nature of enzyme immobilization by polyelectrolyte LbL assembly, the electrostatic conditions are extremely important for an efficient immobilization. We further observed that the immobilization efficiency of ADH on PEM membranes could be increased from 17-86% by changing the enzyme feed solution buffer from MES buffer at pH 6.5 to Tris buffer at pH 8.5 (Figure A1 in Appendix A4).

Table 3.1: Immobilization of ADH by polyelectrolyte LbL assembly on UF membrane substrates. The effects of UF membrane pore size and enzyme feed solution pH on the success of immobilization were tested. The PEM membranes were prepared by depositing three layers of polyelectrolytes (PDADMAC-PSS-PDADMAC, 20 mM polyelectrolyte concentration in 0.5 M NaCl) onto polysulfone UF membranes of different pore sizes. The polyelectrolytes were applied to the membranes for 10 min, followed by two 5-min rinsing cycles with 0.5 M NaCl. Subsequently 4 mL of 100 mg L⁻¹ ADH in MES buffer at pH 6.5 or Tris buffer at pH 8.5 were applied to the membranes for 1.5h. The enzyme feed solutions were poured off of the membranes after the predefined adsorption time and the membranes were washed three times with the feed solution buffer. Immobilization efficiency was determined using Bradford microassay. Protein concentrations of the enzyme feed solution before and after immobilization, as well as the enzyme washing solutions, were calculated from absorbance measurements at 595 nm and were used to calculate the immobilization efficiency. Water permeability was measured gravimetrically. The activity of the catalytic membranes was measured by adding 4 mL of substrate solution (30 mM formaldehyde and 100 μ M NADH in MES buffer at pH 6.5) to the reactor and collecting 2 mL of permeate by filtration at 1 bar applied pressure. The NADH concentrations of the feed, retentate, and permeate were calculated from absorbance measurements at 340 nm, and were used to calculate the conversion and retention of NADH in the reactor.

Tested variables			
Membrane	GR61PP	GR40PP	GR40PP
Pore size (kDa)	20	100	100
Immobilization solvent	MES pH 6.5	MES pH 6.5	Tris pH 8.5
Biocatalytic membrane performance			
Water permeability (L m ⁻² h ⁻¹ bar ⁻¹)	3.0	213.2	113.7
NADH conversion per pass (%)	19.9	37.5	10.9
Immobilization efficiency (%)	8.2	4.1	25.8
Retention of NADH (yes/no)	yes	no	no

The water permeability of biocatalytic membranes prepared by interfacial polymerization was likewise affected by the pore size of the UF membrane substrate (Figure 3.7), as well as by the polymerization time between ADH and TMC (Figure A2 in Appendix A4). When ADH was polymerized on a 20 kDa UF substrate, the water permeability ranged from 8-29 L m⁻² h⁻¹ bar⁻¹, depending on the polymerization time and the mode of immobilization (with or without filtration of the enzyme feed solution). The water permeability decreased as the polymerization time increased, which indicated a successful film growth due to polymerization between ADH and TMC and the degree of cross-linking increased with time. Wang et al. [89] reported similar values in their study where lysozyme was polymerized with TMC on a 20 kDa polyethersulfone UF membrane. The authors found the water flux through the membranes to be 44-60 L m⁻² h⁻¹ at 4 bar, depending on the concentrations of TMC and lysozyme used during fabrication.

We observed an increase in water permeability of ADH membranes when the substrate was changed from a 20 kDa membrane to a 50 kDa membrane. The water permeability increased without compromising the conversion of NADH (Figure 3.7). Up to 70% conversion of NADH was observed during a single pass through the biocatalytic membranes, which was higher than what was observed in experiments with biocatalytic PEM membranes, but lower than with the biocatalytic aluminosilicate nanofiber membranes.

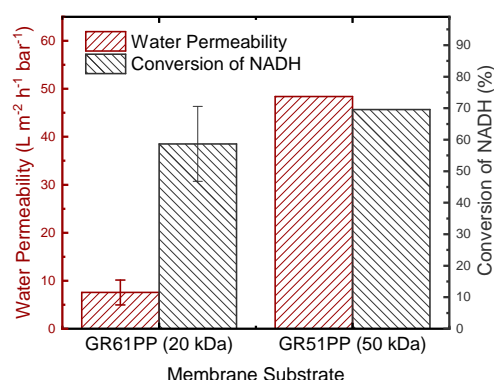


Figure 3.7: Water permeability and NADH conversion per pass through biocatalytic membranes prepared by interfacial polymerization of ADH and TMC. GR61PP and GR51PP UF membranes (polysulfone, 20 and 50 kDa, respectively) were used as substrates for the polymerization. ADH ($3\text{ mL } 133\text{ mg L}^{-1}$ in MES buffer at pH 6.5) was applied to the membrane for 30 min, followed by filtration at 2 bar, subsequently 3 mL of 0.075 wt% TMC in hexane was added to the membrane surface for 10 min. The TMC solution was dumped off of the membranes, the membranes were air-dried and then washed thoroughly with water. The activity of the catalytic membranes was measured by adding 4 mL of substrate solution (30 mM formaldehyde and $100\text{ }\mu\text{M}$ NADH in MES buffer at pH 6.5) to the reactor and collecting 2 mL of permeate by filtration at 4 bar applied pressure. The NADH concentrations of the feed, retentate, and permeate were calculated from absorbance measurements at 340 nm, and were used to calculate the conversion and retention of NADH in the reactor. Water permeability was measured gravimetrically. Protein concentration of the permeate from filtration of the enzyme feed solution was measured by Bradford assay, no enzyme was detected in the permeate which indicated that the immobilization efficiency was 100%.

4 Investigating solute transport in polyelectrolyte multilayer membranes with controllable properties

From the previous discussion and experimental observations, it is clear that the polyelectrolyte LbL assembly method is an interesting option for enzyme immobilization on membranes, as well as on other support structures. When the immobilization is conducted on membranes, the polyelectrolyte LbL assembly serves to provide conditions fit for enzyme immobilization, and simultaneously, it can be used to control the rate of transport through the membrane to provide favorable operating conditions during the enzyme catalyzed reactions [52]. In Section 3.2.3, we saw that the water permeability in PEM membranes decreased steadily upon addition of layers of polyelectrolytes and enzymes to a polymeric MF membrane substrate. Similarly, it has been described how enzyme loading can be increased by immobilizing the enzymes in multiple layers, and furthermore, how enzyme activity and permeate flux can be matched by controlling the number of layers of enzymes and polyelectrolytes deposited on a membrane substrate to ensure optimal substrate conversion upon passing through the membrane (i.e., to match the enzyme activity and substrate retention time in the membrane) [51], [57], [101]. However, while the effect of increasing the number of layers of enzymes and polyelectrolytes in PEM films on the water permeability is well-known, the effects of increasing the number of layers in PEM films, and thereby increasing the thickness of the PEM film, on other membrane properties (e.g., membrane pore size and solute rejection by the membrane) are not well described. Such effects could have important implications for the reaction efficiency in biocatalytic PEM membranes.

We investigated the effects of membrane thickness on solute transport in PEM membranes. To achieve this purpose, it was critical to fabricate PEM membranes where only the thickness of the PEM film was changed, while other properties, such as membrane pore size and surface charge were kept constant. We investigated methods for membrane surface modification by polyelectrolyte LbL assembly for the fabrication of membranes with the desired properties (i.e., membrane thickness, pore size, and surface charge). We then fabricated PEM nanofiltration (NF) membranes with different thicknesses, but similar pore size and surface charge, and studied the transport of neutral and charged solutes through the membranes, as well as the energy barriers to anion transport through the membranes. Energy barriers arise during transport through membranes due to the hindrance imposed by the membranes on the transported solute and solvent molecules. The energy barrier is composed of contributions from all transport mechanisms involved in the transport of a solute through the membrane, but the apparent energy barrier (or the largest energy barrier), which can be calculated from an Arrhenius-type equation, describes the rate-limiting step during transport [56]. Energy barriers to ion transport in NF membranes and membranes with pore sizes similar to the hydrated size of the ions are found to be highly affected by the hydration energy of the ion and the membrane pore size, since the dehydration of the ions at the membrane pore entry is found to be the main contribution to the energy barrier to ion transport through the membranes [122]. By studying the energy barriers to anion transport in membranes of different thicknesses but with similar pore sizes, we could evaluate the importance of ion diffusion inside the membrane pore relative to the ion diffusion into the membrane pore (ion partitioning into

the membrane). The results of this study were reported in Paper 3, *Energy barriers to anion transport in polyelectrolyte multilayer nanofiltration membranes: Role of intra-pore diffusion*, which is attached in Appendix A3.

The objective of the study was to exploit the polyelectrolyte LbL assembly method to fabricate membranes with controlled separation properties (i.e., membrane thickness, pore size, and surface charge) and to calculate energy barriers to ion transport through the membranes to evaluate the effect of membrane thickness on the membrane transport properties. We thus addressed the main objectives O5 and O6 and simultaneously, we tested hypothesis H4, which stated that membrane thickness may be increased without affecting solute rejection by the membrane. While the main objective was to fabricate membranes for solute transport studies in the membranes, the results could be extended to enzyme immobilization and objective O4, regarding membrane modification techniques for enzyme immobilization.

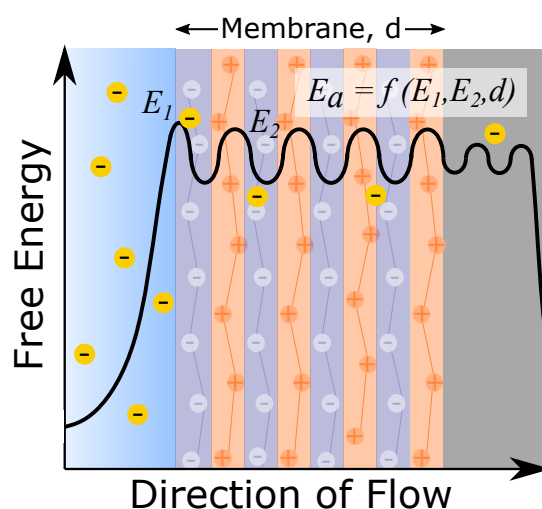


Figure 4.1: Graphical abstract of Paper 3. PEM NF membranes were fabricated by LbL deposition of oppositely charged polyelectrolytes onto UF membrane substrates. The properties of the multilayers were tuned by varying conditions during the multilayer assembly. Energy barriers to anion transport through the membranes were calculated from an Arrhenius-type equation to investigate the effects of membrane thickness and pore size on the energy barriers [56].

4.1 Materials and methods

PEM NF membranes were fabricated by depositing alternating layers of positively and negatively charged polyelectrolytes onto UF membrane substrates by the LbL assembly method. The resulting NF membranes were thin film composite membranes, where the PEM formed the selective layer, and the porous UF substrate formed the support layer. The properties of the selective layer were varied by varying conditions during polyelectrolyte deposition. The membrane thickness was controlled by the number of polyelectrolyte layers, the pore size was decreased by decreasing the concentration of polyelectrolytes in the deposition solutions, and salt annealing was used to control the surface charge. We were thus able to fabricate membranes where one variable was changed (i.e., membrane thickness or pore size), while other variables were kept constant. We used the membranes to study the transport of anions through the membranes, specifically, the effect of membrane thickness on the energy barriers to anion transport through

the membranes. The reader is referred to the Materials and methods section of Paper 3, in Appendix A3, for a detailed description of the experimental procedures.

4.2 Results and discussion

Membrane characterization (membrane thickness, pore size, and surface charge) revealed that we were able to fabricate NF membranes where we changed one membrane property (membrane thickness or pore size) while keeping other membrane properties constant. The membranes could thus be used to investigate the respective effects of membrane thickness and pore size on anion transport through the membranes and the energy barriers to anion transport through the membranes. Furthermore, we applied salt annealing to modify the membrane surface charge, and were able to invert the surface charge of the PEM NF membranes (change it from positive to negative) by applying a high concentration electrolyte solution to the membranes. The membrane characterization confirmed the versatility of the polyelectrolyte LbL assembly method, and showed that it is useful for the fabrication of NF membranes with tunable surface properties.

By increasing the number of bilayers of PDADMAC/PSS from four to ten, the membrane thickness increased from 27.6-76.6 nm, whereas the pore size was not significantly affected and variations in the pore sizes did not follow the increase in membrane thickness. Water permeability of the membranes decreased with increasing membrane thickness, due to increased resistance to transport through thicker membranes. The rejection of glucose and bromide was not significantly affected by the increased membrane thickness on the other hand (Table 4.1). Membrane thickness thus influenced the rate of transport through the membranes, but did not affect the selectivity of the membranes. Solute rejection was mainly decided by the membrane pore size and the properties of the solute, whereas membrane thickness did not influence solute rejection.

Table 4.1: Characterization of PEM NF membranes with different number of bilayers of PDADMAC/PSS fabricated by the alternating deposition of 20 mM polyelectrolyte solutions in 0.5 M NaCl on a UF membrane substrate and transport properties in the membranes

	4 Bilayers	7 Bilayers	10 Bilayers
Thickness (nm)	27.6 ± 3.2	61.6 ± 8.1	76.6 ± 14.3
Pore radius (nm)	0.73 ± 0.09	0.70 ± 0.06	0.74 ± 0.09
Water permeability (L m ⁻² h ⁻¹ bar ⁻¹)	9.01 ± 1.13	8.46 ± 0.91	6.61 ± 0.47
Glucose rejection, R _{obs} (%)	39.6 ± 10.1	43.5 ± 4.5	43.2 ± 2.21
Bromide rejection, R _{obs} (%)	16.3 ± 4.2	12.9.3.2	17.9 ± 2.7

Energy barriers to bromide and fluoride transport through the NF membranes were calculated from an Arrhenius-type equation. The results showed that membrane pore size and ion hydration energy (the energy released upon hydration of an ion) significantly affected the energy barriers to ion transport through the membranes, whereas a significant effect of membrane thickness on the energy barriers was not observed. The effects of pore size and ion hydration energy were explained by the ions undergoing dehydration at the solution-membrane interface as they partitioned from the solution and into the membrane material. Ion dehydration at the membrane pore entry has been found to pose the highest energy barrier to ion transport through membranes with pore sizes similar to the hydrated size of the ion, and be the rate-limiting step during transport through such membranes. More ion dehydration is needed for ions to fit into smaller pores and the energetic cost of

dehydration increases as the hydration energy of the ion increases, which explains the significant effect of membrane pore size and ion hydration energy on the energy barriers. Dehydration is relevant in diffusion controlled transport, but less important in convection controlled transport.

We described the mechanism of ion transport through NF membranes as a series of energy barriers arising due to ion dehydration at the solution-membrane interface and due to diffusion along the thickness of the membrane. The apparent energy barrier is governed by the highest energy barrier arising during transport, which also reveals the rate-limiting step during transport. Ion partitioning into the NF membrane was the rate-limiting step during transport of ions through the membranes, whereas intra-pore diffusion seemingly had negligible effects on anion transport in comparison.

5 Conclusion and future perspectives

5.1 Conclusion

Enzyme immobilization techniques are under continuous development today, more than 100 years after the first report on the topic was published. Research in the field is inspired by current societal and technology trends, as well as potential applications. Likewise, a broader selection of new and improved enzymes and novel immobilization supports are continuously emerging, which provides new opportunities for the development of successful enzyme immobilization systems. The current focus on sustainability is a motivation to continue the development of enzyme immobilization systems.

Enzyme catalysis, employing soluble or immobilized enzymes, is conveniently operated in enzymatic membrane reactors. The membrane retains the enzymes within the process, while substrates and products can freely pass through the membrane, thereby offering reaction mediation by shifting the reaction equilibrium and limiting substrate and product inhibition. Immobilizing enzymes directly on membranes brings several important advantages to the process. First, mass transfer is aided by the pressure-driven convection of substrates through the biocatalytic membrane, thus eliminating diffusion limitations. Furthermore, the membrane offers a large surface area for enzyme immobilization, which affords high enzyme loading, the immobilization inside membrane pores can provide a protective environment for the enzymes, and multi-enzyme immobilization can be done in a spatially controlled manner on the membrane to increase the efficiency of sequential enzyme reactions. Lastly, immobilizing enzymes on membranes is an environmentally friendly and economical option as it brings about process intensification that leads to increased energy-efficiency and reduced waste production, and simultaneously, it eliminates the need for a specific material for enzyme support.

In a pressure-driven membrane operation, substrate transport through the membrane is a single-time event. Therefore, it is critical to consider the enzyme activity and substrate retention time in the membrane to achieve high substrate conversion. Here, the focus should be turned to membranes with high surface area and immobilization methods that allow high enzyme loading for an efficient substrate conversion. Nanofiber membranes, such as the aluminosilicate nanofiber membranes applied in this project, offer advantages in this regard, given their high surface area and porosity which facilitates high enzyme loading. Similarly, the polyelectrolyte LbL assembly method is practical for the ability of controlling enzyme loading and transport properties through such membranes.

Enzymatic membrane reactor operations are faced with the same challenges as membrane operations and enzyme catalysis in general, namely, membrane fouling and loss of enzyme activity with time, respectively. Although enzyme immobilization generally results in enzyme stabilization and prolonged life-time, the useful life of the catalyst is generally shorter than of the membrane, which calls for the regeneration and reuse of the membrane. Some immobilization methods are reversible (e.g., physical adsorption and polyelectrolyte LbL assembly) and allow the removal of deactivated enzymes from the membrane support to reload the membranes with fresh enzymes. Other immobilization methods (which generally offer higher enzyme stability) are irreversible so more drastic methods are needed for the removal of the deactivated enzymes, such as chemical or thermal cleaning methods. Inorganic membrane materials are advantageous in the latter case due to their inherent chemical, thermal, and mechanical stability. Inorganic mem-

branes with immobilized enzymes can be effectively regenerated by harsh chemical and thermal cleaning methods to restore their native properties.

We investigated enzyme immobilization on inorganic materials and the possibility of fabricating inorganic membranes with properties tailored for enzyme immobilization. The immobilization of ADH on inorganic raw materials that are commonly used for membrane fabrication revealed that the enzyme activity and stability were greatly affected by the process conditions as well as the support material and morphology. The buffer selection was important to maintain favorable conditions during reaction and storage. The pH of the reaction mixture was critical for enzyme activity while the electrostatic conditions during storage proved important for colloid stability. The storage stability of silicon carbide powder with immobilized ADH was hampered by agglomeration of the particles during storage due to low colloid stability in the storage buffer used. We observed that the surface area and surface charge of the support were important parameters for high enzyme loading, and the surface charge of the support further affected the enzyme activity by influencing the microenvironment of the enzymes on the support (i.e., negatively charged TiO₂ powder induced local acidification at the surface of the powder, which hampered the activity of physically adsorbed ADH). The inorganic powders were susceptible to surface modification by APTES and glutaraldehyde. The surface modification was advantageous for the immobilization of ADH on TiO₂ due to changes in surface charge by the introduction of new chemical groups to the surface, which provided more favorable conditions for the ADH. The comparison between the activity of physically adsorbed ADH and covalently bonded ADH on TiO₂ indicated the ability to promote conditions for enzyme immobilization by surface modification.

Electrospinning was used for the fabrication of aluminosilicate nanofiber membranes for the immobilization of ADH. The membranes offered a high surface area, high porosity, and a suitable pore size for the immobilization of ADH. High enzyme loading resulted from immobilization in filtration mode (80-96% immobilization efficiency), partially due to the entrapment of enzymes in the nanofibers. The immobilization of ADH on the nanofiber membranes in soaking mode was hampered by mass transfer limitations, resulting in 11-17% immobilization efficiency. The activity and stability of the ADH immobilized in filtration mode was typical for enzyme immobilization by entrapment, that is, we observed high activity retention but low enzyme stability due to enzyme leakage from the membrane. High enzyme activity could potentially be maintained by sealing the membranes by different post-immobilization treatments to prevent enzyme leakage. The aluminosilicate membranes offered favorable conditions for the immobilization of ADH, with high enzyme loading and high activity retention, but the membranes were extremely fragile, which limited their applications. Methods for increasing the stability and flexibility of the membranes would be required to make the membranes useful in pressure-driven filtration. More stable and flexible aluminosilicate nanofiber membranes would have a high potential for the immobilization of ADH and potentially other enzymes.

The immobilization of ADH on polymeric membranes by polyelectrolyte LbL assembly and interfacial polymerization was investigated. We found that the properties of PEM membranes prepared by LbL assembly could be tuned by altering the polyelectrolyte deposition conditions. We varied the pore size, membrane thickness, and surface charge of PEM membranes by varying the number of polyelectrolyte layers, the polyelectrolyte concentrations of the deposition solutions, and by applying salt annealing, respectively. Subsequently, the membranes were used in transport studies to evaluate the effects of membrane thickness and pore size on solute transport in the membranes. We found that the rate of transport was dependent on membrane thickness whereas solute rejection and

energy barriers to anion transport in the membranes were not affected by membrane thickness. The results suggested that the selectivity of the membranes was mainly decided by the relative pore size and properties of the solute, rather than membrane thickness, and that additions of layers of polyelectrolytes to the PEM membranes did not affect solute rejection by the membranes. The results could be extended to enzyme immobilization, as enzyme loading in PEM membranes can be increased by adding layers of enzymes and polyelectrolytes to the membrane, and although the addition would result in increased membrane thickness, it should not influence the selectivity of the membrane.

A novel and facile approach to enzyme immobilization was introduced as immobilization by interfacial polymerization. We tested the immobilization of ADH by polyelectrolyte LbL assembly and interfacial polymerization and found that the success of immobilization changed dramatically by changing the immobilization conditions. We observed up to 70% substrate conversion with biocatalytic membranes prepared by interfacial polymerization and 37.5% conversion with the biocatalytic PEM membranes. These values were lower than what was observed with the aluminosilicate membranes, even at lower permeate flow and thus longer residence times. Nonetheless, the experimental observations and reported studies provided interesting results, which should encourage further research on the subjects.

To summarize, the feasibility of fabricating membranes with properties tailored to the immobilization of ADH was investigated. Two main aspects were considered, i) the fabrication of inorganic membranes with properties tailored for enzyme immobilization, and ii) applying immobilization methods for enzyme immobilization on membranes that could simultaneously be used to control the transport properties of the membranes. The objectives included studying the effects of support material properties and immobilization methods on the catalytic properties of ADH to identify materials and design parameters for the fabrication of membranes with properties tailored to the immobilization of ADH. We found that the surface area and surface charge of the support were particularly important for an efficient enzyme immobilization, and that efficient mass transfer was a critical factor during immobilization to ensure high enzyme loading. Another objective was to study the effects of membrane surface modification on the efficiency of enzyme immobilization as well as on the transport properties of the modified membranes. We observed how surface modification could be applied to promote favorable conditions for enzyme immobilization. For instance, the introduction of functionalizing and activating agents to the surface of TiO_2 powder provided more favorable electrostatic conditions for the immobilization of ADH than on the untreated surface. Furthermore, we demonstrated how the properties of PEM membranes (membrane pore size, thickness, and surface charge) could be modified by controlling the polyelectrolyte deposition conditions, which could be exploited to promote favorable conditions for enzyme immobilization. Solute transport and energy barriers to solute transport in PEM membranes of different thicknesses and pore sizes were studied to evaluate the effects of the surface modification and membrane properties on solute transport in the membranes.

The hypotheses were tested by means of the objectives described above. We found that the material properties of the immobilization support and immobilization methods affected the catalytic properties of immobilized enzymes (H1) and that surface modification could be used to provide suitable conditions for enzyme immobilization (H3). Furthermore, we found that membrane thickness could be increased by addition of layers of polyelectrolytes to a membrane substrate without affecting solute rejection by the membrane (H4). Lastly, we hypothesized that ceramic membranes could be designed and fabricated to provide stable and robust membranes with properties tailored for enzyme

immobilization (H2). The aluminosilicate nanofiber membranes that were fabricated for the project provided favorable conditions for the immobilization of ADH, with high enzyme loading and high activity retention. However, the enzyme stability was hampered by enzyme leakage from the support, and the membranes were very fragile, which limited their applications in pressure-driven operations. Future research should focus on improving the mechanical flexibility of the ceramic membranes and developing immobilization methods with high enzyme stability.

5.2 Future perspectives

The results provided in this study can be used to inspire further research for the development of immobilization supports and immobilization methods for the immobilization of ADH, with potential extrapolation to various other enzymes. Regarding the immobilization support, the inorganic nanofiber membranes provided ideal conditions for efficient enzyme immobilization, namely, a large surface area for high enzyme loading and high porosity for high permeability (and thereby limited mass transfer challenges). For the development of inorganic nanofiber membranes with increased stability and mechanical flexibility, it could be suggested to modify the raw material composition of the electrospinning solution and the processing conditions (e.g., investigate conditions during high temperature calcining or use alternative methods to remove the organic template, such as liquid extraction). Polymeric nanofiber membranes could provide the mechanical flexibility that ceramic nanofibers are lacking, but at the cost of a lower ability of membrane regeneration.

Regarding the immobilization methods, enzyme stability is a key parameter for the widespread implementation of enzymes in industrial processes. Immobilization by polyelectrolyte LbL assembly and interfacial polymerization presented high potential for the preparation of stable biocatalytic membranes with tunable properties. Methods for tuning the surface properties of PEM membranes (i.e., membrane thickness, pore size, and surface charge) were demonstrated and can be used to promote conditions for enzyme immobilization by polyelectrolyte LbL assembly (e.g., favorable pore size and surface charge). The ability to control the properties of biocatalytic membranes prepared by interfacial polymerization is a relatively unexplored avenue, which could provide promising opportunities for the immobilization of a variety of different enzymes. It was further proposed to combine different immobilization methods to enhance the performance of immobilization systems (e.g., to combine entrapment and polyelectrolyte LbL assembly or interfacial polymerization for high enzyme loading and high stability), which affords many possibilities for future investigations.

Bibliography

- [1] C. Lad, N. H. Williams, and R. Wolfenden, “The rate of hydrolysis of phospho-monoester dianions and the exceptional catalytic proficiencies of protein and inositol phosphatases”, *Proceedings of the National Academy of Sciences of the United States of America*, vol. 100, no. 10, pp. 5607–5610, 2003, ISSN: 00278424, 10916490. DOI: 10.1073/pnas.0631607100.
- [2] M. Richter, C. Schulenburg, D. Jankowska, T. Heck, and G. Faccio, “Novel materials through nature’s catalysts”, *Materials Today*, vol. 18, no. 8, pp. 459–467, 2015, ISSN: 18734103, 13697021. DOI: 10.1016/j.mattod.2015.04.002.
- [3] E. M. Abdelraheem, H. Busch, U. Hanefeld, and F. Tonin, “Biocatalysis explained: From pharmaceutical to bulk chemical production”, *Reaction Chemistry and Engineering*, vol. 4, no. 11, pp. 1878–1894, 2019, ISSN: 20589883. DOI: 10.1039/c9re00301k.
- [4] S. Li, X. Yang, S. Yang, M. Zhu, and X. Wang, “Technology prospecting on enzymes: Application, marketing and engineering”, *Computational and Structural Biotechnology Journal*, vol. 2, no. 3, e201209017, e201209017, 2012, ISSN: 20010370. DOI: 10.5936/csbj.201209017.
- [5] J. R. Cherry and A. L. Fidantsef, “Directed evolution of industrial enzymes: An update”, *Current Opinion in Biotechnology*, vol. 14, no. 4, pp. 438–443, 2003, ISSN: 18790429, 09581669. DOI: 10.1016/s0958-1669(03)00099-5.
- [6] R. A. Sheldon and D. Brady, “Broadening the scope of biocatalysis in sustainable organic synthesis”, *Chemsuschem*, vol. 12, no. 13, pp. 2859–2881, 2019, ISSN: 1864564x, 18645631. DOI: 10.1002/cssc.201900351.
- [7] U. T. Bornscheuer, G. W. Huisman, R. J. Kazlauskas, S. Lutz, J. C. Moore, and K. Robins, “Engineering the third wave of biocatalysis”, *Nature*, vol. 485, no. 7397, pp. 185–194, 2012, ISSN: 14764687, 00280836. DOI: 10.1038/nature11117.
- [8] M. V. Arbige, J. K. Shetty, and G. K. Chotani, “Industrial enzymology: The next chapter”, *Trends in Biotechnology*, vol. 37, no. 12, pp. 1355–1366, 2019, ISSN: 18793096, 01677799. DOI: 10.1016/j.tibtech.2019.09.010.
- [9] P. T. Anastas, M. M. Kirchhoff, and T. C. Williamson, “Catalysis as a foundational pillar of green chemistry”, *Applied Catalysis A: General*, vol. 221, no. 1-2, pp. 3–13, 2001, ISSN: 18733875, 0926860x. DOI: 10.1016/s0926-860x(01)00793-1.
- [10] *Sustainable development goals ∴ sustainable development knowledge platform*. [Online]. Available: <https://www.un.org/sustainabledevelopment/sustainable-development-goals/>.
- [11] “Expanding biocatalysis for a sustainable future”, *Nature Catalysis*, vol. 3, no. 3, pp. 179–180, 2020, ISSN: 25201158. DOI: 10.1038/s41929-020-0447-8.
- [12] J. L. Adrio and A. L. Demain, “Microbial enzymes: Tools for biotechnological processes”, *Biomolecules*, vol. 4, no. 1, pp. 117–139, 2014, ISSN: 2218273x. DOI: 10.3390/biom4010117.
- [13] M. J. Burk and S. Van Dien, “Biotechnology for chemical production: Challenges and opportunities”, *Trends in Biotechnology*, vol. 34, no. 3, pp. 187–190, 2016, ISSN: 18793096, 01677799. DOI: 10.1016/j.tibtech.2015.10.007.
- [14] A. L. Demain and J. L. Adrio, “Contributions of microorganisms to industrial biology”, *Molecular Biotechnology*, vol. 38, no. 1, pp. 41–55, 2008, ISSN: 15590305, 10736085. DOI: 10.1007/s12033-007-0035-z.

- [15] R. A. Sheldon and J. M. Woodley, "Role of biocatalysis in sustainable chemistry", *Chemical Reviews*, vol. 118, no. 2, pp. 801–838, 2018, ISSN: 15206890, 00092665. DOI: 10.1021/acs.chemrev.7b00203.
- [16] A. Kumar and S. Singh, "Directed evolution: Tailoring biocatalysts for industrial applications", *Critical Reviews in Biotechnology*, vol. 33, no. 4, pp. 365–378, 2013, ISSN: 15497801, 07388551. DOI: 10.3109/07388551.2012.716810.
- [17] U. Hanefeld, L. Cao, and E. Magner, "Enzyme immobilisation: Fundamentals and application", *Chemical Society Reviews*, vol. 42, no. 15, pp. 6211–6212, 2013, ISSN: 14604744, 03060012. DOI: 10.1039/c3cs90042h.
- [18] C. Mateo, J. M. Palomo, G. Fernandez-Lorente, J. M. Guisan, and R. Fernandez-Lafuente, "Improvement of enzyme activity, stability and selectivity via immobilization techniques", *Enzyme and microbial technology*, vol. 40, no. 6, pp. 1451–1463, 2007.
- [19] B. Brena, P. González-Pombo, and F. Batista-Viera, "Immobilization of enzymes: A literature survey", in *Immobilization of enzymes and cells*, Springer, 2013, pp. 15–31.
- [20] A. A. Homaei, R. Sariri, F. Vianello, and R. Stevanato, "Enzyme immobilization: An update", *Journal of Chemical Biology*, vol. 6, no. 4, pp. 185–205, 2013, ISSN: 18646166, 18646158. DOI: 10.1007/s12154-013-0102-9.
- [21] R. Di Cosimo, J. Mc Auliffe, A. J. Poulouse, and G. Bohlmann, "Industrial use of immobilized enzymes", *Chemical Society Reviews*, vol. 42, no. 15, pp. 6437–6474, 2013, ISSN: 14604744, 03060012. DOI: 10.1039/c3cs35506c.
- [22] S. B. Sigurdardóttir, J. Lehmann, S. Ovtar, J. Grivel, M. Della Negra, A. Kaiser, and M. Pinelo, "Enzyme immobilization on inorganic surfaces for membrane reactor applications: Mass transfer challenges, enzyme leakage and reuse of materials", *Advanced Synthesis and Catalysis*, vol. 360, no. 14, pp. 2578–2607, 2018, ISSN: 16154169, 16154150, 14369966. DOI: 10.1002/adsc.201800307.
- [23] L. Cao, L. van Langen, and R. A. Sheldon, "Immobilised enzymes: Carrier-bound or carrier-free?", *Current Opinion in Biotechnology*, vol. 14, no. 4, pp. 387–394, 2003, ISSN: 09581669, 18790429. DOI: 10.1016/s0958-1669(03)00096-x.
- [24] J. Zdarta, A. S. Meyer, T. Jesionowski, and M. Pinelo, "A general overview of support materials for enzyme immobilization: Characteristics, properties, practical utility", *Catalysts*, vol. 8, no. 2, p. 92, 2018.
- [25] A. Kayvani Fard, G. McKay, A. Buekenhoudt, H. Al Sulaiti, F. Motmans, M. Khraisheh, and M. Atieh, "Inorganic membranes: Preparation and application for water treatment and desalination", *Materials*, vol. 11, no. 1, p. 74, 2018.
- [26] A. R. Studart, U. T. Gonzenbach, E. Tervoort, and L. J. Gauckler, "Processing routes to macroporous ceramics: A review", *Journal of the American Ceramic Society*, vol. 89, no. 6, pp. 1771–1789, 2006.
- [27] L. Treccani, T. Y. Klein, F. Meder, K. Pardun, and K. Rezwan, "Functionalized ceramics for biomedical, biotechnological and environmental applications", *Acta biomaterialia*, vol. 9, no. 7, pp. 7115–7150, 2013.
- [28] P. Zucca and E. Sanjust, "Inorganic materials as supports for covalent enzyme immobilization: Methods and mechanisms", *Molecules*, vol. 19, no. 9, pp. 14 139–14 194, 2014.
- [29] S. A. Ansari and Q. Husain, "Potential applications of enzymes immobilized on/nano materials: A review", *Biotechnology advances*, vol. 30, no. 3, pp. 512–523, 2012.
- [30] S. Chakraborty, H. Rusli, A. Nath, J. Sikder, C. Bhattacharjee, S. Curcio, and E. Drioli, "Immobilized biocatalytic process development and potential application in

- membrane separation: A review”, *Critical reviews in biotechnology*, vol. 36, no. 1, pp. 43–58, 2016.
- [31] I. Eş, J. D. G. Vieira, and A. C. Amaral, “Principles, techniques, and applications of biocatalyst immobilization for industrial application”, *Applied microbiology and biotechnology*, vol. 99, no. 5, pp. 2065–2082, 2015.
- [32] M. Mulder, *Basic principles of membrane technology*. Springer Science & Business Media, 2012.
- [33] G. Rios, M. Belleville, D. Paolucci, and J. Sanchez, “Progress in enzymatic membrane reactors—a review”, *Journal of Membrane Science*, vol. 242, no. 1-2, pp. 189–196, 2004.
- [34] L. Giorno and E. Drioli, “Biocatalytic membrane reactors: Applications and perspectives”, *Trends in biotechnology*, vol. 18, no. 8, pp. 339–349, 2000.
- [35] P. Jochems, Y. Satyawali, L. Diels, and W. Dejonghe, “Enzyme immobilization on/in polymeric membranes: Status, challenges and perspectives in biocatalytic membrane reactors (bmrs)”, *Green chemistry*, vol. 13, no. 7, pp. 1609–1623, 2011.
- [36] Y.-K. Cen, Y.-X. Liu, Y.-P. Xue, and Y.-G. Zheng, “Immobilization of enzymes in/on membranes and their applications”, *Advanced Synthesis & Catalysis*, vol. 361, no. 24, pp. 5500–5515, 2019.
- [37] D. Prazeres and J. Cabral, “Enzymatic membrane bioreactors and their applications”, *Enzyme and Microbial Technology*, vol. 16, no. 9, pp. 738–750, 1994.
- [38] C. Charcosset, “Membrane processes in biotechnology: An overview”, *Biotechnology advances*, vol. 24, no. 5, pp. 482–492, 2006.
- [39] F. Carstensen, A. Apel, and M. Wessling, “In situ product recovery: Submerged membranes vs. external loop membranes”, *Journal of membrane science*, vol. 394, pp. 1–36, 2012.
- [40] B. Van der Bruggen, C. Vandecasteele, T. Van Gestel, W. Doyen, and R. Leyssen, “A review of pressure-driven membrane processes in wastewater treatment and drinking water production”, *Environmental progress*, vol. 22, no. 1, pp. 46–56, 2003.
- [41] N. L. Le, M. Quilitzsch, H. Cheng, P.-Y. Hong, M. Ulbricht, S. P. Nunes, and T.-S. Chung, “Hollow fiber membrane lumen modified by polyzwitterionic grafting”, *Journal of Membrane Science*, vol. 522, pp. 1–11, 2017.
- [42] F. Meng, S.-R. Chae, A. Drews, M. Kraume, H.-S. Shin, and F. Yang, “Recent advances in membrane bioreactors (mbrs): Membrane fouling and membrane material”, *Water research*, vol. 43, no. 6, pp. 1489–1512, 2009.
- [43] E. Ricca, B. Brucher, and J. H. Schrittwieser, “Multi-enzymatic cascade reactions: Overview and perspectives”, *Advanced Synthesis & Catalysis*, vol. 353, no. 13, pp. 2239–2262, 2011.
- [44] S. Ren, C. Li, X. Jiao, S. Jia, Y. Jiang, M. Bilal, and J. Cui, “Recent progress in multienzymes co-immobilization and multienzyme system applications”, *Chemical Engineering Journal*, 2019.
- [45] A. Bruggink, R. Schoevaart, and T. Kieboom, “Concepts of nature in organic synthesis: Cascade catalysis and multistep conversions in concert”, *Organic process research & development*, vol. 7, no. 5, pp. 622–640, 2003.
- [46] R. Xue and J. M. Woodley, “Process technology for multi-enzymatic reaction systems”, *Bioresource technology*, vol. 115, pp. 183–195, 2012.
- [47] I. Wheeldon, S. D. Minter, S. Banta, S. C. Barton, P. Atanassov, and M. Sigman, “Substrate channelling as an approach to cascade reactions”, *Nature chemistry*, vol. 8, no. 4, p. 299, 2016.

- [48] R. J. Peters, M. Marguet, S. Marais, M. W. Fraaije, J. C. Van Hest, and S. Lecommandoux, "Cascade reactions in multicompartmentalized polymersomes", *Angewandte Chemie International Edition*, vol. 53, no. 1, pp. 146–150, 2014.
- [49] E. T. Hwang and S. Lee, "Multienzymatic cascade reactions via enzyme complex by immobilization", *ACS Catalysis*, vol. 9, no. 5, pp. 4402–4425, 2019.
- [50] Z. Wang, M. C. van Oers, F. P. Rutjes, and J. C. van Hest, "Polymersome colloidosomes for enzyme catalysis in a biphasic system", *Angewandte Chemie International Edition*, vol. 51, no. 43, pp. 10 746–10 750, 2012.
- [51] D. G. Ramírez-Wong, C. Coelho-Diogo, C. Aimé, C. Bonhomme, A. M. Jonas, and S. Demoustier-Champagne, "Effects of geometrical confinement in membrane pores on enzyme-based layer-by-layer assemblies", *Applied Surface Science*, vol. 338, pp. 154–162, 2015.
- [52] S. Datta, C. Cecil, and D. Bhattacharyya, "Functionalized membranes by layer-by-layer assembly of polyelectrolytes and in situ polymerization of acrylic acid for applications in enzymatic catalysis", *Industrial & engineering chemistry research*, vol. 47, no. 14, pp. 4586–4597, 2008.
- [53] S. Guedidi, Y. Yurekli, A. Deratani, P. Déjardin, C. Innocent, S. A. Altinkaya, S. Roudesli, and A. Yemenicioglu, "Effect of enzyme location on activity and stability of trypsin and urease immobilized on porous membranes by using layer-by-layer self-assembly of polyelectrolyte", *Journal of Membrane Science*, vol. 365, no. 1-2, pp. 59–67, 2010.
- [54] J. Shi, L. Zhang, and Z. Jiang, "Facile construction of multicompartment multienzyme system through layer-by-layer self-assembly and biomimetic mineralization", *ACS applied materials & interfaces*, vol. 3, no. 3, pp. 881–889, 2011.
- [55] R. M. DuChanois, R. Epsztein, J. A. Trivedi, and M. Elimelech, "Controlling pore structure of polyelectrolyte multilayer nanofiltration membranes by tuning polyelectrolyte-salt interactions", *Journal of Membrane Science*, vol. 581, pp. 413–420, 2019.
- [56] S. B. Sigurdardottir, R. M. DuChanois, R. Epsztein, M. Pinelo, and M. Elimelech, "Energy barriers to anion transport in nanofiltration membranes: Role of intra-pore diffusion", *Journal of Membrane Science*, p. 117 921, 2020.
- [57] S. Arana-Peña, N. S. Rios, C. Mendez-Sanchez, Y. Lokha, D. Carballares, L. R. Gonçalves, and R. Fernandez-Lafuente, "Coimmobilization of different lipases: Simple layer by layer enzyme spatial ordering", *International journal of biological macromolecules*, vol. 145, pp. 856–864, 2020.
- [58] D. Menne, C. Üzüüm, A. Koppelman, J. E. Wong, C. van Foeken, F. Borre, L. Dähne, T. Laakso, A. Pihlajamäki, and M. Wessling, "Regenerable polymer/ceramic hybrid nanofiltration membrane based on polyelectrolyte assembly by layer-by-layer technique", *Journal of Membrane Science*, vol. 520, pp. 924–932, 2016.
- [59] Z. Zhang, J. Muschiol, Y. Huang, S. B. Sigurdardóttir, N. von Solms, A. E. Daugeard, J. Wei, J. Luo, B.-H. Xu, S. Zhang, *et al.*, "Efficient ionic liquid-based platform for multi-enzymatic conversion of carbon dioxide to methanol", *Green Chemistry*, vol. 20, no. 18, pp. 4339–4348, 2018.
- [60] A. Trivedi, M. Heinemann, A. C. Spiess, T. Dausmann, and J. Büchs, "Optimization of adsorptive immobilization of alcohol dehydrogenases", *Journal of bio-science and bioengineering*, vol. 99, no. 4, pp. 340–347, 2005.
- [61] J. Nelson and E. G. Griffin, "Adsorption of invertase.", *Journal of the American Chemical Society*, vol. 38, no. 5, pp. 1109–1115, 1916.
- [62] A. Dwevedi, "100 years of enzyme immobilization", in *Enzyme Immobilization*, Springer, 2016, pp. 1–20.

- [63] M. Bilal, M. Asgher, H. Cheng, Y. Yan, and H. M. Iqbal, "Multi-point enzyme immobilization, surface chemistry, and novel platforms: A paradigm shift in biocatalyst design", *Critical reviews in biotechnology*, vol. 39, no. 2, pp. 202–219, 2019.
- [64] H. Hsieh, "Inorganic membrane reactors", *Catalysis Reviews*, vol. 33, no. 1-2, pp. 1–70, 1991.
- [65] D. N. Tran and K. J. Balkus Jr, "Perspective of recent progress in immobilization of enzymes", *Acs Catalysis*, vol. 1, no. 8, pp. 956–968, 2011.
- [66] M. A. Anderson and G. Sheng, *Microprobes aluminosilicate ceramic membranes*, US Patent 5,268,101, 1993.
- [67] H. Schneider, J. Schreuer, and B. Hildmann, "Structure and properties of mullite—a review", *Journal of the European Ceramic Society*, vol. 28, no. 2, pp. 329–344, 2008.
- [68] C.-H. Lee, J. Lang, C.-W. Yen, P.-C. Shih, T.-S. Lin, and C.-Y. Mou, "Enhancing stability and oxidation activity of cytochrome c by immobilization in the nanochannels of mesoporous aluminosilicates", *The Journal of Physical Chemistry B*, vol. 109, no. 25, pp. 12 277–12 286, 2005.
- [69] Y. Rasouli, M. Abbasi, and S. A. Hashemifard, "Oily wastewater treatment by adsorption–membrane filtration hybrid process using powdered activated carbon, natural zeolite powder and low cost ceramic membranes", *Water Science and Technology*, vol. 76, no. 4, pp. 895–908, 2017.
- [70] B. Nandi, R. Uppaluri, and M. Purkait, "Preparation and characterization of low cost ceramic membranes for micro-filtration applications", *Applied Clay Science*, vol. 42, no. 1-2, pp. 102–110, 2008.
- [71] S. Wanjari, C. Prabhu, T. Satyanarayana, A. Vinu, and S. Rayalu, "Immobilization of carbonic anhydrase on mesoporous aluminosilicate for carbonation reaction", *Microporous and mesoporous materials*, vol. 160, pp. 151–158, 2012.
- [72] K. De Lathouder, D. van Benthem, S. Wallin, C. Mateo, R. F. Lafuente, J. Guisan, F. Kapteijn, and J. Moulijn, "Polyethyleneimine (pei) functionalized ceramic monoliths as enzyme carriers: Preparation and performance", *Journal of Molecular Catalysis B: Enzymatic*, vol. 50, no. 1, pp. 20–27, 2008.
- [73] L. Washmon-Kriel, V. L. Jimenez, and K. J. Balkus Jr, "Cytochrome c immobilization into mesoporous molecular sieves", *Journal of Molecular Catalysis B: Enzymatic*, vol. 10, no. 5, pp. 453–469, 2000.
- [74] A. Rogina, "Electrospinning process: Versatile preparation method for biodegradable and natural polymers and biocomposite systems applied in tissue engineering and drug delivery", *Applied Surface Science*, vol. 296, pp. 221–230, 2014.
- [75] X.-J. Huang, Z.-K. Xu, L.-S. Wan, C. Innocent, and P. Seta, "Electrospun nanofibers modified with phospholipid moieties for enzyme immobilization", *Macromolecular rapid communications*, vol. 27, no. 16, pp. 1341–1345, 2006.
- [76] S. F. Anis, A. Khalil, G. Singaravel, R. Hashaikeh, *et al.*, "A review on the fabrication of zeolite and mesoporous inorganic nanofibers formation for catalytic applications", *Microporous and Mesoporous Materials*, vol. 236, pp. 176–192, 2016.
- [77] M. L. Verma, C. J. Barrow, and M. Puri, "Nanobiotechnology as a novel paradigm for enzyme immobilisation and stabilisation with potential applications in biodiesel production", *Applied microbiology and biotechnology*, vol. 97, no. 1, pp. 23–39, 2013.
- [78] J. Gabrielczyk, T. Duensing, S. Buchholz, A. Schwinges, and H.-J. Jördening, "A comparative study on immobilization of fructosyltransferase in biodegradable polymers by electrospinning", *Applied biochemistry and biotechnology*, vol. 185, no. 3, pp. 847–862, 2018.

- [79] M. M. Aldahri, Y. Q. Almulaiky, R. M. El-Shishtawy, W. Al-Shawafi, A. Alngadh, and R. Maghrabi, "Facile immobilization of enzyme via co-electrospinning: A simple method for enhancing enzyme reusability and monitoring an activity-based organic semiconductor", *ACS omega*, vol. 3, no. 6, pp. 6346–6350, 2018.
- [80] N. R. Mohamad, N. H. C. Marzuki, N. A. Buang, F. Huyop, and R. A. Wahab, "An overview of technologies for immobilization of enzymes and surface analysis techniques for immobilized enzymes", *Biotechnology & Biotechnological Equipment*, vol. 29, no. 2, pp. 205–220, 2015.
- [81] N. Durán, M. A. Rosa, A. D'Annibale, and L. Gianfreda, "Applications of laccases and tyrosinases (phenoloxidases) immobilized on different supports: A review", *Enzyme and microbial technology*, vol. 31, no. 7, pp. 907–931, 2002.
- [82] J. Luo, F. Marpani, R. Brites, L. Frederiksen, A. S. Meyer, G. Jonsson, and M. Pinelo, "Directing filtration to optimize enzyme immobilization in reactive membranes", *Journal of Membrane Science*, vol. 459, pp. 1–11, 2014.
- [83] A. Yu, Y. Wang, E. Barlow, and F. Caruso, "Mesoporous silica particles as templates for preparing enzyme-loaded biocompatible microcapsules", *Advanced Materials*, vol. 17, no. 14, pp. 1737–1741, 2005.
- [84] H. Chen, L.-H. Liu, L.-S. Wang, C.-B. Ching, H.-W. Yu, and Y.-Y. Yang, "Thermally responsive reversed micelles for immobilization of enzymes", *Advanced Functional Materials*, vol. 18, no. 1, pp. 95–102, 2008.
- [85] R. Haddad, S. Cosnier, A. Maaref, and M. Holzinger, "Non-covalent biofunctionalization of single-walled carbon nanotubes via biotin attachment by π -stacking interactions and pyrrole polymerization", *Analyst*, vol. 134, no. 12, pp. 2412–2418, 2009.
- [86] T. Zelinski and H. Waldmann, "Cross-linked enzyme crystals (clecs): Efficient and stable biocatalysts for preparative organic chemistry", *Angewandte Chemie International Edition in English*, vol. 36, no. 7, pp. 722–724, 1997.
- [87] R. Schoevaart, M. Wolbers, M. Golubovic, M. Ottens, A. Kieboom, F. Van Rantwijk, L. Van der Wielen, and R. Sheldon, "Preparation, optimization, and structures of cross-linked enzyme aggregates (cleas)", *Biotechnology and bioengineering*, vol. 87, no. 6, pp. 754–762, 2004.
- [88] M. J. Raaijmakers, T. Schmidt, M. Barth, M. Tutus, N. E. Benes, and M. Wessling, "Enzymatically active ultrathin pepsin membranes", *Angewandte Chemie International Edition*, vol. 54, no. 20, pp. 5910–5914, 2015.
- [89] J. Wang, L. Qin, J. Lin, J. Zhu, Y. Zhang, J. Liu, and B. Van der Bruggen, "Enzymatic construction of antibacterial ultrathin membranes for dyes removal", *Chemical Engineering Journal*, vol. 323, pp. 56–63, 2017.
- [90] J. P. Santos, E. R. Welsh, B. P. Gaber, and A. Singh, "Polyelectrolyte-assisted immobilization of active enzymes on glass beads", *Langmuir*, vol. 17, no. 17, pp. 5361–5367, 2001.
- [91] M. Onda, Y. Lvov, K. Ariga, and T. Kunitake, "Sequential reaction and product separation on molecular films of glucoamylase and glucose oxidase assembled on an ultrafilter", *Journal of fermentation and bioengineering*, vol. 82, no. 5, pp. 502–506, 1996.
- [92] V. Smuleac, D. Butterfield, and D. Bhattacharyya, "Layer-by-layer-assembled microfiltration membranes for biomolecule immobilization and enzymatic catalysis", *Langmuir*, vol. 22, no. 24, pp. 10 118–10 124, 2006.
- [93] J. K. Yong, G. W. Stevens, F. Caruso, and S. E. Kentish, "In situ layer-by-layer assembled carbonic anhydrase-coated hollow fiber membrane contactor for rapid co₂ absorption", *Journal of Membrane Science*, vol. 514, pp. 556–565, 2016.

- [94] N. Dizge, R. Epsztein, W. Cheng, C. J. Porter, and M. Elimelech, "Biocatalytic and salt selective multilayer polyelectrolyte nanofiltration membrane", *Journal of Membrane Science*, vol. 549, pp. 357–365, 2018.
- [95] R. Sarma, M. S. Islam, A.-F. Miller, and D. Bhattacharyya, "Layer-by-layer-assembled laccase enzyme on stimuli-responsive membranes for chloro-organics degradation", *ACS applied materials & interfaces*, vol. 9, no. 17, pp. 14 858–14 867, 2017.
- [96] R. Sarma, M. Islam, M. P. Running, D. Bhattacharyya, *et al.*, "Multienzyme immobilized polymeric membrane reactor for the transformation of a lignin model compound", *Polymers*, vol. 10, no. 4, p. 463, 2018.
- [97] G. Decher, J. Hong, and J. Schmitt, "Buildup of ultrathin multilayer films by a self-assembly process: lii. consecutively alternating adsorption of anionic and cationic polyelectrolytes on charged surfaces", *Thin solid films*, vol. 210, pp. 831–835, 1992.
- [98] X. Zan, B. Peng, D. A. Hoagland, and Z. Su, "Polyelectrolyte uptake by pems: Impact of salt concentration", *Polymer Chemistry*, vol. 2, no. 11, pp. 2581–2589, 2011.
- [99] C.-A. Ghiorghita, F. Bucatariu, and E. S. Dragan, "Influence of cross-linking in loading/release applications of polyelectrolyte multilayer assemblies. a review", *Materials Science and Engineering: C*, p. 110 050, 2019.
- [100] S. Sieber, S. Siegrist, S. Schwarz, F. Porta, S. H. Schenk, and J. Huwyler, "Immobilization of enzymes on plga sub-micrometer particles by crosslinked layer-by-layer deposition", *Macromolecular bioscience*, vol. 17, no. 8, p. 1 700 015, 2017.
- [101] J. K. Yong, J. Cui, K. L. Cho, G. W. Stevens, F. Caruso, and S. E. Kentish, "Surface engineering of polypropylene membranes with carbonic anhydrase-loaded mesoporous silica nanoparticles for improved carbon dioxide hydration", *Langmuir*, vol. 31, no. 22, pp. 6211–6219, 2015.
- [102] D. M. Reurink, J. P. Haven, I. Achterhuis, S. Lindhoud, H. Roesink, and W. M. de Vos, "Annealing of polyelectrolyte multilayers for control over ion permeation", *Advanced materials interfaces*, vol. 5, no. 20, p. 1 800 651, 2018.
- [103] H. M. Fares, Y. E. Ghossoub, R. L. Surmaitis, and J. B. Schlenoff, "Toward ion-free polyelectrolyte multilayers: Cyclic salt annealing", *Langmuir*, vol. 31, no. 21, pp. 5787–5795, 2015.
- [104] B. Khorshidi, T. Thundat, B. A. Fleck, and M. Sadrzadeh, "A novel approach toward fabrication of high performance thin film composite polyamide membranes", *Scientific reports*, vol. 6, p. 22 069, 2016.
- [105] J. R. Werber, S. K. Bull, and M. Elimelech, "Acyl-chloride quenching following interfacial polymerization to modulate the water permeability, selectivity, and surface charge of desalination membranes", *Journal of Membrane Science*, vol. 535, pp. 357–364, 2017.
- [106] W. Xie, G. M. Geise, B. D. Freeman, H.-S. Lee, G. Byun, and J. E. McGrath, "Polyamide interfacial composite membranes prepared from m-phenylene diamine, trimesoyl chloride and a new disulfonated diamine", *Journal of Membrane Science*, vol. 403, pp. 152–161, 2012.
- [107] S. Kroll, C. Brandes, J. Wehling, L. Treccani, G. Grathwohl, and K. Rezwan, "Highly efficient enzyme-functionalized porous zirconia microtubes for bacteria filtration", *Environmental science & technology*, vol. 46, no. 16, pp. 8739–8747, 2012.
- [108] G. Hollermann, R. Dhekane, S. Kroll, and K. Rezwan, "Functionalized porous ceramic microbeads as carriers in enzymatic tandem systems", *Biochemical engineering journal*, vol. 126, pp. 30–39, 2017.

- [109] X. Wang, X. Liu, C. Zhao, Y. Ding, and P. Xu, "Biodiesel production in packed-bed reactors using lipase–nanoparticle biocomposite", *Bioresource technology*, vol. 102, no. 10, pp. 6352–6355, 2011.
- [110] S. Talekar, V. Ghodake, T. Ghotage, P. Rathod, P. Deshmukh, S. Nadar, M. Mulla, and M. Ladole, "Novel magnetic cross-linked enzyme aggregates (magnetic cleas) of alpha amylase", *Bioresource Technology*, vol. 123, pp. 542–547, 2012.
- [111] S. B. Sigurdardóttir, J. Lehmann, J. Grivel, W. (Zhang, A. Kaiser, and M. Pinelo, "Alcohol dehydrogenase on inorganic powders: Zeta potential and particle agglomeration as main factors determining activity during immobilization", *Colloids and Surfaces B: Biointerfaces*, vol. 175, pp. 136–142, 2018, ISSN: 09277765, 18734367. DOI: 10.1016/j.colsurfb.2018.11.080.
- [112] H. Gustafsson, E. M. Johansson, A. Barrabino, M. Odén, and K. Holmberg, "Immobilization of lipase from mucor miehei and rhizopus oryzae into mesoporous silica—the effect of varied particle size and morphology", *Colloids and Surfaces B: Biointerfaces*, vol. 100, pp. 22–30, 2012.
- [113] M. d. de Cazes, M.-P. Belleville, M. Mougél, H. Kellner, and J. Sanchez-Marcano, "Characterization of laccase-grafted ceramic membranes for pharmaceuticals degradation", *Journal of membrane science*, vol. 476, pp. 384–393, 2015.
- [114] H. A. Dabbagh, K. Taban, and M. Zamani, "Effects of vacuum and calcination temperature on the structure, texture, reactivity, and selectivity of alumina: Experimental and dft studies", *Journal of Molecular Catalysis A: Chemical*, vol. 326, no. 1-2, pp. 55–68, 2010.
- [115] J. Xue, T. Wu, Y. Dai, and Y. Xia, "Electrospinning and electrospun nanofibers: Methods, materials, and applications", *Chemical reviews*, vol. 119, no. 8, pp. 5298–5415, 2019.
- [116] J. Long, X. Li, X. Zhan, X. Xu, Y. Tian, Z. Xie, and Z. Jin, "Sol–gel encapsulation of pullulanase in the presence of hybrid magnetic (fe₃o₄–chitosan) nanoparticles improves thermal and operational stability", *Bioprocess and biosystems engineering*, vol. 40, no. 6, pp. 821–831, 2017.
- [117] J. M. Guisan, "Immobilization of enzymes as the 21st century begins", in *Immobilization of enzymes and cells*, Springer, 2006, pp. 1–13.
- [118] Y. Wang and F. Caruso, "Mesoporous silica spheres as supports for enzyme immobilization and encapsulation", *Chemistry of Materials*, vol. 17, no. 5, pp. 953–961, 2005.
- [119] J. Hou, G. Dong, Y. Ye, and V. Chen, "Laccase immobilization on titania nanoparticles and titania-functionalized membranes", *Journal of Membrane Science*, vol. 452, pp. 229–240, 2014.
- [120] A. C. Patel, S. Li, J.-M. Yuan, and Y. Wei, "In situ encapsulation of horseradish peroxidase in electrospun porous silica fibers for potential biosensor applications", *Nano letters*, vol. 6, no. 5, pp. 1042–1046, 2006.
- [121] L. Liu, Z. Liu, H. Bai, and D. D. Sun, "Concurrent filtration and solar photocatalytic disinfection/degradation using high-performance ag/tio₂ nanofiber membrane", *Water research*, vol. 46, no. 4, pp. 1101–1112, 2012.
- [122] R. Epsztein, E. Shaulsky, M. Qin, and M. Elimelech, "Activation behavior for ion permeation in ion-exchange membranes: Role of ion dehydration in selective transport", *Journal of membrane science*, vol. 580, pp. 316–326, 2019.

Appendix

A1 Paper 1: Enzyme Immobilization on Inorganic Surfaces for Membrane Reactor Applications: Mass Transfer Challenges, Enzyme Leakage and Reuse of Materials

Sigyn Björk Sigurdardóttir, Jonas Lehmann, Simona Ovtar, Jean-Claude Grivel, Michela Della Negra, Andreas Kaiser, and Manuel Pinelo

Advanced Synthesis and Catalysis, vol. 360, no. 14, pp. 2578–2607, 2018. DOI:10.1002/adsc.201800307

VIP Very Important Publication

Enzyme Immobilization on Inorganic Surfaces for Membrane Reactor Applications: Mass Transfer Challenges, Enzyme Leakage and Reuse of Materials

Sigyn Björk Sigurdardóttir,^a Jonas Lehmann,^b Simona Ovtar,^b Jean-Claude Grivel,^b Michela Della Negra,^b Andreas Kaiser,^b and Manuel Pinelo^{a,*}

^a Technical University of Denmark, DTU Chemical Engineering, Søtofts Plads, Building 229, 2800 Kgs. Lyngby, Denmark
E-mail: mp@kt.dtu.dk

^b Technical University of Denmark, DTU Energy, Frederiksborgvej 399, 4000 Roskilde, Denmark

Received: March 8, 2018; Revised: April 9, 2018; Published online: June 5, 2018

Abstract: Enzyme immobilization is an established method for the enhancement of enzyme stability and reusability, two factors that are of great importance for industrial biocatalytic applications. Immobilization can be achieved by different methods and on a variety of carrier materials, both organic and inorganic. Inorganic materials provide the advantage of high stability and long service life which, together with the prolonged service life of the immobilized enzyme, can benefit the process economy. However, enzyme immobilization and increased stability often come at the cost of decreased enzyme activity. The main challenges involved in the design of an efficient immobilized enzyme system is to obtain both retention of high enzyme activity, enhanced stability and reusability, which is a complicated task, given the many variables involved, and the large numbers of methods and materials available. Simultaneously, new carrier materials and morphologies are constantly being developed. An investigation of enzyme immobilization systems on inorganic materials, with special emphasis on inorganic membranes, has been conducted in order to evaluate the effects of the immobilization system on the enzyme properties upon immobilization, i.e., activity, stability and reusability. The material properties of the enzyme carriers (particles and membranes) and their effects on the success of immobilization are described here. Furthermore, the reuse of inorganic membranes as enzyme carriers has been investigated and the reported examples show high ability of regeneration. To the best of our knowledge, this is the first review on enzyme immobilization focusing on the three fundamental aspects to consider when dealing with the topic: catalytic properties, enzyme leakage and reusability.

Abbreviations: β -Gal: β -D-galactosidase; ADH: alcohol dehydrogenase; AFM: atomic force microscopy; APTES: 3-aminopropyltriethoxysilane; APTMS: 3-aminopropyltrimethoxysilane; BPA: bisphenol A;

BSA: bovine serum albumin; CA: carbonic anhydrase; CALB: *Candida antarctica* lipase B; CD: circular dichroism; CDI: carbonyldiimidazole; CLEA: cross-linked enzyme aggregates; CLSM: confocal laser scanning microscopy; CNT: carbon nanotube; CPG: controlled pore glass; CRL: *Candida rugosa* lipase; DMeDMOS: dimethyldimethoxysilane; DRIFT: diffuse reflectance Fourier transform infrared; E2: 17 β -estradiol; EDC: *N*-(3-dimethylaminopropyl)-*N'*-ethylcarbodiimide hydrochloride; EDS: electron dispersive spectroscopy; FDH: formate dehydrogenase; FESEM: field emission scanning microscopy; FT-IR: Fourier transform infrared spectroscopy; GA: glutaraldehyde; GCSZn: coal fly ashes glass-ceramic zinc sulfate; GOD: glucose oxidase; GPS: 3-(glycidyloxypropyl)trimethoxysilane; HDMI: hexamethylene diisocyanate; HRP: horseradish peroxidase; IEP: isoelectric point; IPTES: (3-isocyanatopropyl)triethoxysilane; IR: infrared spectroscopy; LbL: layer-by-layer; MCP: metallic ceramic powder; MeTEOS: methyltriethoxysilane; MF: microfiltration; MML: *Mucor miehei* lipase; MNP: magnetic nanoparticle; MPTMS: 3-mercaptopropyltrimethoxysilane; NHS: *N*-hydroxysuccinimidyl; PAH: poly(allylamine hydrochloride); PEI: polyethyleneimine; PEG: polyethylene glycol; PES: polyether sulfone; PM-IRRAS: polarization modulation infrared reflection absorption spectroscopy; pNPA: *para*-nitrophenyl acetate; pNPP: *para*-nitrophenyl palmitate; PSS: polystyrene sulfonate; PTMS: phenyltrimethoxysilane; ROL: *Rhizopus oryzae* lipase; SCAD: *Saccharomyces cerevisiae* alcohol dehydrogenase; SDS: sodium dodecyl sulfate; SDS-2: sodium dodecyl sulfonate; SEM: scanning electron microscopy; TEM: transmission electron microscopy; TEOS: tetraethoxysilane; TGA: thermogravimetric analysis; TLL: *Thermomyces lanuginosa* lipase; TMP: transmembrane pressure; TTIP: titanium tetraisopropoxide; TVL: *Trametes versicolor* laccase; UF: ultrafiltration; VTMS: vinyltrimethylsilane

1	Introduction	4.2	Methods for Characterization of Enzyme Structure
2	Inorganic Support Materials for Enzyme Immobilization	5	Evaluation of Enzyme Properties upon Immobilization
2.1	Material Surface Properties for Enzyme Immobilization on Inorganic Powders	5.1	Activity
2.2	Processing of Inorganic Membranes and Concepts for Enzyme Immobilization	5.2	Stability
3	Techniques for Enzyme Immobilization on Inorganic Materials	5.3	Reusability and Leakage
3.1	Physical Adsorption	6	Reuse of Ceramic Membranes as Supports for Immobilization
3.2	Affinity Attachment	6.1	Chemical Cleaning
3.3	Entrapment/Encapsulation	6.2	Thermal Removal of Fouling
3.4	Covalent Bonding	7	Conclusions
4	Techniques for Characterization of Enzymes on Inorganic Particles	Keywords: enzyme immobilization; enzyme leakage; inorganic materials; reusability of immobilization supports	
4.1	Detection and Visualization of Enzymes on Inorganic Particles		

1 Introduction

Enzyme immobilization is a well-known technique that has been practiced for decades already, finding applications in various fields, ranging from biosensors and bone implants to waste-water treatment facilities, for the degradation of pollutants and bacteria and in organic synthesis.^[1–6] Inorganic membranes have been used as carriers in many of these applications. Immobilizing enzymes on membranes is an attractive option to combine the advantages of both enzymes and membranes; the excellent efficiency of the biocatalyst and the process intensification brought about by the membrane.^[7,8] Moreover, both enzymatic and membrane processes are usually operated under moderate process conditions, resulting in energy efficient and environmentally friendly processes. The advantages of immobilization are exploited as well, i.e., increased enzyme stability and reusability in multiple reaction cycles.^[9–11]

A number of different methods for enzyme immobilization exist, which all have their advantages and disadvantages. These have been reviewed comprehensively before.^[10,12–18] Enzymes are made insoluble upon immobilization, which greatly facilitates the recovery and reuse of the enzyme,^[19] but also introduces the mass transfer challenges of heterogeneous catalysis to the process. Immobilized enzymes often show increased resistance to process conditions as well as improved productivity, they allow continuous processes and cause limited product contamination.^[20–22] With these advantages, the technique can offer improved stability and economy of industrial processes. A few important industrial applications of immobilized enzymes include beverage clarification and the production of high-fructose corn syrup, enzymes immobilized on celite can be obtained commercially for the latter

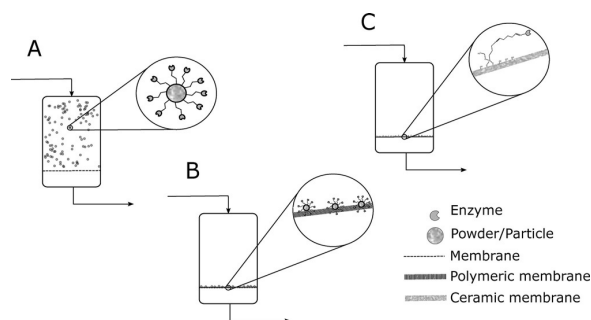


Figure 1. Three configurations of enzymatic membrane reactors with enzymes immobilized on inorganic carriers; inorganic powders or particles with immobilized enzymes suspended in solution and retained by the membrane (**A**), inorganic powders with immobilized enzymes impregnated/immobilized on a polymeric membrane (**B**), enzymes immobilized directly on inorganic membranes (**C**).

process.^[22] Nevertheless, the number of commercial processes involving immobilized enzymes does not reflect the huge research efforts within the field.^[22,23] The reluctance of the industry to applying immobilized enzymes has to do with the drawbacks of the techniques, i.e., loss of activity and cost of fabrication. Enzyme activity is often hampered by immobilization due to conformational changes in the enzyme structure and due to the previously mentioned mass transfer limitations.^[4,19,24–26] Likewise, the immobilization methods can negatively affect the enzyme activity, since they generally involve several steps where the enzyme is subject to, e.g., different reagents, shear forces and varied temperatures for shorter or longer periods, which can be detrimental to the enzyme activity. The effects of immobilization on the enzyme properties, i.e., activity, stability and reusability, vary

Sigyn Björk Sigurdardóttir was born in Iceland, in 1990. She obtained her bachelor degree in chemical engineering from the University of Iceland and master degree in chemical and biochemical engineering from the Technical University of Denmark (DTU). Since 2017, she is a Ph.D. student at DTU, Department of Chemical Engineering, where she is working on enzyme immobilization on inorganic membranes.



Jonas Lehmann was born in Køge, Denmark in 1991. He obtained his bachelor degree in chemistry and master degree in materials and manufacturing engineering both at the Technical University of Denmark. In 2017, he began his work as a Ph.D. student at the Department of Energy Conversion and Storage at the Technical University of Denmark. His research interest is the development and characterization of inorganic materials used for enzyme immobilization.



Simona Ovtar was born in Celje, Slovenia in 1983. She earned her diploma degree in chemistry at the University of Ljubljana, Slovenia and her Ph.D. degree in material science at the Jožef Stefan International Postgraduate School, Slovenia. In 2012 she worked as a research assistant at University of Nova Gorica, Slovenia and from 2013 until 2018 as a postdoctoral researcher at the Department of Energy Conversion and Storage at the Technical University of Denmark. Her research interest is the development of inorganic materials for advanced applications in energy devices and water filtration.



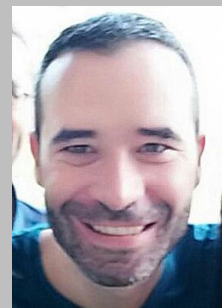
Jean-Claude Grivel was born in Geneva, Switzerland, in 1967. He obtained a Ph.D. in condensed matter physics in 1996 at the University of Geneva (Switzerland). He then worked at the Royal Institute of Technology in Stockholm (Sweden) and for Nordic Superconductor Technologies A/S (Denmark) before joining the Risø National Laboratory as senior scientist in 2000. Since 2012, he is associate professor at the Technical University of Denmark (DTU). His current research activities encompass ceramic and thin film processing as well as characterization for various applications including electro-functional materials and ultrafiltration membranes.



Andreas Kaiser was born in Bremen, Germany, in 1964. He received his Ph.D. in 1994 at the Fraunhofer Institute for Silicate Chemistry (ISC, Germany). He worked at Dornier GmbH (Germany), at the University of St. Andrews (U.K.) and in the group “Materials and Surface Engineering” at Sulzer Innotec AG (Switzerland). In 2004, he joined Risø National Laboratory as senior scientist and he is associate professor at the Technical University of Denmark (DTU) since 2012. His current research interest is in advanced porous materials for gas and liquid separation or in energy devices.



Manuel Pinelo received his Ph.D. degree in chemical engineering in 2005 and has since been working on membrane separation and enzymatic membrane reactors for biorefinery applications at the University College Cork, University of California, Davis, and the Technical University of Denmark (DTU), where he has been working as an associate professor since 2011.



Michela Della Negra, born in Italy in 1970, accomplished her master degree and Ph.D. in chemical sciences at the University of Padova. She continued her academic career as postdoc and assistant professor at Copenhagen University (Denmark) in surface science and nano-biotechnologies. From 2009, she worked as scientist and later as senior researcher at the Technical University of Denmark with a focus on ceramic processing, colloidal chemistry and fabrication of porous multi-layer ceramic structures for energy devices and water filtration membranes. She has also experience as researcher in the private sector with employment at SCF Technologies A/S and Carlsberg A/S.



with the method applied, as well as the enzyme, support and process conditions in question.^[12] There is usually a balance between the stability and activity upon immobilization, and it must be evaluated for each application which immobilization method and carrier are most suitable, considering both the effects on the enzyme properties as well as the cost of immobilization and any specific restrictions/requirements related to the intended application, e.g., in the food or pharmaceutical industries.^[22,24,27–30]

The aim of this review is to investigate enzyme immobilization on inorganic carriers, with a special emphasis on ceramic membranes, and to evaluate the effects of different immobilization systems on the enzyme properties (Figure 1). Inorganic support materials present important advantages over organic materials, such as increased chemical, mechanical and thermal resistance as well as enhanced reusability.^[31,32] Besides membranes, inorganic nanomaterials are of high interest as immobilization support given their high surface-to-volume ratio, which allows high enzyme loadings and minimized mass transfer resistance in the reaction medium.^[17,28]

In order to better understand the interactions between enzymes and inorganic support materials, the important material properties regarding enzyme immobilization, such as pore size and surface charge, are discussed, followed by a discussion on membrane fabrication methods and their effects on the material properties. The different immobilization techniques are briefly introduced, as well as techniques for characterization of the carriers and the immobilized enzymes. Finally, the enzyme properties upon immobilization and reuse of the ceramic membranes are discussed. Numerous examples of enzyme immobilization on different inorganic support materials and by different immobilization methods have been reported in recent papers and have been evaluated here. The focus on the catalytic properties of the immobilized enzyme, enzyme leakage and reusability allows the comparison between the respective methods as well as between the reported results and the general understanding of the different immobilization methods.

2 Inorganic Support Materials for Enzyme Immobilization

The general requirements of support materials for enzyme immobilization have been described elsewhere^[15,16,20,33,34] and the most important properties are briefly summarized below:

(i) Functional groups: A material's functional groups enable the covalent bonding of enzymes;

- (ii) Physical parameters: Particle size, pore structure and active surface area are of great importance, this subject will be explored in detail in the following sections;
- (iii) Chemical stability: The material should be inert towards the enzyme and unaffected by the reaction media after immobilization. This is critical for the cleaning processes for the reuse of ceramic membranes;
- (iv) Microbial resistance: The material should be resistant to contamination by microbial growth;
- (v) Thermal stability: The material should be resistant to chemical or physical changes caused by increased temperature;
- (vi) Mechanical stability: The material should be applicable under different working conditions without deforming or breaking.

Immobilization support materials are usually placed in two categories: organic and inorganic. The focus of this review is on inorganic materials as they do present the required properties mentioned above. Vast numbers of different inorganic support materials and morphologies have been suggested for enzyme immobilization.^[35–41] Traditionally, various silica-based materials have been preferred as inorganic carriers for enzyme immobilization. In that sense, immobilization on celite and controlled pore glass (CPG) have been commonly reported,^[20,21] and commercial processes involving celite as enzyme carrier have been established.^[22] Nevertheless, new materials are constantly being developed, which offer new opportunities for a more efficient immobilization. There is a great interest in highly porous nanoparticles with ultra-high surface area, and therefore silica is still commonly used.^[33] Mesoporous silica, for instance, can offer surface areas larger than $700 \text{ m}^2 \text{ g}^{-1}$.^[42] Other commonly used inorganic particles include titania and zirconia.^[35,42,43] Iron oxide nanoparticles are currently of high interest due to their magnetic properties. The magnetic properties can simplify the cleaning and separation of particles from solution. The separation is achieved by applying a magnetic field to the particle dispersion, which will attract the magnetic nanoparticles (MNPs). MNPs are useful for avoiding the harsh and time-consuming centrifugation steps normally used after enzyme immobilization.^[44] MNPs usually consist of iron oxide coated with a thin layer of silica to avoid agglomeration and to improve the chemical stability.^[44,45] Details of the mentioned examples and other recent examples are listed in Table 1. The active research of enzyme immobilization has led to the development and improvement of new materials used for immobilization of enzymes. While the primary focus of this review is on inorganic membranes, it is still important to review the current state of immobilization on inorganic particles as the research can be

Table 1. Commonly used inorganic particles for enzyme immobilization reported in recent years (2012–2017).

Material	Properties	Enzyme	Application	Ref.
silica	particle size (nm): 40–1000 surface area (m ² /g): 463–606 pore width (nm): 9.1–9.4 total pore volume (cm ³ /g): 0.91–1.18	lipase	hydrolysis of 4-nitrophenyl acetate to 4-nitrophenol	[46]
silica	particle size (nm): 1000–20000 surface area: (m ² /g): 641 pore width (nm): 2–25	<i>Candida rugosa</i> lipase (CRL)	hydrolysis of <i>p</i> -nitrophenyl palmitate (pNPP)	[47]
silica	particle size (nm): 40 pore width (nm): 9	glucose oxidase (GOD) or horseradish peroxidase (HRP)	cascade reaction forming 2,3-diaminophenazine	[48]
silica	particle size (nm): 288–480 surface area (m ² /g): 292–723 pore width (nm): 13.2–14.4 pore volume (cm ³ /g): 0.9–1.8	formaldehyde dehydrogenase	detection of formaldehyde	[42]
zirconia	particle size (nm): 500 surface area (m ² /g): 14 pore width (nm): >50	CRL	hydrolysis of pNPP	[47]
zirconia	particle size (nm): 275 surface area (m ² /g): 70.55 pore width (nm): 12.2 pore volume (cm ³ /g): 0.2	formaldehyde dehydrogenase	detection of formaldehyde	[42]
titania	particle size (nm): 20 surface area (m ² /g): 60	<i>Trametes versicolor</i> laccase (TVL)	biocatalytic degradation of recalcitrant micropollutants	[35]
titania	particle size (nm): 20	<i>P. ostreatus</i> laccase	viocatalytic degradation of recalcitrant micropollutants	[43]
iron oxide	particle size (nm): <30	laccase	decolorization of phenolic azo dyes	[45]
iron oxide	particle size (nm): 25 surface area (m ² /g): 42	CRL	synthesis of pentyl valerate in cyclohexane	[49]

useful for membrane applications. The materials of the inorganic particles considered for enzyme immobilization exhibit different properties, which result in specific advantages and disadvantages, depending on the interactions between the specific inorganic material and the enzyme.

2.1 Material Surface Properties for Enzyme Immobilization on Inorganic Powders

An interesting concept for enzyme immobilization is to not only look at the materials used, but also the possibilities for altering the physical parameters of the materials in order to create an optimal environment for the enzymes. There are many different surface properties that affect the success of immobilization including (i) electrostatic forces, (ii) particle size, and (iii) pore size. These properties have to be specifically tailored towards the enzyme in question as a particular parameter may lead to a successful immobilization of one enzyme while being incompatible with another enzyme, as discussed in the following sections.

2.1.1 Electrostatic Forces

It is critical to consider the electrostatic forces of the support material and the enzyme because these forces have an impact on the efficiency of the immobilization process. The surface chemistry of inorganic particles changes when functionalization agents (Section 3.4.2) and enzymes are attached to the particles, which is a research area that has not yet been fully explored.^[47,50] The pH value at which an enzyme or a particle has an overall neutral charge (zeta potential is zero, $\zeta=0$) is known as the isoelectric point (IEP).^[51] The zeta potential is the potential difference across a particle-liquid phase boundary and it is a key element for indicating the stability of colloidal dispersions. The separation of the zeta potential from the IEP expresses the amount of electrostatic repulsion between particles. At $\zeta=0$ the repulsion is very small and the dispersed particles or enzymes will rapidly agglomerate. For a colloidal dispersion to be moderately stable in water and other polar media, a potential of ± 30 mV is required.^[47]

The electrostatic forces are crucial for immobilization of enzymes on particles by physical adsorption.

During physical adsorption of enzymes a new surface is formed, which shifts the IEP of the inorganic particle towards the IEP of the enzyme. Once a monolayer of enzyme is adsorbed on the inorganic particle surface, the IEP will be identical to that of the enzyme, as demonstrated by Rezwan et al.^[50] In this research, bovine serum albumin (BSA) was physically adsorbed onto alumina particles. By repeating the immobilization process with an increasing amount of enzyme, it could be seen how the IEP is shifted until it became constant as a monolayer of BSA had been formed. Further adsorption was still possible, but not visible by zeta potential measurements.

The zeta potential may also be used as a tool for evaluating the extent of enzyme immobilization. Zivkovic et al.^[47] immobilized CRL onto silica and zirconia powders by physical adsorption using different buffer solutions. By changing the pH of the dispersion, it was possible to change the zeta potential of the particle and enzyme. It was discovered that a higher absolute zeta potential of the particles resulted in a larger amount of adsorbed lipase. Therefore, knowledge of the zeta potential may help in predicting immobilization efficiency. Oppositely charged particles and enzymes should create electrostatically favorable conditions, whereas particles and enzymes of similar charge should lead to repulsion. However, this does not mean that a negatively charged enzyme is unable to attach to a negatively charged particle.^[47] Gustafsson et al.^[46] immobilized two different lipases, from *Mucor miehei* (MML) and *Rhizopus oryzae* (ROL), onto mesoporous silica and found that the enzyme loading of MML was 20% higher compared to that of ROL at pH 6, but lower at a higher pH, indicating that MML loading was more dependent on pH compared to ROL. The support material was mesoporous silica with IEP = ca. 2, whereas the IEPs of MML and ROL are 3.8 and 7.6, respectively. Both silica and MML are thus negatively charged at pH values 5–8, i.e., under the experimental conditions. By increasing the pH, both silica and MML become more negatively charged, resulting in lower enzyme loading. In contrast, ROL loading on silica did not show the same dependence on pH. This could be due to ROL being positively charged or slightly negative (at pH 8) and silica being negatively charged at pH 5–8. However, it is important to note that this example focuses only on enzyme loading and zeta potential, but this is not necessarily the only influential factor.

2.1.2 Particle Size

Particle size can have a great impact on enzyme immobilization. A smaller particle yields a higher surface area which, in principle, translates into more possible space for enzymes to attach. However, the con-

cept is much more complicated. Vertegel et al. demonstrated the influence of particle size in their research where chicken egg lysozyme was physically adsorbed on the surface of silica nanoparticles with three different particle sizes, 4, 20 and 100 nm, under otherwise similar conditions. Enzyme adsorption behaved vastly differently depending on the particle size. For 4 nm silica particles the enzyme was not able to effectively form a layer on the surface, which could be due to the fact that the colloidal particle is around the same size as the enzyme. For 20 nm silica particles the enzyme was effectively immobilized, forming a thin monolayer on the surface. The 20 nm particles also resulted in the highest enzyme activity. The 100 nm silica particles showed the highest enzyme loading, but lower enzyme activity compared to the 20 nm silica particles. As the particle size increases the surface curvature decreases, which can affect the physical adsorption of enzymes. A low surface curvature means that the parts of the enzyme that are not in direct contact with the particle are closer to the surface and thereby more affected by the electrostatic forces. This can cause the enzyme to stretch out on the particle surface resulting in deactivation of the enzyme. It can even lead to multiple layers of enzymes being attached to the surface, which would result in more inactive enzymes. In conclusion, the enzyme immobilization yields different results depending on the particle size.^[52] To support the results Vertegel et al. analyzed the α -helix content of the enzyme, which is a secondary structure located in proteins. The α -helix content was found to decrease with increased particle size. It was concluded that the 20 nm particles had the highest activity as they provided the best combination of sufficiently high enzyme load and α -helix content.

2.1.3 Pore Size of Porous Inorganic Particles

Just like the particle size, smaller pore size results in a higher surface area. However, a pore that is smaller than the enzyme is ineffective as the enzyme cannot be immobilized inside the pore. A suitable pore size also depends on the specific enzyme, some enzymes are more active in compact spaces whereas other enzymes may need bigger pores to unfold. Gustafsson et al.^[53] studied mesoporous silica particles with the same particle size, but with varying pore sizes. In their research, silica particles with pore diameters of 5, 6 and 8.9 nm were used as carriers for the immobilization of either trypsin from bovine pancreas or lipase from *Mucor miehei* by encapsulation. It was discovered that the 6 nm pores were most fitting for trypsin. The diameter of trypsin in this research is 3.8 nm and the 5 nm pores were too narrow, resulting in a decreased diffusion rate. The enzyme loading for

pore sizes 6 and 8.9 nm was almost identical and immobilization occurred instantly. The rapid immobilization could be due to the electrostatic forces since the immobilization was carried out at pH 7.6, meaning that there was a high attraction between the silica particles (IEP around 2) and trypsin (IEP 10.5). While the enzyme loading of trypsin was similar for pore sizes of 6 and 8.9 nm the activity was much higher with the 6 nm pores. An explanation for this could be that the confined space of 6 nm provided the best protection for trypsin, which is required as trypsin undergoes autolysis, i.e., a self-reaction within the enzyme. Performing the same immobilization but with lipase instead of trypsin completely changed the immobilization. The lipase used here is a slightly bigger enzyme, with a diameter of 4.5 nm, compared to the 3.8 nm of the trypsin used. This resulted in poor immobilization for the pore sizes of 5 and 6 nm, as the pores were too narrow. With the 8.9 nm pores the catalytic activity of immobilized lipase actually surpassed that of free lipase, yielding more than double the activity. It is believed that lipase was activated by the hydrophobic/hydrophilic surface interface inside the pores. The surface consists of many hydrophilic silanol groups, however, some of these are converted into hydrophobic siloxanes during the calcination steps of the powder processing. The active sites of lipase are covered by a surface loop. As the enzyme is immobilized it unfolds causing the surface loop to move away from the active sites creating more access to the active sites. Additionally, Gustafsson et al.^[46] immobilized two types of lipase, from *Mucor miehei* and *Rhizopus oryzae*, onto mesoporous silica with the same pore size of 9 nm but with particle sizes of 300 and 1000 nm. It was discovered that the enzyme loading (mg enzyme g⁻¹ particle) was almost identical for both particle sizes, but the enzyme activity differed greatly, with the 300 nm particles having higher specific activity. With bigger particles the length of the pores increases and, according to Gustafsson et al., lipase exerts its catalytic action close to the pore openings so that enzymes located further inside the particle may not contribute to the activity. This underlines the importance of choosing the correct geometric properties of the particles, as they vary depending on the specific enzyme. Even small changes in the geometry can greatly affect the activity of the enzyme. The pores have to be large enough to allow diffusion of enzymes into the pores, but not so large that enzyme unfolding or leakage becomes an issue.^[53–59]

2.2 Processing of Inorganic Membranes and Concepts for Enzyme Immobilization

To combine the good immobilization properties of an inorganic powder with a separation technique, the

powder may be processed into a membrane. Enzyme immobilization on membranes allows for continuous processes where the enzymes are immobilized in/on the membrane and thus kept separated from the end product.^[38,60] The following section provides a short description of the use and implementation of inorganic materials in membranes and the techniques for fabrication of ceramic membranes with different geometries.

Inorganic membrane materials: Membranes may be processed from polymers,^[24] inorganic materials^[60] or a composite mixture where the inorganic powder is implemented as part of a polymer solution.^[35] For this review, the focus is on inorganic membranes. Examples of the most common inorganic materials used for inorganic membranes are alumina, titania, zirconia, silica and silicon carbide.^[61] In fact, these are the same materials as the ones used for enzyme immobilization on inorganic powders, as discussed in the previous section. The important properties of the powders regarding enzyme immobilization also apply to the membranes.

Inorganic membrane geometries: Inorganic membranes have two distinct structures with respect to the morphology through the thickness of the membrane; symmetric and asymmetric. Symmetric membranes have a uniform cross section whereas asymmetric membranes consist of a relatively thick, porous support layer and thinner and denser separation layer(s). Inorganic membrane geometries are commonly either planar, tubular or hollow fibre, as illustrated in Figure 2. For microscopic images of asymmetric structures, the work of Tsuru et al.^[62] is referred to for multi-layered structures and Kingsbury et al.^[63] for hollow fibres. It is also possible to combine geometries as seen in many commercial membranes where tubes are embedded in a planar structure. The relevant membrane configuration for enzyme immobilization is an asymmetric membrane in the range of microfiltration (MF) or ultrafiltration (UF).

2.2.1 Steps in the Fabrication of Inorganic Membranes

As described before, inorganic membranes usually require an asymmetric structure, consisting of a relatively thick, porous support layer with a large pore size (usual thickness several millimeters and pore size in the micron range) and thinner, finely porous separation layers. For example, for a UF membrane with a final separation layer thickness of a few hundred nanometers and a pore size of a few tenths of nanometers, usually, a stepwise addition of layers with decreasing thickness and pore size on top of the porous support is required to reduce excessive pressure drops and to avoid the formation of processing defects in

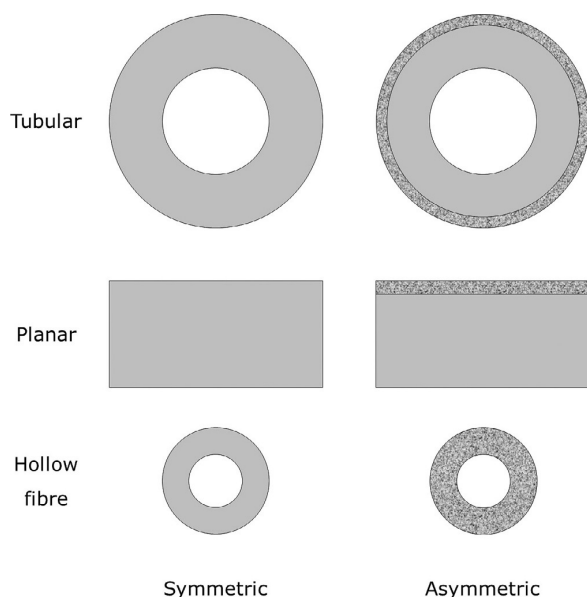


Figure 2. Typical geometries of symmetric and asymmetric membranes.

the final separation layer. The fabrication of such multilayer structures can be achieved by different ceramic processing techniques depending on the final membrane type [micro-/ultra- or nanofiltration (NF)] and on the desired geometry. In the following, the fabrication of ceramic membranes is briefly introduced and the implications are explained on specific geometries.

Inorganic membranes consisting of metal oxides are prepared by methods based on ceramic process-

ing.^[64] This involves the following steps: ceramic powder preparation, shaping, drying, and sintering. The procedure is illustrated in Figure 3, where a schematic for the fabrication of tubular membranes is shown as an example, but the general process is also applicable to other geometries. Normally, fabrication starts with a particle slurry or paste consisting of the inorganic material as a powder mixed with solvent, organic additives and binders. Organic additives are added in order to obtain a stable dispersion and desired rheology of the slurry. Binders are for cohesion between particles and provide strength to avoid crack formation during drying and sintering. The mixture is shaped to form the green body, which is then dried to remove solvents and organic additives and finally sintered. Sintering is the appliance of thermal energy to the powder compact after the shaping step in order to induce grain growth and densification.^[65] Sintering of solids occurs over three stages: initial, intermediate and final. During the initial sintering step, neck formation between particles occurs, the particles merge through diffusion throughout the intermediate stages, and the final sintering stage is the densification and elimination of isolated pores. By controlling the sintering, it is possible to control the microstructural changes and the porosity of the ceramic membrane. A higher temperature leads to more rapid grain growth and densification, which results in a support structure with large particles and a low surface area. To follow up on the general procedure, three specific processes will be discussed further: fabrication of the inorganic porous support structure, the separation layer(s) and hollow fibres.

Inorganic porous support structure: For inorganic porous supports, the material of choice is usually α -

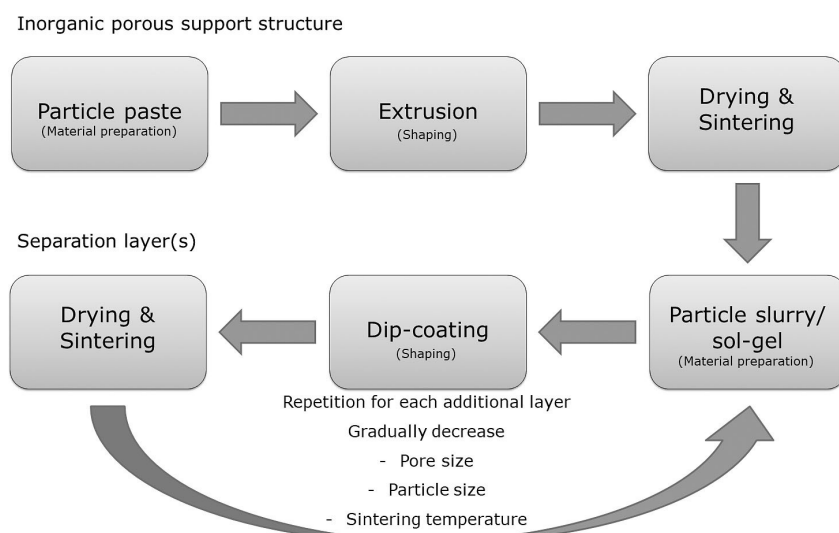


Figure 3. Schematic diagram for the fabrication of inorganic asymmetric tubular membranes.

alumina^[61] and processing starts with raw powder conditioning for alumina. Aluminum is mainly occurring naturally as bauxite [Al(OH)₃], extracted from the earth by mining, and processed to produce alumina powder. Powder properties are important, as large pores (1–15 μm) are a requirement to avoid pressure drops.^[64] To achieve this, the particles must be relatively large since the pore sizes are around three times smaller than the particles. The support must also be sufficiently thick in order to provide mechanical strength. When the powder has been prepared, it is made into a slurry or paste and shaped. To shape the support structure, techniques such as extrusion are used to create tubular structures. The shaping methods for planar shapes are casting or pressing. When the precursor formation is obtained, it is dried followed by high temperature sintering.

Separation layer(s): As the porous support structure has been prepared, one or more separation layers may be deposited on top to achieve MF/UF membranes. Particle and pore sizes of the separation layers are reduced gradually in order to avoid the coating layers from collapsing and sinking into the larger pores of the support. With normal powder processing, it is possible to achieve pore diameters down to 100 nm.^[62] A controlled particle size and narrow particle size distribution of the powder is required, which is achieved by mechanical milling to break down agglomerates. For pore sizes below 100 nm, much finer particles and very narrow particle size distributions are required, the pore size range of 1–50 nm can be more easily obtained by a sol-gel process.^[61,62] In this process, metal alkoxides or inorganic salts are hydrolyzed followed by condensation to form a sol (nanoparticles in solution). An example of this is given here for the preparation of TiO₂ nanoparticles.^[62] Titanium tetraisopropoxide (TTIP) is mixed in an aqueous solution with an acid such as HCl. Hydrolysis and condensation results in the TiO₂ sol. The particle size depends on the concentration of TTIP, the water/acid ratio and duration of hydrolysis. A suitable porous support structure can then be coated with the TiO₂ sol by an appropriate coating technique, for example by dip-coating. Subsequently, the coating is dried and sintered. The sol preparation, the drying and sintering (temperature) of the applied layer must be controlled carefully to achieve a defect-free coating with a very narrow pore size distribution. Lowering the sintering temperature reduces the pore size and increases the porosity.^[66] In conclusion, the fabrication of inorganic multilayer membranes requires an increasing number of complex coating and firing steps if the pore size of the membrane separation layer is to be reduced from MF to UF and NF.

Hollow fibres: Fabrication of hollow fibres differs from the procedures seen for planar and tubular membranes. Here, a combined phase inversion and

sintering technique is used. An example was given by Kingsbury et al. for alumina hollow fibres.^[63] A suspension consisting of alumina particles of three different sizes was prepared, the suspension was extruded through a tube-in-orifice spinneret and into a coagulation bath where the hollow fibres were left in order to complete phase inversion. The fibres were immersed in water to remove *N*-methyl-2-pyrrolidone that was used in the suspension. Finally, the fibres were calcined and sintered to create alumina hollow fibres. This differs from the methods of systematically adding layers as seen for the fabrication of tubular and planar membranes, since asymmetry can be achieved in a single process for hollow fibres. Phase inversion has furthermore the advantage that it creates a structure within the membrane, which consists of an outer sponge-like region with large finger-like voids with low tortuosity.

2.2.2 Effects of Fabrication on Membrane Properties

An important aspect to consider is the structural changes of the ceramic materials caused by the sintering steps. The crystal structure changes depending on the particle size and sintering temperature. A specific example of this would be to look at the crystal structure of titania, which is one of the common materials of inorganic membranes. Ding et al.^[67] investigated the phase transformation of titania from anatase to rutile with three different particle sizes. It was discovered that smaller particles undergo phase changes at lower temperatures compared to bigger particles. This is important for determining the sintering steps and the possibility to either retain or change the crystal structure. Different crystal structures may also show different hydration behavior. The surface hydroxy density is an important factor in enzyme immobilization since the hydroxy groups are used to bind linking agents that can covalently bond with enzymes, which is a topic explained in the upcoming section. The hydroxy groups on inorganic surfaces are eliminated through temperature increase.^[68,69] It is however possible to reacquire the hydroxy groups that are lost after sintering. Hydroxy groups are naturally formed by hydration of water vapor in the atmosphere,^[70] however, this is a slow process. Hummer et al.^[71] investigated the hydration behavior of anatase and rutile and found that 96% of water molecules remained stable on anatase, whereas rutile had a higher tendency to dissociate water to form hydroxy groups and only 75% of the water molecules remained stable on the surface. Instead, the membrane surface may be activated by reaction with chemicals such as hydrogen peroxide in order to form hydroxy groups on the surface.

Locations for enzyme immobilization in asymmetric membrane structures: Depending on the membrane morphology, enzymes can be immobilized in different locations of the asymmetric inorganic membrane structure. As described above, an asymmetric UF/MF inorganic membrane consists of multiple layers where an enzyme could be attached, i.e., the support layer and the separation layer(s), as shown in Figure 4.

The separation layers (a) are very thin, resulting in low overall open pore volume, even though the surface area is high. The support layer (b) on the other hand, is relatively thick giving a high overall pore volume, whereas the surface area is very small because of the large sintered particles. Immobilizing enzymes in area (a) is very likely to result in pore blockage, fouling and a heavily reduced flux as the enzymes are attached to very narrow pores, which is also a problem experienced with polymeric membranes.^[24] Similar issues were also discussed in the previous section on mesoporous particles. Enzymes immobilized in area (b) should not cause any significant reduction in flux as the pore diameter in this layer is sufficiently high. However, with such a low surface area, the enzyme loading is expected to be low and larger pores offer less protection to the enzyme, which can result in heavy enzyme leakage. This leads to different options for enzyme immobilization in inorganic membranes. One option is enzyme immobilization in the inorganic membrane as just described, which will likely result in low enzyme loading. Another option is to modify the surface through surface treatment or the previously mentioned activation, for example, with impregnation of a highly active, high surface area powder. The overall surface area may be increased considerably by this method, which simultaneously increases the enzyme loading potential and provides small narrow spaces for protection of the enzyme and minimized leakage. The inorganic surface of membranes, powders and particles can be made more susceptible to enzyme immobilization by different activation methods, as will be described in the coming section.

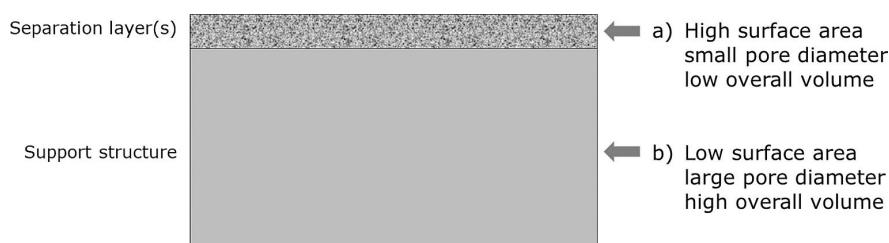


Figure 4. Two distinct areas where enzymes may attach on an inorganic membrane.

3 Techniques for Enzyme Immobilization on Inorganic Materials

Enzyme immobilization is achieved by different physical and chemical methods. The common methods include physical adsorption, entrapment/encapsulation, covalent bonding, affinity attachment and self-immobilization by cross-linking. These methods are illustrated in Figure 5. The last method differs from the others in that it does not require a carrier for the immobilization.^[16,72] The other methods are applicable to inorganic surfaces.

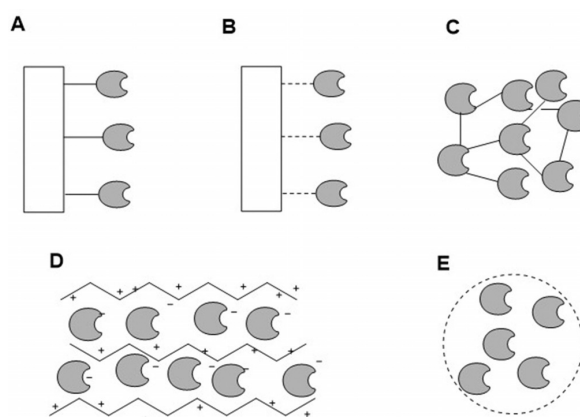


Figure 5. The most common enzyme immobilization techniques illustrated; covalent bonding (A), physical adsorption (B), cross-linking (C), entrapment (D) and encapsulation (E).

3.1 Physical Adsorption

Physical adsorption is one of the most simple immobilization techniques. It is based on physical interactions of the carrier and enzyme such as dipole-dipole, ionic forces, hydrophobic/hydrophilic, van der Waals forces, hydrogen bonding and electrostatic forces. Electro-

static forces play an important role in the physical adsorption onto ceramic materials, since both the ceramic materials and the enzymes are typically charged in aqueous solutions and the degree of adsorption can thereby be controlled by the pH of the solution and/or by the right pairing of enzyme and support material based on their IEPs.^[73,74] The immobilization can be carried out simply by immersing the carrier in the enzyme solution. The enzyme retains much of its activity but typically gains little stability and is easily lost as it leaches from the support.^[16,19,24,25] This can particularly be seen in studies where different immobilization methods have been compared, for instance, TVL physically adsorbed onto TiO₂ nanoparticles lost 50% of its activity after being immersed in buffer for six days, while both covalently bonded and cross-linked TVL on the same carrier retained over 90% activity after the same treatment.^[35] Similarly, the activity retention after eight batches of reaction catalyzed by adenosine deaminase either physically adsorbed or covalently bonded onto TiO₂ microparticles was 10% and 80%, respectively.^[75] On the other hand, the higher activity retention of physically adsorbed enzyme compared to covalently bonded enzyme was seen in a study where the enzyme Esterase EreB from genetically modified *E. coli* was immobilized on TiO₂ membranes, the adsorbed enzyme showed an almost 30% higher pollutant degradation rate than the covalently bonded enzyme, even at lower enzyme loading, or 4.4 mgL⁻¹ physically adsorbed vs. 7.7 mgL⁻¹ covalently bonded enzyme.^[4] In addition to TiO₂ particles and membranes, various types of inorganic supports have been used for enzyme immobilization by physical adsorption, for example, silica, alumina and zirconia membranes, particles and powders.^[4,35,47,76–78]

3.2 Affinity Attachment

Affinity attachment is an alternative immobilization method, which is based on strong, non-covalent bonds that are more specific than the bonds formed in physical adsorption. The specific bonds are formed between affinity tags on the enzyme and carrier, e.g., biotin and avidin/streptavidin or polyhistidine and bivalent metal ions.^[14,72] The affinity tags are either found in the enzyme naturally or they must be attached to the enzyme by genetic engineering.^[18] The strong, yet non-covalent bonds offer both reversibility, high stability and high activity, but a drawback of this method is the often high degree of complexity.^[14,16] A more simple approach to affinity attachment has been described in recent papers, where the enzyme is immobilized by affinity interactions between the enzyme and bivalent metal ions that have been mixed with the enzyme carrier, for example, metal ceramic

powder (MCP) or ceramic hydroxyapatite. The results still show high enzyme activity and stability.^[6,79,80]

3.3 Entrapment/Encapsulation

Enzymes can be entrapped or encapsulated within solid structures, e.g., in membranes and sol-gels, either by incorporating them in the manufacturing process, or by filtering an enzyme solution through a membrane so that the enzymes will be trapped in the pores.^[24] Alternatively, enzymes can be entrapped in a network of polyelectrolytes of alternating charges assembled using a layer-by-layer (LbL) method. For the latter, charged polymers such as polyethyleneimine (PEI), poly(allylamine hydrochloride) (PAH), polystyrene sulfonate (PSS) and chitosan have been applied to grow LbL films on solid supports, e.g., silicon wafers, polymeric and polycarbonate membranes and glass slides. The enzyme is introduced into the growing LbL film by exploiting the electrostatic charges of the enzyme, so that a layer of enzymes is formed and entrapped between the layers of oppositely charged polymers.^[38,81] Entrapment and encapsulation provide a protective microenvironment within the solid supports and have little effect on the enzyme structure, the catalytic efficiency is however often hampered by mass transport limitations.^[18,34,82] Likewise, the enzymes are easily lost due to leakage from the support, therefore, the method is often combined with other methods, such as cross-linking, to enhance the reusability of the enzyme.^[37]

3.4 Covalent Bonding

Covalent bonding provides the strongest interactions between enzyme and carrier and is one of the most widely used immobilization methods.^[16,34] Covalent bonding is a multi-step process that generally requires the promotion of reactive groups on the inorganic surface as a first step, followed by functionalization and activation and lastly reaction with the enzyme. For the purpose of enzyme immobilization, surface activation and functionalization provide the link between the surface and the enzyme in the form of functionalizing and activating agents. The enzyme is then attached to the activating agent, typically through the ϵ -amino group of lysine, the thiol group of cysteine or the carboxylic group of aspartic and glutamic acids.^[16] The procedure and the terminology used here are illustrated in Figure 6, the commonly used functionalizing and activating agents, 3-aminopropyltriethoxysilane (APTES) and glutaraldehyde (GA) are shown.

The covalent methods are complicated in practice, as they require multiple, time-consuming steps and often expensive and/or toxic reagents. The enzyme ac-

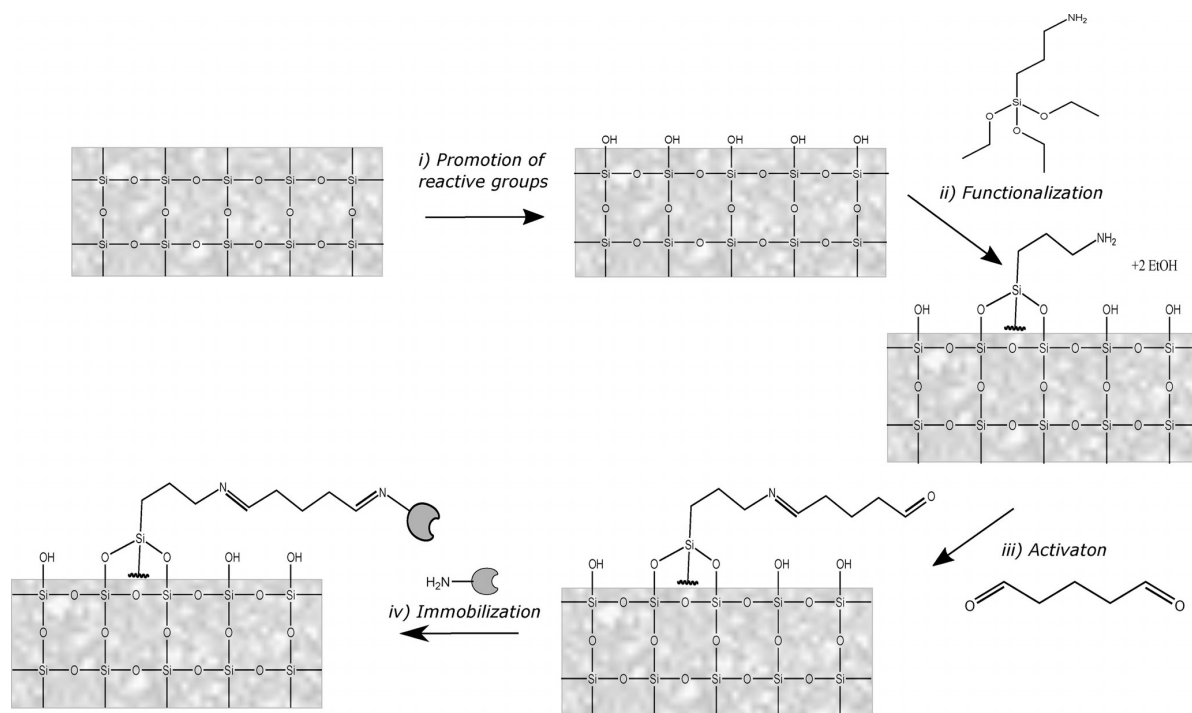


Figure 6. A schematic diagram of the multi-step procedure for covalent immobilization on a ceramic surface. The example shows (i) the promotion of reactive groups on the ceramic surface, (ii) functionalization with APTES (EtOH stands for ethanol), (iii) activation with GA and (iv) immobilization of the enzyme.

tivity often decreases upon covalent immobilization due to conformational changes of the enzyme and/or decreased mobility but, in return, the covalent bonds give high stability and reusability of the catalyst.^[19,34] The properties of the immobilized enzyme can be controlled to a certain extent by the choice of reaction conditions, the functionalizing and activating agents and other factors. A number of functionalizing and activating agents has been successfully used for covalent enzyme immobilization, such as organosilanes, gelatin and PEI for functionalization and GA, carbodiimides and carbonyldiimidazole (CDI) for activation. APTES and GA are without a doubt the most widely used agents.^[34,40] A detailed description of the methods and the chemistry of functionalization by the above-mentioned and more agents on inorganic surfaces, notably silica surfaces, can be found in a recent review by Zucca and Sanjust.^[34] The different steps of surface functionalization prior to immobilization are briefly described below.

3.4.1 Promotion of Reactive Groups on Ceramic Surfaces

Unlike most inorganic surfaces, which naturally exhibit a high degree of hydroxylation,^[34] ceramic materials

generally require the promotion of reactive groups, or surface activation, as a first step of the covalent immobilization strategy. This is due to the absence or lack of reactive groups on the untreated surface,^[13,83] since ceramic materials undergo a decrease in surface area and activity during the fabrication process, e.g., calcining and high temperature sintering.^[73,78,84] Surface activation of ceramic materials entails the promotion of hydroxy groups on the surface. This can be achieved by chemical and physical methods, such as by treatment with acids or bases, or with thermal treatments.^[40,73] A common practice is to combine different methods, notably using chemical methods in conjunction with, e.g., sonication,^[2,29,85] elevated temperatures^[86–89] and/or microwave assistance.^[90–92]

One of the most commonly encountered surface activation agents in the literature is piranha solution (H_2O_2 and H_2SO_4 , ca. 1/3 v/v). The support, for example, silica, alumina and zirconia, is immersed in the piranha solution for up to an hour, sometimes with heating.^[29,41,93–95] Kroll et al.^[93] compared four different surface treatments for the hydroxylation of a zirconia membrane; piranha solution at room temperature and 95 °C, NaOH at 95 °C and a hydrothermal treatment using steam. The highest loading capacity of hydroxy groups was obtained by using piranha solution; the number of OH groups on the surface increased from

0.5 to 1.2 OH/nm², or by a factor of 2.4, as compared to the untreated surface. The piranha solution was more effective than the NaOH and hydrothermal treatments, but the temperature did not affect the loading capacity, as similar loading capacities were obtained with piranha solution at room temperature and 95 °C. Other acidic and chemical treatments are also commonly used, e.g., using concentrated or dilute acids,^[90,96,97] acetone and/or ethanol.^[2,35,98,99] Alternatively, water can be used for surface hydroxylation, as has been successfully applied on alumina and titania surfaces.^[4,11,100]

3.4.2 Functionalization

Functionalization is the introduction of a functionalizing agent to a surface to tailor the surface properties for a specific purpose. The functional groups, for example, hydroxy, epoxy or amine groups, are attached to the surface either covalently or by physisorption.^[40] Enzyme immobilization is one important objective of functionalization, but by far not the only one, the technique is also used for fouling mitigation and to change the adsorptive or hydrophilic character of a surface for removal of heavy metals, gas separation or impregnation of metal catalysts onto surfaces, to name but a few alternatives.^[31,99,101–105] Common functionalizing agents for enzyme immobilization include organic compounds such as organosilanes and polymers such as PEI, polyethylene glycol (PEG) and gelatin.^[40]

Functionalization using polymers is obtained by coating the support with the polymer rather than by forming direct covalent bonds between the polymer and support.^[83] The polymers, usually gelatin or PEI, are water soluble (the branched PEI polymer, not the linear) and contain amino groups that can be further derivatized by the activating agents which are used to attach the enzyme. The polymers are thus activated to form covalent bonds with the enzyme, unlike in the entrapment method where the enzyme is entrapped between polymer layers due to electrostatic forces.^[106,107] This method is conveniently applied to membranes, which can be coated with biopolymers in a simple procedure where a polymer solution is filtered through the membrane. A thin polymer layer can be obtained which is compacted under the pressure applied during filtration.^[4,11,83] PEI is found to provide a hydrophilic environment for the enzyme, has protein stabilizing effects and offers multi-point attachment of the enzyme.^[106,107] The polymer layer, even though very thin, inevitably affects the permeability of the membrane. Chea et al.^[83] found the water permeability of a 0.2 μm alumina membrane to decrease from 1000 L (hm²bar)⁻¹ for the native membrane, to 20 and 4.5 L (hm²bar)⁻¹ for the biocatalytic

membranes prepared with 1 and 10 gL⁻¹ gelatin solutions, respectively. Likewise, the biocatalytic membranes prepared by Cazes et al.^[9] showed a decrease in permeability of 4244 L (hm²bar)⁻¹ for the raw support to below 400 L (hm²bar)⁻¹ for the gelatin coated membranes. In their work, laccase was immobilized on 0.2 μm and 1.4 μm alumina membranes which were functionalized with a gelatin coating and activated with GA. The permeability decreased to 38 and 346 L (hm²bar)⁻¹ for the 0.2 μm and 1.4 μm membranes, respectively, using 1 gL⁻¹ gelatin solution. By increasing the gelatin concentration to 10 gL⁻¹, the permeability further decreased to 10 L (hm²bar)⁻¹ for the 0.2 μm membrane while it was steady at 346 L (hm²bar)⁻¹ for the 1.4 μm membrane. As seen from these numbers, it is important to be able to predict the effects of the immobilization method on the permeability, the separation factor and various other parameters, and to select the support accordingly.

Functionalization by organosilanes is generally achieved by grafting, a process in which the support is treated with the organosilanes, typically trialkoxysilanes, that form a coating of covalently bonded silanes on the surface with an organic functional group extending out into the liquid media.^[34] Trialkoxysilanes have a similar backbone structure of (RO)₃-Si(CH₂)_n-X where R is commonly methyl or ethyl group, n is 3 and X is a functional group. The silicon atom of the trialkoxysilane forms covalent bonds with the hydroxy groups of the carrier surface, releasing one, two or three ROH molecules in the process. The functional group, X, is further derivatized by the activating agent in the following step. Alternative functionalization routes by organosilanes are co-condensation and oligomer hydrolysis, but these are of less importance for enzyme immobilization, especially on membranes.^[34,108,109] Co-condensation and oligomer hydrolysis are mainly used for orthosilicate particles formed by means of sol-gel synthesis. In co-condensation, the functionalization and sol-gel synthesis are obtained in a one-step process where an even distribution of organic functional groups is obtained in the structure of growing sol-gel particles.^[109] Hartono et al.^[110] described the preparation of functionalized mesoporous silica carriers by co-condensation of tetraethoxysilane (TEOS) with either APTES, 3-mercaptopropyltrimethoxysilane (MPTMS), vinyltrimethoxysilane (VTMS) or phenyltrimethoxysilane (PTMS). The amino-functionalized carrier showed the highest cellulase (from *Tricoderma reesei*) loading capacity while the vinyl-functionalized carrier resulted in higher cellulase activity retention. The higher enzyme loading observed was explained by the stronger electrostatic interactions between the negatively charged proteins and positively charged amino-functionalized carrier, as opposed to negatively charged vinyl-functionalized carrier, while the lower activity retention

was explained by the formation of covalent amide bonds between the amine of the APTES and carboxylic acid residues of the proteins, which lead to conformational changes in the enzyme structure and de-formation and/or blocking of the active sites of the enzyme. The immobilization on the vinyl-functionalized carrier was primarily by physical (hydrophobic) interactions between the vinyl functional groups and the enzyme, which provided a suitable microenvironment for the enzyme. A few examples of trialkoxysilanes that have been reported for use in enzyme immobilization are listed in Table 2.

APTES is a popular choice as a functionalizing agent for enzyme immobilization. APTES has been used for the functionalization of several different inorganic carriers, such as ceramics (TiO_2 , Al_2O_3 and SiO_2),^[29,35,41,86] coal-fly ash,^[98] glass^[90,111] and nanosilicalite.^[112] The common choice of APTES can further be seen in Table 5, where a number of recent examples of enzyme immobilization on inorganic carriers has been listed.

Kroll et al.^[5] found that the APTES loading capacity on a ZrO_2 microtube membrane increased with APTES concentration, temperature and incubation time, both in toluene and DI water as solvents. The APTES loading capacity varied from 1.0 to $50.1 \mu\text{g m}^{-2}$ under the operating conditions investigated. Higher APTES loading resulted in higher enzyme loading, and significantly higher, up to 8.5-fold higher, than unspecific enzyme adsorption onto the untreated membrane surface. On the other hand, the permeability of an alumina membrane upon functionalization with APTES was reported by Ranieri et al.^[41] the functionalization resulted in an APTES loading of $1.26 \mu\text{mol cm}^{-2}$ which caused a 37% decrease in the water permeability compared to the native membrane. The water permeability further decreased to

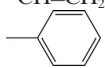
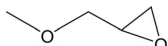
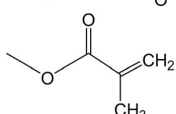
53% of the original permeability by activation with GA and to 12% by the immobilization of lipase.

3.4.3 Activation

Activation is the final step prior to the enzyme immobilization. Activation is the generation of electrophilic groups on the support, which will react with the strong nucleophiles on the proteins. A few examples of activating agents include GA, *N*-(3-dimethylamino-propyl)-*N'*-ethylcarbodiimide hydrochloride (EDC), *N*-hydroxysuccinimidyl (NHS), hexamethylene diisocyanate (HDMI) and CDI.^[11,86,118–121]

Glutaraldehyde is an inexpensive activation agent, and a popular choice for enzyme immobilization. The reaction between the aldehyde group of GA and an amino group of the enzyme is pH dependent and found to take place through either the formation of a Schiff base or Michael-type addition. The formation of a Schiff base is often described, but it is also debated if Schiff base formation is the actual route for activation with GA, given the low stability of the obtained Schiff base under acidic conditions.^[16,27,29,34,98,122] The Schiff base route is generally accepted for other aldehydes, e.g., benzaldehyde.^[123] GA provides a rather long spacer between the enzyme and support, the exact length of the spacer can be controlled with temperature and pH, among other factors, since the monomer is known to exist in equilibrium with at least 12 other di-/oligo- and polymeric forms.^[34,124,125] A comparison of two activating agents, namely GA and HDMI, could be seen in a study where GA and HDMI were used for the activation of PEI-functionalized silica spheres for the subsequent immobilization of lipase from *Thermomyces lanuginosus*. Activation by GA showed the overall best performance, both in

Table 2. Examples of trialkoxysilanes used for the functionalization of inorganic supports in enzyme immobilization.

Functionalizing agent	Organic functional group	Ref.
(3-aminopropyl)triethoxysilane (APTES)	$-\text{NH}_2$	[113]
[3-(methylamino)propyl]triethoxysilane	$-\text{NH}-\text{CH}_3$	[114]
(3-mercaptopropyl)trimethoxysilane (MPTMS)	$-\text{SH}$	[113]
(3-isocyanatopropyl)triethoxysilane (IPTES)	$-\text{N}=\text{C}=\text{O}$	[115]
(3-chloropropyl)triethoxysilane	$-\text{Cl}$	[116]
vinyltrimethoxysilane (VTMS)	$-\text{CH}=\text{CH}_2$	[110]
phenyltrimethoxysilane (PTMS)		[110]
3-(glycidyloxypropyl)trimethoxysilane (GPS)		[117]
3-(trimethoxysilyl)propyl methacrylate		[115]

terms of immobilization efficiency and yield (82% and 88%, respectively, for GA vs. 68% and 73% for HDMI) as well as stability and reusability.^[121]

4 Techniques for Characterization of Enzymes on Inorganic Particles

Characterization of enzymes on particles is an important technique to gain understanding and to determine the success of the immobilization process. Characterization may also provide knowledge on the correlation between enzyme immobilization and activity. A wide variety of techniques exists that not only can be used to detect enzymes, but also characterize their structural behavior and distribution on the surface of the inorganic particles. These are important parameters for optimization of enzyme immobilization but many different techniques are required in order to thoroughly analyze the immobilized enzyme. The characterization techniques have been split into two categories: (i) detection and visualization of enzymes and (ii) enzyme structural behavior on inorganic particles, which will be discussed in the following sections. While the focus in this section is on inorganic particles, it should be mentioned that possibilities for utilizing some of the techniques for characterization of enzymes on ceramic membranes also exist. It is also important to consider that most of the characterization techniques are only useful when comparing the free enzyme to the immobilized enzyme or a free material with the immobilized material.

4.1 Detection and Visualization of Enzymes on Inorganic Particles

Detection and visualization of enzymes on inorganic particles revolves around using a large variety of microscopic or spectroscopic methods. Being able to visualize the immobilized enzymes may give insight into their distribution behavior on the surface or inside the pores. Microscopy can also be used to analyze the stability of inorganic materials when exposed to enzymes. Some of the most interesting methods are discussed in the following section, but for an in-depth list of characterization methods, see Table 3. The table highlights examples of methods used to detect specific enzymes. These methods can obviously be applied to other enzymes and inorganic materials as well.

Fluorescence microscopy: Fluorescence microscopy is a technique that involves a microscope that utilizes fluorescence to generate an image. This can be effectively used for the detection of enzymes that have been tagged with a dye before immobilization on a

support. Matsuura et al. have done extensive research in applying fluorescence microscopy for visual distribution of enzymes on mesoporous silica.^[55,56,126] An interesting approach for detecting multiple enzymes is to apply different dyes to different enzymes. This method enabled the direct visualization of lipase (from *Phycomyces nitens*) and trypsin (from porcine pancreas) on mesoporous silica, and revealed a uniform distribution of the enzymes by fluorescence detection of each individual enzyme and additionally by merging the images.^[56]

Confocal laser scanning microscopy: Confocal laser scanning microscopy (CLSM) is a technique that enables the visualization of enzymes inside the inorganic pore structures of porous powders. This is done by optical sectioning, which makes it possible to observe fluorescence-tagged enzyme distribution inside the particle by 3D reconstruction of 2D images at different depths.^[58] As with fluorescence microscopy the enzymes must first be fluorescence-tagged. This technique is used effectively for detecting enzymes inside particles but also for optimization of the pore diameter by comparing microscopic images of samples with different pore diameters.^[45,58,127,128] A good example of using this technique was reported by Suh et al.,^[58] who investigated the immobilization of BSA on nanoporous silica particles with different pore sizes and used CLSM to visualize the success of immobilization inside the pores.

Scanning electron microscopy and transmission electron microscopy: Electron microscopy is a common technique for surface characterization and is regularly used for surface characterization of the inorganic supports used for enzyme immobilization. Scanning electron microscopy and field emission scanning electron microscopy (SEM and FESEM) are highly efficient for surface characterization – such as particle size, morphology, shape and distribution. Furthermore, it is possible to make a comparison of the inorganic particles before and after immobilization to better visualize the surface morphological changes or if the particles start to agglomerate due to enzyme immobilization.^[35,47,79,129,130] It should be noted that while SEM is excellent for surface characterization, it is unable to directly observe the enzyme. Wu et al.^[79] immobilized amylase onto Cu-MCP and used SEM imaging in order to characterize the enzyme distribution. The fabricated Cu-MCP contained many cracks and characterization showed that enzyme immobilization occurred on the surface, including in the cracks. A decrease in surface area confirmed the immobilization on Cu-MCP and that the enzymes filled the cracks. Hou et al.^[35] complemented SEM analysis with the use of electron dispersive spectroscopy (EDS). In this research, titania nanoparticles were implemented in a polyether sulfone (PES) membrane followed by immobilization of TVL. A cross section of the mem-

Table 3. Methods for the detection and visualization of enzymes on inorganic materials.

Method	Enzyme/Protein	Material	Characterization useful for	Ref.
AFM	GOD, HRP, cellulase, CALB, ^[a] subtilisin Carlsberg, TLL ^[b]	titania, gold, silica	direct qualitative characterization, agglomeration characterization, height distribution	[133,128,136,137]
SEM	lipase, laccase, amylase, ADH ^[c] +FDH, ^[d] CALB, subtilisin Carlsberg, TLL	MNP, silica, MCP, titania, zirconium, zirconia	surface visualization, particle stability and morphology, not directly able to see the enzyme	[35,47,79,128–130,138]
EDS	laccase	titania	elemental composition	[35]
TEM	streptavidin, lipase, SCAD, ^[e] lysozyme, cellulase, laccase	titania, zirconia, magnetite, silica, MNP, carbon nanotube, silica/iron oxide	surface visualization, particle stability and morphology. Enzyme distribution for tagged-enzymes	[45,127,129,131–135]
fluorescence microscopy	lipase, trypsin, glutaminase	silica	direct enzyme distribution visualization. fluorescence-tagged enzymes required	[55,56,126]
CLSM	bovine serum albumin, streptavidin, laccase, CALB, subtilisin Carlsberg, TLL	silica, titania, silica/iron oxide	direct enzyme distribution visualization. fluorescence-tagged enzymes required	[45,58,127,128]
N ₂ adsorption isotherm	lysozyme, α -amylase, hemoglobin, streptavidin	silica, alumina, zirconia, titania	surface area measurements, indirect quantitative characterization inside pores	[57,59,77,127]
zeta potential	BSA, lipase	alumina, silica, zirconia	indirect qualitative characterization, changes in electrostatic potential after immobilization	[47,50]
XPS	GOD, HRP, lipase	titania, gold, silica, MNP, carbon nanotube	elemental composition	[129,134,136,137]
XRD	lysozyme, cytochrome C, myoglobin, α -amylase, laccase	silica, alumina, zirconia, silica/iron oxide	indirect qualitative surface characterization, strain development caused by enzyme interaction	[59,77,139]
Bradford assay	BSA, lysozyme	silica	enzyme load determination by measurement of supernatant	[52,58]
TGA	lipase	zirconia	destructive enzyme determination	[131]
quartz crystal microbalance	HRP, GOD	silica,	<i>in-situ</i> monitoring of enzyme immobilization	[48]

^[a] *Candida antarctica* lipase B.

^[b] *Thermomyces lanuginosa* lipase.

^[c] Alcohol dehydrogenase.

^[d] Formate dehydrogenase.

^[e] *Saccharomyces cerevisiae* alcohol dehydrogenase.

brane was made by fracturing the membranes and coating with chromium. SEM combined with atomic mapping of titanium using EDS resulted in direct visualization of the titania distribution. The analysis concluded that adding 4% titania inside the membranes gave a good distribution of particles on the surface and inside the membrane. Increasing the amount of titania to 6% showed clear signs of agglomeration.

Another commonly used electron microscopy method is the transmission electron microscope (TEM).^[45,127,129,131–135] TEM allows imaging at a much greater resolution than SEM, with the limitation that it provides two-dimensional projections of the structures as the image is created by the transmitting electrons going through the sample. This also means that the sample must be very thin. TEM imaging can be

used to directly visualize any changes that occur to the particles after enzyme immobilization, such as size, shape and agglomeration. Ye et al.^[127] used TEM in order to visualize how the size of titania nanoparticles increased after aminosilanization for 4, 16 and 26 hours. Furthermore, a similar procedure was conducted by Li et al.,^[135] who used TEM to analyze iron oxide nanoparticles before and after binding to SCAD. The results showed that the particles were still well dispersed after immobilization, and that the mean diameter increased from 25 nm to 30 nm. Just like with SEM, direct observation of individual enzymes is not possible with TEM. However, an interesting use of TEM is the immunogold staining procedure, where the enzymes are tagged with gold nanoparticles, making direct observation through TEM

possible. This allows the exact location and visualization of individual enzyme molecules on the surface. Piras et al.^[132] embedded human lysozyme immobilized on SBA-15 mesoporous silica with an LR gold resin and cut it into thin sections of 60–80 nm. Afterwards, two incubation steps were carried out: one with an unlabeled primary antibody followed by a secondary colloidal gold conjugated antibody. The result is gold particles attached to lysozyme and TEM imaging is able to detect the individual gold particles.

Atomic force microscopy: An additional method of visualization of individual molecules is atomic force microscopy (AFM). AFM is a microscopic technique that allows visualization at a single-molecule level with sub-nanometer accuracy. AFM is an effective technique for surface characterization of as-received, functionalized and enzyme-immobilized inorganic particles as it allows precise surface measurements for enzyme distribution, agglomeration and height measurements.^[133,128,136,137] Ahmad et al.^[133] used AFM as a way to analyze the distribution of cellulase from *Aspergillus niger* onto titania nanoparticles by either physical adsorption or covalent bonding. This was done by creating 2D and 3D imaging showing the height distribution of titania nanoparticles before and after immobilization. The titania nanoparticles revealed a very smooth surface with almost no peaks in the height distribution. However, the physically adsorbed cellulase was visible by the presence of large height increases in localized areas, indicating that the enzyme was not uniformly adsorbed onto the surface, but rather agglomerated on the surface. Covalently bonded cellulase showed much more promising results, with an overall increase in height compared to the original surface, indicating the presence of enzyme but with a more uniform distribution with only few signs of agglomeration. Furthermore, analysis of the enzyme activity revealed that the covalently immobilized enzyme performed much better, which could be due to the improved distribution and thereby fewer inactive enzymes caused by agglomeration.

4.2 Methods for Characterization of Enzyme Structure

Enzymes are macromolecules and their shape/conformation is influenced by their environment. Conformational changes of enzymes can be induced by many factors, such as differences in temperature or pH, as well as by interactions and bonding between the enzyme and a support material. Therefore, a structural characterization of the enzymes after immobilization can provide important information about the success of immobilization and enzyme activity.^[140] In the materials section it was described how the enzyme structure can change due to strong interactions with inorganic particles. Some of the most interesting methods for characterization of the structure of immobilized enzymes are discussed in the coming section, but for an in-depth list of methods, see Table 4. The table highlights examples of methods used to detect conformational changes of specific enzymes. These methods can obviously be applied to other enzymes and inorganic materials as well.

Circular dichroism: Circular dichroism (CD) is a spectroscopic technique that has been used for structural analysis of enzymes.^[52,54,57,134,139] CD can be used to detect the secondary structures of enzymes, such as α -helices and β -sheets. By comparing the contents of secondary structures between free and immobilized enzymes, it is possible to estimate the structural loss caused by immobilization. These structures have highly defined bands in the CD spectrum and any intensity decrease will signal the loss of structure. Vertegel et al.^[52] immobilized chicken egg lysozyme on silica nanoparticles of different sizes by physical adsorption. Using CD, they were able to see the effect of particle size and pH on the enzyme secondary α -helix structure. The intensity of the bands was converted to the content of α -helicity for direct comparison between the different experiments. Similarly, Sang et al.^[54] investigated how the pore diameter of silica particles affected the secondary structure of chicken egg lysozyme and equine heart myoglobin. It

Table 4. Characterization of enzyme structures on inorganic particles.

Method	Enzyme	Material	Characterization useful for	Ref.
Raman spectroscopy	laccase	gold, silver, thiols	structural characterization	[144]
CD	lysozyme, cytochrome C, myoglobin, hemo-globin, lipase	silica, carbon nanotube	structural characterization of active sites on enzymes	[52,54,57,134,139]
IR	α -amylase, lysozyme, streptavidin, lipase, SCAD, lysozyme, myoglobin, cellulase, laccase	zirconia, silica, alumina, titania, zirconia, magnetite, silica metal ceramic powder, germanium crystals	characterization of functional groups of the particle and enzyme. qualitative confirmation of enzyme immobilized on to particle	[44,47,54,59,77,79,127,131,133,135,142,143]

was discovered that for lysozyme, α -helix and β -turn were mostly unaffected by increasing the pore diameter, and they saw an increase in the β -sheet content. For myoglobin there was a significant loss of α -helix content with increasing pore diameter, indicating that myoglobin preferred a confined space close to its own dimensions. The relative activity decreased with higher pore diameter, and the loss of structure characterized with CD is a useful tool to help understand why the enzyme activity decreases.

Infrared spectroscopy: Infrared spectroscopy (IR) is a spectroscopic characterization technique that is widely used for characterization and identification of enzymes on inorganic supports. The different types that are used are diffuse reflectance Fourier transform infrared (DRIFT),^[59] polarization modulation infrared reflection absorption spectroscopy (PM-IRRAS),^[141] and the most commonly used Fourier transform infrared spectroscopy (FT-IR).^[44,47,54,79,127,131,133,135,142,143] FT-IR is an excellent way to follow the success of functionalization and immobilization. By enzyme immobilization, the vibration bands change and new vibration bands, corresponding to the newly formed bonds between enzyme and support, appear. It is thus possible to follow the structural changes caused by enzyme immobilization. A good example is provided by Ye et al.,^[127] who attached biotin to functionalized titania nanoparticles. The process was followed by FT-IR after each step in order to characterize the presence of functional groups and biotin.

5 Evaluation of Enzyme Properties upon Immobilization

As indicated in previous chapters, the immobilization of enzymes can have positive or negative effects on the enzyme activity, stability and reusability. In general, covalent attachment is found to enhance stability and reusability while it often leads to decreased activity. The opposite is observed for physical adsorption, in which the activity retention is generally high, but the enzyme is easily lost as it leaches from the support.^[4,12,35] Shorter spacers and multi-point attachment increase the rigidity of the immobilized enzyme and immobilization inside porous structures provides a protective environment for the enzymes. These factors can enhance the stability of the immobilized enzyme while the activity is more likely to be negatively affected.^[12,13,16,145] A vast number of different immobilization strategies has been described in recent papers, these strategies and their influences on the enzyme properties were investigated and are summarized below.

5.1 Activity

Enzyme immobilization can result in enhanced enzyme activity,^[6,53] although a decrease in enzyme activity is more common. The activity is affected by conformational changes of the enzyme, decreased mobility and mass transfer limitation within the nano-/microporous structures of the carriers, as well as by the conditions of the immobilization procedure.^[91] In addition to the immobilization method applied, the activity retention is strongly influenced by the properties of the carrier, such as surface charge, particle size and pore size.

Pore size and mass transfer: The relation between enzyme activity and pore size of the carrier can be seen in studies where enzymes have been immobilized onto carriers of different pore sizes, under otherwise similar conditions. For instance, bovine liver catalase was covalently immobilized *via* APTES and GA onto controlled pore glass (CPG) beads of different pore sizes; 70, 100 and 214 nm. The highest enzyme loading and specific activity was obtained on the surface of the 70 nm CPG beads, which presented the highest surface area and thereby availability for enzyme immobilization.^[120] On the contrary, silica graphite matrices of different pore sizes; 7, 14 and 21 nm, were used as carriers for the immobilization of GOD for the fabrication of a biosensor. The enzyme was covalently immobilized using aminopropyltrimethoxysilane (APTMS) and GA. The enzyme loading was highest for the largest pores, 21 nm, and decreased with decreasing pore size. The enzymes (7.0 \times 5.5 \times 8.0 nm) could more readily diffuse into the larger pores than the smaller ones, explaining the higher enzyme loading despite smaller surface area.^[1] In addition to enzyme loading, the pore size is also important regarding the accessibility of the substrates to the enzyme, as the substrates and products are subject to increased mass transfer limitations within smaller pore structures. The effects of mass transfer limitations on the activity of immobilized carbonic anhydrase (CA) from bovine erythrocytes could be seen by comparing the reaction efficiency with two different substrates; CO₂ on the one hand and *para*-nitrophenyl acetate (pNPA) on the other hand. The CA was immobilized in an LbL film composed of PEI, PAH, PSS and the enzyme. By increasing the number of layers in the film, and thereby the enzyme loading, the hydrolysis rate of pNPA remained steady while the hydrolysis rate of CO₂ increased linearly, indicating that the larger pNPA molecules were limited by mass transfer through the polymer network so that they could only reach the enzyme in the most superficial layer, while the smaller, gaseous CO₂ could readily diffuse through the network.^[81] The effects of the pore size on mass transfer were also seen in a study by Biro et al.,^[82] who studied the entrapment of β -D-

galactosidase (β -Gal) from *Kluyveromyces lactis* in an organic-inorganic sol-gel where they varied the composition of the sol-gel. No activity was detected when β -Gal was entrapped in a sol-gel obtained solely from methoxysilanes while high activity retention could be obtained in sol-gels obtained from ethoxysilanes. The difference was explained by the more compact structure of the methoxysilane-obtained sol-gel than the ethoxysilane one, and thereby more mass transfer limitations. The importance of the composition of the sol-gel was further demonstrated by introducing alkylated silanes, dimethyldimethoxysilane (DMeDMOS) and methyltriethoxysilane (MeTEOS), to the sol-gel preparation, and varying the ratios of TEOS:DMeDMOS and TEOS:MeTEOS, the resulting activity varied from *ca.* 0–84 U g⁻¹. The optimal composition was found to be 7:1 TEOS:MeTEOS. The presence of the alkyl groups resulted in larger pores but also led to hydrophobization of the sol-gel, so the optimal ratio was a balance between mass transfer limitations and hydrophobicity. The effects of pore size are thus a balance between surface area and mass transfer resistance, but also depend on the specific enzyme. A suitable pore size for a successful immobilization has been reported to be in the range of 3–9 times that of the enzyme dimensions,^[146] or in the upper limit of the mesoporous range, around 10–50 nm,^[34,72] and the lower limit of the macroporous range, 50–70 nm.^[147] Covalent immobilization is favored when the pore size is considerably larger (around five times) than the enzyme dimensions.^[120] When membranes are used as immobilization support, the situation is somewhat different, since the permeability of the membrane must be taken into account. Hence, the pore sizes of membranes used as support for enzyme immobilization have been reported in the range of 200–1400 nm. The mass transfer is aided by the fact that the biocatalyst is stationary in/on the membrane where it comes in contact with the substrate as the substrate is forced through the membrane under applied pressure.

Immobilization on ceramic membranes: This procedure has been widely practiced, as this set-up allows a continuous operation with simultaneous product removal.^[148] A few studies involving covalent immobilization on ceramic membranes show both increased, decreased and unaffected enzyme activity upon immobilization.^[4,41,149] For instance, covalently immobilized CRL retained nearly all of its activity when immobilized on an alumina hollow fibre membrane through APTES and GA. Under optimal immobilization conditions, the enzyme retained 93% of its observed specific activity compared to the free enzyme.^[41] Thomsen et al.^[148] immobilized a thermophilic β -glycosidase CelB from *Pyrococcus furiosus* on the γ -aluminum coated walls of a microreactor *via* APTES and GA. The immobilized enzyme retained

50% of the activity of the soluble enzyme. An even greater decrease in activity was seen when esterase EreB from genetically modified *E. coli* was immobilized on TiO₂ tubular membranes. In this study, Cazes et al.^[4] compared two immobilization methods and a free enzyme set-up for the enzymatic degradation of erythromycin, a pollutant found in some waste-waters. The enzyme was immobilized by adsorption onto the untreated membrane and by covalent attachment *via* gelatin and GA. The activity decreased sharply upon immobilization – less than 20% of the substrate was converted after five minutes reaction, while all the substrate was converted within one minute by the free enzyme under similar process conditions. The results showed that the activity of the covalently immobilized enzyme was lower, but more stable during multiple reaction cycles than the activity of the adsorbed enzyme. The same was seen with chicken egg lysozyme immobilized on zirconia membranes by covalent bonding through APTES and EDC on the one hand and physical adsorption on the other hand. The enzyme loading was around six times higher for the covalently immobilized enzyme than the adsorbed enzyme, however, the activity retention was higher for the adsorbed enzyme, which had an about four times higher specific activity than the covalently immobilized enzyme.^[93] Cazes et al.^[9,149] immobilized TVL on an α -alumina tubular membrane (pore size of 0.2 μ m) using gelatin and GA for covalent attachment. The activity of the immobilized enzyme was higher than that of the free enzyme, the Michaelis constant, K_M , was about 4–5 times lower for the immobilized enzyme in activity assays with two different substrates. In a reaction with tetracycline, degradation yields of 30% and 56% were reached with the free and immobilized laccase, respectively.^[149] On the same subject, the effect of the membrane pore size was investigated by comparing the degradation rate on membranes with pore sizes 0.2 and 1.4 μ m. It was found that the degradation rate was always higher with the larger pore-size membrane. Characterization of the enzyme-grafted membranes revealed that the gelatin, and thus the enzymes, were only found on the surface of the 0.2 μ m membrane, while for the 1.4 μ m membrane, the gelatin and the enzymes were found on the surface as well as inside the membrane pores, thus allowing higher enzyme loading.^[9] The higher activity of the 1.4 μ m membrane could also be explained by higher flux through the membrane, and thereby reduced mass transfer limitations.

Enzyme loading: This is another one of many important aspects of enzyme immobilization, as high enzyme loading generally results in high activity. A carrier with high surface area and availability for enzyme immobilization is favorable regarding high enzyme loading. There is, however, an optimal enzyme concentration for a given support, above

which the relative activity decreases since a too high enzyme concentration can result in enzyme aggregation, crowding within pores or formation of multilayers on the carrier surface with subsequent mass transfer challenges.^[37,73] Several reports of optimal enzyme activity at intermediate enzyme loading are found in the literature.^[6,9,75,81,82,150] For instance, the activity of β -Gal entrapped in a silica sol-gel was investigated under different enzyme concentrations (4–10 mg protein mmol⁻¹ silane). The highest activity was observed with intermediate protein loadings, 6.22 g protein mmol⁻¹ silane.^[82] Pectinex 3XL, a commercial mixture of pectinases, xylanases and cellulases, was covalently immobilized onto magnetic nanoparticles. All three enzyme showed highest activity at intermediate enzyme loadings, or 55 U of the investigated range of 25–75 U.^[150] Similar results were seen in the study on immobilized laccase by Cazes et al.,^[9] the enzymatic activity was investigated at enzyme concentrations of 1–20 g L⁻¹, and for both membranes, 0.2 and 1.4 μ m pore size, the highest activity was seen at a concentration of 5 g L⁻¹. In the study with CA immobilized by entrapment in an LbL film, the enzyme loading could be increased by a factor of around 140. This was achieved by immobilizing the CA on mesoporous silica nanoparticles, 110 nm in diameter, in the LbL film. The high enzyme loading resulted in increased absolute activity, however, the specific activity decreased from 3.5 to 0.067 μ mol min⁻¹ μ g⁻¹ CA for the enzyme entrapped in the LbL film in the absence and presence of silica particles, respectively. The decrease in specific activity was explained by diffusion limitations within the mesoporous silica nanoparticles.^[81] Enzyme loading is an important consideration in terms of optimal utilization of the enzyme.

The activity retention of the immobilized enzyme varies from low to high. Physical adsorption tends to result in higher activity retention than covalent bonding, likewise, high activity retention is obtained by entrapment, which is consistent with the common descriptions of these methods. The role of the carrier is evident, as seen from the variation in enzyme activity depending on the pore size, hydrophobicity and other parameters of the carrier. Fortunately, there is a large number of carriers available, and likewise, the properties can often be tailored to fit the needs of the specific enzyme, as seen with the sol-gel entrapped β -Gal.

5.2 Stability

Enzyme immobilization generally results in enhanced enzyme stability, regardless the immobilization method used. The stability can be seen as increased half-life and increased activity retention with varying temperature and pH, as compared to the free enzyme. The increased thermal and pH stability can

be explained by the enzyme becoming more rigid upon binding to a support. The covalent or physical bonds prevent, to a certain extent, the deformation of the enzyme's active sites and enzyme denaturation. A high enzyme stability is of paramount importance for industrial applications.

Ranieri et al.^[41] covalently immobilized CRL on an alumina hollow fibre membrane with APTES and GA, the immobilized enzyme was highly stable, no apparent decrease in activity was seen after six reaction cycles over 18 days. Kjellander et al.^[118] covalently immobilized glutathione transferase from *Drosophila melanogaster* on nanoporous alumina membranes with APTES and CDI as functionalizing and activating agents, respectively. The immobilization resulted in a slight decrease in activity compared to the free enzyme due to mass transport limitations, but the stability of the immobilization was high, with about 70% activity remaining after six days of storage and multiple reaction cycles. The immobilization allowed multiple reuse of the enzyme and simultaneous sterilization of the product. Immobilization of the thermophilic β -glycosidase CelB from *Pyrococcus furiosus* on the γ -aluminum coated walls of a microreactor via APTES and GA resulted in high stability. The immobilized enzyme could be operated in a continuous reaction at 80 °C for several days at a stable conversion of lactose (about 70%).^[148] The immobilization of lipase from porcine pancreas on MCP (ceramic powder mixed with metal hydroxide precipitates) with Ni²⁺ ions as chelating agents resulted in improved thermal and storage stability compared to the free enzyme.^[6] The thermal and pH stability of *Klebsiella pneumonia* pullulanase was improved upon immobilization by entrapment in a silica sol-gel in the presence of magnetic chitosan/Fe₃O₄ particles, where the enzyme was either free in the sol-gel or covalently bonded on the magnetic particles. The half-life at 60 °C increased from about 75 minutes for the free enzyme to more than 300 minutes for the immobilized enzymes; the activity retention of the immobilized enzymes was 52% and 69% at the end of reaction after 300 minutes, for the free enzyme in sol-gel and the enzyme covalently bonded on magnetic particles in the sol-gel, respectively.^[37]

The sol-gel entrapped β -Gal showed increased thermal and pH stability as compared to the soluble enzyme. The soluble enzyme was completely inactivated after 2 hours incubation at 50 °C while the immobilized enzyme was fully active after 8 hours incubation at the same temperature. The pH optima shifted from pH 7.5 to pH 8 after immobilization, and the immobilized enzyme had higher activity at a wider pH range than the soluble enzyme. The immobilized enzyme showed overall high stability, with over 90% activity retention after 20 days of storage at 4 °C and 60% activity retention after five reaction cycles. The

largest decrease in activity was seen after the first cycle, which is most likely due to loss of enzymes that were already poorly entrapped, 30% of the initial activity was lost in the first cycle while the activity decreased only by about 10% in the next four cycles.^[82]

The thermal stability of CRL was enhanced upon immobilization by physical adsorption on silica and zirconia powders. The half-life at 60 °C increased from 10 minutes for the free enzyme to 40 and 120 minutes for the enzyme immobilized on silica and zirconia, respectively. The enzyme-support interactions, electrostatic attractions and hydrophobic interactions could prevent unfolding of the enzyme at elevated temperature and restrict the enzyme movements, resulting in higher thermal stability. The same factor, that is, increased rigidity, caused a decrease in activity of the same immobilized enzyme, as mentioned previously. The high thermal stability of lipase immobilized on zirconia was further explained by the morphology of the zirconia particles, the characterization of the particles revealed a hollow spherical structure. The enzymes were adsorbed inside the spheres, which provided a protective environment for the enzyme. The stability of the immobilized lipase could also be seen on the high reusability, more than 90% activity retained after eight reuse cycles on both supports, and still around 40–60% activity retained after 20 recycles.^[47]

The higher enzyme stability achieved by covalent immobilization compared to physical adsorption could be seen in a study by Hou et al.,^[35] who compared different immobilization techniques for the preparation of biocatalytic membranes for pollutant degradation in waste-water treatment. They immobilized TVL on TiO₂ nanoparticles, which they subsequently loaded onto polymeric membranes. The immobilization was done by (i) physical adsorption onto untreated TiO₂ nanoparticles and (ii) physical adsorption onto APTES-functionalized TiO₂ nanoparticles, (iii) covalent bonding through APTES and GA and finally (iv) by physical adsorption onto APTES-functionalized TiO₂ nanoparticles, followed by cross-linking of the enzymes with GA.

Regarding immobilization on the particles, the highest activity retention and lowest enzyme loading was obtained by covalent immobilization, the opposite was seen for the cross-linked enzymes and intermediate activity recovery and enzyme loading for physical adsorption. The higher activity recovery of the covalently bonded laccase than the physically adsorbed laccase was explained by the use of centrifugation during the immobilization procedure. The shear stress posed on the enzyme can have detrimental effects on the enzyme activity, due to possible changes in the enzyme conformation. The increased rigidity of the covalently immobilized laccase proves beneficial in this case as it protects the enzyme when subject to

high shear stress. The higher stability of covalently immobilized laccase was also seen by investigating the residual activity after storing in a buffer for several days. After six days of storage, the activity retention of the physically adsorbed enzyme was around 50% while for the covalently bonded and cross-linked enzymes, more than 90% activity was retained after 20 days.

Immobilization is an effective method to increase the stability of enzymes and thereby prolong their useful life-time, as seen from the examples above. Again, the immobilization method and the carrier influence the stability, whereby covalent immobilization is the most efficient method in terms of enhanced enzyme stability.

5.3 Reusability and Leakage

Efficient immobilization will minimize loss of enzyme due to leakage from the support. Covalent immobilization generally provides the strongest bonds between enzyme and support and thereby the lowest degree of leakage. Many examples of prolonged enzyme activity and multiple reuses have been described in the literature. For instance, covalently immobilized β -glucosidase showed 81% glucose yield after six reaction cycles of 18 hours, compared to 100% in the first cycle. The enzyme was covalently immobilized on silicalite nanoparticles through APTES and GA. The strong, covalent bond prevented enzyme leakage, and the decrease in glucose yield was assigned to the natural decay in enzyme activity rather than enzyme leakage.^[112] Glutathione transferase was covalently immobilized on a nanoporous alumina membrane through APTES and CDI. No sign of enzyme leakage was observed in the system. Kjellander et al.^[118] could demonstrate this by real-time monitoring of the product formation in a flow-through set-up. A steady rate of product formation was detected as long as there was a flow of substrates through the membrane, but as soon as the flow was stopped, the product formation stopped as well, meaning that no enzymes leaked through the membrane that could otherwise continue the conversion of substrates. The comparison between covalently bonded and physically adsorbed enzyme could be seen in a study on chicken egg lysozyme immobilized on a zirconia membrane. The loss of lysozyme in a dead-end flow was 1.2 $\mu\text{g h}^{-1}$ for the covalently immobilized lysozyme whereas it was 4.2 $\mu\text{g h}^{-1}$ for the physically adsorbed lysozyme. Furthermore, the enzyme loading was considerably higher for the covalently immobilized lysozyme, so the relative loss was 0.2% of the covalently immobilized and 2.5% of the physically adsorbed enzyme per hour of filtration. The loss of enzyme increased by increasing the flow rate through the membrane.^[93] Similarly, the effects of

different enzyme-carrier interactions on enzyme leakage were observed in a study where *Trichoderma reesei* cellulase was immobilized onto non-, amino-, and vinyl-functionalized mesoporous silica particles. The primary interactions between the enzyme and the three carriers were hydrogen bonds (physical), amide bond (covalent) and hydrophobic interactions (physical), respectively. The enzyme leakage varied from non-detectable for the covalently immobilized enzyme, to approximately 2% with the hydrophobic interactions and 7% with the hydrogen bonding. It was also observed that enzyme leakage increased with higher enzyme loading, regardless of the carrier used, which was explained by the higher enzyme concentration gradient between the carrier and the surrounding media at higher enzyme loadings.^[110] Several studies have shown that enzyme leakage is often more pronounced in the first reaction cycle and becomes lower and more stable in the subsequent reaction cycles, since the enzymes that are already poorly immobilized will be lost in the first reaction or washing cycle.^[37,82,90,100] Furthermore, the enzyme concentration gradient between the carrier and surrounding media decreases with the loss of enzyme, which also affects the rate of enzyme leakage.^[110]

Enzyme reusability is one of the most important objectives of enzyme immobilization, therefore great efforts have been made in order to minimize enzyme leakage. For this matter, it can be beneficial to combine different immobilization methods for their advantages. Long et al.^[37] demonstrated this with a sol-gel entrapped pullulanase. The enzyme was immobilized in a silica sol-gel in the presence of magnetic chitosan/Fe₃O₄ particles. By adding a covalent step to the immobilization, the enzyme was covalently bonded to the magnetic particles *via* APTES prior to entrapment within the sol-gel. This strategy resulted in increased operational stability and decreased leakage. The residual activity after six reaction cycles increased from 72 to 81% by adding the cross-linking step to the immobilization. The relative activity of adenosine deaminase after eight batches increased from below 10% to around 80% by adding GA to the immobilization strategy.^[75] The enzyme was immobilized on APTES functionalized TiO₂ microparticles by three different methods; physical adsorption, covalent attachment through GA and finally covalent attachment through GA followed by cross-linking of the enzymes with GA. The relative enzyme activity after eight batches was approximately 10%, 50% and 80% with the three different methods, respectively. The physically immobilized enzyme retained the highest activity compared to the free enzyme, 84.4%, which was around 7.8% higher than the activity retained by the covalently immobilized enzyme. The GA prevented enzyme leaching and loss of activity by stabilizing the enzyme through multi-point attachments. In a

more specific approach, Xu et al.^[151] used ConA, a protein that agglutinates glycoproteins, to immobilize two commonly used glycoenzymes, HRP and laccase, onto activated carbon. In this two-step immobilization method, the ConA was adsorbed onto activated carbon and then the enzyme was attached to ConA through affinity attachment. The enzyme leakage and deactivation were significantly reduced by the presence of ConA and furthermore, the activity was enhanced compared to the enzyme adsorbed directly onto the support. The activity retention for laccase immobilized in the presence of ConA was 98% after 10 cycles of incubation, filtration and activity assay and still 80% after 25 cycles, while the laccase adsorbed onto activated carbon in the absence of ConA lost all its activity after 22 cycles. The activity retention of HRP immobilized on activated carbon with and without ConA was 50% after 25 cycles and zero after 12 cycles, respectively. The effect of ConA was compared to that of cross-linking with GA. The immobilization with GA resulted in similar reusability, that is, both methods could efficiently prevent enzyme leakage, but the immobilization with GA resulted in a considerable loss of activity. The balance between leakage prevention and activity retention upon cross-linking with GA was reported in a study by Bhangé et al.,^[152] who investigated the effect of GA concentration for the immobilization of bile salt hydrolase on APTES-functionalized mesoporous silica, SBA-15. By increasing the GA concentration from 0.025–1%, both leakage and activity decreased. In this case, the activity decreased steeply from 0.1–1% GA, it was therefore concluded that the minimum amount of GA should be used that offers sufficient stability with minimum loss of activity.

The examples provided above are listed in Table 5, along with other recently reported enzyme immobilizations on inorganic supports. From this discussion, it can be concluded that enzyme stability and reusability can be significantly increased by immobilization. The common immobilization methods have been covered in numerous examples and the results mostly support the general understanding of enzyme immobilization, for example, the higher activity retention by physical immobilization and higher stability of covalently immobilized enzymes. The popular choice of APTES and GA is clearly seen, as these agents have been used with a number of different enzymes and support materials. Still, the variety of different methods and materials used and their different effects on the enzyme properties only highlight the complications involved in choosing the right immobilization method and carrier for a given enzyme and adjustment of the various parameters involved. The discussion has been restricted to inorganic support materials and it has been shown that ceramic materials provide a suitable support for enzyme immobilization. Although immo-

Table 5. Examples of immobilized enzymes from recent papers (2014–2017); support materials and morphologies, immobilization methods, functionalizing and activating agents and enzyme properties upon immobilization.

Support	Pore size	Enzyme	Immobilization method	Functionalizing agent	Activating agent	Activity retention ^[a,b]	Stability	Reusability ^[c]	Ref.
Al ₂ O ₃ tubular membrane	0.8 μm	<i>Candida antarctica</i> lipase B (CALB)	covalent bonding	gelatin	GA	– ^[c]	–	–	[11]
TiO ₂ tubular membrane	0.8 μm	<i>Candida antarctica</i> lipase B (CALB)	covalent bonding	gelatin	GA	–	–	–	
Al ₂ O ₃ hollow fibre membrane	–	CRL	covalent bonding	APTES	GA	93%	+	ca. 100% A.R. after 6 cycles	[41]
TiO ₂ tubular membrane	1.4 μm	esterase (EreB)	covalent bonding	gelatin	GA	2–20%	/	stable activity over 100 h	[4]
TiO ₂ tubular membrane	1.4 μm	esterase (EreB)	physical adsorption	–	–	7–40%	/	ca. 80% A.R. after 4 cycles	
Al ₂ O ₃ monochannel tubular membrane	0.2 μm	TVL	covalent bonding	gelatin	GA	13%	+	ca. constant degradation rate over 200 h	[9]
Al ₂ O ₃ monochannel tubular membrane	1.4 μm	TVL	covalent bonding	gelatin	GA	15%	+	ca. constant degradation rate over 200 h	
alumina membrane	0.2 μm	glutathione transferase from <i>Drosophila melanogaster</i>	covalent bonding	APTES	CDI	12–21%	+	70% A.R. after 6 days of storage and repeated use	[18]
Al ₂ O ₃ /SiO ₂ microbeads	79 nm	glucose oxidase, catalase	covalent bonding	APTES	EDC/NHS	÷	+	61% A.R. after 72 h in continuous flow-through	[20]
MCM-41 mesoporous silica spheres	2.4 nm	lipase from <i>Thermomyces lanuginosus</i>	Physical adsorption	–	–	52%	+	70% A.R. after 12 cycles	[21]
MCM-41 mesoporous silica spheres	2.4 nm	Lipase from <i>Thermomyces lanuginosus</i>	physical adsorption	PEI	–	62%	+	ca. 75% A.R. after 12 cycles	
MCM-41 mesoporous silica spheres	2.4 nm	lipase from <i>Thermomyces lanuginosus</i>	physical adsorption	PEI + succinic anhydride	–	58%	+	ca. 80% A.R. after 12 cycles	
MCM-41 mesoporous silica spheres	2.4 nm	Lipase from <i>Thermomyces lanuginosus</i>	Covalent bonding	PEI	GA	82%	+	85% A.R. after 12 cycles	
MCM-41 mesoporous silica spheres	2.4 nm	lipase from <i>Thermomyces lanuginosus</i>	covalent bonding	PEI	HDMI	68%	+	ca. 75% A.R. after 12 cycles	
TiO ₂ nanoparticles	–	TVL	covalent bonding	APTES	GA	79%	+	ca. 90% A.R. after 18 days in buffer	[35]
TiO ₂ nanoparticles	–	TVL	covalent + cross-linking	APTES	GA	24%	+	ca. 85% A.R. after 18 days in buffer	
TiO ₂ nanoparticles	–	TVL	physical adsorption	APTES	–	48%	+	ca. 50% A.R. after 18 days in buffer	
TiO ₂ nanoparticles	–	TVL	physical adsorption	–	–	40%	+	ca. 45% A.R. after 18 days in buffer	
TiO ₂ microparticles	20 nm	adenosine deaminase	physical adsorption	APTES	–	84%	–	ca. 10% A.R. after 8 cycles	[75]
TiO ₂ microparticles	20 nm	adenosine deaminase	covalent bonding	APTES	GA	78%	–	ca. 50% A.R. after 8 cycles	

Table 5. (Continued)

Support	Pore size	Enzyme	Immobilization method	Functionalizing agent	Activating agent	Activity retention ^[a,b]	Stability	Reusability ^[c]	Ref.
TiO ₂ microparticles	20 nm	adenosine deaminase	covalent + cross-linking	APTES	GA	–	–	80% A.R. after 8 cycles	
SBA-15 mesoporous silica	6.5 nm	bile salt hydrolysatase	covalent + cross-linking	APTES	GA	163%	+	–	[152]
SBA-15 powder	2–25 nm	CRL	physical adsorption	–	–	÷	+	>90% A.R. after 8 cycles	[47]
ZrO ₂ powder	> 50 nm	CRL	physical adsorption	–	–	÷	+	>90% A.R. after 8 cycles	[150]
MNPs	–	pectinex 3XL (pectinase, xylanase and cellulase)	–	APTES	GA	58–87%	+	87–97% A.R. after 6 cycles	[36]
MNPs	–	<i>Cerrera</i> laccase	covalent bonding + CLEA ^e	APTES	GA	47%	–	–	[37]
MNPs/chitosan	–	pullulanase from <i>Klebsiella pneumoniae</i>	entrapment	APTES	GA	84%	+	72% A.R. after 6 cycles	[37]
MNPs/chitosan	–	pullulanase from <i>Klebsiella pneumoniae</i>	entrapment + cross-linking	APTES	GA	–	+	81% A.R. after 6 cycles	
fumed silica micro-particles	–	laccase from <i>M. thermophila</i>	covalent bonding	APTES	GA	59%	+	ca. 60%/11% after 10 cycles on BPA/E2 ^[f]	[153]
magnetized fumed silica microparticles	–	laccase from <i>M. thermophila</i>	covalent bonding	APTES	GA	55%	+	50%/50% after 10 cycles on BPA/E2	[98]
GCSZn ^[g] powder	91 μm ²	baker's yeast invertase	covalent bonding	APTES	GA	+	÷	91/30% A.R. after 10 cycles at 25/60°C	[98]
coal fly ash ceramics	–	baker's yeast invertase	covalent bonding	APTES	GA	85%	+	ca. constant hydrolysis rate in 10 cycles	[98]
ceramic monolith (2MgO/2Al ₂ O ₃ /5SiO ₂)	–	TVL	covalent bonding	APTES	GA	16%	–	57% A.R. after 9 cycles	[99]
porous glass beads	–	laccase from <i>Myceliophthora thermophila</i>	covalent bonding	APTES	GA	40%	–	ca. 66% A.R. after 4 cycles	
porous glass beads	–	glucose oxidase from <i>Aspergillus niger</i>	covalent bonding	APTES	GA	78%	–	–	
nanosilicite	–	β-glucosidase from almonds	covalent bonding	APTES	GA	63%	–	85% A.R. after 5 cycles	[112]
Al ₂ O ₃ ceramic discs	0.56 μm	alkaline phosphatase from chicken intestine	covalent + cross-linking	APTES	EDC/NHS	56%	–	–	[154]
YSZ ceramic discs	0.53 μm	alkaline phosphatase from chicken intestine	covalent + cross-linking	APTES	EDC/NHS	65%	–	–	
Al ₂ O ₃ /SiO ₂ ceramic wafer	–	urease	covalent bonding	APTES	GA	–	+	stable response for up to 21 days	[87]
inorganic-organic sol-gel	1.5 nm	β-D-galactosidase from <i>Kluyveromyces fragilis</i>	entrapment	–	–	–	+	70% A.R. after 5 cycles	[82]
activated carbon	–	horseradish peroxidase	physical adsorption	ConA	–	÷	+	50% A.R. after 25 cycles	[151]

Table 5. (Continued)

Support	Pore size	Enzyme	Immobilization method	Functionalizing agent	Activating agent	Activity retention ^[a,b]	Stability	Reusability ^[c]	Ref.
MCP	–	laccase lipase from porcine pancreas, type II	physical adsorption affinity attachment	ConA Ni ²⁺ ions	– –	÷ 216%	+	80% A.R. after 25 cycles ca. 35% A.R. after 5 cycles	^[6]
MCP	–	lipase from porcine pancreas, type II	affinity attachment	Ni ²⁺ entrapped in chitosan	–	164%	+	58% A.R. after 5 cycles	^[155]

^[a] Activity compared to free enzyme, when available in percentages.

^[b] Properties compared to free enzyme: ÷ lower, / comparable, + higher.

^[c] Activity retention after *n* cycles compared to first cycle.

^[d] Information not available/applicable.

^[e] Cross-linked enzyme aggregates.

^[f] BPA/E2 (bisphenol A/17 β -estradiol) as substrates.

^[g] Coal fly ashes glass-ceramic support with zinc sulfate.

bilization allows the use of enzymes in continuous processes, the different lifetimes of the enzymes and the ceramic material calls for the reuse of the ceramic material.

6 Reuse of Ceramic Membranes as Supports for Immobilization

One of the main advantages of ceramic materials and membranes is their relatively long service life, despite the inevitable fouling and loss of catalytic activity in the case of immobilized enzymes. Fouling is one of the main challenges of membrane processes. Fouling is the reversible or irreversible deposition of solutes on the membrane, gel- or cake-layer formation and pore blocking, which lead to decreased flux through the membrane and thereby decreased process efficiency. Enzymes and proteins in general are especially known to cause fouling due to their size and adsorption on the membrane.^[101,105,156] The relative size of the enzymes and the membrane pores plays an important role in fouling, as do the characteristics of the enzymes and the membrane surface, e.g., surface charge and hydrophobicity. An enzyme of dimensions smaller or comparable to the membrane pore is more likely to cause pore narrowing and pore blocking as it can diffuse into the pore and adsorb to the pore walls, or simply be stuck in the pore under the convective flux through the membrane. Cake-layer formation occurs when the enzyme is larger than the nominal pore size. This relation is not exclusive to enzymes, rather it is general for all foulants.^[157] Fouling due to enzyme adsorption is mainly a problem with free enzymes, while the adsorption can in fact be exploited as an immobilization method.^[158] In that sense, the gel-layer formation caused by fructosyl transferase was exploited to immobilize the enzyme on a TiO₂ membrane, initially, the enzyme passed through to the permeate, but with the build-up of a gel-layer, it could be immobilized in the gel-layer and thereby retained within the bioreactor.^[159] For a successful immobilization, the membrane pore size and the size of the enzyme as well as immobilization method must be considered together so that enzyme loading and activity retention are maximized, while the loss of membrane permeability is minimized. The permeability is less affected by immobilization in larger pore size membranes since the immobilized enzymes (and functionalizing/activating agents) fill up relatively less volume of larger pores than smaller pores.^[9,147] The activity retention is particularly important regarding immobilization on membranes, since inactive enzymes end up as membrane fouling. Many methods for fouling mitigation have been established, such as tailoring of the chemical and surface properties of the mem-

branes, as well as mechanical methods such as back-flushing and membrane vibration.^[26,105,156] Increasing the feed temperature can also result in decreased fouling of ceramic membranes due to the lower viscosity and mass transfer coefficient of the feed solution.^[157] When immobilized enzymes are involved, they pose an additional challenge on the membrane reusability, as the enzymes will eventually lose their catalytic activity and must be replaced by fresh enzymes. However, the high chemical, mechanical and thermal resistance of the ceramic material makes it possible to restore the native properties of the material by different cleaning and thermal treatments.^[11,41] The foulants are thus removed and the catalytic membrane can be regenerated by repeating the immobilization with fresh enzymes.

6.1 Chemical Cleaning

Chemical cleaning with NaOH as cleaning agent is commonly used in order to remove proteins and enzymes from membranes.^[55] Alkaline cleaning agents, often combined with oxidizing agents such as NaClO for oxidation decomposition, promote the disintegration of large organic particles and colloids and their detachment from the membrane. As these particles are broken down to smaller subunits, they can permeate through the membrane and thereby be removed from the feed.^[157,160] Acid cleaning, using strong inorganic acids, is often used to remove metal ion deposits from membranes. The order of the alkali and acid cleaning procedures is important with respect to the nature of the foulants that are removed by the different procedures. The alkali cleaning is used first to remove proteins, polysaccharides and other organic foulants that are usually larger molecules forming a cake-layer on the membrane surface. Subsequently the acid-cleaning is applied for the removal of metal ions that are attached to the membrane surface and inside the membrane pores, and are only exposed after the organic fouling has been removed.^[157] Several examples of efficient membrane regeneration by chemical cleaning have been reported. Ranieri et al.^[41] immobilized CALB on an alumina hollow fibre membrane, they were able to restore the native membrane flux completely after removal of the enzyme by a cleaning procedure. A basic detergent solution, containing NaOH and NaOCl, was filtered through the membrane at elevated temperature (80 °C), followed by rinsing with water. Aneur et al.^[11] immobilized CALB on TiO₂ and Al₂O₃ tubular membranes by covalent attachment. The membranes were firstly coated with a gelatin layer and then GA acted as a cross-linker between the enzyme and the membrane. In their work, the ceramic membranes were regenerated by a two-step washing procedure,

first using NaOH and then HNO₃ at elevated temperature (60–80 °C). The membranes were first soaked in the solutions for some time and then transmembrane pressure was applied to clean the membrane pores. After the cleaning procedure, the catalytic membrane could be regenerated using the same immobilization procedure as before. The effects of chemical cleaning of a ceramic membrane utilized in an anaerobic membrane bioreactor were investigated by Mei et al.^[160] In an *ex-situ* cleaning test, the fouled membrane could be efficiently cleaned by alkali and acid cleaning, using NaOH and HCl, so that the original membrane resistance was restored. The chemical cleaning was integrated into the anaerobic process by back-flushing. The effects of using NaOH were seen by comparing the increase in transmembrane pressure (TMP) where *in-situ* back-flushing was performed with NaOH on the one hand and DI water on the other. The rate of increase in TMP was approximately 5.5 times higher using DI water compared to NaOH.^[160]

The removal of physically adsorbed enzymes from inorganic supports can be carried out by a simple procedure using eluents, where the enzyme is desorbed from the carrier and into the solvent solution. Liu et al.^[161] used three different eluents, sodium dodecyl sulfate (SDS), sodium dodecyl sulfonate (SDS-2) and NaCl, to elute lysozyme from a zeolitic imidazolate framework (ZIF-8). They found SDS to be the most efficient eluent, the adsorption efficiency was practically unaffected in four lysozyme reloading cycles, while the adsorption efficiency decreased using SDS-2 and NaCl as eluents, and no enzyme was adsorbed in the fourth cycle using these two eluents. Similarly, Ji et al.^[162] used SDS for the detachment of laccase physically adsorbed onto carbon nanotubes (CNTs) that had been loaded and cross-linked onto a polymeric membrane. The laccase removal efficiency was 85%, which was reached by soaking the membrane in the SDS solution for 24 h under orbital shaking. The membrane was subsequently dried at 100 °C for 5 min and reloaded with fresh laccase solution by the same immobilization procedure as before. High reloading capacity was obtained, with 70% of the initial laccase activity remaining after the fourth reloading cycle, which proved the efficiency of the CNT-coated membrane regeneration.

6.2 Thermal Removal of Fouling

In addition to chemical cleaning, thermal treatments can be applied for the regeneration of ceramic membranes as a result of their high thermal resistance. Such methods have been demonstrated by Benito et al.,^[163] who were able to regenerate two alumina membranes, α -alumina with a pore size of 98 nm and

γ -alumina with a pore size of 6 nm, by high temperature treatment at 500 °C. The membranes were subject to calcination after filtration of oily waste-water, for the volatilization of the oil adsorbed on the membrane. The thermal treatment, calcination at 500 °C for two hours, allowed the regeneration of the membranes, eliminating the external fouling on the surface as well as the internal fouling in the membrane pores, without altering their native properties. Dafinov et al.^[164] were able to regenerate the original water permeability of an alumina membrane by heating at 250 °C for one hour. The membranes, a composite tubular membrane with γ -alumina skin layer and α -alumina support, had been functionalized with different alcohols for hydrophobization, making them more suitable for filtration under acidic conditions.

The regeneration of the ceramic membranes can be carried out by these harsh chemical and thermal methods without causing membrane swelling or other damage owing to the inherent properties of the ceramic materials. The regeneration is essential in order to exploit the full service life of the membrane and hence allowing a more cost-effective use, as the capital cost of ceramic membranes is relatively high in comparison to polymeric membranes.^[94]

7 Conclusions

The immobilization of enzymes on inorganic materials, with special emphasis on ceramic membranes, has been surveyed through numerous recent examples from the literature. One of the main motivations to use inorganic materials, as opposed to organic materials, for example, polymeric membranes, is their long service life and capability of regeneration. This was supported by examples of chemical and thermal treatments for the regeneration of ceramic membranes, which showed efficient restoration of the native membrane properties. Besides the capability of regeneration, inorganic materials prove suitable as carriers for enzyme immobilization, as high enzyme activity retention, enhanced stability and reusability can be obtained. The complications involved with enzyme immobilization are the balance between the enzyme properties upon immobilization, notably activity and stability, while the large number of parameters involved, as well as methods and materials available make optimization a difficult task. Some general conclusions can be derived from the discussion conducted here, such as that physical adsorption proves better in obtaining high enzyme activity while covalent bonding results in higher stability, which is consistent with the general description of these methods.^[4,35] Likewise, the preferred pore size for enzyme immobilization on nanostructural materials and particles lies in the range of 10–70 nm, these dimensions can provide

a high surface area, a protective environment within the pores yet limited mass transfer limitations.^[34,147] Immobilization on membranes usually requires larger pore sizes to compensate for the requirements of high flux. Pore sizes in the range of 0.2–1.4 μm have been commonly reported.^[4,11,118] Although enzyme immobilization has been practiced for a long time, the lack of generalization leaves space for improvement, new methods as well as new carrier materials and morphologies are constantly emerging and enzyme immobilization is still an active research field.

Acknowledgements

This work was supported by The Danish Council for Independent Research, Grant no.: 6111-00232B.

References

- [1] E. M. Caldas, D. Novatzky, M. Deon, E. W. de Menezes, P. F. Hertz, T. M. H. Costa, L. T. Arenas, E. V. Benvenuti, *Microporous Mesoporous Mater.* **2017**, *247*, 95–102.
- [2] E. Verné, S. Ferraris, C. Vitale-Brovarone, S. Spriano, C. L. Bianchi, A. Naldoni, M. Morra, C. Cassinelli, *Acta Biomater.* **2010**, *6*, 229–240.
- [3] D. Becker, S. Rodriguez-Mozaz, S. Insa, R. Schoevaart, D. Barceló, M. De Cazes, M. P. Belleville, J. Sanchez-Marcano, A. Misovic, J. Oehlmann, M. Wagner, *Org. Process Res. Dev.* **2017**, *21*, 480–491.
- [4] M. de Cazes, M. P. Belleville, E. Petit, M. Salomo, S. Bayer, R. Czaja, J. De Gunzburg, J. Sanchez-Marcano, *Biochem. Eng. J.* **2016**, *114*, 70–78.
- [5] S. Kroll, L. Treccani, K. Rezwani, G. Grathwohl, *J. Memb. Sci.* **2010**, *365*, 447–455.
- [6] Z. Wu, W. Qi, M. Wang, R. Su, Z. He, *J. Mol. Catal. B Enzym.* **2014**, *110*, 32–38.
- [7] U. T. Bornscheuer, G. W. Huisman, R. J. Kazlauskas, S. Lutz, J. C. Moore, K. Robins, *Nature* **2012**, *485*, 185–194.
- [8] X. Dong, W. Jin, N. Xu, K. Li, *Chem. Commun.* **2011**, *47*, 10886–10902.
- [9] M. de Cazes, M. P. Belleville, M. Mougél, H. Kellner, J. Sanchez-Marcano, *J. Memb. Sci.* **2015**, *476*, 384–393.
- [10] R. A. Sheldon, *Adv. Synth. Catal.* **2007**, *349*, 1289–1307.
- [11] S. Ben Ameer, C. Luminița Gîjiu, M. P. Belleville, J. Sanchez, D. Paolucci-Jeanjean, *J. Memb. Sci.* **2014**, *455*, 330–340.
- [12] C. Mateo, J. M. Palomo, G. Fernandez-Lorente, J. M. Guisan, R. Fernandez-Lafuente, *Enzyme Microb. Technol.* **2007**, *40*, 1451–1463.
- [13] A. K. S. Nisha S, G. N. Nisha S, *Chem. Sci. Rev. Lett.* **2012**, *1*, 148–155.
- [14] W. Liu, L. Wang, R. Jiang, *Top. Catal.* **2012**, *55*, 1146–1156.
- [15] S. Datta, L. R. Christena, Y. R. S. Rajaram, *3 Biotech* **2013**, *3*, 1–9.

- [16] N. R. Mohamad, N. H. C. Marzuki, N. A. Buang, F. Huyop, R. A. Wahab, *Biotechnol. Biotechnol. Equip.* **2015**, *29*, 205–220.
- [17] S. A. Ansari, Q. Husain, *Biotechnol. Adv.* **2012**, *30*, 512–523.
- [18] S. Chakraborty, H. Rusli, A. Nath, J. Sikder, C. Bhattacharjee, S. Curcio, E. Drioli, *Crit. Rev. Biotechnol.* **2016**, *36*, 43–58.
- [19] I. Eş, J. D. G. Vieira, A. C. Amaral, *Appl. Microbiol. Biotechnol.* **2015**, *99*, 2065–2082.
- [20] L. Cao, *Carrier-Bound Immobilized Enzymes: Principles, Application and Design*, Wiley-VCH, Weinheim, **2006**.
- [21] L. Cao, *Curr. Opin. Chem. Biol.* **2005**, *9*, 217–226.
- [22] R. DiCosimo, J. McAuliffe, A. J. Poulouse, G. Bohlmann, *Chem. Soc. Rev.* **2013**, *42*, 6437.
- [23] A. Dwevedi, *Enzyme Immobilization, Advances in Industry, Agriculture, Medicine, and the Environment*, Springer International Publishing, Berlin, Heidelberg, **2016**.
- [24] P. Jochems, Y. Satyawali, L. Diels, W. Dejonghe, *Green Chem.* **2011**, *13*, 1609.
- [25] D. Brady, J. Jordaan, *Biotechnol. Lett.* **2009**, *31*, 1639–1650.
- [26] F. Carstensen, A. Apel, M. Wessling, *J. Memb. Sci.* **2012**, *394–395*, 1–36.
- [27] R. A. Sheldon, S. van Pelt, *Chem. Soc. Rev.* **2013**, *42*, 6223–6235.
- [28] M. L. Verma, C. J. Barrow, M. Puri, *Appl. Microbiol. Biotechnol.* **2013**, *97*, 23–39.
- [29] N. Aissaoui, J. Landoulsi, L. Bergaoui, S. Boujday, J. F. Lambert, *Enzyme Microb. Technol.* **2013**, *52*, 336–343.
- [30] I. V. Pavlidis, M. Patila, U. T. Bornscheuer, D. Gournis, H. Stamatis, *Trends Biotechnol.* **2014**, *32*, 312–320.
- [31] S. R. Hosseinabadi, K. Wyns, A. Buekenhoudt, B. Van Der Bruggen, D. Ormerod, *Sep. Purif. Technol.* **2015**, *147*, 320–328.
- [32] N. S. A. Mutamim, Z. Z. Noor, M. A. A. Hassan, A. Yuniarto, G. Olsson, *Chem. Eng. J.* **2013**, *225*, 109–119.
- [33] M. Hartmann, X. Kostrov, *Chem. Soc. Rev.* **2013**, *42*, 6277–6289.
- [34] P. Zucca, E. Sanjust, *Molecules* **2014**, *19*, 14139–14194.
- [35] J. Hou, G. Dong, Y. Ye, V. Chen, *J. Memb. Sci.* **2014**, *452*, 229–240.
- [36] J. Yang, Y. Lin, X. Yang, T. B. Ng, X. Ye, J. Lin, *J. Hazard. Mater.* **2017**, *322*, 525–531.
- [37] J. Long, X. Li, X. Zhan, X. Xu, Y. Tian, Z. Xie, Z. Jin, *Bioprocess Biosyst. Eng.* **2017**, *40*, 821–831.
- [38] D. G. Ramirez-Wong, C. Coelho-Diogo, C. Aimé, C. Bonhomme, A. M. Jonas, S. Demoustier-Champagne, *Appl. Surf. Sci.* **2015**, *338*, 154–162.
- [39] M. S. Crosley, W. T. Yip, *J. Phys. Chem. B* **2017**, *121*, 2121–2126.
- [40] L. Treccani, T. Y. Klein, F. Meder, K. Pardun, K. Rezwani, *Acta Biomater.* **2013**, *9*, 7115–7150.
- [41] G. Ranieri, R. Mazzei, Z. Wu, K. Li, L. Giorno, *Molecules* **2016**, *21*, 345.
- [42] Y. Masuda, S. Kugimiya, K. Kato, *J. Asian Ceram. Soc.* **2014**, *2*, 11–19.
- [43] C. Ji, L. N. Nguyen, J. Hou, F. I. Hai, V. Chen, *Sep. Purif. Technol.* **2017**, *178*, 215–223.
- [44] C. C. S. Fortes, A. L. Daniel-da-Silva, A. M. R. B. Xavier, A. P. M. Tavares, *Chem. Eng. Process. Process Intensif.* **2017**, *117*, 1–8.
- [45] H. Wang, W. Zhang, J. Zhao, L. Xu, C. Zhou, L. Chang, L. Wang, *Ind. Eng. Chem. Res.* **2013**, *52*, 4401–4407.
- [46] H. Gustafsson, E. M. Johansson, A. Barrabino, M. Odén, K. Holmberg, *Colloids Surfaces B Biointerfaces* **2012**, *100*, 22–30.
- [47] L. T. Izrael Živković, L. S. Živković, B. M. Babić, M. J. Kokunešoski, B. M. Jokić, I. M. Karadžić, *Biochem. Eng. J.* **2015**, *93*, 73–83.
- [48] H. Gustafsson, A. Küchler, K. Holmberg, P. Walde, *J. Mater. Chem. B* **2015**, *3*, 6174–6184.
- [49] S. Yi, F. Dai, C. Zhao, Y. Si, *Sci. Rep.* **2017**, *7*, 9806.
- [50] K. Rezwani, L. P. Meier, M. Rezwani, J. Vörös, M. Textor, L. J. Gauckler, *Langmuir* **2004**, *20*, 10055–61.
- [51] S. P. Hudson, S. White, D. Goradia, H. Essa, B. Liu, L. Qiao, Y. Liu, J. C. Cooney, B. K. Hodnett, E. Magner, *ACS Symp. Ser.* **2008**, *986*, 49–60.
- [52] A. A. Vertegel, R. W. Siegel, J. S. Dordick, *Langmuir* **2004**, *20*, 6800–6807.
- [53] H. Gustafsson, C. Thörn, K. Holmberg, *Colloids Surfaces B Biointerfaces* **2011**, *87*, 464–471.
- [54] L.-C. Sang, M.-O. Coppens, *Phys. Chem. Chem. Phys.* **2011**, *13*, 6689–6698.
- [55] S.-i. Matsuura, R. Ishii, T. Itoh, S. Hamakawa, T. Tsunoda, T. Hanaoka, F. Mizukami, *Chem. Eng. J.* **2011**, *167*, 744–749.
- [56] S.-i. Matsuura, R. Ishii, T. Itoh, T. Hanaoka, S. Hamakawa, T. Tsunoda, F. Mizukami, *Microporous Mesoporous Mater.* **2010**, *127*, 61–66.
- [57] Y. Urabe, T. Shiomi, T. Itoh, A. Kawai, T. Tsunoda, F. Mizukami, K. Sakaguchi, *ChemBioChem* **2007**, *8*, 668–674.
- [58] C. W. Suh, M. Y. Kim, J. B. Choo, J. K. Kim, H. K. Kim, E. K. Lee, *J. Biotechnol.* **2004**, *112*, 267–277.
- [59] A. Vinu, V. Murugesan, O. Tangermann, M. Hartmann, *Chem. Mater.* **2004**, *16*, 3056–3065.
- [60] G. M. Rios, M. P. Belleville, D. Paolucci, J. Sanchez, *J. Memb. Sci.* **2004**, *242*, 189–196.
- [61] M. Lee, Z. Wu, K. Li, *Advances in Ceramic Membranes for Water Treatment*, Elsevier, **2015**.
- [62] T. Tsuru, *J. Sol-Gel Sci. Technol.* **2008**, *46*, 349–361.
- [63] B. F. K. Kingsbury, K. Li, *J. Memb. Sci.* **2009**, *328*, 134–140.
- [64] K. Li, *Preparation of Ceramic Membranes 2.1*, in: *Ceramic Membranes for Separation and Reaction*, Wiley, Chichester, **2007**.
- [65] K. S. Joong, *Sintering*, Elsevier, **2005**.
- [66] B. Das, B. Chakraborty, P. Barkakati, *Ceram. Int.* **2016**, *42*, 14326–14333.
- [67] X. Ding, X. Liu, Y. He, *J. Mater. Sci. Lett.* **1996**, *15*, 1789–1791.
- [68] C. Y. Wu, K. J. Tu, J. P. Deng, Y. S. Lo, C. H. Wu, *Materials (Basel)*. **2017**, *10*, 566.
- [69] R. Mueller, H. K. Kammler, K. Wegner, S. E. Pratsinis, *Langmuir* **2003**, *19*, 160–165.
- [70] T. H. Ho, S. J. Chang, C. C. Li, *Mater. Chem. Phys.* **2016**, *172*, 1–5.

- [71] D. R. Hummer, J. D. Kubicki, P. R. C. Kent, P. J. Heaney, *J. Phys. Chem. C* **2013**, *117*, 26084–26090.
- [72] F. Jia, B. Narasimhan, S. Mallapragada, *Biotechnol. Bioeng.* **2014**, *111*, 209–222.
- [73] N. Carlsson, H. Gustafsson, C. Thörn, L. Olsson, K. Holmberg, B. Åkerman, *Adv. Colloid Interface Sci.* **2014**, *205*, 339–360.
- [74] L. Derr, N. Hildebrand, S. Köppen, S. Kunze, L. Trecani, R. Dringen, K. Rezwani, L. Colombi Ciacchi, *Biointerphases* **2016**, *11*, 011007.
- [75] W. Zhuang, Y. Zhang, L. He, R. An, B. Li, H. Ying, J. Wu, Y. Chen, J. Zhou, X. Lu, *Microporous Mesoporous Mater.* **2017**, *239*, 158–166.
- [76] R. du Preez, K. G. Clarke, L. H. Callanan, S. G. Burton, *J. Mol. Catal. B Enzym.* **2015**, *119*, 48–53.
- [77] R. Reshmi, G. Sanjay, S. Sugunan, *Catal. Commun.* **2007**, *8*, 393–399.
- [78] R. Reshmi, G. Sanjay, S. Sugunan, *Catal. Commun.* **2006**, *7*, 460–465.
- [79] Z. Wu, W. Qi, M. Wang, Y. Wang, R. Su, Z. He, *Biochem. Eng. J.* **2013**, *77*, 190–197.
- [80] Q. Liu, X. Kong, C. Zhang, Y. Chen, Y. Hua, *J. Sci. Food Agric.* **2013**, *93*, 1953–1959.
- [81] J. K. J. Yong, J. Cui, K. L. Cho, G. W. Stevens, F. Caruso, S. E. Kentish, *Langmuir* **2015**, *31*, 6211–6219.
- [82] E. Biró, D. Budugan, A. Todea, F. Péter, S. Klébert, *Journal Mol. Catal. B Enzym.* **2016**, *123*, 81–90.
- [83] V. Chea, D. Paolucci-Jeanjean, M. P. Belleville, J. Sanchez, *Catal. Today* **2012**, *193*, 49–56.
- [84] W. Wan, Y. Feng, J. Yang, S. Xu, T. Qiu, *J. Eur. Ceram. Soc.* **2015**, *35*, 2163–2170.
- [85] Y. X. Bai, Y. F. Li, Y. Yang, L. X. Yi, *Process Biochem.* **2006**, *41*, 770–777.
- [86] S. Tanvir, J. Pantigny, P. Boulnois, S. Pulvin, *J. Memb. Sci.* **2009**, *329*, 85–90.
- [87] K. Malecha, E. Remiszewska, D. G. Pijanowska, *Sensors Actuators B Chem.* **2014**, *190*, 873–880.
- [88] J. Lin, J. A. Siddiqui, R. M. Ottenbrite, *Polym. Adv. Technol.* **2001**, *292*, 285–292.
- [89] N. Kaltenborn, M. Sax, F. A. Müller, L. Müller, H. Dieker, A. Kaiser, R. Telle, H. Fischer, *J. Am. Ceram. Soc.* **2007**, *90*, 1644–1646.
- [90] R. Plagemann, J. von Langermann, U. Kragl, *Eng. Life Sci.* **2014**, *14*, 493–499.
- [91] B. El-Zahab, D. Donnelly, P. Wang, *Biotechnol. Bioeng.* **2008**, *99*, 508–514.
- [92] A. Dyal, K. Loos, M. Noto, S. W. Chang, C. Spagnoli, K. V. P. M. Shafi, A. Ulman, M. Cowman, R. A. Gross, *J. Am. Chem. Soc.* **2003**, *125*, 1684–1685.
- [93] S. Kroll, C. Brandes, J. Wehling, L. Treccani, G. Grathwohl, K. Rezwani, *Environ. Sci. Technol.* **2012**, *46*, 8739–8747.
- [94] J. Bartels, M. N. Souza, A. Schaper, P. Árki, S. Kroll, K. Rezwani, *Environ. Sci. Technol.* **2016**, *50*, 1973–1981.
- [95] B. Besser, T. Veltzke, J. A. H. Dreyer, J. Bartels, M. Baune, S. Kroll, J. Thöming, K. Rezwani, *Microporous Mesoporous Mater.* **2015**, *217*, 253–261.
- [96] K. Nishizawa, M. Nakajima, H. Nabetani, *Biotechnol. Bioeng.* **2000**, *68*, 92–97.
- [97] O. E. Shapovalova, D. Levy, D. Avnir, V. V. Vinogradov, *Colloids Surfaces B Biointerfaces* **2016**, *146*, 731–736.
- [98] R. P. Dos Santos, J. Martins, C. Gadelha, B. Cavada, A. V. Albertini, F. Arruda, M. Vasconcelos, E. Teixeira, F. Alves, J. Lima Filho, V. Freire, *Sci. World J.* **2014**, DOI: 10.1155/2014/154651.
- [99] J. Kujawa, W. Kujawski, *ACS Appl. Mater. Interfaces* **2016**, *8*, 7509–7521.
- [100] E. Magnan, I. Catarino, D. Paolucci-Jeanjean, L. Preziosi-Belloy, M. P. Belleville, *J. Memb. Sci.* **2004**, *241*, 161–166.
- [101] F. Wang, J. Lee, J. H. Ha, I. H. Song, *Mater. Lett.* **2017**, *191*, 200–202.
- [102] V. V. Tomina, N. V. Stolyarchuk, I. V. Melnyk, V. M. Kochkodan, Y. L. Zub, A. Chodosovskaja, A. Kareiva, *Prot. Met. Phys. Chem. Surfaces* **2016**, *52*, 55–60.
- [103] B. Besser, A. Ahmed, M. Baune, S. Kroll, J. Thöming, K. Rezwani, *ACS Appl. Mater. Interfaces* **2016**, *8*, 26938–26947.
- [104] Y. Liu, M. Peng, H. Jiang, W. Xing, Y. Wang, R. Chen, *Chem. Eng. J.* **2017**, *313*, 1556–1566.
- [105] N. F. Ishak, N. A. Hashim, M. H. D. Othman, P. Monash, F. M. Zuki, *Ceram. Int.* **2017**, *43*, 915–925.
- [106] P. Lozano, A. B. Pérez-Marín, T. De Diego, D. Gómez, D. Paolucci-Jeanjean, M. P. Belleville, G. M. Rios, J. L. Iborra, *J. Memb. Sci.* **2002**, *201*, 55–64.
- [107] J. J. Virgen-Ortíz, J. C. Dos Santos, Á. Berenguer-Murcia, O. Barbosa, R. C. Rodrigues, R. Fernandez-Lafuente, *J. Mater. Chem. B* **2017**, *7461*–7490.
- [108] D. Kołodyńska, T. M. Budnyak, Z. Hubicki, V. A. Tertykh, *Sol-Gel Derived Organic-Inorganic Hybrid Ceramic Materials for Heavy Metal Removal*, in: *Sol-gel Based Nanoceramic Materials: Preparation, Properties and Applications*, (Ed.: A. K. Mishra), Springer, **2017**, pp 253–2745.
- [109] V. V. Tomina, N. V. Stolyarchuk, I. V. Melnyk, V. M. Kochkodan, Y. L. Zub, *Microporous Mesoporous Mater.* **2015**, *209*, 66–71.
- [110] S. B. Hartono, S. Z. Qiao, J. Liu, K. Jack, B. P. Ladewig, Z. Hao, G. Qing, M. Lu, *J. Phys. Chem. C* **2010**, *114*, 8353–8362.
- [111] A. V. P. Albertini, J. L. Silva, V. N. Freire, R. P. Santos, J. L. Martins, B. S. Cavada, P. G. Cadena, P. J. Rolim Neto, M. C. B. Pimentel, C. R. Martínez, A. L. F. Porto, J. L. Lima Filho, *Chem. Eng. J.* **2013**, *214*, 91–96.
- [112] Y. Carvalho, J. M. A. R. Almeida, P. N. Romano, K. Farrance, P. Demma Carà, N. Pereira, J. A. Lopez-Sanchez, E. F. Sousa-Aguiar, *Appl. Biochem. Biotechnol.* **2017**, *182*, 1619–1629.
- [113] M. E. Marques, A. A. P. Mansur, H. S. Mansur, *Appl. Surf. Sci.* **2013**, *275*, 347–360.
- [114] M. Ortega-Muñoz, J. Morales-Sanfrutos, A. Megia-Fernandez, F. J. Lopez-Jaramillo, F. Hernandez-Mateo, F. Santoyo-Gonzalez, *J. Mater. Chem.* **2010**, *20*, 7189–7196.
- [115] K. Solanki, N. Grover, P. Downs, E. E. Paskaleva, K. K. Mehta, L. Lee, L. S. Schadler, R. S. Kane, J. S. Dordick, *Sci. Rep.* **2013**, *3*, 1–6.
- [116] Y. X. Bai, Y. F. Li, Y. Yang, L. X. Yi, *J. Biotechnol.* **2006**, *125*, 574–582.

- [117] G. Yao, D. Qi, C. Deng, X. Zhang, *J. Chromatogr. A* **2008**, *1215*, 82–91.
- [118] M. Kjellander, A. M. A. Mazari, M. Boman, B. Mannervik, G. Johansson, *Anal. Biochem.* **2014**, *446*, 59–63.
- [119] R. Xu, Y. Si, F. Li, B. Zhang, *Environ. Sci. Pollut. Res.* **2015**, *22*, 3838–3846.
- [120] G. Hollermann, R. Dhekane, S. Kroll, K. Rezwani, *Biochem. Eng. J.* **2017**, *126*, 30–39.
- [121] M. Khoobi, S. F. Motevalizadeh, Z. Asadgol, H. Forootanfar, A. Shafiee, M. A. Faramarzi, *Biochem. Eng. J.* **2014**, *88*, 131–141.
- [122] O. S. Sakr, G. Borchard, *Biomacromolecules* **2013**, *14*, 2117–2135.
- [123] F. M. Bautista, J. M. Campelo, A. García, A. Jurado, D. Luna, J. M. Marinas, A. A. Romero, *J. Mol. Catal. B Enzym.* **2001**, *11*, 567–577.
- [124] I. Migneault, C. Dartiguenave, M. J. Bertrand, K. C. Waldron, *Biotechniques* **2004**, *37*, 790–802.
- [125] O. Barbosa, C. Ortiz, Á. Berenguer-Murcia, R. Torres, R. C. Rodrigues, R. Fernandez-Lafuente, *RSC Adv.* **2014**, *4*, 1583–1600.
- [126] S. Matsuura, T. Yokoyama, R. Ishii, T. Itoh, E. Tomon, S. Hamakawa, T. Tsunoda, F. Mizukami, H. Nanbu, T. Hanaoka, *Chem. Commun.* **2012**, *48*, 7058–7060.
- [127] L. Ye, R. Pelton, M. A. Brook, *Advances* **2007**, *29*, 5630–5637.
- [128] J. C. Cruz, P. H. Pfromm, R. Szożkiewicz, M. E. Rezac, *Process Biochem.* **2014**, *49*, 830–839.
- [129] Y. Ren, J. G. Rivera, L. He, H. Kulkarni, D.-K. Lee, P. B. Messersmith, *BMC Biotechnol.* **2011**, *11*, 63.
- [130] Y. S. Zimmermann, P. Shahgaldian, P. F. X. Corvini, G. Hommes, *Appl. Microbiol. Biotechnol.* **2011**, *92*, 169–178.
- [131] Y. Z. Chen, C. T. Yang, C. B. Ching, R. Xu, *Langmuir* **2008**, *24*, 8877–8884.
- [132] M. Piras, A. Salis, M. Piludu, D. Steri, M. Monduzzi, *Chem. Commun.* **2011**, *47*, 7338–7340.
- [133] R. Ahmad, M. Sardar, *Indian J. Biochem. Biophys.* **2014**, *51*, 314–320.
- [134] M. L. Verma, M. Naebe, C. J. Barrow, M. Puri, *PLoS One* **2013**, *8*, 16–18.
- [135] G. Y. Li, K. L. Huang, Y. R. Jiang, D. L. Yang, P. Ding, *Int. J. Biol. Macromol.* **2008**, *42*, 405–412.
- [136] A. Curulli, A. Cusmà, S. Kaciulis, G. Padeletti, L. Pandolfi, F. Valentini, M. Viticoli, *Surf. Interface Anal.* **2006**, *38*, 478–481.
- [137] S. Libertino, F. Giannazzo, V. Aiello, A. Scandurra, F. Sinatra, M. Renis, M. Fichera, *Langmuir* **2008**, *24*, 1965–1972.
- [138] S. S. Vidya Bhat, *Enzym. Eng.* **2013**, *02*, DOI: 10.4172/2329-6674.1000117.
- [139] Y. S. Chaudhary, S. K. Manna, S. Mazumdar, D. Khushalani, *Microporous Mesoporous Mater.* **2008**, *109*, 535–541.
- [140] F. Secundo, *Chem. Soc. Rev.* **2013**, *42*, 6250–6261.
- [141] A. Kreider, S. Sell, T. Kowalik, A. Hartwig, I. Grunwald, *Colloids Surfaces B Biointerfaces* **2014**, *116*, 378–382.
- [142] V. Dandavate, H. Keharia, D. Madamwar, *Process Biochem.* **2009**, *44*, 349–352.
- [143] J. Schartner, K. Gavriljuk, A. Nabers, P. Weide, M. Muhler, K. Gerwert, C. Kötting, *ChemBioChem* **2014**, *15*, 2529–2534.
- [144] A. Michota-Kaminska, B. Wrzosek, J. Bukowska, *Appl. Spectrosc.* **2006**, *60*, 752–757.
- [145] D.-H. Zhang, L.-X. Yuwen, L.-J. Peng, *J. Chem.* **2013**, *2013*, 1–7.
- [146] Ö. Alptekin, S. S. Tükel, D. Yildirim, D. Alagöz, *J. Mol. Catal. B Enzym.* **2009**, *58*, 124–131.
- [147] L. Bayne, R. V. Ulijn, P. J. Halling, *Chem. Soc. Rev.* **2013**, *42*, 9000.
- [148] M. S. Thomsen, B. Nidetzky, *Biotechnol. J.* **2009**, *4*, 98–107.
- [149] M. De Cazes, M. P. Belleville, E. Petit, M. Llorca, S. Rodríguez-Mozaz, J. De Gunzburg, D. Barceló, J. Sanchez-Marcano, *Catal. Today* **2014**, *236*, 146–152.
- [150] M. Perwez, R. Ahmad, M. Sardar, *Int. J. Biol. Macromol.* **2017**, *103*, 16–24.
- [151] W. Xu, Y. Yong, Z. Wang, G. Jiang, J. Wu, Z. Liu, *ACS Sustain. Chem. Eng.* **2017**, *5*, 90–96.
- [152] P. Bhang, N. Sridevi, D. S. Bhang, A. Prabhune, V. Ramaswamy, *Int. J. Biol. Macromol.* **2014**, *63*, 218–224.
- [153] M. Gamallo, Y. Moldes-Diz, G. Eibes, G. Feijoo, J. M. Lema, M. T. Moreira, *Biocatal. Biotransformation* **2017**, *2422*, 1–11.
- [154] A. Aminian, B. Shirzadi, Z. Azizi, K. Maedler, E. Volkmann, N. Hildebrand, M. Maas, L. Treccani, K. Rezwani, *Mater. Sci. Eng. C* **2016**, *69*, 184–194.
- [155] Y. Qu, Z. Wu, R. Huang, W. Qi, R. Su, Z. He, *RSC Adv.* **2016**, *6*, 64581–64588.
- [156] S. Prakash, M. B. Karacor, S. Banerjee, *Surf. Sci. Rep.* **2009**, *64*, 233–254.
- [157] W. Li, G. Ling, F. Lei, N. Li, W. Peng, K. Li, H. Lu, F. Hang, Y. Zhang, *Sep. Purif. Technol.* **2018**, *190*, 9–24.
- [158] J. Luo, F. Marpani, R. Brites, L. Frederiksen, A. S. Meyer, G. Jonsson, M. Pinelo, *J. Memb. Sci.* **2014**, *459*, 1–11.
- [159] A. Ur Rehman, Z. Kovacs, H. Quitmann, M. Ebrahimi, P. Czermak, *Sep. Sci. Technol.* **2016**, *51*, 1537–1545.
- [160] X. Mei, P. J. Quek, Z. Wang, H. Y. Ng, *Bioresour. Technol.* **2017**, *240*, 25–32.
- [161] G. Liu, Y. Xu, Y. Han, J. Wu, J. Xu, H. Meng, X. Zhang, *Dalt. Trans.* **2017**, *46*, 2114–2121.
- [162] C. Ji, J. Hou, V. Chen, *J. Memb. Sci.* **2016**, *520*, 869–880.
- [163] J. M. Benito, M. J. Sánchez, P. Pena, M. A. Rodríguez, *Desalination* **2007**, *214*, 91–101.
- [164] A. Dafinov, R. Garcia-Valls, J. Font, *J. Memb. Sci.* **2002**, *196*, 69–77.

A2 Paper 2: Alcohol dehydrogenase on inorganic powders: Zeta potential and particle agglomeration as main factors determining activity during immobilization

Sigyn Björk Sigurdardóttir, Jonas Lehmann, Jean-Claude Grivel, Wenjing Zhang, Andreas Kaiser, and Manuel Pinelo

Colloids and Surfaces B: Biointerfaces, vol. 175, pp. 136–42, 2018. doi:10.1016/j.colsurfb.2018.11.080.



Contents lists available at ScienceDirect

Colloids and Surfaces B: Biointerfaces

journal homepage: www.elsevier.com/locate/colsurfb

Alcohol dehydrogenase on inorganic powders: Zeta potential and particle agglomeration as main factors determining activity during immobilization



Sigyn Björk Sigurdardóttir^a, Jonas Lehmann^b, Jean-Claude Grivel^b, Wenjing Zhang^b,
Andreas Kaiser^b, Manuel Pinelo^{a,*}

^a Technical University of Denmark, DTU Chemical Engineering, Søtofts Plads, Building 229, 2800 Kgs. Lyngby, Denmark

^b Technical University of Denmark, DTU Energy, Frederiksborgvej 399, 4000, Roskilde, Denmark

ARTICLE INFO

Keywords:

Enzyme immobilization
Inorganic powders
Alcohol dehydrogenase
Colloid stability

ABSTRACT

Alcohol dehydrogenase from *Saccharomyces cerevisiae* was immobilized on different inorganic support materials, i.e. powders of Al₂O₃, SiC, TiO₂ and YSZ-8, by covalent bonding and physical adsorption. The raw powders were characterized by scanning electron microscopy, BET surface area, particle size distribution and ζ-potential measurements. Enzyme activity retention, storage stability and recyclability were evaluated on the basis of the measured support material properties. Preliminary experiments showed that the buffer selection was a critical factor. The properties of both the enzyme and the powders varied considerably between the buffers used; namely Tris-HCl (100 mM, pH 7) and MES (40 mM, pH 6.5) buffers. The enzyme activity was higher and more stable in the MES buffer, whereas the commonly used Tris buffer was problematic due to apparent incompatibility with formaldehyde. In MES, the order of decreasing activity of covalently bonded enzyme was on SiC > YSZ-8 > Al₂O₃ > TiO₂. The lower performance of TiO₂ was ascribed to the negative ζ-potential of the material, which impeded an efficient immobilization. Particle agglomeration, caused by low colloidal stability of the particles in MES buffer, hampered the storage stability of the immobilized systems. The results from this study show the advantages and limitations of using nanoparticles as immobilization supports, and highlight which properties of nanoparticles must be considered to ensure an efficient immobilization.

1. Introduction

A common approach to stabilize enzymes for their viable applications in industrial processes is to immobilize them on solid supports [1,2]. Using inorganic materials as immobilization support has many advantages, including superior thermal, mechanical and microbial stability, prolonged service life and ability of regeneration of their native properties by thermal and chemical cleaning methods. Various inorganic support structures and morphologies have been proposed for enzyme immobilization, including nanoparticles and membranes [3]. Nanomaterials provide the advantages of high surface-to-volume ratio and limited mass transfer resistance, which allows both high enzyme loading and high activity retention [4–6]. Nevertheless, the design of an optimized immobilized enzyme system still faces the challenge of pairing the enzyme with a suitable support and a suitable immobilization method, as the success of immobilization is highly dependent on these factors. For instance, the effects of the nature and properties of the support material on enzyme activity and stability was demonstrated by Masuda et al. [7,8], who immobilized formaldehyde

dehydrogenase (FaldDH) on mesoporous silica and zirconia particles. The catalytic properties of FaldDH immobilized on mesoporous silica varied with the pore size of the support and the functionalization agent used. Of the seven pore sizes investigated, the highest activity of physically adsorbed enzyme was observed on particles with pores of similar size as the enzyme dimensions. The activity was further enhanced by functionalizing the support with phenyltriethoxysilane, owing to favorable hydrophobic interactions between the enzyme and the functionalized support [7]. In a subsequent study by the same group, the catalytic activity and thermal stability of FaldDH were further improved by immobilization on mesoporous zirconia, instead of silica [8]. Silica is one of the most commonly used materials for enzyme immobilization [9]. Other inorganic nanoparticles have however attracted high interest recently, e.g. magnetic nanoparticles for their ease of separation from a medium [3], and gold nanoparticles (AuNPs) for their high biocompatibility [10]. The latter were applied for the immobilization of bovine serum amine oxidase on core-shell AuNPs, consisting of a gold core and polymeric shell. The particle-enzyme complex finds potential applications in cancer therapy. Both enzyme

* Corresponding author.

E-mail address: mp@kt.dtu.dk (M. Pinelo).

<https://doi.org/10.1016/j.colsurfb.2018.11.080>

Received 4 October 2018; Received in revised form 23 November 2018; Accepted 28 November 2018

Available online 29 November 2018

0927-7765/ © 2018 Elsevier B.V. All rights reserved.

activity and loading were highly dependent on pH; enzyme loading increased at acidic conditions due to more favorable electrostatic interactions, while activity was highest at neutral conditions where the enzyme structure was intact [10]. The importance of selecting the right immobilization method for a given enzyme is likewise important, and was clearly seen in a recent study by Zhang et al. [11], who used three different immobilization methods for five different enzymes on three different polymeric membranes. Electrostatic adsorption resulted in the highest activity retention for four out of five enzymes, while hydrophobic adsorption was suitable for only two out of five enzymes. Covalent bonding resulted in high enzyme loading but lower activity retention due to conformational changes posed on the enzymes. The results can be used as a platform for the selection of immobilization method to ensure high enzyme activity and stability.

Alcohol dehydrogenase (ADH) is an enzyme whose industrial applications are hampered by its instability [12], e.g. free ADH employed in an enzymatic membrane reactor was almost completely deactivated after 90 min (4 cycles) of operation [13]. ADH catalyzes the reversible oxidation of alcohols to aldehydes/ketones [14]. One important application of ADH is in the cascade conversion of CO₂ to methanol (MeOH), a conversion route that is of high interest nowadays for its ability to produce MeOH as fuel or a building block chemical, while simultaneously contributing to the sequestration of CO₂ from the atmosphere [15–17]. In this enzymatic conversion, CO₂ is converted to MeOH by formate dehydrogenase (FateDH), FaldDH and ADH, with formic acid and formaldehyde (Fald) as intermediate products, and the simultaneous oxidation of the cofactor NADH in each step. This route was already suggested two decades ago by Obert and Dave [18], and has been widely studied since. The unfavorable thermodynamic of the reverse combustion can be overcome by the enzymatic catalysis [19], but not without complications. In addition to the consumption of the costly cofactor, NADH, the process suffers from low activity and stability of the enzymes involved, which has been the main factor in yet preventing the scale-up of the process [12,15]. Consequently, the immobilization of ADH has been the subject of numerous recent studies, in attempts to enhance its stability and other catalytic parameters [20–26].

The aim of this study is to investigate the interactions between ADH and different inorganic support materials, based on the fundamental properties of these materials. For this purpose, we used four inorganic raw powders of materials that are commonly used for enzyme immobilization, namely Al₂O₃, SiC, TiO₂ and yttria stabilized zirconia (YSZ-8). ADH was immobilized on the powders by two different methods; physical adsorption (PA) and covalent bonding (CB). The activity and stability of the immobilized enzymes are explained based on different powder properties, i.e., ζ -potential, surface area and particle size distribution. Moreover, the effects of two different buffers on enzyme- and powder colloidal stabilities are discussed, just as the interactions between the two. Low colloidal stability influences the degree of particle agglomeration, which has negative effects on the enzyme stability. The final objective of this work is to identify the main characteristics of inorganic raw materials in an enzyme environment that promotes optimal enzyme catalytic properties and stability. Such information can be of guidance for the optimization and utilization of other enzyme-material systems to ensure high enzyme performance.

2. Materials and methods

2.1. Chemicals and enzymes

Alcohol dehydrogenase from *Saccharomyces cerevisiae* (yeast ADH, EC 1.1.1.1), β -nicotinamide adenine dinucleotide reduced disodium salt hydrate (NADH, $\geq 97\%$), Anatase-TiO₂, Fald (37% in H₂O), (3-aminopropyl)triethoxysilane (APTES, 99%), glutaraldehyde (GA, 25% in H₂O), 2-(*N*-Morpholino)ethanesulfonic acid, MES potassium salt, Trizma[®] base, hydrochloric acid (37%) were purchased from Sigma-Aldrich (Steinheim, Germany). Ethanol (EtOH, 99%) was from WVR

(Søborg, Denmark). Roti[®]-Nanoquant 5x concentrate was purchased from Carl Roth GmbH (Karlsruhe, Germany). Non-commercial SiC ceramic powder was provided by LiqTech Intl. (Ballerup, Denmark), α -Al₂O₃ from Nanostructured and Amorphous Materials inc. (Texas, USA) and YSZ-8 from Tosoh Corporation (Tokyo, Japan).

2.2. Powder characterization

Particle size distribution (PSD) was analyzed using a Beckman Coulter LS13320 (Beckman Coulter Inc., USA). The powder concentration of the suspensions was 1 wt%, using deionized (DI) water as solvent. The suspensions were continuously kept in motion before entering the equipment to avoid potential sedimentation. *Surface area* was calculated from BET (Brunauer-Emmett-Teller) measurements using an Autosorb 1 (Quantachrome Instruments, USA). The powder was degassed for 3 h at 300 °C, followed by 1 h of measurements in N₂-gas. ζ -*Potential* was calculated using a Zetaprobe Analyzer (Colloidal Dynamics LLC, USA). The equipment was calibrated before each experiment to ensure high quality results. The powders were analyzed under mild stirring of 150 rpm, using single-point measurements and 1 wt% concentration in two different buffers; 100 mM Tris-HCl at pH 7 and 40 mM MES at pH 6.5 (hereinafter called Tris and MES buffers, respectively). The setting calculates ζ -potential over time at the pH values of the buffers. *Powder morphology* was characterized by scanning electron microscopy (SEM) using a Zeiss Merlin microscope (Carl Zeiss, Germany) with an accelerating voltage of 5 kV, generating the image from secondary electrons.

2.3. Immobilization procedures

ADH was immobilized on the powders by PA (ADH-PA) and CB (ADH-CB). For PA, 10 mg of powder and 10 mL of enzyme solution (20 mg/L) were mixed for 90 min, at room temperature (RT) and 100 rpm. For CB, 10 mg of powder was first functionalized with APTES (90 min, 70 °C, 700 rpm) and activated with GA (30 min, RT, 700 rpm) before immobilization. The activated powder was then mixed with 10 mL of enzyme solution for 90 min, at RT and 100 rpm. A detailed description is given in Supplementary material. A detailed scheme of the immobilization protocols is given in Fig. 1.

2.4. Activity of free and immobilized enzyme

Enzyme activity was assessed by the catalyzed conversion of Fald to MeOH with simultaneous oxidation of the cofactor NADH to NAD⁺. The reaction was monitored by measuring the absorbance of NADH at 340 nm throughout the reaction, since NADH has an absorbance maximum at this wavelength whereas NAD⁺ does not. A decrease in absorbance is observed as NADH is oxidized and Fald is converted to MeOH. The reaction conditions were as follows: 10 mL reaction volume, 30 mM Fald, 100 μ M NADH, 1 g/L powder in MES buffer, pH 6.5, RT and 100 rpm. The reactions were initiated by the addition of NADH to the reactor. Samples were filtered with a 0.22 μ m syringe filter to remove the powder and transferred to a semi-micro UV-cuvette for absorbance measurements on a UV-1280 spectrophotometer (SHIMADZU Corp., Japan). The activity of free enzyme was measured at enzyme concentrations of 0–20 mg/L in MES buffer, with 30 mM Fald and 100 μ M NADH. The free enzyme reactions were conducted on a Corning 96-well flat bottom UV microplate, the absorbance at 340 nm was measured on a Tecan Infinite[®] M200 plate reader (Tecan Trading AG, Switzerland).

2.5. Storage stability

Storage stability of ADH-PA and ADH-CB on SiC powder was investigated. The immobilized enzyme was suspended in MES buffer and stored in 2 mL aliquots at 4 °C. A free enzyme solution in MES buffer

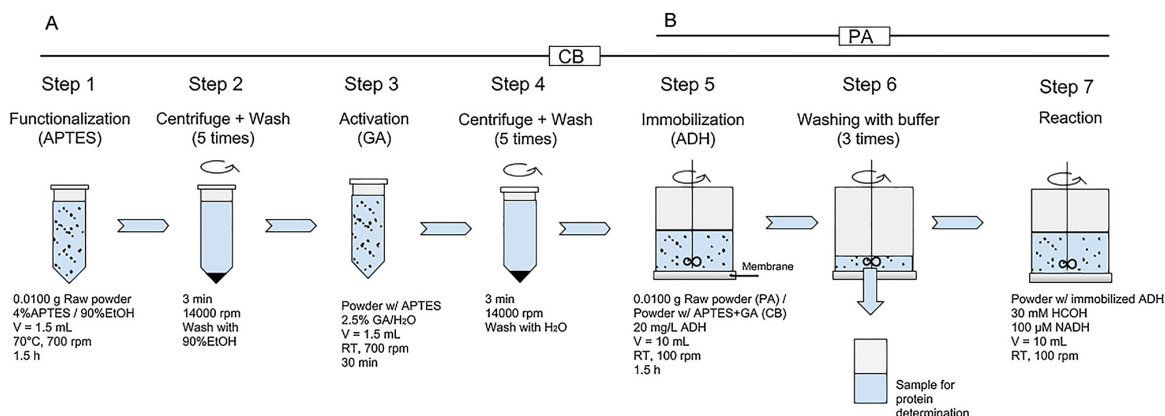


Fig. 1. Scheme of immobilization protocols, steps 1–7 for CB, steps 5–7 for PA.

was prepared and stored at 4 °C. The activity of the free and immobilized enzymes was measured after 0–40 days storage in the buffer. The storage buffer was filtered from the powder with a GRM0,1PP membrane before the reactions, the permeate was stored for protein determination and investigation of enzyme leakage. The reactions were conducted by the same procedure as the activity studies described above.

2.6. Recyclability

The activity retention of ADH-PA and ADH-CB on SiC powder in multiple reaction cycles was investigated. The enzyme activity was measured in eight consecutive reaction cycles. The reaction conditions were similar as described above. Samples were collected after 10 min of reaction. After each reaction cycle, the reaction mixture was filtered from the powder and the powder was washed once with 10 mL of MES buffer. The subsequent reaction cycle was initiated by adding fresh reaction mixture to the reactor.

2.7. Protein determination

Enzyme loading and leakage were determined with Roti Nanoquant assay, which is a modified Bradford assay that can be used for detection of extremely low protein amounts, down to 200 ng according to the manufacturer. The absorbance at 590 nm and 450 nm is measured, and the quotient of the two gives linearity. The sample concentration can thus be read from a standard curve, which was made with ADH.

3. Results and discussion

3.1. Buffer selection

Tris-HCl buffer is a commonly used buffer in enzyme catalyzed reactions at physiological pH, including reactions with ADH [16,21,23,24]. In our initial experiments with the immobilized ADH catalyzed conversion of Fald to MeOH in Tris buffer, the enzyme stability was very low. pH measurements of the reaction mixtures revealed that upon adding Fald to the Tris buffer for the preparation of a 30 mM solution, the pH dropped to around 5, rendering the enzyme more or less inactive. Evers et al. mentioned a similar drop in pH upon mixing Fald in a Tris buffered solution at a neutral pH, and deemed it critical to avoid using Tris buffer for the Fald fixation of RNA [27]. The above results suggested that the buffer capacity of the Tris buffer was hampered by reaction with Fald. Tris can react with Fald to make stable intramolecular cyclic products, and this reactivity is indeed commonly exploited to quench Fald reactivity and cross-linking activity [28,29]. In light of these complications, a different buffer was suggested, and of the tested MES and MOPS (4-Morpholinepropanesulfonic acid) buffers at pH 5.5–7.5, the MES buffer at pH 6.5 was found to provide suitable conditions for the reactions and the highest enzyme activity. pH 6.5 was elsewhere found to be the optimal pH for the three enzyme cascade reaction of CO₂ to MeOH, catalyzed by FaldDH and ADH [30]. The pH of the reaction mixture in MES buffer was unaffected by Fald. Furthermore, the spontaneous degradation of NADH was much lower in a 30 mM Fald mixture prepared in MES buffer than in Tris buffer, or 0.04 ± 0.01 and 0.56 ± 0.10 μM/min in MES and Tris, respectively. This is likely since NADH is generally more unstable at lower pH [31].

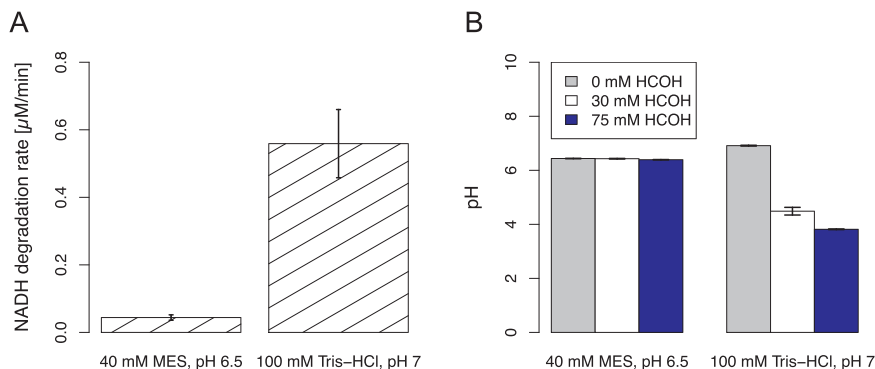


Fig. 2. (Left) Spontaneous degradation of NADH in Tris and MES buffers. Solution concentrations: 30 mM Fald, 100 μM NADH, no enzyme. (Right) Changes in pH of MES and Tris buffers upon addition of Fald. Error bars report standard deviation of three independent measurements.

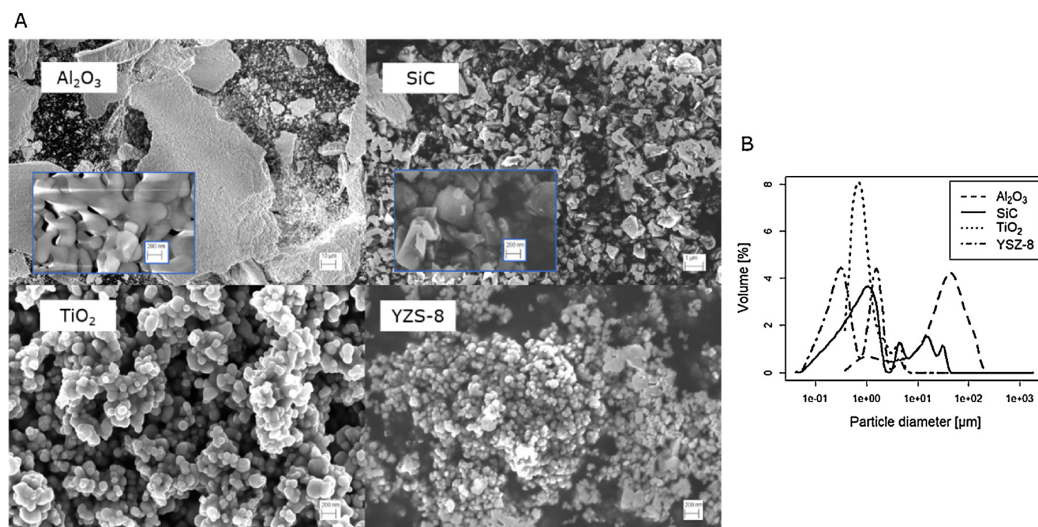


Fig. 3. (A) SEM figures and (B) PSD of raw Al₂O₃, SiC, TiO₂ and YSZ-8 powders. PSD was measured at 1 wt% powder concentration in DI water.

The degradation is especially important considering that NADH is commonly used to monitor reactions, and the spontaneous degradation must be accounted for in activity measurements [21,24]. The observations just discussed are illustrated in Fig. 2 and highlight the importance of carefully selecting all process conditions for optimized performance. Considering these results, the MES buffer was selected for further experiments with ADH.

3.2. Powder characterization

The properties of the support largely decide the success of immobilization. The powder properties investigated here were the PSD, BET surface area and ζ -potential, in addition to visualization by SEM. The PSD and BET surface area contain information about the available surface area for immobilization while the ζ -potential is important regarding the electrostatic interactions between the enzyme and support.

3.2.1. Powder morphology

The SEM images of Al₂O₃, SiC, TiO₂ and YSZ-8 powders are shown in Fig. 3A. The figures reveal the different morphologies of the powders. The TiO₂ and YSZ-8 powders seem to have similar morphologies, composed of fine, spherical particles with a narrow PSD. The SiC particles are relatively fine, but with irregular sizes and shapes and coarse surfaces. The Al₂O₃ particles are likewise irregular in size and shape, large particles with flat surfaces are observed on the SEM figure of Al₂O₃.

The observations from the SEM images are supported by PSD measurements (Fig. 3B). From the PSD, the Al₂O₃ particles measure an order of magnitude bigger than the other particles, with an average particle diameter of 46.0 μm, compared to 0.7–3.7 μm for the other particles (Table 1). However, given the irregular and flat surfaces of the Al₂O₃ particles, it is likely that the particle size is overestimated due to assumption of spherical particles. The SiC powder has a somewhat wide

PSD - in addition to the average particle diameter of 3.7 μm, there is a considerable amount of larger particles, up to 40 μm in size, indicating that SiC could be prone to agglomeration. Small particles provide numerous advantages for immobilization over large particles, notably, higher surface area and higher particle concentration in a suspension. Furthermore, mass transfer limitations are reduced, both regarding particle mobility in solution, i.e. increased Brownian motion, [32,33] as well as regarding diffusion of species within the particles [34,35].

The BET surface areas of the four powders are given in Table 1, and mostly reflect the results of the PSD measurements. The Al₂O₃ powder has the lowest BET surface area, or 5.4 m²/g, compared to 11.5–13.4 m²/g for the other powders. This difference is rather small, considering the difference in PSD, which supports the suggestion that the size of the Al₂O₃ powder is overestimated due to the flat shapes of the particles. The finest powder, YSZ-8, has the largest BET surface area, followed by SiC and TiO₂. The irregular surfaces and presence of very small SiC particles, down to 0.1 μm as revealed by the PSD, could explain the higher surface area of SiC than of TiO₂, despite larger average particle size.

3.2.2. ζ -Potential

In addition to the morphology, the electrostatic properties of the support materials play an important role in enzyme immobilization. The ζ -potential of the powders were measured in both Tris and MES buffers and the results are given in Table 1. The results vary considerably between the two buffers; the ζ -potential is generally higher in the Tris buffer than in the MES buffer, except for TiO₂. TiO₂ is the only powder resulting in a negative ζ -potential and a higher absolute value in MES than Tris, or -42.25 and -35.02 mV, respectively. The observed change in ζ -potential of the TiO₂ is most likely a result of a lower salt concentration of the MES buffer as compared to the Tris buffer. Generally, the ζ -potential decreases with increasing salt concentration since the electrical double layer (fixed and diffuse layer of counter ions

Table 1

Properties of Al₂O₃, SiC, TiO₂ and YSZ-8 powders. Where applicable, values are means \pm SD (n = at least 2).

Powder	IEP from literature [38]	ζ -potential (Tris) [mV]	ζ -potential (MES) [mV]	BET surface area [m ² /g]	Average particle diameter from PSD [μm]
Al ₂ O ₃	8–9	32.4 \pm 0.2	12.5 \pm 0.3	5.4	46.0
SiC	2.5–3.5	63.4 \pm 0.6	2.8 \pm 0.1	13.0	3.7
TiO ₂	5–7	–35.0 \pm 2.8	–42.3 \pm 1.5	11.5	1.2
YSZ-8	7.5–9.5	33.5 \pm 0.2	8.1 \pm 0.1	13.4	0.7

around a surface) is compressed in the presence of salts [36]. However, the opposite is seen for the other powders - the Al_2O_3 , SiC and YSZ-8 powders are only slightly positively charged in the MES buffer, with ζ -potentials of 12.51, 2.08 and 8.09, respectively, whereas the ζ -potentials of these powders are 32.44, 63.41 and 33.45 mV in the Tris buffer. A possible explanation for the drop in ζ -potential, despite a lower ionic concentration, can be found in the nature of the ionic compounds of the two buffers. As the Al_2O_3 , SiC and YSZ-8 powders are positively charged in both buffers, the counter ions in the Tris and MES buffers are Cl^- and MES^- ($\text{C}_6\text{H}_{12}\text{NO}_4\text{S}^-$), respectively. Weak electrolytes, such as the MES^- , can adsorb to particle surfaces by hydrogen and van der Waals bonds, in addition to electrostatic forces [36,37]. At the same time, the diffusion of MES^- ions back to the bulk is slower than of the Cl^- ions due to their size. Hence, the adsorption of MES^- ions on the surface of the positively charged powders might explain the low ζ -potential of these powders in the MES buffer.

3.3. Properties of free and immobilized ADH

3.3.1. Activity of ADH immobilized on inorganic powders

The activity of ADH immobilized on the four powders by PA and CB is shown in Fig. 4, where a faster consumption of NADH means higher enzyme activity. The activity retention is generally high, except for TiO_2 . Regarding the Al_2O_3 , SiC and YSZ-8 powders, the activity retention of ADH-PA is higher than that of ADH-CB, which is consistent with what is generally seen when comparing these two immobilization methods [3]. The lower activity retention of ADH-CB can be caused by a number of reasons, notably conformational changes in the enzyme structure by the formation of covalent bonds and increased mass transfer limitations [39,40]. The latter arises since the particles can undergo cross-linking in the activation step with GA, thereby decreasing the available surface area and increasing the mass transfer limitations within the particle clusters. Moreover, the covalent attachment by GA can result in unfavorable orientation of the enzyme, so that the active sites are blocked [16]. Despite these negative effects on the enzyme activity, covalent bonds generally provide robustness, and therefore, CB is often favored in terms of increased operational stability and decreased enzyme leaching. From Fig. 4, it may be observed how the enzyme activity is lower on the Al_2O_3 particles than on SiC and YSZ-8, which can be explained by the lower BET surface area of the Al_2O_3 particles.

The special case here is the TiO_2 powder, where the immobilization results in low activity retention, especially with ADH-PA. This is likely explained by the negative ζ -potential of TiO_2 in the MES buffer at pH

6.5. ADH is likewise negatively charged at pH 6.5 (IEP 5.4–5.8), which leads to electrostatic repulsion between the TiO_2 powder and the ADH, and thereby low enzyme loading. This is especially important for PA, where the electrostatic forces play a central role in the immobilization [41]. Consistently, the results here show almost zero activity retention of ADH-PA on TiO_2 . The other three powders had a slight positive surface charge, thereby providing favorable electrostatic conditions for ADH-PA. The electrostatic forces are less important for CB. The surface chemistry of the support is altered by functionalization and activation, as new functional groups and new charges are introduced to the surface [42,43]. The introduction of GA would typically result in increased positive charge on the surface under the conditions at hand. This change in surface charge was demonstrated by Vasconcellos et al. [42], who measured the ζ -potential of six different nanozeolite supports for enzyme immobilization, both untreated supports, as well as amino-functionalized (with aminopropyltrimethoxysilane) and GA activated. The introduction of the functionalizing and activating agents resulted in increased positive ζ -potential, for instance, the ζ -potential of an untreated zeolite composed of SiO_2 , TiO_2 and Na_2O in DI water was -34.4 mV, while the amino-functionalized surface had a ζ -potential of +19.6 mV and the further GA activated surface had a ζ -potential of +30.2 mV [42]. The shift in ζ -potential from negative to positive allows a more efficient immobilization of ADH on the surface of the activated TiO_2 particles than on the raw TiO_2 particles, as can be seen by comparing the two reaction curves for TiO_2 in Fig. 4.

3.3.2. Storage stability of free and immobilized ADH

The storage stability of ADH was investigated by measuring the enzyme activity after storage in MES buffer for up to 40 days. For these experiments, ADH was immobilized on SiC, which was chosen from the four powders based on the performance in the activity studies. The results for free and immobilized enzymes are shown in Fig. 5A. The results are presented as relative activity, compared to the activity of freshly prepared enzyme solution or immobilized enzyme (day 0). The free enzyme seems to be highly stable, since the relative activity was still $85 \pm 4\%$ at day 40, which is much higher than for the immobilized enzymes, where the relative activity at day 40 was $30 \pm 22\%$ and $3 \pm 4\%$ for ADH-PA and ADH-CB, respectively. It must be noted that the activity retention of ADH-PA was still high after 21 days, or $94 \pm 12\%$. With ADH-CB on the other hand, the activity retention decreases steadily and the enzyme was more or less inactive after 21 days. These results are in apparent contradiction to what is generally observed, where CB normally provides higher stability than PA [44–47]. However, the behavior of the CB samples observed here

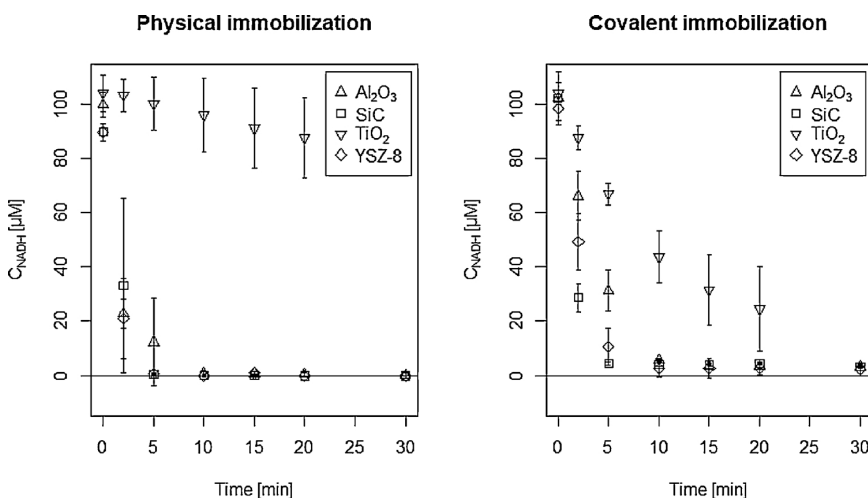


Fig. 4. Activity of ADH-PA (left) and ADH-CB (right) immobilized on Al_2O_3 , SiC, TiO_2 and YSZ-8 powders. Activity was measured as the decrease in NADH concentration, which was measured by absorbance at 340 nm. Reaction conditions: 10 mL reaction volume, 30 mM Fald, 100 μM NADH, RT, 100 rpm, MES buffer, pH 6.5. Error bars report standard deviation of at least two independent measurements.

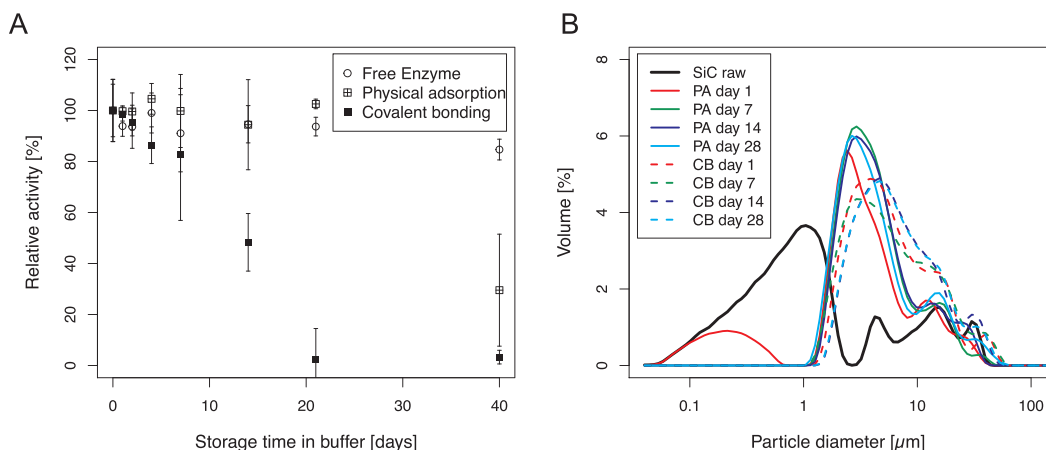


Fig. 5. (A) Effects of storage in MES buffer on activity of free ADH, ADH-PA and ADH-CB immobilized on SiC powder. Reaction conditions: 10 mL reaction volume, 30 mM Fald, 100 μ M NADH, RT, 100 rpm, MES buffer, pH 6.5. (B) PSD of raw SiC and SiC with ADH-PA and ADH-CB showing effects of storage in MES buffer on particle agglomeration. Error bars report standard deviation of at least two independent measurements.

may be explained by the particularities of the employed system, especially the use of fine powders as immobilization supports.

Considering the free ADH, the MES buffer seems to generally provide a good environment, as seen by the high storage stability in the buffer. Similar experiments in the Tris buffer showed a much more pronounced decrease in enzyme activity with storage. ADH is negatively charged in both buffers, which might induce the interactions between the enzyme and the positively charged Tris molecules ($\text{NH}_3\text{C}(\text{CH}_2\text{OH})_3^+$), while resulting in better dispersion in the presence of the negatively charged MES^- molecules and lower ionic concentration. This hypothesis can be supported by the findings of Cugia et al. [37] who measured the mobility of positively charged lysozyme in different buffers and found the highest mobility to be in Tris buffer, the only positively charged buffer investigated.

Regarding the immobilized enzymes, the observed decrease in activity was mainly caused by enzyme leakage and mass transfer limitations. The enzyme loss due to leakage was calculated from protein concentration measurements of the storage buffer, and was found to be around 3–8% for both ADH-PA and ADH-CB. Mass transfer limitations seemed to be a more critical factor here. This was detected by the formation of particle agglomerates in the buffer during storage. The mass transfer limitations increase with the size of the agglomerates, thereby resulting in decreased activity. This observation was investigated further by measuring the PSD of the powder with immobilized enzyme after storing in buffer for 1–28 days. The results are presented in Fig. 5B, and clearly show the agglomeration of the particles, notably the particles with ADH-CB. The mean particle diameter increased from 3.7 μm for the raw powder to 4.4 and 7.0 μm for powder with ADH-PA and ADH-CB, respectively, after one day of storage in MES buffer. The particles with ADH-CB immediately formed large agglomerates, likely due to cross-linking of the particles during the GA activation step, which helps explaining the immediate and dramatic decrease in the activity of ADH-CB. The particles with ADH-PA formed smaller agglomerates that increased in size during storage.

In addition to the agglomeration, the observed difference in activity retention of the enzymes might be explained by the immobilization efficiency (IE). The IE of ADH-PA and ADH-CB was 65.2% and 39.5%, respectively. With a smaller initial amount of enzyme to catalyze the reactions (lower IE of ADH-CB than ADH-PA), the decrease in activity due to natural decay, leakage, mass transfer limitations etc., will be more pronounced.

3.3.3. Recyclability of ADH on SiC

One of the main objectives of enzyme immobilization is to extend the lifetime of the catalyst to allow its repeated use in multiple reaction cycles and/or in continuous processes. To investigate the recyclability performance of ADH immobilized on SiC powder, the immobilized enzyme was used in eight consecutive reaction cycles. The results are presented in Fig. S1. After the eight reaction cycles, the activity retentions of ADH-PA and ADH-CB were $49 \pm 4\%$ and $32 \pm 18\%$, respectively. The decrease in enzyme activity is mainly explained by the mechanical stress on the enzyme in the reaction set-up. Furthermore, the repeated agitation and filtration could induce the aggregation of the powder particles with subsequent mass transfer restrictions, as was also suggested by Gao et al. [45] who used a similar recycling and washing procedure for the recycling of carbonic anhydrase immobilized on TiO_2 nanoparticles. The residual activity of ADH-CB is somewhat lower than of ADH-PA. On the other hand, the rate of decrease in activity is similar for the two immobilization methods, except the decrease in activity is only detected after the third cycle for ADH-PA instead of after the first cycle for ADH-CB. This could indicate that the enzyme is mostly immobilized on the outer surface of the particles, and is thereby equally exposed to the external conditions. Immobilization on outer surfaces does not result in as high stabilization as immobilization inside porous structures [15]. The delay observed here is likely because of the higher IE of ADH-PA than ADH-CB, which in these experiments were measured to be 76.6% and 25.1%, respectively.

4. Conclusions

The results obtained here have confirmed some fundamental aspects of enzyme immobilization on solid surfaces. The importance of electrostatic forces for physical adsorption of enzymes was seen by the different activity retention of ADH on the four inorganic powders investigated, i.e. high activity retention was achieved where the powder and enzyme had opposite surface charge while the activity retention was low in the case of similar surface charges. The surface area is likewise an important factor, the lower surface area of the Al_2O_3 powder as compared to the SiC and YSZ-8 powders resulted in lower observed activity. Furthermore, the immobilization efficiency by CB was considerably lower than by PA, which was presumably due to cross-linking of the particles in the activation step with GA, resulting in decreased surface area available for immobilization. The results obtained revealed both advantages and disadvantages of using nanoparticles as support for enzyme immobilization. The nanoparticles

proved to be good immobilization supports regarding high Brownian motion and high activity retention. Furthermore, the nanoparticles were easily recovered from a reaction medium by filtration, which facilitates their use in multiple reaction cycles. On the other hand, the storage stability of the immobilized enzyme suffered from agglomeration of the nanoparticles in the MES buffer. This highlighted the necessity to find a suitable buffer, considering both the reaction conditions and suspension stability, in order to fully exploit the advantages of nanoparticles in future applications.

Conflict of interest

The authors declare that they have no conflict of interest.

Acknowledgement

This work was supported by The Danish Council for Independent Research, Grant no.: 6111-00232B.

Appendix A. Supplementary data

Supplementary material related to this article can be found, in the online version, at doi:<https://doi.org/10.1016/j.colsurfb.2018.11.080>.

References

- [1] R.A. Sheldon, *Adv. Synth. Catal.* 349 (2007) 1289–1307.
- [2] M.L. Verma, C.J. Barrow, M. Puri, *Appl. Microbiol. Biotechnol.* 97 (2013) 23–39.
- [3] S.B. Sigurdardóttir, J. Lehmann, S. Ovtar, J. Grivel, M. Della Negra, A. Kaiser, M. Pinelo, *Adv. Synth. Catal.* 360 (14) (2018) 2578–2607, <https://doi.org/10.1002/adsc.201800307>.
- [4] E. Aslani, A. Abri, M. Pazhang, *Colloids Surf. B: Biointerfaces* 170 (2018) 553–562.
- [5] J.N. Talbert, J.M. Goddard, *Colloids Surf. B: Biointerfaces* 93 (2012) 8–19.
- [6] H. Jia, G. Zhu, P. Wang, *Biotechnol. Bioeng.* 84 (2003) 406–414.
- [7] Y. Masuda, S.I. Kugimiya, K. Murai, A. Hayashi, K. Kato, *Colloids Surf. B: Biointerfaces* 101 (2013) 26–33.
- [8] Y. Masuda, S. Kugimiya, K. Kato, *J. Asian Ceram. Soc.* 2 (2014) 11–19.
- [9] T. Jesionowski, J. Zdzarta, B. Krajewska, *Adsorption* 20 (2014) 801–821.
- [10] I. Venditti, T.F. Hassanein, I. Fratoddi, L. Fontana, C. Battocchio, F. Rinaldi, M. Carafa, C. Marianecchi, M. Diociaiuti, E. Agostinelli, et al., *Colloids Surf. B: Biointerfaces* 134 (2015) 314–321.
- [11] H. Zhang, J. Luo, S. Li, Y. Wei, Y. Wan, *Langmuir* 34 (2018) 2585–2594.
- [12] A. Trivedi, M. Heinemann, A.C. Spiess, T. Dausmann, J. Büchs, *J. Biosci. Bioeng.* 99 (2005) 340–347.
- [13] J. Luo, A.S. Meyer, G. Jonsson, M. Pinelo, *Bioresour. Technol.* 147 (2013) 260–268.
- [14] S.B. Raj, S. Ramaswamy, B.V. Plapp, *Biochemistry* 53 (2014) 5791–5803.
- [15] M. Zezzi do Valle Gomes, A.E.C. Palmqvist, *Colloids Surf. B: Biointerfaces* 163 (2018) 41–46.
- [16] F. Marpani, M. Pinelo, A.S. Meyer, *Biochem. Eng. J.* 127 (2017) 217–228.
- [17] S. Schlager, A. Dibenedetto, M. Aresta, D.H. Apaydin, L.M. Dumitru, H. Neugebauer, N.S. Sariciftci, *Energy Technol.* 5 (2017) 812–821.
- [18] R. Obert, B.C. Dave, *J. Am. Chem. Soc.* (1999) 12192–12193.
- [19] F.S. Baskaya, X. Zhao, M.C. Flickinger, P. Wang, *Appl. Biochem. Biotechnol.* 162 (2010) 391–398.
- [20] M.H. Liao, D.H. Chen, *Biotechnol. Lett.* 23 (2001) 1723–1727.
- [21] B. Zeuner, N. Ma, K. Berendt, A.S. Meyer, P. Andric, J.H. Jørgensen, M. Pinelo, *J. Chem. Technol. Biotechnol.* 93 (10) (2018) 2952–2961, <https://doi.org/10.1002/jctb.5653>.
- [22] C. Hoffmann, H. Silau, M. Pinelo, J.M. Woodley, A.E. Daugaard, *Mater. Today Commun.* 14 (2018) 160–168.
- [23] S.W. Xu, Y. Lu, J. Li, Z.Y. Jiang, H. Wu, *Ind. Eng. Chem. Res.* 45 (2006) 4567–4573.
- [24] S. Xu, Y. Lu, Z. Jiang, H. Wu, *J. Mol. Catal. B: Enzym.* 43 (2006) 68–73.
- [25] P. Han, X. Song, H. Wu, Z. Jiang, J. Shi, X. Wang, W. Zhang, Q. Ai, *Ind. Eng. Chem. Res.* 54 (2015) 597–604.
- [26] X. Ji, Z. Su, P. Wang, G. Ma, S. Zhang, *ACS Nano* 9 (2015) 4600–4610.
- [27] L.E. David, C.B. Fowler, B.R. Cunningham, J.T. Mason, T.J. O’Leary, *J. Mol. Diagn.* 13 (2011) 282–288.
- [28] E.A. Hoffman, B.L. Frey, L.M. Smith, D.T. Auble, *J. Biol. Chem.* 290 (2015) 26404–26411.
- [29] B.W. Sutherland, J. Toews, J. Kast, *J. Mass Spectrom.* (2008) 699–715.
- [30] R. Cazelles, J. Drone, F. Fajula, O. Ersen, S. Moldovan, A. Galarneau, *New J. Chem.* 37 (2013) 3721–3730.
- [31] L. Rover, J.C.B. Fernandes, G.D.O. Neto, L.T. Kubota, E. Katekawa, S.H.P. Serrano, *Anal. Biochem.* 260 (1998) 50–55.
- [32] S. Sieber, S. Siegrist, S. Schwarz, F. Porta, S.H. Schenk, J. Huwyler, *Macromol. Biosci.* 17 (2017) 1–10.
- [33] M.L. Verma, M. Puri, C.J. Barrow, *Crit. Rev. Biotechnol.* 36 (2016) 108–119.
- [34] S.A. Ansari, Q. Husain, *Biotechnol. Adv.* 30 (2012) 512–523.
- [35] R.A. Meryam Sardar, *Biochem. Anal. Biochem.* 04 (2015), <https://doi.org/10.4172/2161-1009.1000178>.
- [36] G. Kontogeorgis, S. Kiil, *Introduction to Applied Colloid and Surface Chemistry*, Wiley, 2016.
- [37] F. Cugia, M. Monduzzi, B.W. Ninham, A. Salis, *RSC Adv.* 3 (2013) 5882–5888.
- [38] M. Kosmulski, *Adv. Colloid Interface Sci.* 251 (2018) 115–138.
- [39] I. Eş, J.D.G. Vieira, A.C. Amaral, *Appl. Microbiol. Biotechnol.* 99 (2015) 2065–2082.
- [40] M. de Cazes, M.P. Belleville, E. Petit, M. Salomo, S. Bayer, R. Czaja, J. De Gunzburg, J. Sanchez-Marcano, *Biochem. Eng. J.* 114 (2016) 70–78.
- [41] N. Carlsson, H. Gustafsson, C. Thörn, L. Olsson, K. Holmberg, B. Åkerman, *Adv. Colloid Interface Sci.* 205 (2014) 339–360.
- [42] A. de Vasconcelos, A.H. Miller, D.A.G. Aranda, J.G. Nery, *Colloids Surf. B: Biointerfaces* 165 (2018) 150–157.
- [43] W. Zhuang, L. He, J. Zhu, J. Zheng, X. Liu, Y. Dong, J. Wu, J. Zhou, Y. Chen, H. Ying, *Colloids Surf. B: Biointerfaces* 145 (2016) 785–794.
- [44] T.R.B. Ramakrishna, T.D. Nalder, W. Yang, S.N. Marshall, C.J. Barrow, *J. Mater. Chem. B: Mater. Biol. Med.* 6 (2018) 3200–3218.
- [45] S. Gao, M. Mohammad, H.-C. Yang, J. Xu, K. Liang, J. Hou, V. Chen, *ACS Appl. Mater. Interfaces* 9 (2017) 42806–42815.
- [46] N. Dizge, R. Epsztein, W. Cheng, C.J. Porter, M. Elimelech, *J. Membr. Sci.* 549 (2018) 357–365.
- [47] M. Vinoba, M. Bhagiyalakshmi, S.K. Jeong, Y.I.I. Yoon, S.C. Nam, *Colloids Surf. B: Biointerfaces* 90 (2012) 91–96.

A3 Paper 3: Energy barriers to anion transport in polyelectrolyte multilayer nanofiltration membranes: Role of intra-pore diffusion

Sigyn B. Sigurdardottir, Ryan M. DuChanois, Razi Epsztein, Manuel Pinelo, Menachem Elimelech

Journal of Membrane Science, vol. 603, p. 117921, 2020. doi:10.1016/j.memsci.2020.117921



Contents lists available at ScienceDirect

Journal of Membrane Science

journal homepage: <http://www.elsevier.com/locate/memsci>

Energy barriers to anion transport in polyelectrolyte multilayer nanofiltration membranes: Role of intra-pore diffusion

Sigyn B. Sigurdardottir^{a,b}, Ryan M. DuChanois^a, Razi Epsztein^{a,c,**}, Manuel Pinelo^b, Menachem Elimelech^{a,*}

^a Department of Chemical and Environmental Engineering, Yale University, New Haven, CT, 06520-8286, USA

^b Department of Chemical and Biochemical Engineering, Technical University of Denmark, DTU, Søtofts Plads, Building 229, 2800, Kgs. Lyngby, Denmark

^c Faculty of Civil and Environmental Engineering, Technion – Israel Institute of Technology, Haifa 32000, Israel

ARTICLE INFO

Keywords:

Nanofiltration membrane
Energy barrier
Layer-by-layer assembly
Membrane thickness
Ion transport

ABSTRACT

We investigated the relative contributions of intra-pore diffusion (via membrane thickness) and partitioning into nanofiltration (NF) membrane pores (via membrane pore size and ion hydration energy) to the apparent energy barriers for ion transport in NF membranes. Using polyelectrolyte layer-by-layer assembly, we independently altered NF membrane thickness as well as membrane pore size and then determined the apparent energy barriers to bromide and fluoride transport through the fabricated membranes. Membrane thickness and pore size were estimated using an AFM scratch technique and the hydrodynamic pore transport model, respectively. By increasing the number of polyelectrolyte bilayers from four to ten, the polyelectrolyte film thickness increased from 28 to 77 nm, while the apparent energy barriers to bromide transport through the membranes with four, seven, and ten bilayers were negligibly affected (4.4, 3.4, and 3.9 kcal mol⁻¹, respectively, at 1.7 bar). Instead, we found that solute flux and the apparent energy barriers to ion transport were significantly affected by both membrane pore size and ion hydration energy. Overall, our results support the traditional energy barrier-based models for ion transport in membranes and the recently proposed notion that ion dehydration at the solution-membrane interface is the rate-limiting step during transport through NF membranes.

1. Introduction

Nanofiltration (NF) is a pressure-driven membrane separation process in which a semi-permeable membrane acts as a selective barrier that separates salts and low molecular-weight solutes from a solution [1–3]. The separation properties of NF membranes lie between those of reverse osmosis (RO) and ultrafiltration (UF) membranes, and thus the solute transport mechanism in NF membranes is based on both diffusion and convection, as well as electromigration [4,5]. The most recognized solute rejection mechanisms of NF membranes are Donnan (charge) and steric (size) exclusion [6–8], which can be exploited for the removal of target solutes, product concentration, and solvent recovery from a feed stream [9–11]. Applications of NF (e.g., in the textile, food, pharmaceutical, and biorefinery industries) focus mainly on water softening and wastewater treatment [12–20].

As solute rejection in NF is mainly controlled by the size and charge of the membrane pores and the species passing through the pores [4], it

follows that selectivity for species of similar size and charge is often limited [7,21–24]. Nevertheless, certain selectivity trends have been observed during the separation of ions of similar hydrated size and charge [22,25], which have mainly been ascribed to the respective hydration energies of the ions [22,26]. A higher hydration energy implies a higher energetic cost of ion dehydration, while the need for ion dehydration increases as the pore size decreases [22,25,27–33]. Numerous studies have demonstrated how higher hydration energy can enhance steric exclusion of an ion when the hydrated size of the ion is similar to the membrane pore size, since the water shells surrounding the ion are less easily removed or distorted during passage through the membrane pores [4,25,27,34–37]. Ion dehydration, as an ion-specific effect, can thus be considered an additional mechanism involved in ion selectivity.

Besides influencing ion rejection, ion hydration energy and dehydration are also reflected in the energy barrier to ion transport through NF membranes [37]. Energy barriers arise when a membrane imposes a hindrance to transport. The energy barriers amount to the energy

* Corresponding author.

** Corresponding author. Technion - Israel Institute of Technology, Israel.

E-mail addresses: raziepsztein@technion.ac.il (R. Epsztein), menachem.elimelech@yale.edu (M. Elimelech).

<https://doi.org/10.1016/j.memsci.2020.117921>

Received 23 October 2019; Received in revised form 23 December 2019; Accepted 2 February 2020

Available online 3 February 2020

0376-7388/© 2020 Elsevier B.V. All rights reserved.

required for solute transport to occur, which includes contributions from all transport mechanisms involved (convection, diffusion, and electrical mobility) [20,25]. Furthermore, the energy barriers due to diffusion depend on the respective rate constants for diffusion at the solution-membrane interface (solute partitioning into the membrane) and inside the membrane [38].

The transport of solutes through membranes with pore sizes similar to the size of the hydrated solute involves partitioning of the solutes into the membrane, followed by diffusion through the membrane [22,39]. The diffusion step can be described as solutes hopping between equilibrium positions, such as vacant sites [38,40] and sites of favorable chemical/electrostatic interactions [41–44]. Notably, the diffusion of dehydrated ions inside membrane pores is strongly influenced by local charge stabilization, as the point charge of the ions is exposed upon dehydration and thereby interacts more strongly with electrically charged sites of the pore walls. This transport has been described as jump diffusion and can lead to slower ion permeation through the membrane [44].

With the series of hindrances offered by the membrane pore entry and interior, the solutes can be considered to traverse multiple transition states during transport — i.e., momentary high-potential-energy and unstable configurations — much like those described by the transition-state theory for chemical reactions [40,45]. The energy barriers associated with the individual transition-states cannot be evaluated separately due to the limited number of measurable parameters involved in transport [38]. However, an apparent representative energy barrier to solute transport through membranes can be quantified experimentally using a single-barrier Arrhenius-type equation, which describes the solute flux (analogous to a chemical reaction rate constant) as a function of temperature [22,37,46].

Molecular dynamics simulations and ion transport experiments reveal that when the membrane pore size is similar to the hydrated size of the ion (such as in NF membranes), ion dehydration at the pore entry is the main contribution to the apparent energy barrier [22,25,46]. For instance, Cory et al. [28,29] investigated energy barriers to ion transport in carbon nanotubes (CNTs) using molecular dynamics simulations, and showed that the energy barriers were controlled by the CNT diameter and the hydration energy of the ions, whereas the energy barriers were unaffected by the length of the CNTs. Unlike the frictionless transport in CNTs, polymeric NF membranes are tortuous, and the local chemical properties may vary throughout the length of the pores. Solute experience various resistances during transport through such membranes, such as physical and chemical interactions with the pore walls [29], and they are assumed to overcome numerous transport-related energy barriers inside the membrane pores [29,38]. The contribution of these intra-pore energy barriers to the apparent energy barrier in NF membranes has yet to be shown experimentally. Notably, while energy barriers arise due to a series of local hindrances, the question whether the energy barrier for ion transport accumulates along the membrane thickness has not been answered. Hence, the contribution of the intra-pore energy barriers may be evaluated by investigating the effect of membrane thickness on the apparent energy barriers to transport in NF membranes.

NF membranes are generally composed of a thin, selective separation layer, and a thicker, porous support layer. The separation layer primarily controls transport through the membrane and is where energy barriers arise. The separation layer in commercial membranes is most commonly fabricated by interfacial polymerization, a technique where a polymeric film is synthesized at an aqueous-organic interface [5,14,18]. An alternative method for the fabrication of the separation layer is polyelectrolyte (PE) layer-by-layer (LbL) assembly. In this method, a polyelectrolyte multilayer (PEM) is assembled on top of the porous support by alternating deposition of oppositely charged PEs to form a film with separation performance in the range of NF membranes [6,8,47,48]. The LbL assembly method has gained attention for its simplicity and versatility [49].

The properties of PEM films can be controlled by numerous fabrication parameters. For instance, the pore size and layer thickness can be tuned by controlling the concentrations of PEs and background ionic strength of the deposition solutions [6], the film thickness can be increased by addition of layers [43,47,49–52], and the surface charge can be controlled by the terminating PE [7,16,43]. Moreover, the surface charge can be dramatically changed, or even reversed, by incorporating salt annealing in the fabrication procedure [41,53–55]. Given the highly controllable properties of PEM films, PE LbL assembly is a practical method for fabrication of tailor-made membranes for specific applications, such as investigating the effects of membrane thickness on the apparent energy barriers to ion transport through NF membranes.

In this work, we used PE LbL assembly to study energy barriers to ion transport in NF membranes of different thicknesses. By carefully controlling the LbL deposition conditions, we first fabricated PEM NF membranes of various thicknesses but similar pore size and surface charge. We then measured experimental energy barriers to ion transport through the membranes and found that (i) increased membrane thickness does not result in significantly higher energy barriers to ion permeation and (ii) the intra-pore diffusion creates a relatively low barrier. Conversely, we found that energy barriers are dependent on ion hydration energy as well as NF membranes pore size, corroborating previous experimental and molecular dynamics studies. Our work provides experimental evidence that energy barriers to ion transport in NF arise primarily due to ion dehydration effects at the water-membrane interface and can be used to guide the design of selective membrane materials.

2. Materials and methods

2.1. Materials and chemicals

Commercial polysulfone (PSf) ultrafiltration (UF) membranes (Sepro Membranes, Oceanside, CA, USA) with molecular weight cut-off of 20 kDa were used as the substrate for PE LbL self-assembly. Poly (diallyldimethylammoniumchloride) (PDADMAC; MW 150,000–200,000 g mol⁻¹; 20% wt. in water), poly(sodium 4-styrenesulfonate) (PSS; MW 70,000 g mol⁻¹), erythritol, glucose, xylose, sodium bromide (NaBr), and sodium fluoride (NaF) were purchased from Sigma Aldrich (St. Louis, MO, USA). Sodium chloride (NaCl), isopropanol, and glycerol were purchased from J.T. Baker Chemicals (Phillipsburg, NJ, USA); hydrochloric acid (HCl) from AmericanBio (Natick, Massachusetts, USA); and sodium hydroxide (NaOH) from Avantor (Center Valley, Pennsylvania, USA). Silicon wafers (Mechanical Grade 1996) were provided by UniversityWafer, Inc. (South Boston, MA, USA). Deionized (DI) water (MilliPore, Billerica, MA, USA) was used for solution preparation, membrane compaction, and cleaning the filtration system.

2.2. Fabrication of NF membranes by LbL assembly

Before deposition of the PEs onto the PSf UF membrane substrate, the PSf membrane was immersed in 25% isopropanol and shaken at 60 rpm for 30 min, followed by thorough rinsing with DI water in three 30-min cycles. The pretreated PSf membrane was stored in DI water at 4°C overnight before use. For LbL assembly, the pretreated PSf membrane was clamped between a glass plate and a polytetrafluoroethylene (PTFE) frame with the active side facing up (the exposed membrane area was approximately 40 cm²) [6,47]. The frame was placed on a rotary shaker, which was set to 60 rpm, and then 10 mL of cationic and anionic PE solutions were deposited onto the PSf membrane in an alternating fashion with intermediate rinsing cycles. PDADMAC and PSS were chosen as cationic and anionic PEs, respectively, because they are both charged over the normal operational pH [8,37].

The PE concentration of the deposition solution used was either 0.8 or 20 mM, calculated with respect to the monomer molar mass. The PE

concentration was decreased to fabricate membranes with smaller pore sizes, as described in our previous work [6]. In both cases, the PEs were dissolved in DI water with 0.5 M NaCl as the background ionic strength, and a 0.5 M NaCl solution was used for rinsing. As the pristine PSf membrane has a negative surface zeta potential (Fig. S2), LbL assembly was initiated by the deposition of cationic PDADMAC onto the substrate. The PSf membrane was exposed to the PDADMAC solution for 10 min, followed by two 5-min rinsing cycles to remove any loosely adsorbed PDADMAC. Subsequently, the PSS solution was applied to the substrate for 10 min, followed by two 5-min rinsing cycles. These six steps concluded the first bilayer. PEM NF membranes with four, seven, and ten bilayers were fabricated to produce PEM NF membranes of different thicknesses. The subsequent bilayers were fabricated in a similar manner as described above, except for the top bilayer, where salt annealing was introduced [53,55]. The PEM was annealed by applying 10 mL of 2 M NaCl for 30 min to the membrane prior to depositing the terminating PSS layer. After LbL assembly, the PEM NF membranes were immersed in 15% wt. glycerol for 4 h, and then air-dried overnight at room temperature. The membranes were thoroughly rinsed with DI water before use.

2.3. NF system, water flux and solute rejection measurements

Filtration experiments were conducted in a bench-scale crossflow system, with flat-sheet membranes placed in plate-and-frame cells. The effective membrane surface area was 20.02 cm². Feed solution recirculated between the membrane cells and a feed tank at a crossflow velocity of 0.21 m s⁻¹. The temperature of the feed solution was controlled by a heater/chiller system (± 1 °C). The membranes were compacted overnight at high pressure—9.7 bar (140 psi) before filtrations of salt solutions and 13.8 bar (200 psi) before filtrations of organic solutions—using DI water. Pure water flux was measured gravimetrically at the beginning of each experiment and then a concentrated stock solution was added to the feed tank to reach either 4 mM NaF/NaBr or 50 mg L⁻¹ total organic carbon (TOC) (glucose/erythritol/xylose). Additionally, filtration of a mixed anion solution containing 2 mM of each NaCl, NaF, and NaBr was conducted. Filtrations of salt solutions were conducted at 1.7, 5.2, and 6.9 bar (25, 75, and 100 psi), and at 22, 28, 34, and 40 °C for each operational pressure. Filtrations of organic solutions were conducted at 4.1, 6.2, 8.3, and 10.3 bar (60, 90, 120, and 150 psi), and 25 °C. The system was stabilized for 30 min at each pressure and temperature, after which samples of the feed and permeate were collected to determine membrane water flux (gravimetrically) and solute rejection. Ion concentration of single salt solutions was measured using an electrical conductivity meter (Oakton Instruments, Vernon Hills, IL, USA) and mixed salt solutions were measured with ion chromatography (Dionex DX-500 with an AS14A IonPac column). Organic concentration was measured using a TOC analyzer (TOCV-CSH, Shimadzu Corp., Japan). The observed rejection, R_{obs} , was calculated using the equation:

$$R_{obs} = \left(1 - \frac{c_p}{c_f}\right) \times 100\% \quad (1)$$

where c_p and c_f are the solute concentrations of the permeate and feed, respectively. Water permeability of the PEM NF membranes was calculated from water flux measured during filtrations of 4 mM NaBr at 22 °C, and at 1.7, 5.2, and 6.9 bar (25, 75, and 100 psi).

2.4. Membrane characterization

PEM film thickness was evaluated using atomic force microscopy (AFM). For this purpose, the PEM films were fabricated on atomically smooth silicon wafers, with 1 mL of PE and rinse solutions applied to the substrate using small PTFE frames. Similar to the procedure described in Section 2.2, the PEM films were formed by alternating deposition of

PDADMAC and PSS to the substrate for 10 min, with two 5-min intermediate rinsing cycles, and salt annealing to the terminating bilayer. The PEM samples were rinsed with DI water and air-dried overnight. Before AFM scanning, the dry PEM films were scratched with a needle without damaging the silicon wafer. PEM samples were measured using a Bruker Dimension FastScan AFM (Santa Barbara, CA, USA) equipped with a Bruker FastScan-B cantilever (5 nm tip radius) in ScanAsyst mode. AFM images of the edge of the scratch were captured at a scan rate of 3 Hz. Height profiles across the scratch were obtained by an image analysis software, NanoScope Analysis v1.9 (Bruker), using the section tool. The height difference between the PEM film and the bare silicon wafer revealed the dry PEM film thickness. PEM thicknesses are reported as the average and standard deviation of six measurements (three scratches on two PEM films). Statistical difference was assessed using one-way ANOVA and the results are reported as p -values.

An estimation of the average pore size of the PEM NF membranes was calculated using the hydrodynamic pore transport model [56]. The model assumes the membrane to be a bundle of cylindrical capillary tubes of constant radii and uses rejection data of neutral organic solutes for the pore size estimation, as was described previously by our group [6, 18,57]. Solute flux and rejection data for erythritol (MW 122 g mol⁻¹), xylose (MW 150 g mol⁻¹) and glucose (MW 180 g mol⁻¹) were collected during single solute filtrations using the crossflow system, filtration conditions, and analytical methods described in Section 2.3. These data were fed to the hydrodynamic pore transport model, and the average membrane pore radius was estimated from transport data for each organic solute. Estimated pore sizes and standard deviations are reported based on the results obtained from erythritol, xylose and glucose rejections. Statistical difference was assessed using one-way ANOVA and the results are reported as p -values. The model has been described in detail by Deen [56] and Nghiem et al. [57], and a short description of the method is provided in the Supplementary Material.

The surface zeta potential of the PEM NF membranes was calculated from streaming potential measurements using an electro-kinetic analyzer with an asymmetric clamping cell (EKA, Brookhaven Instruments, Holtsville, NY, USA) as described elsewhere [8,14]. The surface zeta potential was determined at pH 5, 7, and 9 using a constant background electrolyte concentration of 1 mM KCl and 0.1 mM KHCO₃. PEM NF membranes were prepared on PSf UF substrate by the method described in Section 2.2, except using a bigger PTFE frame and 20 mL of PE and rinse solutions. The results are reported as the average and standard deviation of two independent samples, with eight streaming potential measurements per sample.

2.5. Determination of energy barriers to ion transport

Experimental energy barriers to ion transport through the PEM NF membranes were determined from an Arrhenius-type equation:

$$J_s = A \exp\left(-\frac{E_a}{RT}\right) \quad (2)$$

where J_s is the ion flux through the membrane, A is a pre-exponential factor, E_a is the experimental energy barrier, R is the universal gas constant, and T is the absolute temperature. A linearized form of Eq. (2) describes the natural logarithm of ion flux through the membrane as a function of the inverse of the absolute temperature:

$$\ln J_s = \ln A - \frac{E_a}{RT} \quad (3)$$

Energy barriers to ion transport through the PEM NF membranes were calculated from the slope of the line resulting from Eq. (3). The ion flux, J_s , was calculated at different feed temperatures from experimental data according to:

$$J_s = J_w c_p \quad (4)$$

where J_w is the water flux through the membrane and c_p is the ion concentration in the permeate. The ion flux was normalized to the feed concentration at each sampling to eliminate any effect of feed concentration variability due to sampling and solvent evaporation at elevated temperatures. Energy barriers to water transport were calculated in a similar manner as for ion transport, except using water flux instead of solute flux in Eq. (3).

Water flux and rejection data for fluoride, bromide, and chloride were collected in single and mixed sodium salt filtrations, using the crossflow system, filtration conditions, and analytical methods described in Section 2.3. The experimental energy barriers to water and ion transport in the PEM NF membranes with four, seven, and ten bilayers were calculated from these data. The average and standard deviation are reported from at least three independently fabricated membranes. Statistical difference was assessed using one-way ANOVA and Welch two-sample *t*-tests, and the results are reported as *p*-values.

3. Results and discussion

3.1. Characterization of PEM NF membranes

The aim of this study was to investigate the effect of intra-pore ion transport on energy barriers in NF membranes. To do so, we fabricated PEM NF membranes of different thicknesses by changing the number of bilayers of PDADMAC/PSS deposited on a PSf UF substrate. The PEM fabrication conditions were selected so that only the thickness of the PEM NF membranes changed by addition of bilayers, while changes in membrane pore size and surface charge were minimized. We estimated the PEM thickness, average pore size, and surface zeta potential using AFM, the hydrodynamic pore transport model, and an electro kinetic analyzer, respectively, to quantify variations in these membrane properties.

For thickness measurements, PEMs with four, seven, and ten bilayers of PDADMAC/PSS were fabricated on atomically smooth silicon wafers. After assembly, the PEM films were dried and then scratched with a needle before imaging with AFM (Fig. S1). A scan of the edge of the scratch revealed the height difference between the PEM and the bare silicon wafer, which corresponded to the dry PEM thickness (Fig. 1A–C). The PEM thickness increased from 28 to 77 nm for PEMs with four to ten bilayers ($p < 0.001$, Fig. 1C). The observed PEM film growth was linear with an average bilayer thickness of 7.9 nm, which is in good agreement with results reported elsewhere for similar systems [6,50,52,58]. The measured PEM thickness indicates the increase in thickness of the separation layers of the PEM NF membranes with addition of bilayers, although the thickness may not be directly comparable to the PEMs on porous UF membranes. When PEMs are assembled on porous substrates, the PEM growth begins in a pore regime (filling of the pores) before it reaches the film regime (increasing film thickness) [50,53]. Here, we deposited at least four bilayers onto the PSf UF substrate to be within the film regime across all experiments.

The average pore sizes of the PEM NF membranes were estimated using the hydrodynamic pore transport model. Membranes with four, seven, and ten bilayers of PDADMAC/PSS were fabricated on PSf UF substrates and applied in filtrations of neutral organic solutes (erythritol, xylose, and glucose). The pore size calculations were based on rejection data for the solutes (Table S2), as described elsewhere [6,57]. Pore sizes were seemingly not affected by the number of bilayers in the PEM films, as the average estimated pore radii were calculated to be 0.73, 0.70, and 0.74 nm for the PEM NF membranes with four, seven, and ten bilayers, respectively ($p = 0.76$, Fig. 1C). Similarly, the variation in surface zeta potential among the PEM NF membranes with different number of bilayers was small and assumed not to affect the energy barrier measurements (Fig. 1D). The control over surface charge was achieved by applying salt annealing to the PEM NF membranes during fabrication. Preliminary experiments showed that the surface zeta

potential of PEM NF membranes with two, four, and eight bilayers of PDADMAC/PSS fabricated without salt annealing became increasingly positive with addition of bilayers, even with PSS (anionic) as the terminating PE (Fig. S2). This phenomenon has been commonly explained by overcompensation of PDADMAC in the PEM due to an uneven adsorption of PDADMAC and PSS to the film, which results in accumulation of excess PDADMAC with addition of bilayers [51,53,58]. Salt annealing has been proposed as a method to restore the stoichiometric balance between PDADMAC and PSS in PEM films [55]. Briefly, the mobility of the PEs within the PEM is enhanced by exposure to high salt concentration (>1.5 M NaCl), whereby the excess, extrinsic PDADMAC sites (charge-neutralized by salt counter-ions from the deposition solution) are evenly dispersed through the PEM, allowing a higher uptake of PSS at the surface in the following deposition cycle [55]. By applying salt annealing, we were able to produce membranes with different number of bilayers but similar, negative surface charges (Fig. 1D).

The filtration performance of the PEM NF membranes (water permeability and solute rejection, Table 1) supports the results obtained from characterization. Water permeability decreased from 9.01 to 6.61 $\text{L m}^{-2} \text{h}^{-1} \text{bar}^{-1}$ upon increasing the number of bilayers from four to ten ($p < 0.01$), which can be explained by higher resistance to water flux in thicker membranes [12]. Notably, the decrease in water flux was not inversely proportional to the increase in membrane thickness, which indicates that partitioning into the membrane imposed a higher resistance to transport than diffusion inside the membrane [38]. Glucose and bromide rejection remained similar for the three membranes ($p > 0.57$ for both solutes), which is in agreement with results from the hydrodynamic pore transport model and electro kinetic analyzer, respectively. The similarity in the rejection values is also consistent with predictions of a pore transport model proposed by Bowen and Welfoot [59], who showed that rejection of uncharged solutes and ions is independent of membrane thickness.

Membrane thickness increased significantly with the addition of bilayers to the PEMs while pore size and surface zeta potential were comparatively unaffected (Fig. 1). The similarity in pore size was particularly important for measurements of energy barriers to ion transport through the membranes, given the reported effect of steric hindrance on ion dehydration (i.e., greater need for ion dehydration when ions pass through smaller membrane pores) [25]. Thus, the characterization proves the usefulness of the PEM NF membranes for studying the effect of membrane thickness on energy barriers to ion transport in NF membranes.

3.2. Effects of membrane thickness on apparent energy barriers to ion transport

We applied PEM NF membranes of varying thicknesses (with four, seven, and ten bilayers of PDADMAC/PSS) in filtrations of ionic solutions and calculated the energy barriers to ion transport through the membranes, according to the linearized Arrhenius equation (Eq. (3)). In an attempt to limit the dominating effect of ion dehydration at the pore

Table 1
Water permeability and solute rejection of PEM NF membranes.

	4 Bilayers 20 mM PE	7 Bilayers 20 mM PE	10 Bilayers 20 mM PE
Water permeability ^a ($\text{L m}^{-2} \text{h}^{-1} \text{bar}^{-1}$)	9.01 ± 1.13	8.46 ± 0.91	6.61 ± 0.47
Bromide rejection, R_{obs}^b (%)	16.3 ± 4.2	12.9 ± 3.2	17.9 ± 2.7
Glucose rejection, R_{obs}^c (%)	39.6 ± 10.1	43.5 ± 4.5	43.2 ± 2.1

^a Filtration of bromide solution (4 mM NaBr), at 22 °C, pH 5.7, and 1.7, 5.2, and 6.9 bar.

^b Measured at 22 °C, 6.9 bar, and pH 5.7, feed concentration 4 mM NaBr.

^c Measured at 25 °C, 6.2 bar, and pH 5.7, feed concentration 50 mg L⁻¹ TOC.

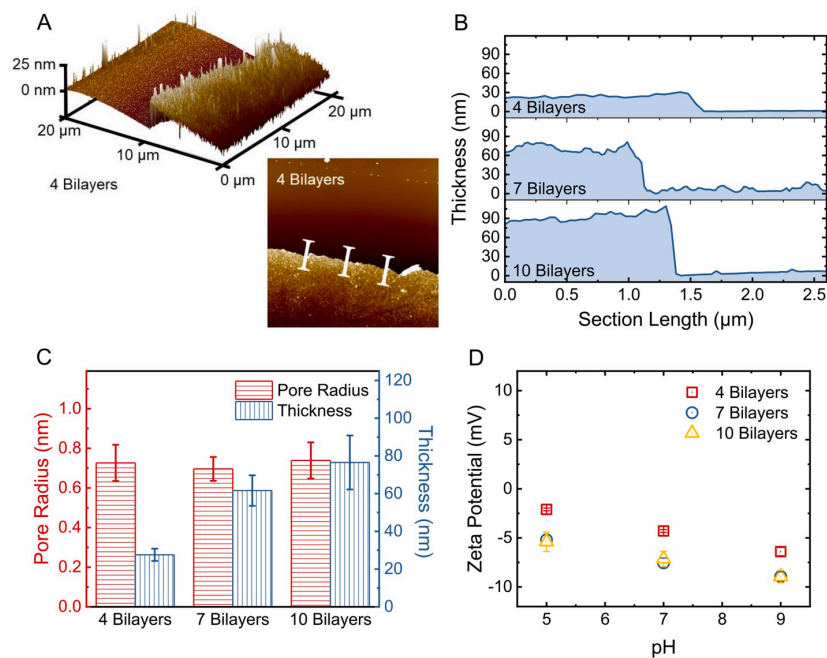


Fig. 1. Characterization of PEM films and PEM NF membranes prepared with four, seven, and ten bilayers using 20 mM PDADMAC/PSS deposition solutions. (A) Sample AFM images ($20 \times 20 \mu\text{m}$, 3-D and 2-D) of a dry PEM film with four bilayers of PDADMAC/PSS on a silicon wafer. Before imaging, a scratch was generated by dragging a needle across the dry PEM film. The images show the topology of the PEM film and the bare silicon wafer around one edge of the scratch. (B) Sample height profiles of PEM films obtained from AFM. The thickness of the PEM films was calculated from the height profiles as the difference in height between the PEM film (thicker part) and the bare silicon wafer (thinner part). Three different scratches on two independent coupons were measured. (C) Average estimated pore size ($p = 0.76$) and thickness ($p < 0.001$) of PEM NF membranes and films, respectively. PEM NF membranes were fabricated on Psf UF substrate. Pore size was determined from the hydrodynamic pore transport model, using rejection of erythritol, xylose, and glucose in single-solute filtration experiments at applied pressures of 4.1, 6.2, 8.3, and 10.3 bar (60, 90, 120, and 150 psi). Experimental conditions: feed concentration 50 mg L^{-1} TOC, crossflow velocity 0.21 m s^{-1} , and temperature $25 \text{ }^\circ\text{C}$. (D) Surface zeta potential of PEM NF membranes fabricated on Psf UF substrate. The surface zeta potential was calculated from eight streaming potential measurements on two independent coupons using a constant background electrolyte concentration of 1 mM KCl and 0.1 mM KHCO_3 . The pH was adjusted using hydrochloric acid (HCl) and sodium hydroxide (NaOH). (For interpretation of the references to colour in this figure legend, the reader is referred to the Web version of this article.)

entry on the apparent energy barrier, we used bromide ions with relatively low hydration energy and PEM NF membranes with average pore sizes larger than the hydrated size of the ions in our study. By using such a system, the potential effect of membrane thickness, i.e., the contribution of the transport resistance arising within the membrane, on the apparent energy barrier should have become more evident.

Bromide flux through the membranes was measured at temperatures ranging from 22 to $40 \text{ }^\circ\text{C}$ and operating pressures of 1.7–6.9 bar (Fig. 2). An increase in the two operating parameters led to an increase in bromide flux. Generally, solute flux increases at higher pressure (up to a certain critical pressure) mostly due to enhanced convective flow [25,60], while higher temperature leads to increased diffusion, decreased water viscosity, and potentially altered membrane pore structure (e.g., due to fusion of adjacent pores) [61–63]. The effect of temperature on the PEM pore sizes and water viscosity was investigated by comparing the calculated energy barriers for water and ion transport through the membranes (Fig. S3). The energy barriers for water were always lower than for ions, so the observed increase in bromide flux at higher temperatures cannot be explained entirely by increased pore size or decreased water viscosity. Rather, an additional ion-specific mechanism (i.e., ion dehydration) was involved in bromide transport in addition to convection, which resulted in higher energy barriers to bromide transport than water transport. The relatively small difference between the energy barriers for water and bromide transport (especially in the membranes with larger pore size) suggests, however, that bromide transport through the membranes was significantly affected by convection. In addition to the influence of pressure and temperature, bromide flux decreased with membrane thickness, which can be explained by increased resistance to convective and diffusive transport [12]. However, the reduction in bromide flux was comparatively lower than the increase in membrane thickness, suggesting that hindrance to transport was composed of another major barrier than intra-pore

diffusion, such as ion dehydration at the solution-membrane interface.

Arrhenius plots were produced from bromide fluxes at different temperatures by plotting the natural logarithm of the bromide flux against the inverse of the absolute temperature (Fig. 3A). The linearity of the Arrhenius plots verifies the occurrence of thermally activated transport through the membranes, and the slopes of the Arrhenius plots were thus used to calculate the apparent energy barriers (Fig. 3B) [38]. The energy barriers to bromide transport in PEM NF membranes of different thicknesses ranged from 3.4 to $4.4 \text{ kcal mol}^{-1}$; these barriers are comparable to energy barriers calculated elsewhere for commercial NF and ion-exchange membranes [22,37]. Notably, the data do not show a relationship between the energy barriers and membrane thickness. More specifically, the energy barriers do not increase with increased membrane thickness, suggesting that the apparent energy barrier is not an accumulative parameter with respect to membrane thickness; instead, it represents the local energy barrier of the rate-limiting step. Our results thus support previously published models on diffusion in membranes describing solute transport as sequential (and local) barriers in series, rather than a single accumulative barrier over the membrane [38].

Similar observations have been described previously by Epsztein et al. [22,37] who found energy barriers to ion transport in ion-exchange membranes to be comparable to those for NF membranes, despite ion-exchange membranes being much thicker than NF membranes. The authors concluded that the energy barriers were mainly due to ion dehydration at the pore entry, in agreement with previous studies [22, 25,46]. According to transport models based on the transition-state theory [38], if the energy barrier due to intra-pore diffusion is significant, solute flux will depend inversely on membrane thickness. Here, the relatively minor effect of thickness on solute flux (Fig. 2) suggests that the barrier at the solution-membrane interface is the rate-limiting step and therefore poses the most significant barrier for solute transport.

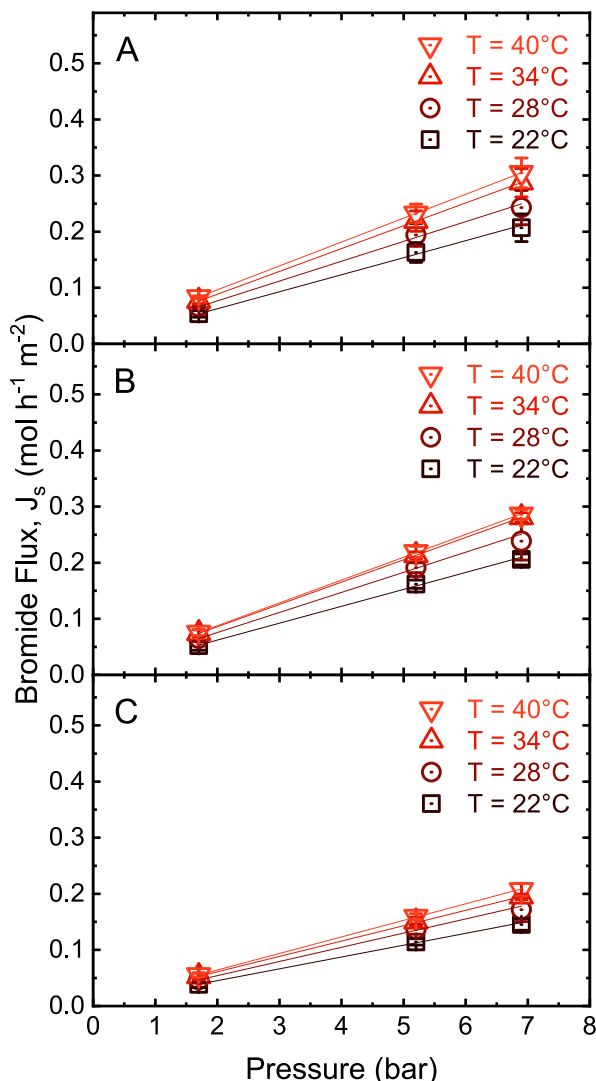


Fig. 2. Bromide flux through PEM NF membranes with (A) four, (B) seven, and (C) 10 bilayers of PDADMAC/PSS. Membranes were prepared by deposition of 20 mM polyelectrolyte solutions onto a PSf UF substrate. Bromide flux was measured during filtration of 4 mM NaBr solutions at 1.7, 5.2, and 6.9 bar (25, 75, and 100 psi). Rejection was calculated from conductivity measurements of the feed and permeate. Experimental conditions: crossflow velocity of 0.21 m s⁻¹, pH 5.7. Error bars report standard deviations of four independently fabricated membranes.

Although the average pore size was relatively large in our experiments and transport was dominated by convection rather than diffusion, some pores may still force bromide ions to partially dehydrate or, at least, rearrange their hydration shells at the pore entrance.

3.3. Effect of hydration energy, pore size, and pressure on apparent energy barriers to ion transport

To verify that ion dehydration governs the apparent energy barrier, we studied the effects of ion hydration energy and membrane pore size on energy barriers to ion transport in PEM NF membranes. We fabricated PEM NF membranes with different pore sizes by varying the concentrations of PEs in the deposition solutions from 0.8 to 20 mM, which

resulted in membranes with average estimated pore radii of 0.62 and 0.70 nm, respectively, as estimated from the hydrodynamic pore transport model. We then determined the energy barriers to bromide transport through those membranes (Fig. 4B). The effect of ion hydration energy on energy barriers was investigated by comparing bromide and fluoride transport (hydration energies of 75.3 and 111.1 kcal mol⁻¹, respectively [22]) in PEM NF membranes with seven bilayers of PDADMAC/PSS and an average estimated pore radius of 0.62 nm (Fig. 4A).

Both higher ion hydration energy (fluoride) and smaller membrane pore size (0.8 mM PE) resulted in increased energy barriers to ion transport through the PEM NF membranes (Fig. 4 and Fig. S4), in contrast to increased membrane thickness (Fig. 3B). As such, hydration energy and pore size had a greater effect on energy barriers than membrane thickness, which suggests that partial ion dehydration controls the apparent energy barrier to ion transport in NF membranes. Welch two-sample *t*-tests showed significant differences in energy barriers for bromide and fluoride ions ($p = 0.01$ – 0.05) as well as for the pore sizes ($p = 0.02$ – 0.16), where the p -values vary depending on the applied pressure. Larger differences may have been observed in membranes with pore sizes more comparable to the hydrated size of the ions, where diffusive transport is relatively more important in comparison to convective transport.

Energy barriers to ion transport in membranes have been found to decrease to some extent upon increasing the operating pressure, notably when the ions experience a high resistance to partitioning into the membrane due to high ion hydration energy and narrow pores [25]. Considering that the apparent energy barrier is calculated from the Arrhenius-type equation where solute flux is described as a function of temperature, the decrease in energy barriers at higher pressure (or higher water permeation velocity) may be the result of increased contribution of convective transport over diffusive transport at higher pressure [1,20]. The temperature dependence of diffusion thereby becomes comparatively less important for solute flux, which can be observed as a decrease in the apparent energy barrier at higher pressure. We evaluated the effects of pressure on the energy barriers and found that pressure effects were generally not apparent, with the exception of fluoride transport through the denser membrane studied (pore radius of 0.62 nm, Fig. 4A). The pressure effect was thus more pronounced as the need for ion dehydration was higher, in agreement with reported observations [25,62]. The energy barrier to fluoride transport decreased significantly with pressure ($p < 0.001$), while no pressure effects on the energy barriers to bromide transport were observed at the operating pressures applied here, suggesting that bromide transport was largely convection-controlled. Based on these observations, pressure may potentially be exploited to tune the selectivity of NF membranes towards ions of similar hydrated size and charge.

3.4. Mechanisms of ion transport through PEM NF membranes

The apparent energy barrier to solute transport in membranes was originally described by a membrane diffusion model derived from the transition-state theory [38]. According to this model, the apparent energy barrier is dependent on both the energy barriers to intra-pore diffusion and the energy barrier due to solute partitioning into the membrane. Similarly, the transport of ions through a PEM NF membrane may be described as a sequence of energy barriers that arise due to ion partitioning into the membrane pores and diffusion across the membrane thickness (Fig. 5) [38,64]. Although the apparent energy barrier theoretically depends on both steps, it is governed by the rate-limiting step during transport, or the step that imposes a higher energy barrier [38]. We found that membrane thickness did not affect the apparent energy barriers calculated here, indicating that the apparent energy barrier is not an accumulative parameter with respect to thickness. Instead, the apparent energy barrier represents a single local barrier as described by the membrane diffusion model [38]. Notably, the relatively

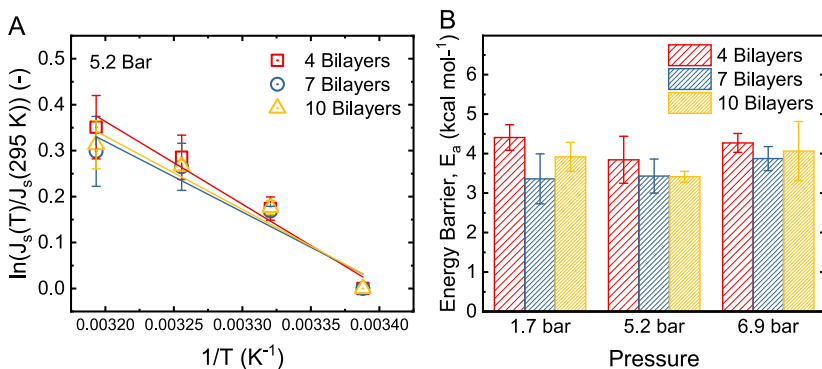


Fig. 3. (A) Arrhenius plots and (B) experimental energy barriers to bromide transport through PEM NF membranes with four, seven, and ten bilayers of PDADMAC/PSS. Membranes were prepared by deposition of 20 mM PE solutions onto a PSf UF substrate. (A) Bromide flux was determined during filtration of 4 mM NaBr at 22, 28, 34, and 40 °C; 5.2 bar (75 psi); crossflow velocity of 0.21 m s^{-1} ; and pH 5.7. The bromide flux was normalized to the flux at 22 °C (295 K) and the natural logarithm of the normalized flux was plotted against the inverse of the absolute temperature, according to the linearized Arrhenius equation. (B) Energy barriers were calculated from the slopes of the Arrhenius plots at applied pressures of 1.7, 5.2, and 6.9 bar (25, 75, and 100 psi), under the same conditions as in (A) ($p = 0.23, 0.41,$ and 0.32 for 1.7, 5.2, and 6.9 bar, respectively). Error bars report standard deviations of four independently fabricated membranes.

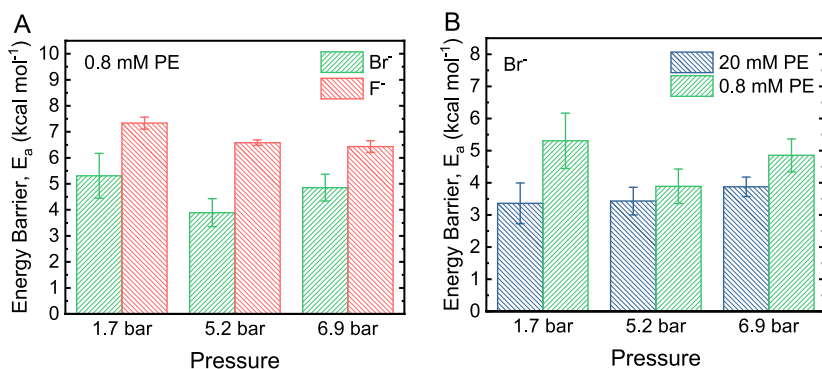


Fig. 4. (A) Experimental energy barriers to transport of anions of different hydration energies ($\text{Br}^- = 75.3 \text{ kcal mol}^{-1}$; $\text{F}^- = 111.1 \text{ kcal mol}^{-1}$) through PEM NF membranes with seven bilayers of PDADMAC/PSS (Welch two-sample t -tests; $p = 0.05, 0.01,$ and 0.02 for 1.7, 5.2, and 6.9 bar, respectively). Membranes were prepared by deposition of 0.8 mM PE solutions onto a PSf UF substrate. (B) Experimental energy barriers to bromide transport through PEM NF membranes of different pore sizes (Welch two-sample t -tests; $p = 0.02, 0.16,$ and 0.03 for 1.7, 5.2, and 6.9 bar, respectively). PEM NF membranes were prepared by deposition of seven bilayers of 20 mM (pore radius = 0.70 nm) and 0.8 mM (pore radius = 0.62 nm) PDADMAC/PSS onto a PSf UF substrate. The energy barriers were calculated from flux and rejection data from filtration of single salt solutions (4 mM NaBr or 4 mM NaF) at 22, 28, 34, and 40 °C; crossflow velocity of 0.21 m s^{-1} ; and pH 5.7. The energy barriers were calculated from the slope of Arrhenius plots, where the natural logarithm of ion flux through the membranes was plotted against the inverse of the absolute temperature. Error bars report standard deviations of three independently fabricated membranes.

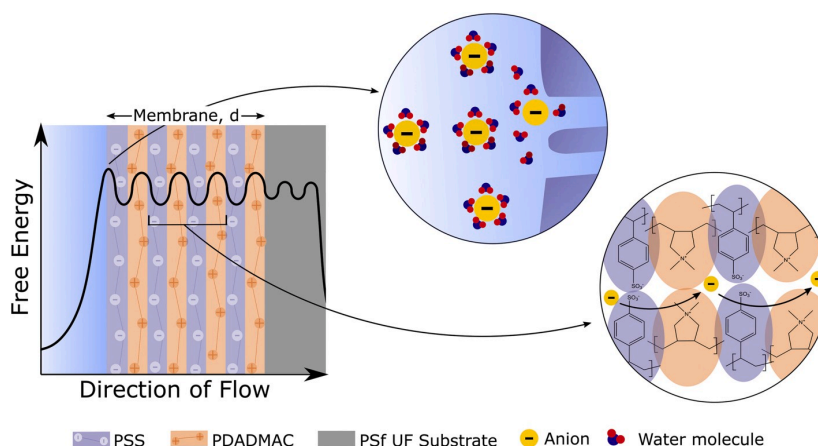


Fig. 5. Schematic description of energy barriers to anion transport through PEM NF membranes. The main energy barrier arises at the membrane-water interface, where ions undergo dehydration, or deformation of their hydration shells, before they enter the pore. The ions overcome further energy barriers as they move through the membrane and hop between vacant sites and between charged groups of the membrane.

small effect of thickness on ion flux, even with the local charge stabilization of the dehydrated ion during diffusion through the membranes, suggests that transport was mainly controlled by ion partitioning into the membrane, i.e. ion dehydration at the solution-membrane interface, and not by diffusion inside the membrane.

While ion rejection and the apparent energy barriers to ion transport were unaffected by increasing membrane thickness, water permeability and solute flux decreased to some extent due to a greater resistance to water transport. Membrane thickness thus somewhat influenced the rate of transport through the membranes but did not play a role in ion selectivity. The selectivity of the membranes was solely dictated by the pore size of the membrane and properties of the ions. Once a solute has crossed the largest energy barrier at the pore entry, the solute traverses the membrane without being significantly affected by the pore interior [38].

4. Conclusion

We investigated the role of intra-pore diffusion in the apparent energy barriers to ion transport in NF membranes. PEM NF membranes were prepared using PE LbL assembly, where one membrane property (either membrane thickness or pore size) was varied while other membrane properties were kept constant. The apparent energy barriers to bromide and fluoride transport through the membranes were calculated from an Arrhenius-type equation. We found no distinguishable effect on the apparent energy barriers to bromide transport when changing membrane thickness, whereas both ion hydration energy and membrane pore size significantly affected the apparent energy barriers. The results indicate that the apparent energy barriers to ion transport were mainly controlled by ion dehydration at the water-membrane interface (i.e., in entering or partitioning into the pore) rather than intra-pore diffusion. This observation was supported by predictions of a membrane diffusion model previously derived from the transition-state theory, which shows that solute permeation (translated to the apparent energy barrier here) is independent of membrane thickness when transport is controlled by partitioning of the solute into the membrane. The results highlight the important role of ion dehydration at the water-membrane interface in controlling ion rejection by NF membranes and simultaneously eliminate membrane thickness as a parameter involved in ion dehydration-based selectivity.

Declaration of competing interest

The authors declare that they have no known competing financial interests or personal relationships that could have appeared to influence the work reported in this paper.

CRedit authorship contribution statement

Sigyn B. Sigurdardottir: Conceptualization, Methodology, Formal analysis, Investigation, Writing - original draft, Writing - review & editing, Visualization. **Ryan M. DuChanois:** Conceptualization, Methodology, Investigation, Writing - original draft, Writing - review & editing. **Razi Epsztein:** Conceptualization, Methodology, Investigation, Writing - original draft, Writing - review & editing, Supervision. **Manuel Pinelo:** Supervision, Funding acquisition, Writing - review & editing. **Menachem Elimelech:** Resources, Supervision, Funding acquisition, Writing - review & editing.

Acknowledgements

This work was supported by The Danish Council for Independent Research, Grant no.: 6111-00232B. In addition, we acknowledge the support received from the National Science Foundation (NSF) through the Engineering Research Center for Nanotechnology-Enabled Water Treatment (EEC-1449500). Facilities used for AFM were supported by

the Yale Institute of Nanoscale and Quantum Engineering (YINQE) under NSF MRSEC DMR 1119826. We also acknowledge the NSF Graduate Research Fellowship awarded to R.M.D. and the postdoctoral fellowship (to R. E.) provided from the United States-Israel Binational Agricultural Research and Development (BARD) Fund, Fellowship Number FI-549-2016.

Appendix A. Supplementary data

Supplementary data to this article can be found online at <https://doi.org/10.1016/j.memsci.2020.117921>.

References

- [1] J. Luo, Y. Wan, Effect of highly concentrated salt on retention of organic solutes by nanofiltration polymeric membranes, *J. Membr. Sci.* 372 (2011) 145–153, <https://doi.org/10.1016/j.memsci.2011.01.066>.
- [2] N. Hilal, H. Al-Zoubi, N.A. Darwish, A.W. Mohammad, M. Abu Arabi, A comprehensive review of nanofiltration membranes: treatment, pretreatment, modelling, and atomic force microscopy, *Desalination* 170 (2004) 281–308, <https://doi.org/10.1016/j.desal.2004.01.007>.
- [3] N.N. Bui, M.L. Lind, E.M. V Hoek, J.R. McCutcheon, Electrospun nanofiber supported thin film composite membranes for engineered osmosis, *J. Membr. Sci.* (2011) 385–386, <https://doi.org/10.1016/j.memsci.2011.08.002>, 10–19.
- [4] B. Tansel, J. Sager, T. Rector, J. Garland, R.F. Strayer, L. Levine, M. Roberts, M. Hummerick, J. Bauer, Significance of hydrated radius and hydration shells on ionic permeability during nanofiltration in dead end and cross flow modes, *Separ. Purif. Technol.* 51 (2006) 40–47, <https://doi.org/10.1016/j.seppur.2005.12.020>.
- [5] J.R. Werber, C.O. Osuji, M. Elimelech, Materials for next-generation desalination and water purification membranes, *Nat. Rev. Mater.* 1 (2016) 16018, <https://doi.org/10.1038/natrevmats.2016.18>.
- [6] R.M. DuChanois, R. Epsztein, J.A. Trivedi, M. Elimelech, Controlling pore structure of polyelectrolyte multilayer nanofiltration membranes by tuning polyelectrolyte-salt interactions, *J. Membr. Sci.* 581 (2019) 413–420, <https://doi.org/10.1016/j.memsci.2019.03.077>.
- [7] R. Epsztein, W. Cheng, E. Shauly, N. Dizge, M. Elimelech, Elucidating the mechanisms underlying the difference between chloride and nitrate rejection in nanofiltration, *J. Membr. Sci.* 548 (2018) 694–701, <https://doi.org/10.1016/j.memsci.2017.10.049>.
- [8] W. Cheng, C. Liu, T. Tong, R. Epsztein, M. Sun, R. Verduzco, J. Ma, M. Elimelech, Selective removal of divalent cations by polyelectrolyte multilayer nanofiltration membrane: role of polyelectrolyte charge, ion size, and ionic strength, *J. Membr. Sci.* 559 (2018) 98–106, <https://doi.org/10.1016/j.memsci.2018.04.052>.
- [9] I. Koyuncu, D. Topacik, Effect of organic ion on the separation of salts by nanofiltration membranes, *J. Membr. Sci.* 195 (2002) 247–263, [https://doi.org/10.1016/S0376-7388\(01\)00559-2](https://doi.org/10.1016/S0376-7388(01)00559-2).
- [10] L.S. White, A.R. Nitsch, Solvent recovery from lube oil filtrates with a polyimide membrane, *J. Membr. Sci.* 179 (2000) 267–274, [https://doi.org/10.1016/S0376-7388\(00\)00517-2](https://doi.org/10.1016/S0376-7388(00)00517-2).
- [11] J. Luo, Y. Wan, Effects of pH and salt on nanofiltration—a critical review, *J. Membr. Sci.* 438 (2013) 18–28, <https://doi.org/10.1016/j.memsci.2013.03.029>.
- [12] B. Su, T. Wang, Z. Wang, X. Gao, C. Gao, Preparation and performance of dynamic layer-by-layer PDADMAC/PSS nanofiltration membrane, *J. Membr. Sci.* (2012) 423–424, <https://doi.org/10.1016/j.memsci.2012.08.041>, 324–331.
- [13] R. Zhang, Y. Su, X. Zhao, Y. Li, J. Zhao, Z. Jiang, A novel positively charged composite nanofiltration membrane prepared by bio-inspired adhesion of polydopamine and surface grafting of poly(ethylene imine), *J. Membr. Sci.* 470 (2014) 9–17, <https://doi.org/10.1016/j.memsci.2014.07.006>.
- [14] Y.C. Chiang, Y.Z. Hsub, R.C. Ruaan, C.J. Chuang, K.L. Tung, Nanofiltration membranes synthesized from hyperbranched polyethyleneimine, *J. Membr. Sci.* 326 (2009) 19–26, <https://doi.org/10.1016/j.memsci.2008.09.021>.
- [15] D. Menne, C. Üzümlü, A. Koppelman, J.E. Wong, C. van Foeken, F. Borre, L. Dähne, T. Laakso, A. Pihlajamäki, M. Wessling, Regenerable polymer/ceramic hybrid nanofiltration membrane based on polyelectrolyte assembly by layer-by-layer technique, *J. Membr. Sci.* 520 (2016) 924–932, <https://doi.org/10.1016/j.memsci.2016.08.048>.
- [16] J. De Groot, D.M. Reurink, J. Ploegmakers, W.M. De Vos, K. Nijmeijer, Charged micropollutant removal with hollow fiber nanofiltration membranes based on polycation/polyzwitterion/polyanion multilayers, *ACS Appl. Mater. Interfaces* 6 (2014) 17009–17017, <https://doi.org/10.1021/am504630a>.
- [17] S.T. Morthensen, S.B. Sigurdardottir, A.S. Meyer, H. Jørgensen, M. Pinelo, Separation of xylose and glucose using an integrated membrane system for enzymatic cofactor regeneration and downstream purification, *J. Membr. Sci.* 523 (2017) 327–335, <https://doi.org/10.1016/j.memsci.2016.10.017>.
- [18] C. Boo, Y. Wang, I. Zucker, Y. Choo, C.O. Osuji, M. Elimelech, High performance nanofiltration membrane for effective removal of perfluoroalkyl substances at high water recovery, *Environ. Sci. Technol.* 52 (2018) 7279–7288, <https://doi.org/10.1021/acs.est.8b01040>.
- [19] A.W. Mohammad, Y.H. Teow, W.L. Ang, Y.T. Chung, D.L. Oatley-Radcliffe, N. Hilal, Nanofiltration membranes review: recent advances and future prospects, *Desalination* 356 (2015) 226–254, <https://doi.org/10.1016/j.desal.2014.10.043>.

- [20] S. Bhattacharjee, J.C. Chen, M. Elimelech, Coupled model of concentration polarization and pore transport in crossflow nanofiltration, *AIChE J.* 47 (2001) 2733–2745, <https://doi.org/10.1002/aic.690471213>.
- [21] S.U. Hong, R. Malaisamy, M.L. Bruening, Separation of fluoride from other monovalent anions using multilayer polyelectrolyte nanofiltration membranes, *Langmuir* 23 (2007) 1716–1722, <https://doi.org/10.1021/la061701y>.
- [22] R. Epszstein, E. Shaulsky, M. Qin, M. Elimelech, Activation behavior for ion permeation in ion-exchange membranes: role of ion dehydration in selective transport, *J. Membr. Sci.* 580 (2019) 316–326, <https://doi.org/10.1016/j.memsci.2019.02.009>.
- [23] S.T. Morthensen, J. Luo, A.S. Meyer, H. Jørgensen, M. Pinelo, High performance separation of xylose and glucose by enzyme assisted nanofiltration, *J. Membr. Sci.* 492 (2015) 107–115, <https://doi.org/10.1016/j.memsci.2015.05.025>.
- [24] S. Faucher, N. Aluru, M.Z. Bazant, D. Blankschtein, A.H. Brozena, J. Cummings, J. Pedro De Souza, M. Elimelech, R. Epszstein, J.T. Fourkas, A.G. Rajan, H.J. Kulik, A. Levy, A. Majumdar, C. Martin, M. McEldrew, R.P. Misra, A. Noy, T.A. Pham, M. Reed, E. Schwegler, Z. Siwy, Y. Wang, M. Strano, Critical knowledge gaps in mass transport through single-digit nanopores: a review and perspective, *J. Phys. Chem. C* 123 (2019) 21309–21326, <https://doi.org/10.1021/acs.jpcc.9b02178>.
- [25] L.A. Richards, B.S. Richards, B. Corry, A.I. Schäfer, Experimental energy barriers to anions transporting through nanofiltration membranes, *Environ. Sci. Technol.* 47 (2013) 1968–1976, <https://doi.org/10.1021/es303925r>.
- [26] M. Zvolak, J. Wilson, M. Di Ventura, Dehydration and ionic conductance quantization in nanopores, *J. Phys. Condens. Matter* 22 (2010) 454126, <https://doi.org/10.1088/0953-8984/22/45/454126>.
- [27] L.A. Richards, A.I. Schäfer, B.S. Richards, B. Corry, The importance of dehydration in determining ion transport in narrow pores, *Small* 8 (2012) 1701–1709, <https://doi.org/10.1002/sml.201102056>.
- [28] B. Corry, Designing carbon nanotube membranes for efficient water desalination, *J. Phys. Chem. B* 112 (2008) 1427–1434, <https://doi.org/10.1021/jp709845u>.
- [29] L.A. Richards, A.I. Schäfer, B.S. Richards, B. Corry, Quantifying barriers to monovalent anion transport in narrow non-polar pores, *Phys. Chem. Chem. Phys.* 14 (2012) 11633–11638, <https://doi.org/10.1039/c2cp41641g>.
- [30] Y. Ruan, Y. Zhu, Y. Zhang, Q. Gao, X. Lu, L. Lu, Molecular dynamics study of Mg²⁺/Li⁺ separation via biomimetic graphene-based nanopores: the role of dehydration in second shell, *Langmuir* 32 (2016) 13778–13786, <https://doi.org/10.1021/acs.langmuir.6b03001>.
- [31] K. Li, Y. Tao, Z. Li, J. Sha, Y. Chen, Selective ion-permeation through strained and charged graphene membranes, *Nanotechnology* 29 (2018), 035402, <https://doi.org/10.1088/1361-6528/aa9b0c>.
- [32] S. Zhu, R.S. Kingsbury, D.F. Call, O. Coronell, Impact of solution composition on the resistance of ion exchange membranes, *J. Membr. Sci.* 554 (2018) 39–47, <https://doi.org/10.1016/j.memsci.2018.02.050>.
- [33] O.N. Samoylova, E.I. Calixte, K.L. Shuford, Molecular dynamics simulations of ion transport in carbon nanotube channels, *J. Phys. Chem. C* 119 (2015) 1659–1666, <https://doi.org/10.1021/jp5103669>.
- [34] L. Paugam, C.K. Diawara, J.P. Schlumpf, P. Jaouen, F. Quémeunier, Transfer of monovalent anions and nitrates especially through nanofiltration membranes in brackish water conditions, *Separ. Purif. Technol.* 40 (2004) 237–242, <https://doi.org/10.1016/j.seppur.2004.02.012>.
- [35] L. Wang, M.S.H. Boutilier, P.R. Kidambi, D. Jang, N.G. Hadjiconstantinou, R. Karnik, Fundamental transport mechanisms, fabrication and potential applications of nanoporous atomically thin membranes, *Nat. Nanotechnol.* 12 (2017) 509–522, <https://doi.org/10.1038/nnano.2017.72>.
- [36] K. Sint, B.Y. Wang, P. Kral, Selective ion passage through functionalized graphene nanopores, *J. Am. Chem. Soc.* 131 (2009) 16448–16449, <https://doi.org/10.1021/ja903655u>.
- [37] R. Epszstein, E. Shaulsky, N. Dizge, D.M. Warsinger, M. Elimelech, Role of ionic charge density in donnan exclusion of monovalent anions by nanofiltration, *Environ. Sci. Technol.* 52 (2018) 4108–4116, <https://doi.org/10.1021/acs.est.7b06400>.
- [38] B.J. Zvolinski, H. Eyring, C.E. Reese, Diffusion and membrane permeability, *J. Phys. Colloid Chem.* 53 (1949) 1426–1453, <https://doi.org/10.1021/j150474a012>.
- [39] M. Ding, A. Szymczyk, A. Ghoufi, On the structure and rejection of ions by a polyamide membrane in pressure-driven molecular dynamics simulations, *Desalination* 368 (2015) 76–80, <https://doi.org/10.1016/j.desal.2015.01.003>.
- [40] T. Arfin, Rafiuddin, Metal ion transport through a polystyrene-based cobalt arsenate membrane: application of irreversible thermodynamics and theory of absolute reaction rates, *Desalination* 284 (2012) 100–105, <https://doi.org/10.1016/j.desal.2011.08.042>.
- [41] T.R. Farhat, J.B. Schlenoff, Doping-controlled ion diffusion in polyelectrolyte multilayers: mass transport in reluctant exchangers, *J. Am. Chem. Soc.* 125 (2003) 4627–4636, <https://doi.org/10.1021/ja021448y>.
- [42] S. Na, T. Steinbrecher, T. Koslowski, Thermodynamic integration network approach to ion transport through protein channels: perspectives and limits, *J. Comput. Chem.* 39 (2018) 2539–2550, <https://doi.org/10.1002/jcc.25615>.
- [43] T.R. Farhat, J.B. Schlenoff, Ion transport and equilibria in polyelectrolyte multilayers, *Langmuir* 17 (2001) 1184–1192, <https://doi.org/10.1021/la001298>.
- [44] H. Nada, T. Sakamoto, M. Henmi, T. Ogawa, M. Kimura, T. Kato, Environmental Science Ions in Sub-nano Channels of Nanostructured, 2019, <https://doi.org/10.1039/c9ew00842j>.
- [45] D.G. Truhlar, B.C. Garrett, Variational transition state theory, *Annu. Rev. Phys. Chem.* 35 (1984) 159–189.
- [46] J. Abraham, K.S. Vasu, C.D. Williams, K. Gopinadhan, Y. Su, C.T. Cherian, J. Dix, E. Prestat, S.J. Haigh, I.V. Grigorieva, P. Carbone, A.K. Geim, R.R. Nair, Tunable sieving of ions using graphene oxide membranes, *Nat. Nanotechnol.* 12 (2017) 546–550, <https://doi.org/10.1038/nnano.2017.21>.
- [47] N. Dizge, R. Epszstein, W. Cheng, C.J. Porter, M. Elimelech, Biocatalytic and salt selective multilayer polyelectrolyte nanofiltration membrane, *J. Membr. Sci.* 549 (2018) 357–365, <https://doi.org/10.1016/j.memsci.2017.12.026>.
- [48] S.U. Hong, R. Malaisamy, M.L. Bruening, Optimization of flux and selectivity in Cl⁻/SO₄²⁻ separations with multilayer polyelectrolyte membranes, *J. Membr. Sci.* 283 (2006) 366–372, <https://doi.org/10.1016/j.memsci.2006.07.007>.
- [49] X. Zan, B. Peng, D.A. Hoagland, Z. Su, Polyelectrolyte uptake by PEMs: impact of salt concentration, *Polym. Chem.* 2 (2011) 2581–2589, <https://doi.org/10.1039/c1py00280e>.
- [50] E. Hübsch, V. Ball, B. Senger, G. Decher, J.C. Voegel, P. Schaaf, Controlling the growth regime of polyelectrolyte multilayer films: changing from exponential to linear growth by adjusting the composition of polyelectrolyte mixtures, *Langmuir* 20 (2004) 1980–1985, <https://doi.org/10.1021/la0361870>.
- [51] M. Adusumilli, M.L. Bruening, Variation of ion-exchange capacity, ζ potential, and ion-transport selectivities with the number of layers in a multilayer polyelectrolyte film, *Langmuir* 25 (2009) 7478–7485, <https://doi.org/10.1021/la900391q>.
- [52] T. Radeva, V. Milkova, I. Petkanchin, Electro-optics of colloids coated with multilayers from strong polyelectrolytes: surface charge relaxation, *J. Colloid Interface Sci.* 266 (2003) 141–147, [https://doi.org/10.1016/S0021-9797\(03\)00533-2](https://doi.org/10.1016/S0021-9797(03)00533-2).
- [53] D.M. Reurink, J.P. Haven, I. Achterhuis, S. Lindhoud (Erik), H.D.W. Roesink, W. M. de Vos, Annealing of polyelectrolyte multilayers for control over ion permeation, *Adv. Mater. Interfaces.* 5 (2018) 1800651, <https://doi.org/10.1002/admi.201800651>.
- [54] J.A. Jaber, J.B. Schlenoff, Counterfoils and water in polyelectrolyte multilayers: a tale of two polycations, *Langmuir* 23 (2007) 896–901, <https://doi.org/10.1021/la061839g>.
- [55] H.M. Fares, Y.E. Ghoussoub, R.L. Surmaitis, J.B. Schlenoff, Toward ion-free polyelectrolyte multilayers: cyclic salt annealing, *Langmuir* 31 (2015) 5787–5795, <https://doi.org/10.1021/la504910y>.
- [56] W.M. Deen, Hindered transport of large molecules in liquid-filled pores, *AIChE J.* 33 (1987) 1409–1425.
- [57] L.D. Nghiem, A.I. Schäfer, M. Elimelech, Removal of natural hormones by nanofiltration Membranes : measurement, modeling, and mechanisms, *Environ. Eng. 38* (2004) 1888–1896, <https://doi.org/10.1021/es034952r>.
- [58] R.A. Ghostine, R.M. Jisr, A. Lehaf, J.B. Schlenoff, Roughness and salt annealing in a polyelectrolyte multilayer, *Langmuir* 29 (2013) 11742–11750, <https://doi.org/10.1021/la401632x>.
- [59] W.R. Bowen, J.S. Welfoot, Modelling the performance of membrane nanofiltration-critical assessment and model development, *Chem. Eng. Sci.* 57 (2002) 1121–1137, [https://doi.org/10.1016/S0009-2509\(01\)00413-4](https://doi.org/10.1016/S0009-2509(01)00413-4).
- [60] B. Van der Bruggen, M. Mänttäri, M. Nyström, Drawbacks of applying nanofiltration and how to avoid them : a review, *Separ. Purif. Technol.* 63 (2008) 251–263, <https://doi.org/10.1016/j.seppur.2008.05.010>.
- [61] V. Freger, T.C. Arnot, J.A. Howell, Separation of concentrated organic/inorganic salt mixtures by nanofiltration, *J. Membr. Sci.* 178 (2000) 185–193, [https://doi.org/10.1016/S0376-7388\(00\)00516-0](https://doi.org/10.1016/S0376-7388(00)00516-0).
- [62] H.H. Kim, J.H. Kim, Y.K. Chang, Removal of potassium chloride by nanofiltration from ion-exchanged solution containing potassium clavulanate, *Bioproc. Biosyst. Eng.* 33 (2010) 149–158, <https://doi.org/10.1007/s00449-009-0360-7>.
- [63] R.R. Sharma, S. Chellam, Temperature and concentration effects on electrolyte transport across porous thin-film composite nanofiltration membranes: pore transport mechanisms and energetics of permeation, *J. Colloid Interface Sci.* 298 (2006) 327–340, <https://doi.org/10.1016/j.jcis.2005.12.033>.
- [64] R.W. Tsien, D. Noble, A transition state theory approach to the kinetics of conductance changes in excitable membranes, *J. Membr. Biol.* 1 (1969) 248–273, <https://doi.org/10.1007/BF01869785>.

A4 Experimental results of immobilization of alcohol dehydrogenase by polyelectrolyte layer-by-layer assembly and interfacial polymerization

Selected results of experiments with the immobilization of ADH by polyelectrolyte LbL assembly and interfacial polymerization are presented below.

The effect of the pH of the enzyme feed solution on the immobilization efficiency when ADH was immobilized on PEM membranes is shown in Figure A1. The adsorption of ADH onto the PEM membranes increased by increasing the pH of the enzyme feed solution from pH 6.5 to pH 8.5, presumably due to more favorable electrostatic conditions between the ADH and the positively charged membrane. The effect of polymerization time between ADH and TMC on water permeability and NADH conversion in biocatalytic membranes prepared by interfacial polymerization are presented in Figure A2. The water permeability decreased as the polymerization time between ADH and TMC was increased, which indicated a successful film growth due to polymerization between ADH and TMC. The NADH conversion upon passing through the biocatalytic membranes increased slightly with polymerization time, possibly since the lower water permeability resulted in longer retention time within the membrane.

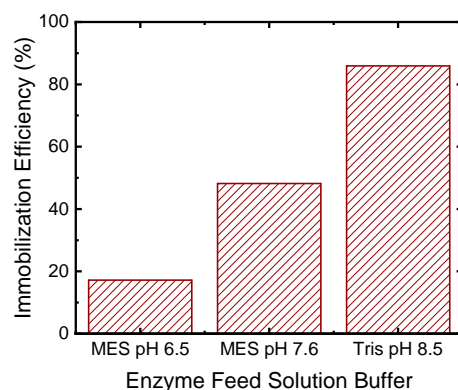


Figure A1: Effects of the pH of the enzyme feed solution on the immobilization of ADH on PEM membranes. The membranes were prepared by depositing polystyrene sulfonate (PSS) and Poly(diallyldimethylammonium chloride) (PDADMAC) onto a GRM0.1PP MF membrane substrate. For enzyme immobilization at pH 6.5 and 7.6, the PEM membranes were prepared by filtering 10 mL of 0.01% PDADMAC in 0.2 M NaCl through the membranes at 1 bar, followed by static deposition of one layer of PSS (10 mL, 0.1 wt%, 20 min) and one layer of PDADMAC (10 mL, 0.1 wt%, 20 min), with two 5-min rinsing cycles with 0.2 M NaCl between layers. Enzyme immobilization on the membranes was conducted by applying 5 mL of 10 mg L⁻¹ ADH in MES buffer at pH 6.5 (or pH 7.6, where the pH was raised by adding drops of 1M NaOH to the enzyme solution) for 30 minutes followed by filtration at 1 bar. For enzyme immobilization at pH 8.5, the GRM0.1PP membrane was first treated with PDA and PEI by applying 10 mL of a 1,82 g/L dopamine-HCl and 0,09 g/L PEI solution in 50 mM Tris buffer at pH 8.5, at 100 rpm, room temperature, for 1h. Subsequently, 10 mL of a 0.01% PSS solution in 0.2 M NaCl was filtered through the membranes at 1 bar, followed by 20-min static deposition of one layer of PDADMAC (10 mL, 0.1 wt%), with two five minutes rinsing cycles with 0.2 M NaCl between layers. Enzyme immobilization on the membrane was conducted by applying 5 mL of 10 mg L⁻¹ ADH in Tris buffer at pH 8.5 for 30 minutes followed by filtration at 1 bar.

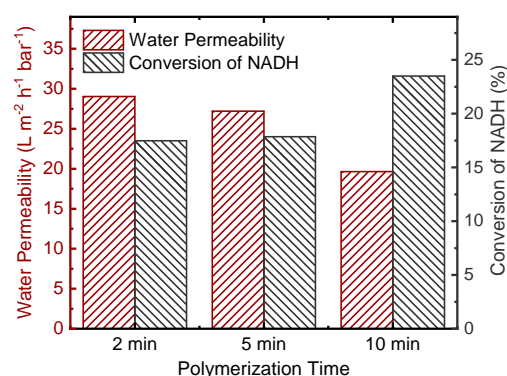


Figure A2: Water permeability and NADH conversion per pass through biocatalytic membranes prepared by interfacial polymerization of ADH and TMC. GR61PP UF membrane (polysulfone, 20 kDa) was used as a substrate for the polymerization. ADH (0.7 mL 571 mg L⁻¹ in MES buffer at pH 6.5) was applied to the membrane for 30 min, subsequently, 3 mL of 0.075 wt% TMC in hexane was added to the membrane surface and the ADH and TMC were left to polymerize for 2, 5, and 10 min. The TMC solution was dumped off of the membranes, the membranes were air-dried for 2 min and then washed thoroughly with water. The activity of the catalytic membranes was measured by adding 4 mL of substrate solution (30 mM formaldehyde and 100 μ M NADH in MES buffer at pH 6.5) to the reactor and collecting 2 mL of permeate by filtration at 4 bar applied pressure. The NADH concentrations of the feed, retentate, and permeate were calculated from absorbance measurements at 340 nm, and were used to calculate the conversion and retention of NADH in the reactor. Water permeability was measured gravimetrically.

A5 Supplementary material

Electronic supplementary material for papers 2 and 3 is provided below.

Immobilization of alcohol dehydrogenase on inorganic powders: Zeta potential, surface area and particle agglomeration as main factors determining activity

Sigyn Björk Sigurdardóttir^a, Jonas Lehmann^b, Jean-Claude Grivel^b, Wenjing Zhang^b, Andreas Kaiser^b, Manuel Pinelo^{a*}

^aTechnical University of Denmark, DTU Chemical Engineering, Søltøfts Plads, Building 229, 2800 Kgs. Lyngby, Denmark, ^bTechnical University of Denmark, DTU Energy, Frederiksborgvej 399, 4000 Roskilde, Denmark. *Corresponding author

Supplementary material

S1. Immobilization procedures

The immobilization was conducted in an Amicon 2010 stirred cell (Millipore, USA), with 10 mL working volume and membrane projection area of 4.1 cm². First, a GRM0,1PP microfiltration membrane (polysulfone, 0.1 μm pore diameter) was prepared by immersing in 50% EtOH for 5 minutes, after which it was mounted in the cell and washed twice with 10 mL of DI water. Subsequently, powder and enzyme solution (10 mL of 20 mg/L ADH in MES buffer) were added to the cell, where the immobilization was conducted for 90 min at room temperature (RT) and 100 rpm. After immobilization, the enzyme solution was removed by filtration and the powder was washed three times with 10 mL of MES buffer to ensure complete removal of any non-immobilized enzyme. The filtration permeates were collected for protein determination. For PA, 10 mg of as-received powder and 10 mL of a freshly prepared enzyme solution were added to the cell and the immobilization was proceeded as just described. For CB, the powder was functionalized and activated before immobilization. These two steps were conducted in 1.5 mL microcentrifuge tubes and mixing was done on a Thermomixer Compact (Eppendorf, Germany). For functionalization, 10 mg of as-received powder and 1.5 mL of 4% APTES in 90% EtOH were mixed for 90 min at 70°C and 700 rpm. Subsequently, the powder suspension was centrifuged at 14000 rpm for 3 min on a Sigma 1-15 microcentrifuge (DJB labcare, UK), the APTES solution was removed and the powder was washed five times by re-suspending in 90% EtOH with intermediate centrifugation cycles (3 min at 14000 rpm). After washing, the powder was dried for 1h at 60°C in an incubator (BINDER, Germany). For activation, the powder was suspended in 1.5 mL of 2.5% GA in H₂O and mixed for 30 min at RT and 700 rpm. GA was removed by centrifugation and the powder was washed with MilliQ water in a similar manner as after functionalization. The powder was dried for 1.5h at 60°C in the incubator. Finally, the powder was transferred to the filtration cell and the immobilization was conducted by the same procedure as described above.

S2. Recyclability of ADH on SiC

The activity of ADH-PA and ADH-CB on SiC in eight consecutive reaction cycles is shown in Figure S1.

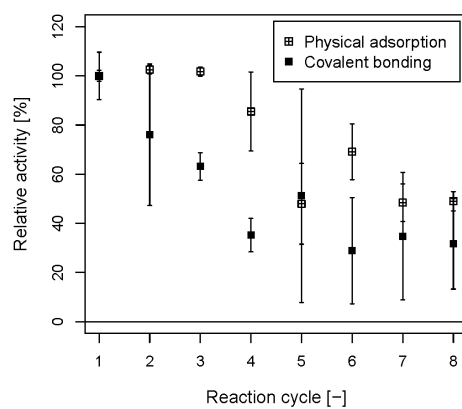


Figure S1: Relative activity of ADH-PA and ADH-CB immobilized on SiC as a function of reuse cycle. Reaction conditions: 10 mL reaction volume, 30 mM Fald, 100 μ M NADH, RT, 100 rpm, MES buffer, pH 6.5. Each reaction cycle lasted 10 minutes, after which the NADH concentration was measured. Error bars report standard deviation of at least two independent measurements.

Supplementary Material

Energy Barriers to Ion Transport in Nanofiltration Membranes: Role of Intra-Pore Diffusion

Sigyn B. Sigurdardottir,^{1,2} Ryan M. DuChanois,¹ Razi Epsztein,^{1,3,*} Manuel Pinelo,² Menachem Elimelech^{1,*}

¹ Department of Chemical and Environmental Engineering, Yale University, New Haven, Connecticut 06520-8286, USA

² Department of Chemical and Biochemical Engineering, Technical University of Denmark, DTU, Søtofts Plads, Building 229, 2800 Kgs, Lyngby, Denmark

³ Faculty of Civil and Environmental Engineering, Technion – Israel Institute of Technology, Technion City, Haifa 32000, Israel

(* Emails: menachem.elimelech@yale.edu; raziepsztein@technion.ac.il)

Number of Pages: 9

Number of Figures: 4

Number of Tables: 2

Hydrodynamic pore transport model. In the model described by Deen [1] and Nghiem et al. [2], we assume neutral, spherical solutes to enter the membrane pores, which are described as a bundle of capillaries of the same radii. When only steric interactions are considered, the ratio of the solute radius (r_s) and pore radius (r_p) is described by the distribution coefficient (Φ) according to the equation [3]:

$$\Phi = \frac{\langle c' \rangle}{c} = \left(1 - \frac{r_s}{r_p}\right)^2 = (1 - \lambda)^2 \quad (\text{S1})$$

Where $\langle c' \rangle$ is the average solute concentration inside the pore and c is the solute concentration at the pore entrance. Knowing Φ and the solute radius, the pore radius can be solved from Eq. S1.

The distribution coefficient (Φ) is involved in the real rejection (R_r) by the membrane, which describes the difference in solute concentrations just outside the membrane pores on the feed and permeate sides. The real rejection is described by the following equation:

$$R_r = 1 - \frac{c_L}{c_0} = 1 - \frac{\Phi K_c}{1 - \exp(-\text{Pe})(1 - \Phi K_c)} \quad (\text{S2})$$

Where c_0 and c_L are the solute concentrations at the membrane surfaces facing the feed and permeate, respectively, K_c is a hydrodynamic hindrance coefficient for convection and Pe is the Peclet number of the membrane [3]. The calculation of K_c and Pe is described elsewhere [2].

The real rejection can be calculated from the observed rejection, which is measured from the bulk feed concentration, by applying film theory that takes concentration polarization at the membrane surface into account. The relation between the real and observed rejections according to film theory is given by Eq. S3:

$$\ln\left(\frac{1-R_r}{R_r}\right) = \ln\left(\frac{1-R_o}{R_o}\right) - \frac{J_v}{k_f} \quad (\text{S3})$$

Where J_v is the water flux and k_f is the mass transfer coefficient for the solute.

The real rejection, R_r , can be obtained from Eq. S3 using data collected in filtrations of neutral organic solutes (water flux and observed rejection). Subsequently, R_r is used in Eq. S2 to solve for ΦK_c and Pe , using an iterative procedure (Solver, Microsoft Excel). The ratio of r_s and r_p (λ) can then be solved for knowing ΦK_c and Pe , since these parameters are functions of λ . Finally, the pore radius can be found from Eq. S1. The pore radius is calculated for each organic solute used, and the average estimated pore radius for each membrane is found as the average pore radius calculated for each solute. The results are presented in table S2.

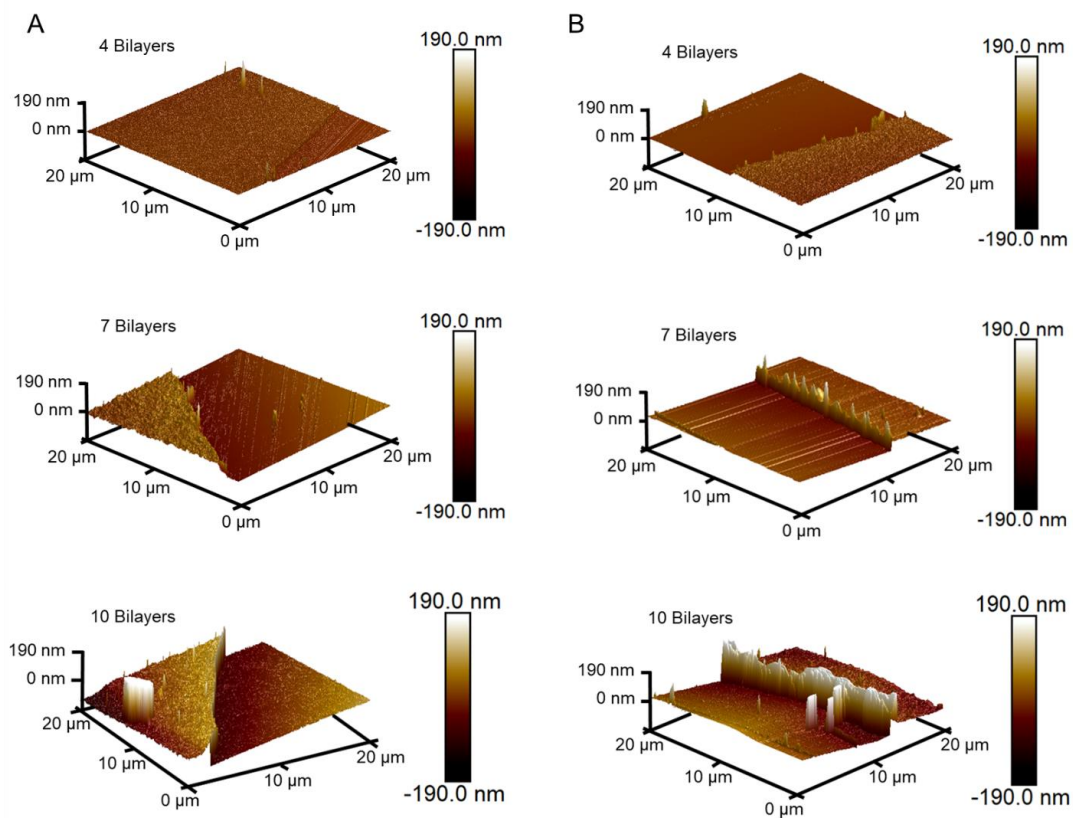


Fig. S1. Sample AFM images ($20 \times 20 \mu\text{m}$) used for thickness measurements of dry PEM films. PEM films with four, seven, and ten bilayers of PDADMAC/PSS were fabricated by depositing (A) 0.8 mM and (B) 20 mM polyelectrolyte solutions onto a silicon wafer. Before imaging, a scratch was generated by dragging a needle across the dry PEM film. The images show the topology of the PEM film and the bare silicon wafer around one edge of the scratch.

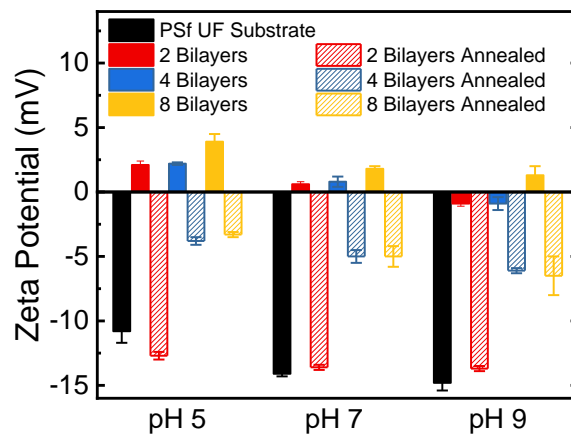


Fig. S2. Surface zeta potential of PSf UF substrate and PEM NF membranes with two, four, and eight bilayers of PDADMAC/PSS (20 mM) fabricated on PSf UF substrate with and without salt annealing. By salt annealing, the PEM films were subjected to 2 M NaCl for 30 minutes prior to the deposition of the terminating PSS layer. The surface zeta potential was calculated from eight streaming potential measurements using a constant background electrolyte concentration of 1 mM KCl and 0.1 mM KHCO_3 . The pH was adjusted using hydrochloric acid (HCl) and sodium hydroxide (NaOH).

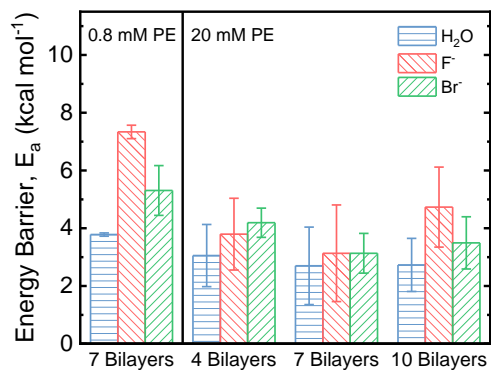


Fig. S3. Energy barriers to water and anion transport through PEM NF membranes with four, seven, and ten bilayers of PDADMAC/PSS. Membranes were prepared by deposition of 0.8 mM or 20 mM polyelectrolyte solutions onto a PSf UF substrate. Experimental conditions: single salt solutions of 4 mM NaF (H₂O, F⁻) or 4 mM NaBr (Br⁻), 1.7 bar (25 psi), crossflow velocity of 0.21 m s⁻¹, pH 5.7. Error bars report standard deviations of three independently fabricated membranes.

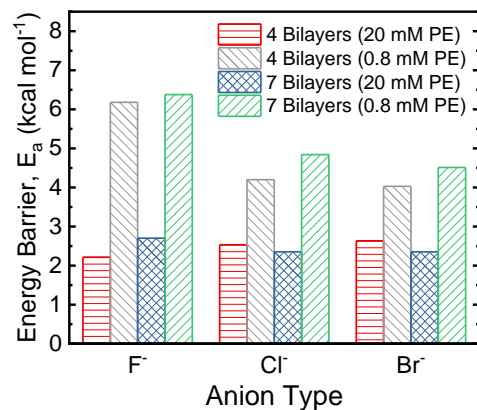


Fig. S4. Energy barriers to transport of different anions through PEM NF membranes of different thicknesses and pore sizes. Membranes were fabricated by depositing either four or seven bilayers of 0.8 mM or 20 mM PDADMAC/PSS onto a PSf UF substrate. Membranes fabricated with deposition solutions of 0.8 mM (pore radius = 0.62 nm) and 20 mM (pore radius = 0.70 nm) polyelectrolyte (PE) represent small and large pores, respectively. Hydration energies of ions are: F⁻ (111.1 kcal mol⁻¹), Cl⁻ (81.3 kcal mol⁻¹), and Br⁻ (75.3 kcal mol⁻¹). Experimental conditions: mixed ion solution with 2 mM of each NaF, NaCl, and NaBr; 6.9 bar (100 psi); crossflow velocity of 0.21 m s⁻¹; pH 5.7. Rejection of anions was measured by anion chromatography.

Table S1. Characterization of PEM films and PEM NF membranes.

	4 Bilayers 0.8 mM PE	7 Bilayers 0.8 mM PE	10 Bilayers 0.8 mM PE	4 Bilayers 20 mM PE	7 Bilayers 20 mM PE	10 Bilayers 20 mM PE
Thickness (nm)	13.6 ± 0.7	63.5 ± 8.6	123.0 ± 4.7	27.6 ± 3.2	61.6 ± 8.1	76.6 ± 14.3
Pore radius (nm)	0.64 ± 0.08	0.62 ± 0.05	0.70 ± 0.07	0.73 ± 0.09	0.70 ± 0.06	0.74 ± 0.09
Zeta potential (mV)	2.1 ± 0.1 ^a -2.0 ± 0.4 ^b -3.0 ± 0.4 ^c	4.5 ± 1.1 ^a 2.1 ± 1.7 ^b 1.5 ± 2.1 ^c	5.6 ± 0.5 ^a 2.2 ± 0.6 ^b 0.3 ± 0.7 ^c	-2.1 ± 0.1 ^a -4.3 ± 0.1 ^b -6.4 ± 0.4 ^c	-5.2 ± 0.0 ^a -7.6 ± 0.5 ^b -9.0 ± 0.5 ^c	-5.4 ± 1.0 ^a -7.2 ± 0.8 ^b -9.0 ± 0.6 ^c
Water permeability (L m ⁻² h ⁻¹ bar ⁻¹)	6.98 ^d	5.42 ± 0.24	3.64 ^d	9.01 ± 1.13	8.46 ± 0.91	6.61 ± 0.47

^a pH 5^b pH 7^c pH 9^d Filtration of mixed ion solution (2 mM of each NaCl, NaF, NaBr), at 22°C; 1.7, 5.2, and 6.9 bar.

Table S2. Properties of organic solutes and outputs (λ , pore radius) from the hydrodynamic pore transport model. The average estimated pore sizes were calculated in an optimization process using flux and rejection data from filtrations of organic solutes.

Organic tracer	MW (g mol ⁻¹)	Diffusivity ^a (10 ⁻¹⁰ m ² s ⁻¹)	Stokes Radius ^b , r _s (nm)	$\lambda = r_s/r_p$	Pore radius, r _p (nm)
<i>Membrane: 4 Bilayers (20 mM PE)</i>					
Erythritol	122	8.4	0.263	0.317	0.831
Xylose	150	7.5	0.290	0.422	0.687
Glucose	180	6.8	0.324	0.490	0.661
Average					0.726
<i>Membrane: 4 Bilayers (0.8 mM PE)</i>					
Erythritol	122	8.4	0.263	0.357	0.737
Xylose	150	7.5	0.290	0.484	0.599
Glucose	180	6.8	0.324	0.554	0.585
Average					0.640
<i>Membrane: 7 Bilayers (20 mM PE)</i>					
Erythritol	122	8.4	0.263	0.349	0.754
Xylose	150	7.5	0.290	0.414	0.701
Glucose	180	6.8	0.324	0.511	0.634
Average					0.696
<i>Membrane: 7 Bilayers (0.8 mM PE)</i>					
Erythritol	122	8.4	0.263	0.391	0.673
Xylose	150	7.5	0.290	0.464	0.626
Glucose	180	6.8	0.324	0.567	0.571
Average					0.623
<i>Membrane: 10 Bilayers (20 mM PE)</i>					
Erythritol	122	8.4	0.263	0.312	0.844
Xylose	150	7.5	0.290	0.417	0.696
Glucose	180	6.8	0.324	0.479	0.676
Average					0.739
<i>Membrane: 10 Bilayers (0.8 mM PE)</i>					
Erythritol	122	8.4	0.263	0.337	0.779
Xylose	150	7.5	0.290	0.429	0.676
Glucose	180	6.8	0.324	0.495	0.655
Average					0.703

^a Calculated using the Wilke and Chang equation.

^b Calculated using Stokes-Einstein equation

- [1] W.M. Deen, Hindered Transport of Large Molecules in Liquid-Filled Pores, *AIChE J.* 33 (1987) 1409–1425.
- [2] L.D. Nghiem, A.I. Schafer, M. Elimelech, Removal of Natural Hormones by Nanofiltration Membranes : Measurement, Modeling, and Mechanisms, *Environ. Eng.* 38 (2004) 1888–1896. doi:10.1021/es034952r.
- [3] M. Xie, L.D. Nghiem, W.E. Price, M. Elimelech, Relating rejection of trace organic contaminants to membrane properties in forward osmosis: Measurements, modelling and implications, *Water Res.* 49 (2014) 265–274. doi:10.1016/j.watres.2013.11.031.